THE SOLUTION OF TRANSIENT AND STEADY-STATE MAGNETIC FIELDS WITH PARTICULAR REFERENCE TO NUMERICAL METHODS

R.L. Stoll
Department of Electrical Engineering,
University of Southampton.

1. Introduction

The vector diffusion equation for a low frequency magnetic field $\underline{H}$ can be written in the form[1]

$$\nabla^2\underline{H} = \sigma \frac{dB}{dH}\frac{\partial \underline{H}}{\partial t} - \text{grad}\left(\underline{H}\cdot\frac{1}{\mu}\,\text{grad}\,\mu\right) - \frac{1}{\sigma}\,(\text{grad}\,\sigma)\times\text{curl}\,\underline{H} \qquad (1)$$

Although the conductivity σ is usually constant within each conductor, it is expressed here as a function of space because this can sometimes facilitate setting up the computation scheme. The permeability μ is similarly treated, but, in addition, may be a function of $\underline{H}$. The constituent equation is assumed to take the form $\underline{B} = \mu\underline{H}$ where $\underline{B}$ and $\underline{H}$ are not necessarily linearly related but the magnetic material is isotropic and has no hysteresis effect. For example, the magnetisation characteristic may be approximated by the Frohlich curve

$$\underline{B} = \frac{\underline{H}}{a + bH} \qquad (2)$$

from which $\mu = (a + bH)^{-1}$.

Problems in which the magnetic field is described by eqn.1 are known as initial boundary value problems: the initial ($t = 0$) state of $\underline{H}$ must be defined over the space domain and Dirichlet, Neumann or mixed boundary conditions specified for $t > 0$. However, in the special case of sinusoidal excitation, with the additional constraint $\mu = \mu_o\mu_r$, a simpler boundary value problem can be achieved by defining a complex vector $\overline{\underline{H}}$ which is related to the instantaneous vector $\underline{H}$ by

$$\underline{H} = \text{Re}\left[\overline{\underline{H}}\, e^{j\omega t}\right] \qquad (3)$$

so that eqn.1 reduces to

$$\nabla^2\overline{\underline{H}} = j\omega\sigma\mu\overline{\underline{H}} - \text{grad}\left(\overline{\underline{H}}\cdot\frac{1}{\mu}\,\text{grad}\,\mu\right) - \frac{1}{\sigma}\,(\text{grad}\,\sigma)\times\text{curl}\,\overline{\underline{H}} \qquad (4)$$

Use of the vector potential $\underline{A}$, defined as curl $\underline{A} = \underline{B}$ and div $\underline{A} = 0$ (Sarma[2] shows that a nonzero divergence may be helpful in some low frequency problems), also yields similar real and complex second-order partial differential equations, the real equation being

$$\nabla^2\underline{A} = \sigma\mu\left(\frac{\partial \underline{A}}{\partial t} + \text{grad}\,V\right) - \frac{1}{\mu}\,(\text{grad}\,\mu)\times\text{curl}\,\underline{A} \qquad (5)$$

where V is a scalar electric potential.

Considering problems involving two space co-ordinates x and y and time, then if there is only one component of $\underline{H}$, H_z say, which is independent of z, i.e. the current density is a function of x and y, eqn.1 reduces to the convenient symmetrical form

$$\frac{\partial}{\partial x}\left(\rho\frac{\partial H_z}{\partial x}\right) + \frac{\partial}{\partial y}\left(\rho\frac{\partial H_z}{\partial y}\right) = \frac{dB_z}{dH_z}\frac{\partial H_z}{\partial t} \qquad (6)$$

where ρ is the resistivity. Alternatively, if there is only one component of current density J_z, it is convenient to use the resulting single component of vector potential A_z, and eqn.5 yields

$$\frac{\partial}{\partial x}\left(\nu\frac{\partial A_z}{\partial x}\right) + \frac{\partial}{\partial y}\left(\nu\frac{\partial A_z}{\partial y}\right) = \sigma\frac{\partial A_z}{\partial t} + \sigma\frac{\partial V}{\partial z} = \sigma\frac{\partial A_z}{\partial t} - J_s \qquad (7)$$

where ν is the reluctivity. The term $\frac{\partial V}{\partial z}$ is the negative of the impressed electric field strength E_z, so that $-\sigma\frac{\partial V}{\partial z} = J_s$ is the impressed source current density, if any.

Where a problem has natural boundaries, the differential formulation is preferable, especially in view of the research effort that has been put into the theory of differential equations, but it is also possible to set up an integral equation that sums the contribution of all the field sources. Interesting examples of integral formulations solved numerically are given by Haznadar[3] and Silvester[4].

2. Types of Solution

At the risk of oversimplification we can divide the various types of mathematical solution into three categories.

(a) First there is the analytical solution in which the independent variable or parameter of interest, e.g. the magnetic field distribution or a single quantity such as impedance, can be expressed algebraically in terms of the system constants (conductivity, frequency etc.) and the independent variables (the space and time co-ordinates). Needless to say the expression involved may be a complicated series, for example, and numerical substitution may be necessary before the influence of a given parameter can be determined. Examples of this type of solution are the separation of variables method and the finite, or infinite, Fourier

transform. Such methods are limited to relatively simple linear problems.

(b) Secondly, there is the almost entirely numerical approach in which the problem is discretised in some way so that we can work with a set of numbers instead of with a continuous variable and therefore with a matrix equation instead of a partial-differential equation. This is the basis of the finite-difference and finite-element methods which will be discussed in Section 3. An interesting variation is the coupled electric and magnetic network approach developed by Carpenter[5,6] which makes use of the magnetic scalar potential, instead of the vector potential, by confining the current flow to thin conducting sheets and is a powerful way of translating an eddy-current problem into numerical form.

(c) Thirdly, there is the type of method that can most appropriately be described as mixed, containing both analytical and numerical components. They usually arise because a full numerical method is found to be too time consuming on the available computer system, or because the analyst is determined not to obey Parkinson's law but to seek an economic solution. An outstanding example is the method outlined by Hockney[7] for the solution of Poisson's equation in a rectangular region, but also applicable to Helmholtz equation and to other two-dimensional co-ordinate systems, in which one dimension of the problem is reduced by the application of a finite Fourier transform. The partial-differential equation is thus reduced to a set of ordinary-differential equations which can then be solved numerically. There are various refinements which increase the speed of the solution, and the method should be appropriate for multi-region eddy-current problems, where the interfaces are parallel to the direction in which the transform is applied.

A different approach due to Silvester[8,9] regards each term in a double Fourier series solution for a long rectangular bar as a single eddy-current mode for which an equivalent R-L circuit can be set up. The terms in the series form a complete set of orthogonal functions and so there is no coupling between the set of equivalent circuits. In more general terms we can say that the current in a conductor flows in an infinite number of independent spatial patterns (modes), its distribution between the modes being dictated by the form of the excitation. Thus the method had the advantage that any form of time-dependent excitation can be handled by the same set of circuit equations or matrix equation, and it is particularly useful in being able to handle situations in which it is either not possible or not convenient to formulate an initial boundary value problem. In this sense the method is an alternative to the numerical solution of an integral equation formulation of the problem.

We will now briefly consider some numerical methods which are particularly important if we wish to include magnetic saturation.

3. Numerical Solutions

Problems that require numerical treatment divide naturally into two broad classes; linear steady state, and nonlinear steady state and transient. All nonlinear solutions are essentially the same because a steady-state solution must pass through a numerical transient which will be similar to the real transient for the given initial (switch-on) conditions.

Time-dependent magnetic field equations of the diffusion type have been solved numerically by both finite differences and finite elements, although the time co-ordinate has always been discretised by finite differences. The common feature of the methods is that, at each time step, they yield a large set of difference equations which are usually arranged to be linear and have to be solved either by elimation or by an iterative process of some sort.

In the finite-difference method, the complete differential operator is replaced by a finite-difference operator which sets up discrete values of the dependent variable at the nodes of a regular grid consisting (usually) of rectangular cells. The derivation and programming of the method is relatively straightforward compared with the finite-element approach, which, in its simplest form, sets up an array of triangular elements covering the space domain of the problem and forces the dependent variable to vary linearly over the surface of each element. Thus the local variable is defined by its values at the three vertex nodes. One of the advantages of finite elements is that their size is readily varied so that the field can be accurately represented in regions of rapid spatial variation without using an excessive number of elements. In a nonlinear quasi-static problem the set of algebraic equations is generated by minimising the energy functional[10]

$$F = \int\int \left\{ \int_0^B \nu B \, dB - AJ \right\} dx \, dy \qquad (8)$$

for which the original partial-differential equation is the Euler equation. One way of introducing the time dependence is to regard J in eqn.8 as consisting of both the source current density J_s and the eddy current density $-\sigma \frac{\partial A}{\partial t}$ from eqn.7, i.e. $J = J_s - \sigma \frac{\partial A}{\partial t}$, and to 'graft on' a finite-difference expression for the time derivative after the minimisation process[11]. Eqn.8, with J regarded as an instantaneous injected current, must now more properly be referred to as a functional associated with energy because, due to the ohmic losses, the new system is no longer energy conserving. Whatever the formal difficulties the hybrid scheme appears to work. Results for linear complex problems have already been reported[12,13], and a relatively simple nonlinear problem has been solved using the Galerkin technique[14].

3.1 A finite-difference algorithm for eqn.7.

It is possible to proceed directly via Taylor's theorem, but a simpler result can be achieved if eqn.7 is written in the form

$$\mathrm{curl}_z \left(\underline{a}_x \nu \frac{\partial A_z}{\partial y} - \underline{a}_y \nu \frac{\partial A_z}{\partial x}\right) = J_s - \sigma \frac{\partial A_z}{\partial t} \qquad (9)$$

FIG. 1

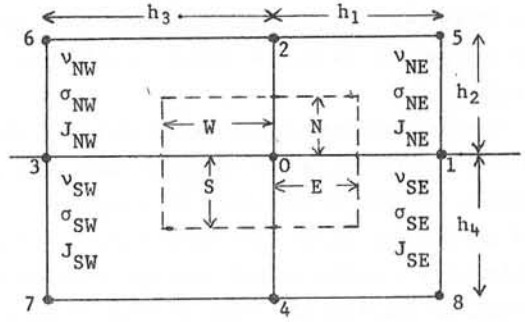

Integrating eqn.9 over the cross-section of the secondary cell shown dotted in Fig.1, applying Stokes' theorem and following a procedure similar to that given in Reference 1 for the complex form of eqn.9, the following explicit finite-difference equation for advancing from time step k to k + 1 is obtained.

$$(\alpha_1 + \alpha_2 + \alpha_3 + \alpha_4) A_{o,k} - (\alpha_1 A_{1,k} + \alpha_2 A_{2,k} + \alpha_3 A_{3,k} + \alpha_4 A_{4,k})$$

$$= I_{o,k} - Q_{o,k} \frac{A_{o,k+1} - A_{o,k}}{\Delta t} \qquad (10)$$

where $\alpha_1 = (N\nu_{NE} + S\nu_{SE})\, h_1^{-1}$

$\alpha_2 = (E\nu_{NE} + W\nu_{NW})\, h_2^{-1}$

$\alpha_3 = (N\nu_{NW} + S\nu_{SW})\, h_3^{-1}$

$\alpha_4 = (E\nu_{SE} + W\nu_{SW})\, h_4^{-1}$

$I_o = NE\, J_{NE} + NWJ_{NW} + SE\, J_{SE} + SWJ_{SW}$

and $Q_o = NE\, \sigma_{NE} + NW\, \sigma_{NW} + SE\, \sigma_{SE} + SW\, \sigma_{SW}$

All these parameters can be functions of time, i.e. the time-step counter k, including the coefficients α_1, α_2, etc. if the problem is nonlinear. The truncation error of the algorithm is $O(h^2 + \Delta t)$ when h is the larger of h_1, h_2, etc. The algorithm is also explicit in the sense that the new potential $A_{o,k+1}$ at node 0 can be obtained directly. However, such a scheme is known to have a very limited stability range, and modifications are necessary. These are most conveniently discussed in terms of a one-dimensional field solution.

3.2 One-dimensional algorithms and comments on extension to two dimensions

Consider the one-dimensional version of eqn.6 with constant conductivity, namely:-

$$\frac{\partial^2 H_z}{\partial y^2} = \sigma \frac{dB_z}{dH_z} \frac{\partial H_z}{\partial t} = \beta \frac{\partial H_z}{\partial t} \qquad (11)$$

The simple explicit difference form of eqn.11 is

$$H_{i,k+1} = rH_{i+1,k} + (1 - 2r) H_{i,k} + rH_{i-1,k} \qquad (12)$$

where $r = \Delta t / \beta h^2 \leqslant \frac{1}{2}$ for stability. Alternatively, the simple implicit equation using a backward instead of forward time difference equation is[15,23]

$$H_{i+1,k+1} + (-2 - \tfrac{1}{r}) H_{i,k+1} + H_{i-1,k+1} = -\tfrac{1}{r} H_{i,k} \qquad (13)$$

with no restriction on r. The penalty we have to pay for this stability is to solve all the new values at time k+1 simultaneously. However, the coefficient matrix is tridiagonal and so the matrix equation is simple to solve.

Application of eqns.12 and 13 at alternate time steps produces the well-known Crank-Nicolson algorithm

$$H_{i+1,k+1} + 2(-1 - \tfrac{1}{r}) H_{i,k+1} + H_{i-1,k+1} = -H_{i+1,k} + 2(1 - \tfrac{1}{r}) H_{i,k} - H_{i-1,k} \qquad (14)$$

which has an improved truncation error $O(h^2 + (\Delta t)^2)$ and is stable for all linear problems and a wide range of nonlinear ones. When r is a function of H, a two-step predictor-corrector algorithm is usually incorporated[15] in order to be able to maintain a relatively large time step.

The Crank-Nicolson equation is an implicit one so that its extension to two-dimensional problems is rather inefficient because of the large number of equations to be solved simultaneously at each time step. For this an iterative solution (e.g. successive over-relaxation) is faster than elimination because, since the change in nodal values from one time step to the next is small, only a few iterations are needed. However, a modified version of the method in two dimensions is the Peaceman-Rachford alternating-direction implicit (ADI) method[16,24] where the nodal equations on first the rows and then the columns of the space grid are treated alternately as implicit sets.

It is tempting to seek an explicit method that is stable and can be extended to two-dimensional solutions. One possibility is the hopscotch method devised by Gourlay[17] and summarised in Reference 1. Basically it derives from the alternate application of eqns.12 and 13 to the nodes on each time step so that the space-time plane can be pictured as a chess board of black (explicit) and white (implicit) squares. The resulting scheme is explicit and is effectively a faster version of the DuFort-Frankel[18,25] scheme (although some of this advantage is lost in non-linear problems) where $H_{i,k}$ in eqn.12 is replaced by $\frac{1}{2}(H_{i,k+1} + H_{i,k-1})$ to give

$$H_{i,k+1} = H_{i,k-1} + \frac{2r}{2r+1}(H_{i+1,k} - 2H_{i,k-1} + H_{i-1,k}) \qquad (15)$$

The truncation error is $O(h^2 + (\Delta t)^2 + (\Delta t/h)^2)$ which indicates that Δt must be much smaller than h. Closer investigation shows that the optimum value of Δt for minimum error lies near $\frac{\beta h^2}{\sqrt{12}}$ for a linear problem[18]. For nonlinear solutions with high saturation, where β may decrease to a low value (typically about 4) for part of the cycle, the situation is not clear. The above condition would suggest $\Delta t \approx h^2$, but the method then involves as much computation as the simple explicit method. The time step must therefore be larger and a greater error tolerated, although the error can still be less than that with the simple scheme.

3.3. Analytical expression for the magnetisation curve

Numerical methods are both faster and less likely to become unstable if an analytical expression is used for the magnetisation curve instead of interpolating from a set of experimental values. In any case the experimental values should be smoothed before use, especially if the incremental permeability is required. A large number of mathematical expressions have been examined by Trutt, Erdelyi and Hopkins[19] and the Frohlich curve (eqn.2) emerges as a good compromise between accuracy and simplicity. In fact the curve is excellent for materials like mild steel but not so good for silicon steels (electrical machine laminations) which have a pronounced 'knee' in their characteristic. It will be seen from eqn.2 that as H increases the magnitude of B tends to the constant value b^{-1}, i.e. the curve has zero slope. On the other hand, the magnetisation curve for steel maintains a constant slope μ_o after the saturation point (B_s, H_s). When working well into saturation, it is therefore essential to make up the characteristic in two parts; the Frohlich curve for $B < B_s$ and the straight line $B = B_o + \mu_o H$ when $B > B_s$. The constant B_o can be shown to be given by bB_s^2. Thus the incremental slope and reluctivity when $B < B_s$ are given by

$$\frac{dB}{dH} = \frac{a}{(a + bH)^2} \qquad (16)$$

and

$$\nu = \frac{a}{1-bB} \qquad (17)$$

and, when $B > B_s$ by

$$\frac{dB}{dH} = \mu_o \qquad (18)$$

and

$$\nu = \frac{1}{\mu_o}\left(1 - \frac{B_o}{B}\right) \qquad (19)$$

The constants in the Frohlich equation must be such that the saturation point (B_s, H_s) lies on the curve and the slope is μ_o when $H = H_s$. After a little manipulation we obtain

$$\left.\begin{aligned} a &= \mu_o (H_s/B_s)^2 \\ \text{and} \quad b &= (1 - \sqrt{\mu_o a})\, B_s^{-1} \end{aligned}\right\} \qquad (20)$$

An important point to note is that, if the problem is being solved in terms of the vector potential, H or ν should be expressible explicity

in terms of B, and hence the derivatives of A, and preferably not in a form that necessitates making successive approximations to H.

3.4 The DuFort-Frankel scheme in two dimensions with variable coefficients

The two-dimensional equation in H_z for constant conductivity is, from eqn.6,

$$\frac{\partial^2 H_z}{\partial x^2} + \frac{\partial^2 H_z}{\partial y^2} = \sigma \frac{dB_z}{dH_z} \frac{\partial H_z}{\partial t} \qquad (21)$$

For a square mesh in the x,y plane of side h, the DuFort-Frankel finite-difference equation is

$$\left.\begin{aligned} H_{i,j,k+1} &= H_{i,j,k-1} + \frac{2r}{4r+1} \\ &(H_{i-1,j,k} + H_{i,j-1,k} + H_{i,j+1,k} + H_{i+1,j,k} - 4\, H_{i,j,k-1}) \end{aligned}\right\} \qquad (22)$$

where i,j is the integer address of a node in the x,y plane. The coefficient r is the same as in eqn.15 for the one-dimensional solution and contains the incremental permeability, which, if the Frohlich representation is being used, is given by eqns.16 and 18. However, we need to express H in eqn.16 in terms of the nodal values. Examining eqns.15 and 22 we see that they involve nodal values on three time levels (k-1,k, and k+1), and , if we view the space-time domain as a multi-dimensional chess board, the finite-difference equations separate into two sets, one associated with the white cubes and the other with the black. Thus, if we allow r to be expressed as a function of $H_{i,j,k}$ we are forcing a white value into the black set, or vice-versa. Such a mixture has been found to cause instability and it is therefore necessary for r to contain black (or white) values only. The unknown $H_{i,j,k+1}$ cannot appear in r because the finite-difference equation would no longer be linear in the unknown value, and therefore the average

$$H = \tfrac{1}{4} (H_{i-1,j,k} + H_{i,j-1,k} + H_{i,j+1,k} + H_{i+1,j,k}) \qquad (23)$$

is used in eqn.16.

If we now turn to a two-dimensional finite-difference scheme in terms of the vector potential component A_z, again taking a square mesh and constant conductivity, and assuming zero source current density for simplicity, eqn.10 reduces to the simple explicit form

$$\begin{aligned} A_{o,k+1} = \tfrac{1}{2}C \{&(\nu_{NE}+\nu_{SE})A_{1,k} + (\nu_{NE}+\nu_{NW})A_{2,k} \\ &+ (\nu_{NW}+\nu_{SW})A_{3,k} + (\nu_{SE}+\nu_{SW})A_{4,k}\} \\ &+ \{1-C\,(\nu_{NE}+\nu_{NW}+\nu_{SE}+\nu_{SW})\}A_{o,k} \end{aligned} \qquad (24)$$

where $C = \Delta t/\sigma h^2$. The DuFort-Frankel equation is obtained by replacing $A_{o,k}$ by $\tfrac{1}{2}(A_{o,k+1} + A_{o,k-1})$.

Whereas the incremental permeability in eqn.22 (in the coefficient r) is effectively a node centred value, the reluctivities in eqn.24 are cell centred (see Fig.1). For example, using eqn.17,

$$\nu_{NE} = \frac{a}{1-bB_{NE}}$$

where B_{NE} is the magnitude of the flux density in cell NE of Fig.1. Since $B_x = \partial A/\partial y$ and $B_y = -\partial A/\partial x$, the most obvious finite-difference expression for B_{NE} is given by

$$B_{NE} = (B_{xNE}^2 + B_{yNE}^2)^{\frac{1}{2}} = \left[\{\tfrac{1}{2}\left(\frac{A_{2,k}-A_{o,k}}{h_1} + \frac{A_{5,k}-A_{1,k}}{h_1}\right)\}^2 + \{\tfrac{1}{2}\left(\frac{A_{1,k}-A_{o,k}}{h_2} + \frac{A_{5,k}-A_{2,k}}{h_2}\right)\}^2\right]^{\frac{1}{2}} \qquad (25)$$

In the DuFort-Frankel equivalent of eqn.24 use of eqn.25 involves a mixture of black and white nodal values. However, in practice, this mixture appears weak enough to avoid instability if the scheme is used with care, particularly in the choice of h (typically 0.5mm).

3.5 Two-dimensional linear steady-state solutions

The complex equivalent of eqn.10 can be obtained by inspection. The set of finite-difference equations is now stationary in the sense that a single elimination process only is required. However, due to the sparsity of the coefficient matrix, iterative methods are usually preferable where each iteration can be thought of as a step forward in solution time. Indeed iterative methods have been found to converge faster for complex than for real arrays of the same size. Apart from the A D I method already mentioned which has been found suitable for problems involving several thousand equations, there is the simpler complex version of the well-known successive over-relaxation (SOR) method[20]. The only difficulty with SOR is the estimation of the complex accelerating factor[21].

A method of interest, proposed by Stone[22], is based on the realisation that the relatively good convergence of ADI methods is due to the component of direct elimination in the iterative process. Stone's strongly implicit iterative method (SIIM) has an increased implicit content and excellent convergence, but at the expense of a substantial increase in computer store requirement (about five times that for SOR). In a simple problem involving 600 internal nodes, SOR required 53 and SIIM 14 iterations, the latter being approximately 10 per cent faster in time[1]. However, as the number of nodes increases the time advantage of SIIM also increases.

REFERENCES

1. STOLL, R.L. : 'The analysis of eddy currents', Clarendon Press, Oxford, 1974, pp. 5, 99, 83, 112.
2. SARMA, M.S. : 'Potential functions in electromagnetic field problems', IEEE Trans. on magnetics, Vol. MAG-6, 1970,pp.513-18.
3. HAZNADAR, Z. and MATJAN, J. : 'Numerical solution of skin effect in systems of straight conductors, Elektrotehnika, Zagreb, Vol. 5, 1970.
4. SILVESTER, P. : 'Dynamic resistance and inductance of slot-embedded conductors', IEEE Trans. Power App. Syst., Vol.87, 1968, pp. 250-56.
5. CARPENTER, C.J. : 'Three-dimensional numerical solution of eddy-currents in thin plates', Proc. Instn. Elect. Engrs, Vol.122, 1975, pp.681-8.
6. CARPENTER, C.J. : 'Finite-element network models and their application to eddy-current problems', ibid. Vol.122, 1975, pp. 455-62.
7. HOCKNEY, R.W. : 'A fast direct solution of Poisson's equation using Fourier analysis, Journal of the Association for Computing Machinery, Vol.12, 1965, pp.95-113.
8. SILVESTER, P. : 'Eddy-current modes in linear solid iron bars', Proc. Instn. Elect. Engrs., Vol.112, 1965, pp.1589-94.
9. SILVESTER, P. : 'The accurate calculation of skin effect in conductors of complicated shape', IEEE Trans. Power App. Syst., Vol. PAS-87, 1968, pp.735-41.
10. SILVESTER, P. and CHARI, M.V.K. : 'Finite element solution of saturable magnetic field problems', ibid., Vol.89, 1970, pp. 1642-48.
11. FLATABO, N. : 'Transient Heat conduction problems in power cables solved by the finite element method', ibid., Vol.92, 1973, pp. 56-63.
12. CHARI, M.V.K. : 'Finite-element solution of the eddy-current problem in magnetic structures', ibid., Vol.93, 1974, pp.62-69.
13. DONEA, J., GIULIANI, S., and PHILIPPE, A. : 'Finite elements in the solution of electromagnetic induction problems', Int. Journal for numerical methods in Engineering, Vol.8, 1974, pp.359-67.
14. FOGGIA, A., SABONNADIERE, J.C. and SILVESTER, P. : 'Finite element solution of saturated travelling magnetic field problems', ibid., Vol.94, 1975, pp.866-71.
15. ROSENBERG, D.U. von : 'Methods for the numerical solution of partial differential equations', Elsevier, New York, 1969, pp.20, 57.
16. PEACEMAN, D.W. and RACHFORD, H.H. : 'The numerical solution of elliptic differential equations', J. Soc. ind. appl. math., Vol.3, 1955, pp. 28-41.
17. GOURLAY, A.R. : 'Hopscotch: a fast second-order partial differential equation solver', J. Inst. Math. Appl., Vol.6, 1970, pp. 375-90.
18. DUFORT, E.C. and FRANKEL, S.P. : 'Stability conditions in the numerical treatment of parabolic differential equations', Mathl. Tabl. Natn. Res. Coun., Wash., Vol . 7, 1953, pp. 135-52.
19. TRUTT, F.C., ERDELYI, E.A., and HOPKINS, R.E. : 'Representation of the magnetic characteristics of D.C. machines for computer use', IEEE Trans. Power App. Syst., Vol.87, 1968, pp.665-9.
20. AMES, W.F. : 'Numerical methods for partial differential equations' Nelson, 1969.
21. STOLL, R.L. : 'Solution of linear steady-state eddy-current problems by complex successive over-relaxation', Proc. Instn. Elect. Engrs, Vol. 117, 1970, pp. 1317-23.
22. STONE, H.L. : 'Iterative solution of implicit approximations of multidimensional differential equations', SIAM J. Numer. Anal., Vol.5, 1968, pp. 530-58.
23. ZAKRZEWSKI, K. and PIETRAS, F. : 'Method of calculating the electromagnetic field and power losses in ferromagnetic materials, taking into account magnetic hysteresis', Proc. Instn. Elect. Engrs., Vol. 118, 1971, pp.1679-85.
24. MUHLHAUS, J. : 'On the solution of 2-dimensional saturable eddy-current problems by the ADI technique', ibid. Vol. 123, 1976, pp.183-6.
25. LIM, K.K., and HAMMOND, P. : 'Numerical method for determining the electromagnetic field in saturated steel plates', ibid., Vol.119, 1972, pp.1667-74.

Discussion following paper:

(Munro, IBM) 1. The method which you described for generating the finite difference equations was for rectangular meshes. Is this method also applicable to general quadrilateral meshes which are not necessarily parallel to the coordinate axes?

2. Can you comment on the speed of convergence of the ADI method for problems in which there are large changes in material properties (eg permeability) within the solution region?

(R Stoll) In reply to Dr Munro's first question, the method I describe for setting up a finite-difference equation in 2 dimensions using surface integration and Stokes' theroem can be applied in 3 dimensions and other coordinate systems. However, the 'box' used should conform to the coordinate systems selected.

In the second case, I have not used the ADI method sufficiently to be able to give a firm answer, but I suspect ADI will suffer in the same way as other iterative schemes in static or steady-state problems, although probably rather less so in view of the direct component of the method.

(Miller, University of Leeds) I would like to comment briefly on Mr Munro's question. The integration method described by Dr Stoll for discretising the differential equation can indeed be used for irregular polygonal meshes.

It has been claimed that discretisation by the integration method automatically gives properties to the coefficient matrix of the linear equations which guarantee convergence in iterative solution. Certainly this appears to be in tune with 2-D problems but at Leeds we have had the difficulty that these properties (in particular, diagonal dominance) appear to be lost when going to 3-D problems.

Refs Bronne, B T Ph D Thesis Leeds University
Varga, Matrix Iterative Analysis

(Schomberg, Philips GmbH) You mentioned the Hopscotch method, where one has "white" and "black" mesh points arranged in such a way that the white mesh points are surrounded by black ones and vice versa, and where one updates the corresponding "white" and "black" potentials alternatively. There seems tobe a strong resemblance to the SOR method with "white-black" (or "odd-even") ordering of the mesh points, which is applicable to elliptic finite difference equations. Could you comment on this?

(Stoll,) Although Hopscotch is primarily designed for use with parabolic equations, the question concerns its use for stationary problems, ie as on iterative method. It can be shown to be equivalent to the Gauss-Seidel and SOR methods with odd-even ordering of the nodes.

The Prediction of Machine End-region Fluxes, allowing for Eddy Current Losses in Thick Components

by

T.W. Preston, A.B.J. Reece

1. Introduction

As unit ratings of turbine-generators increase, it is becoming essential to make accurate prediction of flux distribution, and associated induced losses in the machine end-zone, so that the risk of damage from overheating of components can be avoided.

Prediction of end-region leakage fields, allowing for irregular boundaries and internal components, such as the screen and clamping plate, can only be carried out numerically. The work described in Ref. (1) outlines a finite-element method for determining the scalar potential distribution in the end-region: scalar potential was used because it allows simple treatment of boundaries, and, compared with vector potential, only a single function has to be calculated. Economy of nodes was obtained by assuming that all end-zone functions vary sinusoidally around the periphery, thereby reducing the problem to one in the radial-axial plane only, whilst still retaining the essential 3-dimensional geometry of the end-region. In this way, the complex boundary outline can be represented adequately, but the magnetic effect of the boundary can only be represented by either an infinitely-permeable surface (the Dirichlet condition) or an infinitely-conducting surface (the Neumann condition).

The infinitely-conducting boundary condition has often been used to allow for eddy current effects in conducting boundaries, by setting a surface which has wholly tangential flux at a depth related to the skin depth below the real surface. This treatment is very approximate, and falls down badly when dealing with a highly permeable conducting surface, since no allowance can be made for the high permeability within the skin depth. A fully 3-dimensional vector potential approach would overcome this difficulty, but it would prove expensive to use, as three solutions would be required to obtain all flux densities, and boundary conditions could prove awkward. Although scalar potential is not normally used in problems involving eddy currents, the following sections show that the use of complex potential with a new boundary condition which allows for frequency, permeability and resistivity to represent "thick" components can give excellent results.

2. Development of Boundary Condition

The effect of induced currents beneath the surface of a conducting surface is dealt with by relating the flux distribution beneath the surface to the density normal to the surface. In the formulation of the boundary condition, the following assumptions are made:-

(i) The thickness of the conductor is greater than the depth of penetration.

(ii) Flux flows entirely parallel to the surface once inside the member.

(iii) Flux decays exponentially with depth, as in 1-dimensional theory.

The flux entering normal to the surface of a conducting member can be equated to the integrated value of the tangential flux from the surface to an infinite depth. Fig. 1 shows a tiny element of the conducting member, and by consideration of flux entering and leaving the element, the following equations are derived:-

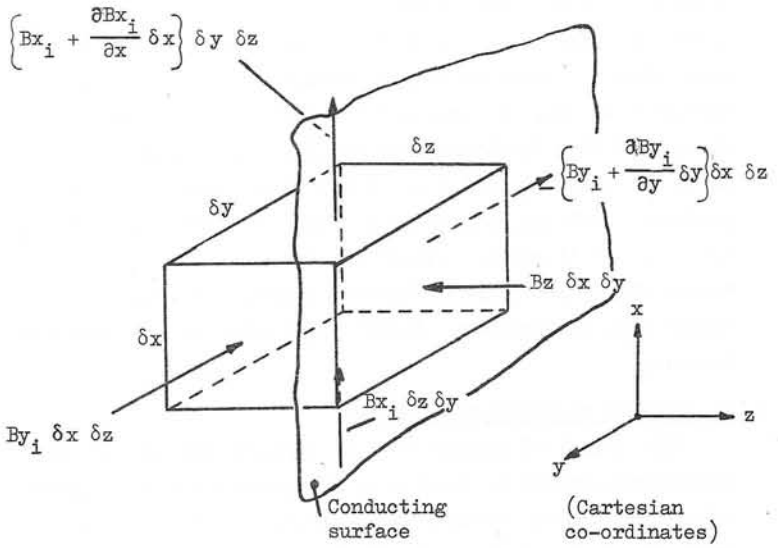

Fig. 1

Therefore, equating fluxes:

$$Bz\ \delta y\ \delta x = \int_0^\infty \frac{\partial By_i}{\partial y}\ \delta x\ \delta y\ dz + \int_0^\infty \frac{\partial Bx_i}{\partial x}\ \delta x\ \delta y\ dz$$

which, with Assumption (iii) and the continuity conditions at the interfaces, reduces to:

$$Bz_{(air)} = \frac{\mu_i(1 - j)\delta}{2}\left\{\frac{\partial By_{(air)}}{\partial y} + \frac{\partial Bx_{(air)}}{\partial x}\right\} \quad \ldots\ldots (1)$$

where: μ_i = relative permeability of conducting member

$\delta = \left\{\frac{2\rho}{\mu_o \mu_i \omega}\right\}^{\frac{1}{2}}$

ρ = resistivity

ω = angular frequency

Thus the effect of induced currents beneath a surface can be represented by a boundary condition at the surface.

3. Analytic Check

To check the validity of the assumptions made in formulating the boundary condition, the expression for flux density in a machine gap (obtained by using the derivative boundary condition) was compared with the exact analytical solution.

(i) Exact solution

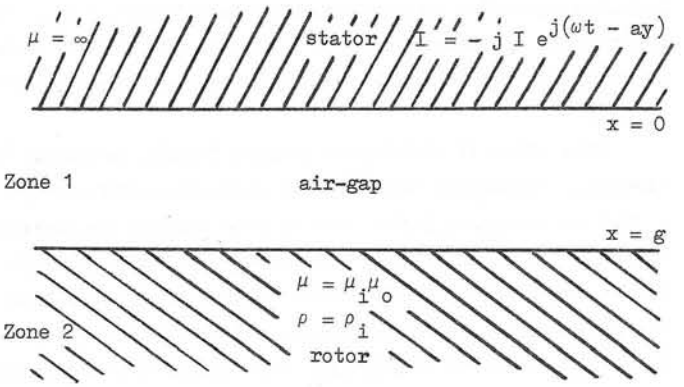

Fig. 2

Fig. 2 shows the air-gap and rotor iron in a Cartesian co-ordinate system, and the resulting equation for flux density in Zone 1 is:

$$Bx = \frac{\mu_o I\left\{\cosh a(x - g) - \frac{c}{a\ \mu_i}\sinh a(x - g)\right\}}{\sinh ag + \frac{c}{a\ \mu_i}\cosh ag} \quad \ldots\ldots (2)$$

where: $c^2 = a^2 + j\ \omega\ b^2$

$a = 2\pi/T$

$b^2 = \mu_o \mu_i / \rho_i = 2/\delta^2 \omega$

$\delta = (2\ \rho_i / \mu_o \mu_i\ \omega)^{\frac{1}{2}}$

T = double pole pitch

(ii) Boundary solution

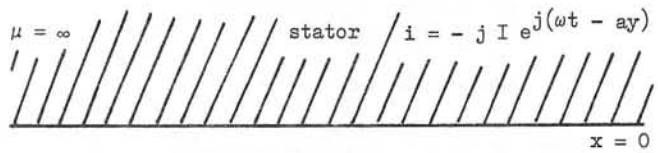

$$Bx = \frac{(1 - j)}{2} \delta \mu_i \frac{\partial By}{\partial y}$$

Fig. 3

Fig. 3 illustrates the same example, treated as a single-zone problem, with the boundary condition given by Eqn. (1) representing the rotor. The resulting equation for the air-gap density is:

$$Bx = \frac{j \mu_o I\left\{\cosh a(x - g) - \frac{(1 + j)}{a \delta \mu_i} \sinh a(x - g)\right\}}{\sinh ag + \frac{(1 + j)}{a \delta \mu_i} \cosh ag} \quad \ldots\ldots (3)$$

Eqns. (2) and (3) differ only in the coefficients of the $\sinh a(x - g)$ and $\cosh ag$ terms, and if a^2 is negligibly small compared with the ωb^2 term, the equations become identical: this requires δ/T to be small.

In order to establish a value of δ/T which will give acceptable accuracy, calculations were made on the problem illustrated in Fig. 2, with the permeability of the rotor iron varied from 1-1,000 (this gives a variation of δ/T of about 30:1).

The results of these calculations are given in Fig. 4, and show that there is little error introduced in the real component of Bx over the whole range, but the error in the imaginary component becomes significant for $\mu_i < 10$: this corresponds to a δ/T ratio of 0.09. Thus, if the δ/T ratio is less than about 0.09, the error resulting from the use of the boundary method should be insignificant. Typically, the δ/T ratio for the screen of a turbine-generator is 0.0018.

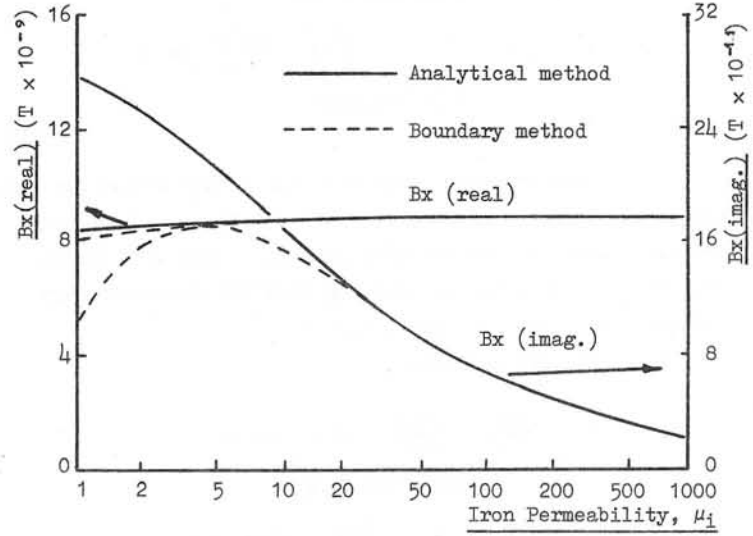

Fig. 4

4. Finite-element Representation of the Boundary Condition

In Ref. (1), a conducting boundary was considered as infinitely-conducting, i.e there was no allowance for flux penetration into the conducting boundary. The new boundary condition, which allows for flux penetration, can be written in scalar potential form by re-arranging Eqn. (1) as:

$$\frac{\partial U}{\partial z} = \frac{(1 - j)}{2} \delta \mu_i \left\{\frac{\partial^2 U}{\partial y^2} + \frac{\partial^2 U}{\partial x^2}\right\} \quad \ldots\ldots (4)$$

To enable this type of boundary to be represented in finite-element terms requires Eqn. (4) to be re-formulated in variational form and added to the existing functional. The basis of the method is outlined in Ref. (2), and when applied to the present problem results in the following functional:-

$$X = \tfrac{1}{2}\iiint_V \left\{\left(\frac{\partial U}{\partial x}\right)^2 + \left(\frac{\partial U}{\partial y}\right)^2 + \left(\frac{\partial U}{\partial z}\right)^2\right\} dx\, dy\, dz$$

end-region term

$$- \frac{(1-j)}{2}\,\delta\,\mu_i \iint_S \left\{\left(\frac{\partial U}{\partial x}\right)^2 + \left(\frac{\partial U}{\partial y}\right)^2\right\} dx\, dy$$

boundary term

..... (5)

The volume integral relates to the volume within the end-region, whereas the surface integral relates only to those boundary surfaces carrying eddy currents. Eqn. (5) can be reduced by a dimension by assuming that all functions vary sinusoidally around the periphery.

Thus Eqn. (5) becomes:

$$X = \tfrac{1}{2}\iint \left\{\left(\frac{\partial U}{\partial x}\right)^2 + \left(\frac{\partial U}{\partial z}\right)^2 + a^2U^2\right\} dx\, dz$$

end-region term

$$- \frac{(1-j)}{2}\,\mu_i\,\frac{\delta}{2}\int \left\{\left(\frac{\partial U}{\partial z}\right)^2 + a^2U^2\right\} dx$$

boundary term

..... (6)

The above functional is extremised by differentiating with respect to the unknown potential, U, and equating to zero, i.e.

$$\frac{\partial X}{\partial U} = 0 \qquad \text{..... (7)}$$

The numerical form of Eqn. (7) is obtained, as described in Ref. (1), by representing the area within the end-region term (Eqn. (6)) by triangular elements, but the boundary term is given by a line integral only, and thus has to be represented by a "line" or "bar" element, as shown in Fig. 5:

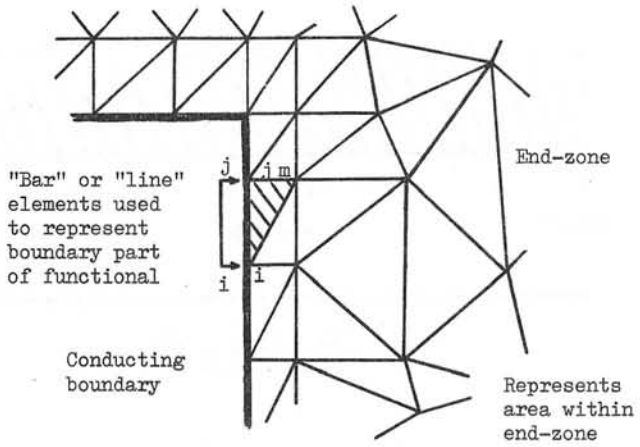

Fig. 5

As with the triangular element, the "bar" element can be represented in numerical form by assuming the potential varies linearly between the nodes. This leads to the following expression, which is added to the extremised functional only for nodes on conducting boundaries:-

$$\frac{\partial X_{(\text{boundary})}}{\partial U_i} = \frac{(1-j)}{12l}\,\delta\,\mu_i \times \{(6 + 2a^2l^2)U_i + (-6 + a^2l^2)U_j\}$$

where l = length of "bar" element

The validity of the bar element representation of conducting boundaries was checked by calculating the scalar potential within the air-gap of a turbine-generator for which an analytical solution was available. Several solutions were obtained for various values of pole-pitch, permeability and resistivity. Figs. 6-7 show that the bar element representation agrees well with the analytical solution, and better than the extreme boundary conditions previously used.

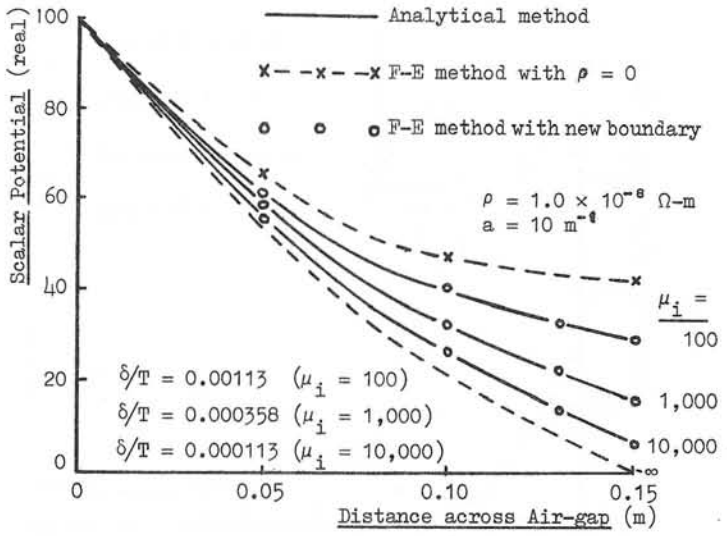
Analytical method
F-E method with ρ = 0
F-E method with new boundary
ρ = 1.0 × 10⁻⁸ Ω-m
a = 10 m⁻¹
μi =
100
1,000
10,000
∞
δ/T = 0.00113 (μi = 100)
δ/T = 0.000358 (μi = 1,000)
δ/T = 0.000113 (μi = 10,000)
Scalar Potential (real)
Distance across Air-gap (m)
0
20
40
60
80
100
0.05
0.10
0.15

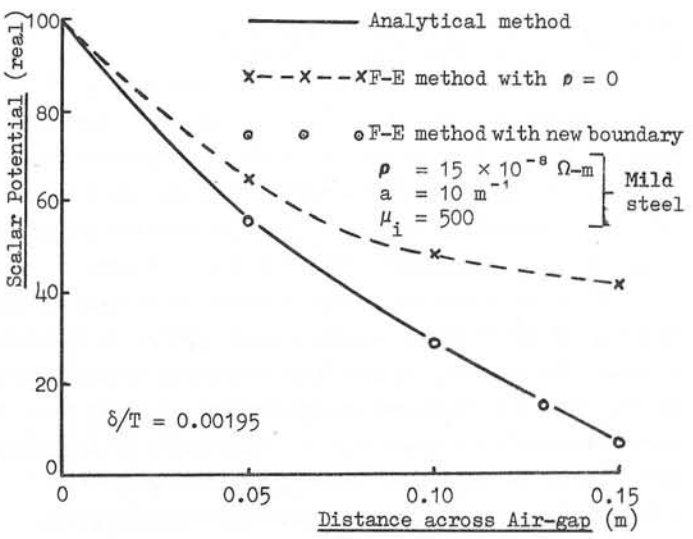
Analytical method
F-E method with ρ = 0
F-E method with new boundary
ρ = 15 × 10⁻⁸ Ω-m
a = 10 m⁻¹
μi = 500
Mild steel
δ/T = 0.00195
Scalar Potential (real)
Distance across Air-gap (m)
0
20
40
60
80
100
0.05
0.10
0.15

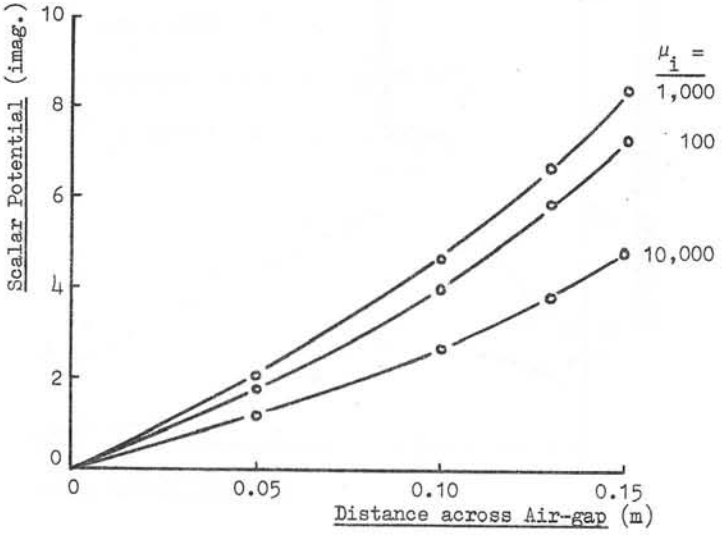
μi =
1,000
100
10,000
Scalar Potential (imag.)
Distance across Air-gap (m)
0
2
4
6
8
10
0.05
0.10
0.15

Fig. 6

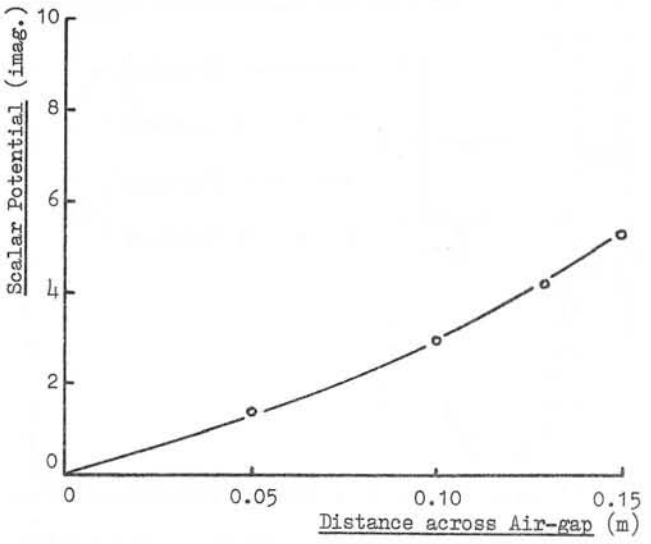
Scalar Potential (imag.)
Distance across Air-gap (m)
0
2
4
6
8
10
0.05
0.10
0.15

Fig. 7

5. Application of New Boundary Approach to a 660 MW Turbine-generator End-region

Recently the stator-core and end-region of a 660 MW turbine-generator was extensively instrumented, and all components of flux density near the screen surface and (where possible) the clamping plate surface were measured under open- and short-circuit excitations. Loss intensities around the screen were also measured, using the $\partial\theta/\partial t$ method.

These measurements enabled a check to be made on the validity of the boundary approach when applied to an actual machine. To do this, it was first necessary to re-formulate all the previous equations in cylindrical co-ordinates. With these re-formulated equations, all components of flux density were calculated within the end-region, with particular attention being given to the screen and clamping plate surfaces. Figs. 8-10 compare the numerical and measured values of flux density near the screen surface for open- and short-circuit excitations. In all cases the agreement is good. Similarly, Figs. 11-12 compare the surface loss intensity around the screen for open- and short-circuit excitations respectively.

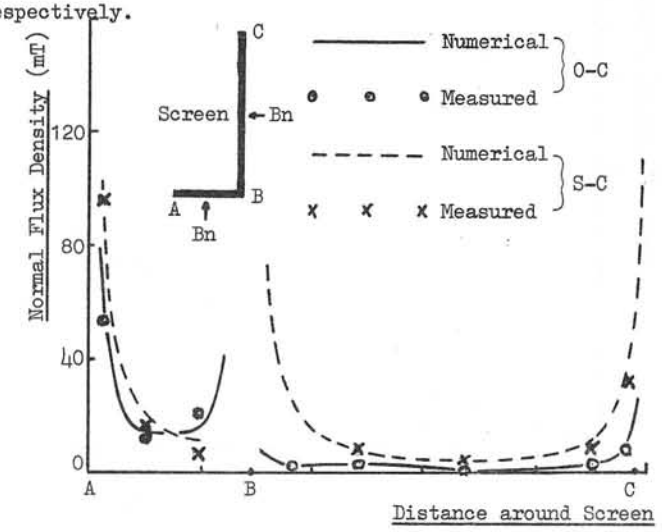

Fig. 8

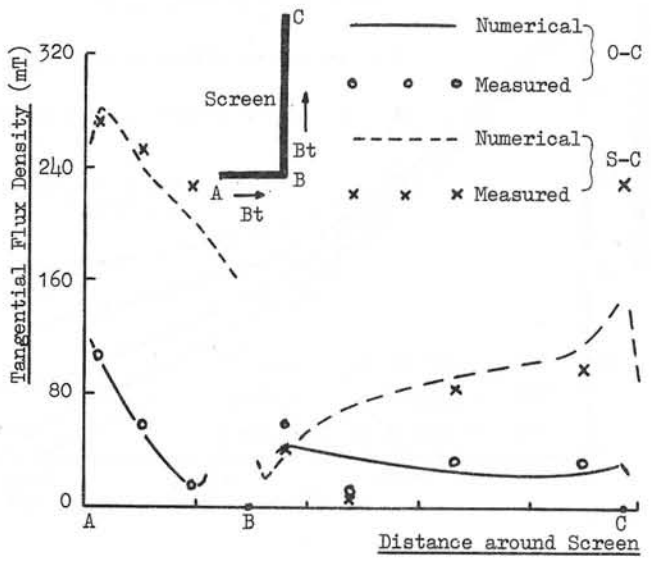

Fig. 9

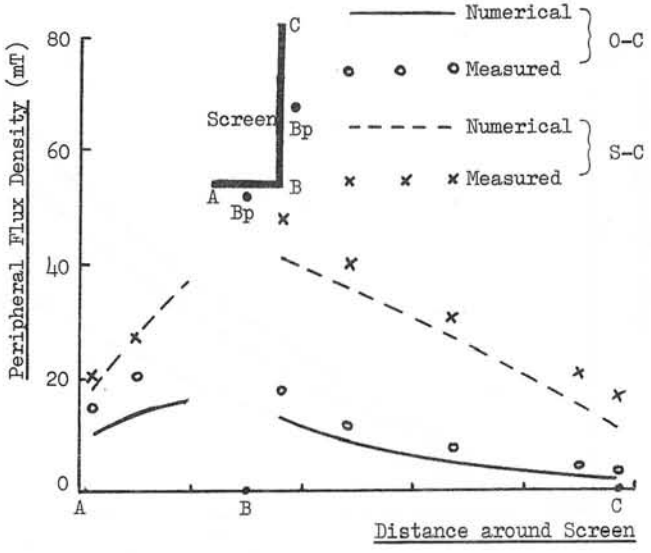

Fig. 10

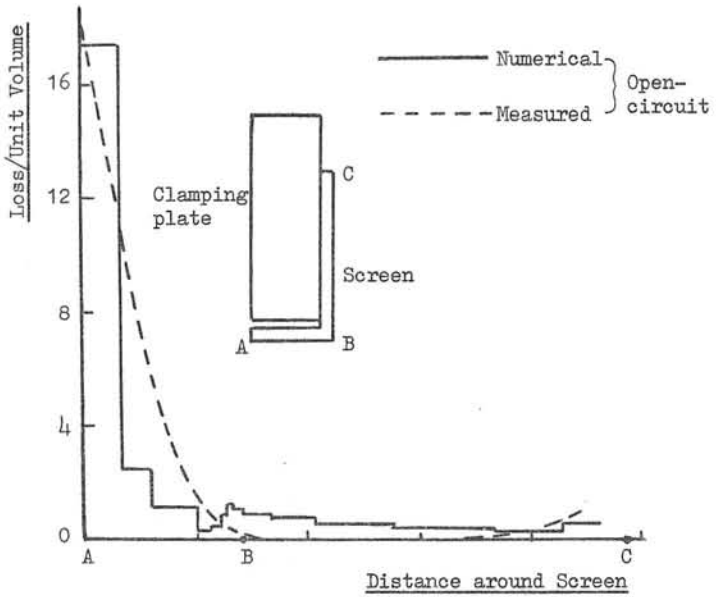

Fig. 11

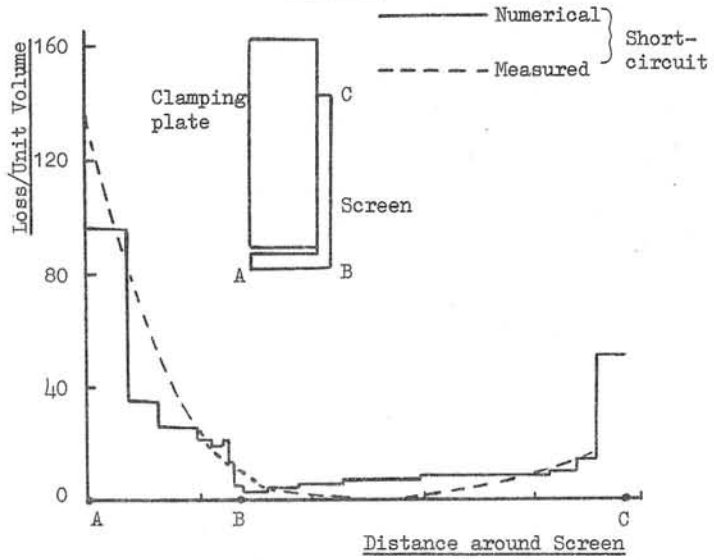

Fig. 12

From Figs. 8-11 it is evident that the new boundary method gives very satisfactory agreement with measurements.

The advantage of the boundary approach is its ability to represent the effect of induced currents in "thick" conducting members, without having to arbitrarily position the boundary surface below the physical surface, as was done in the earlier treatment of conducting boundaries. Also, the magnetic property of the member is more accurately represented.

6. Conclusions

A method has been developed in which the effect of induced currents in conducting magnetic members can be represented in terms of the normal derivative of scalar potential. It has been shown to give reasonable accuracy for various test cases, providing the δ/T ratio is smaller than about 0.09, and when applied to a specially instrumented 660 MW generator gave results in good agreement with the measured values of flux density and loss intensity.

References

(1) Preston, T.W.,
"The prediction of turbine-generator end-winding fields",
Universities Power Engineering Conference - 1975:
The University of Aston in Birmingham.

(2) Berg, B.W.,
"Calculus of variations",
Chapter 16 - 'Handbook of Engineering Mechanics',
W.Flügge, McGraw-Hill.

This work was carried out in the Stafford Laboratory of G.E.C. Power Engineering Ltd. with the support of the C.E.G.B.

Discussions following paper:

(Miller) The paper raises the question, under what conditions can the surface of a magnetic material be represented by a 'zero-permeability' boundary condition, established by the reaction of eddy currents? There is evidence that under certain conditions, for example, when the magnetic 'circuit' is mainly in air, the classical skin-depth parameter $\delta = \nu(p/\omega\mu)$ is less significant than the product $\mu_r\delta$ (μr = relative permeability), in the sense that the criterion $h/\mu r\delta > 1$ implies 'zero permeability' or inductance - limited eddy current reaction field. (h is a characteristic dimension of the conducting material). It has been found both theoritically and experimentally* that the criterion $h/\mu r\delta > 1$ gives a reliable indication of 'inductance limited' eddy currents in the particular application of finding underground insulated pipes inductively.

* Glennie E B and Miller T J E 'Inductive detection of Buried Metallic pipes' Proc. IEE May 1975.

(Preston, GEC Stafford) I thank Mr Miller for his remarks on the representation of a magnetic boundary by a zero permeability surface. If reference is made to Fig (6) in the paper it is clearly shown that the more permeable the surface becomes the larger is the error introduced by the use of a zero permeability boundary. Thus for magnetic materials the $\mu r\delta$ product is a better criterion than δ in accessing the suitability of the zero permeability boundary condition.

Semi-analytical Computation of Magnetic Fields, Eddy Currents and Forces in Electrodynamic Levitation Systems

by

E.-D. Krause and L. Urankar

Siemens AG, Erlangen (W. Germany)

1. Introduction

In the last few years various magnet and track configurations have been proposed for magnetically levitated high-speed vehicles for future transport systems. The basic principles of all such arrangements fall into two categories (Figure 1):

Attractive (Ferromagnetic) Principle and
Repulsive (Inductive) Principle.

In systems using the first, attractive forces between magnets mounted on the vehicle and a ferromagnetic track (solid or laminated) produce levitation.

Systems using the repulsive principle depend upon Lenz's law, which implies that a magnetic field generated by induced currents opposes the primary field.

Two essentially different basic classes of track configurations have been suggested for systems of the second category. One uses metallic loops, the other compact metallic sheets.

Among the magnet arrangements there are again two classes: single magnet and double magnet, respectively. The single magnet class consists of a magnet on the vehicle which moves above a metallic track. Such a system is called the normal flux system. The other system comprises two magnets between which the track is located. The polarity of the magnets, i.e. the direction of the energising currents is such that the fields tend to cancel each other (null flux system) or such that the fields add up (brake flux system).

All these basic systems may be used either for lift of guidance alone or for both lift and guidance together.

In order to simplify the mathematical formulation of the problem, we restrict ourselves to the electromagnetic aspect only and to basic systems with infinite sheet track of arbitrary thickness. Then the basic systems between the dotted lines in Figure 1 can be treated mathematically together as a boundary value problem for magnetic fields. The geometrical arrangement for a theoretical analysis is shown in Figure 2. An infinite metallic sheet of arbitrary thickness d, conductivity σ_S and permeability μ_S is situated between two excitation current systems which are mounted on the moving vehicle in a distance $2\,h_0$ apart and which consist of plane magnet coils of arbitrary form. The midplane of the sheet corresponds to the z=0 plane of the coordinate system which is assumed to be moving with the coils. The excitation systems denoted by j=1 above and 2 below are in parallel planes at distances h_j from the sheet track surfaces, move with a constant velocity in any direction and carry currents, the number of ampere turns being I_j.

A general velocity vector in any direction has been introduced in the model so that intrinsic damping in the levitation systems can be analysed. But the lateral and vertical components of the velocity are assumed to be small compared with the forward velocity, say in the x-direction.

2. Basic Equations

In the following analysis we assume the excitation system to be stationary, so that the sheet track moves with a velocity $\underline{v}$ in the opposite direction. The electric and magnetic fields in the moving sheet track are obtained through Lorentz transformation. Since the track is a good electrical conductor, the displacement current is zero and hence the magnetic field at any fixed point in the moving track is equal to that in the stationary one.

The eddy current in the track is

$$\mu_S \underline{J}^{(S)} = \mu_S \sigma_S \underline{E} + (\underline{\lambda} \times \underline{B}^{(i)}) \qquad (1)$$

where $\underline{\lambda} = \mu_S \sigma_S \underline{v}$ and $\underline{B}^{(i)} = \underline{B}^{(S)} + \underline{B}^{(E)}$ i.e. the total magnetic flux density in the track is the sum of magnetic flux densities due to the eddy current and excitation current, respectively.

Since now $\mu_S \underline{J}^{(S)} = \nabla \times \underline{B}^{(S)}$, we obtain from (1) after taking the rotation and noting that $\nabla \cdot \underline{B} = 0$ and $\nabla \times \underline{E} = 0$, the differential relation

$$\nabla^2 \underline{B}^{(S)} = (\underline{\lambda} \cdot \nabla)\, \underline{B}^{(i)} \qquad (2)$$

Inside the track sheet the excitation magnetic flux density satisfies $\nabla^2 \underline{B}^{(E)} = 0$, so that (2) reduces to the following Maxwell-Minkowski wave equation for the magnetic flux density in the track

$$\nabla^2 \underline{B}^{(i)} - (\underline{\Lambda} \cdot \nabla)\, \underline{B}^{(i)} = 0 \qquad (3)$$

Outside the sheet track we have to solve

$$\nabla^2 \underline{B}^{(e)} = 0 \qquad (4)$$

Both the exterior and interior flux densities, $\underline{B}^{(e)}$ and $\underline{B}^{(i)}$, are divergence free and are interconnected through the following boundary conditions

$$\underline{n} \cdot \underline{B}^{(i)} = \underline{n} \cdot \underline{B}^{(e)} \qquad (5a)$$

$$\underline{t} \cdot \underline{B}^{(i)} = \mu_r\, (\underline{t} \cdot \underline{B}^{(e)}) \qquad (\mu_r = \mu_S/\mu_0) \qquad (5b)$$

where $\underline{n}$ and $\underline{t}$ are outward normal and tangent unit vectors, respectively, at any arbitrary point on the sheet track surface.

3. Analytical Part of the Method

The central point of the method is a two-dimensional infinite Fourier transform defined by

$$\underline{B}(\underline{k};z) = \frac{1}{4\pi^2} \int_{-\infty}^{+\infty} dx \int_{-\infty}^{+\infty} dy\; e^{-ik_x x}\, e^{-ik_y y}\, \underline{B}\,(\underline{r}) \qquad (6a)$$

(where $\underline{k} = (k_x, k_y)$ and $\underline{r} = (x,y,z)$) and its inverse

$$\begin{aligned} \underline{B}(\underline{r}) &= \mathrm{Re} \int_{-\infty}^{+\infty} dk_x \int_{-\infty}^{+\infty} dk_y\; e^{+ik_x x}\, e^{+ik_y y}\, \underline{B}(\underline{k};z) \\ &= \mathrm{Re} \int_{-\infty}^{+\infty} dk_x \int_{-\infty}^{+\infty} dk_y\; \underline{B}(\underline{k};\underline{r}) \end{aligned} \qquad (6b)$$

The functions $\underline{B}(\underline{k};\underline{r})$ are then taken to be the Fourier components of the magnetic flux densities constituting the solutions of the equations (3), (4) and the boundary conditions (5a, b).

3.1. Ansatz for Solutions

In order to solve the boundary value problem we now make, similar to [1], following Ansatz for the solutions $\underline{B}(\underline{k};\underline{r})$ in regions 1, 2 and 3 (s. Figure 2).

Regions 1 and 2:

$$\begin{aligned} B_p^{(ej)} &= B_p^{(Ej)}(\underline{k};\underline{r}) + \tilde{B}_p^{(j)}(\underline{k};\underline{r}) \\ &= \left[B_p^{(Ej)}(\underline{k};z) + a_p^{(j)}(\underline{k})\, e^{\mp kz}\right] e^{ik_x x} \begin{Bmatrix} \cos(k_y y) \\ \sin(k_y y) \\ \cos(k_y y) \end{Bmatrix} \quad (p=x,y,z) \end{aligned} \qquad (7)$$

where $k = (k_x^2 + k_y^2)^{1/2}$ and the column term corresponds, from the top, to the components $p = x,y,z$. $\underline{B}^{(Ej)}$ is the excitation field of the excitation coil j in region j and thus $\tilde{\underline{B}}^{(1)}$ ($\tilde{\underline{B}}^{(2)}$) corresponds to the contribution from the field components in the upper (lower) region due to the eddy current in the track sheet and the lower (upper) excitation coil. The upper sign corresponds to j=1 while the lower one to j=2.

Region 3:

$$B_p^{(i)} = \left[b_p(\underline{k})\, e^{\alpha z} + c_p(\underline{k})\, e^{-\alpha z}\right] e^{ik_x x} \begin{Bmatrix} \cos(k_y y) \\ \sin(k_y y) \\ \cos(k_y y) \end{Bmatrix} \quad (p=x,y,z) \qquad (8)$$

The subsidiary condition $(\nabla \times \underline{B})_z = 0$ (which is not a real restriction in the infinite sheet model because of the natural boundary conditions at infinity) allows us to determine the Fourier coefficients in the Ansatz uniquely for each (k_x,k_y)-pair.

3.2. Eddy Current and Force Expressions

The forces between the track sheet and the excitation current system can be calculated in two different ways.

I. The eddy current density in the track sheet is given by

$$\underline{J}^{(S)} = \frac{1}{\mu_S} (\nabla \times \underline{B}^{(i)}) \qquad (9)$$

Substituting the inverse transform of (8) in this expression, we get the Fourier representation of the eddy current density.

With the help of the inverse transform of the excitation field the force density $\underline{P}$ on the track sheet can now be calculated as

$$\underline{P}(\underline{r}) = \underline{J}^{(S)}(\underline{r}) \times \underline{B}^{(E)}(\underline{r}) \qquad (10)$$

where $\underline{B}^{(E)} = \underline{B}^{(E1)} + \underline{B}^{(E2)}$. Integrating over the volume of the sheet track we obtain the global force between the track and the excitation system

$$\underline{F} = \iiint_{R_S} dx\, dy\, dz\; \underline{P}(x,y,z) \qquad (11)$$

This approach is used when the spatial distribution of the eddy current and force components in the track are needed. This is the case during mechanical outlay of the track system.

II. If, on the contrary, only global forces are to be calculated, the expression

$$\underline{F} = \iiint_{R_E} dx\, dy\, dz \left[\underline{J}^{(E)} \times (\underline{B}^{(e)} - \underline{B}^{(E)})\right]$$

is much more convenient to use. With the help of (7), this then reduces to

$$\underline{F} = \sum_{j=1}^{2} \iiint_{R_{Ej}} dx\, dy\, dz \left[\underline{J}^{(Ej)} \times \underline{\tilde{B}}^{(j)}\right] \qquad (12)$$

which is physically equivalent to (11), as action and reaction are equal and opposite.

For sufficiently simple systems, the volume integral in (12) can be performed before calculating the inverse Fourier transform. In this case (12) can be expressed as

$$\underline{F} = \int_{-\infty}^{+\infty} dk_x \int_{-\infty}^{+\infty} dk_y\, \underline{f}\,(\underline{k};\, B_x^{(E1)}(\underline{k};d/2),\, B_x^{(E2)}(\underline{k};-d/2)) \qquad (13)$$

where $B_x^{(E1)}(\underline{k};d/2)$ and $B_x^{(E2)}(\underline{k};-d/2)$ are Fourier transforms of the x-components of the excitation field at the upper and lower track sheet surfaces, respectively.

4. Numerical Part of the Method

Now we discuss the numerical computations of eddy current and force densities as well as the global force. The former shall be dealt with fast Fourier transform, the latter by means of numerical quadrature. Finally, we compare both methods from the standpoint of computation time and efficiency.

4.1. Fast Fourier Transform (FFT)

To calculate the eddy current and force densities in the track it is necessary to compute several integrals of the type

$$\left.\begin{matrix} A^{(cos)}(x,y) \\ A^{(sin)}(x,y) \end{matrix}\right\} = \int_{-\infty}^{+\infty} dk_x \int_{-\infty}^{+\infty} dk_y\, e^{ik_x x} \left\{\begin{matrix} \cos(k_y y) \\ \sin(k_y y) \end{matrix}\right\} A(k_x,k_y) \qquad \begin{matrix} (14a) \\ (14b) \end{matrix}$$

Introducing the total inverse Fourier transform $A^{(tot)}(x,y)$, we obtain

$$A^{(cos)}(x,y) = \frac{1}{2}\left[A^{(tot)}(x,y) + A^{(tot)}(x,-y)\right] \qquad (15a)$$

$$A^{(sin)}(x,y) = -\frac{i}{2}\left[A^{(tot)}(x,y) - A^{(tot)}(x,-y)\right] \qquad (15b)$$

We now choose two even numbers n_1 and n_2, and calculate the integral (14) on a net of $n_1 \cdot n_2$ equidistant points ordered symmetrically about the origin:

$$x_{l_1} = \Delta x \cdot (l_1 - 1 - n_1/2)$$

$$y_{l_2} = \Delta y \cdot (l_2 - 1 - n_2/2)$$

For each (x,y)-pair we integrate in k-space by applying the trapezoidal rule to a similar net of $n_1 \cdot n_2$ equidistant points:

$$k_{x,j_1} = \Delta k_x \cdot (j_1 - 1 - n_1/2)$$

$$k_{y,j_2} = \Delta k_y \cdot (j_2 - 1 - n_2/2)$$

$$A^{(tot)}(x_{l_1},y_{l_2}) = \Delta k_x\, \Delta k_y \sum_{j_1=1}^{n_1} \sum_{j_2=1}^{n_2} W_{j_1,j_2}\, e^{i(k_{x,j_1}\cdot x_{l_1} + k_{y,j_2}\cdot y_{l_2})} \cdot A(k_{x,j_1},k_{y,j_2}) \qquad (16)$$

$(l_1 = 1,\ldots,n_1;\ l_2 = 1,\ldots,n_2)$

Herein W_{j_1,j_2} are weight factors of the trapezoidal rule (1, 1/2 or 1/4).

The $n_1 \cdot n_2$ double sums (16) can be evaluated most effectively in the formalism of fast Fourier transform (FFT) which is applicable under following conditions

$$\Delta x \cdot \Delta k_x = 2\pi/n_1\,, \quad \Delta y \cdot \Delta k_y = 2\pi/n_2$$

If, in addition, the numbers n_1 and n_2 are powers of two, the computation time is minimum and (16) takes the form

$$A^{(tot)}(x_{l_1},y_{l_2}) = (-1)^{l_1+l_2}\, \Delta k_x\, \Delta k_y \sum_{j_1=1}^{n_1} \sum_{j_2=1}^{n_2} (-1)^{j_1+j_2}\, W_{j_1,j_2} \cdot A(k_{x,j_1},k_{y,j_2}) \cdot \exp\left\{2\pi i\left[(j_1-1)(l_1-1)/n_1 + (j_2-1)(l_2-1)/n_2\right]\right\} \qquad (17)$$

4.2. Numerical Quadrature

The double integral (13) for the global force is not in the form of an inverse Fourier transform. Figure 3 shows the structure of one such typical integrand which must be computed by means of numerical quadrature.

For this purpose the first quadrant in the k_y-direction is separated into different strips of width $2\Delta k_y$ as shown in Figure 4. In each strip the step length for k_x-integration is adjusted to the structure of the integrand. The starting step length $\Delta k^{(a)}$ is chosen same for both the coordinates in such a way that for the oscillating function of the highest frequency occuring in the

integrand there are at least 3 integration nodes in a quarter period. Each strip is divided into rectangles of size $4\Delta k_x \cdot 2\Delta k_y$. For an integral over such a rectangle two approximate values are determined from integrals over elementary rectangles (denoted by the subscript erec) according to product Simpson's rule (s. Figure 4).

$$F_{rec}^{(coarse)} = F_{erec}(2\Delta k_x)$$

$$F_{rec}^{(fine)} = F_{erec}^{(l)}(\Delta k_x) + F_{erec}^{(r)}(\Delta k_x)$$

The integrals $F_{rec}^{(fine)}$ over each rectangle are then summed to give the strip integral F_{str}; the strip integrals in turn are summed to give the total integral F_{tot}. Integration over all the 4 quadrants is performed by taking together in each integral F_{erec} the integrals over the mirror elementary rectangles I-IV.

The k_x-step length is controlled with the help of both the approximate values $F_{rec}^{(fine)}$ and $F_{rec}^{(coarse)}$. Let

$$\Delta F_{rec} = F_{rec}^{(fine)} - F_{rec}^{(coarse)}$$

and

$$F_{temp} = F_{tot} + F_{str} + F_{rec}^{(fine)}$$

where F_{temp} is the temporary value of the total integral. We also introduce 3 accuracy parameters ε_1, ε_2 and ε_3 satisfying $\varepsilon_1 < \varepsilon_2 < \varepsilon_3$. Then, if $|\Delta F_{rec}| < \varepsilon_1 |F_{temp}|$, the step length Δk_x is doubled; if $|\Delta F_{rec}| > \varepsilon_3 |F_{temp}|$, then Δk_x is halved; in all other cases it remains unchanged.

The integration in a strip stops when

$$|F_{rec}^{(fine)}| \leq \varepsilon_2 |F_{temp}|$$

is fulfilled. In the computer code we use

$$\varepsilon_1 = 10^{-(p+1)}, \quad \varepsilon_2 = 10^{-p}, \quad \varepsilon_3 = 10^{-(p-1)}$$

where p can be freely choosen.

If the k_y-step is also determined with the help of approximate values of the integral, the computation time would become unduly large. To avoid it, we use an heuristic way. If w_{max} is the highest frequency of the oscillating functions in the integrand depending upon k_y, an upper bound for the k_y-step length is defined by

$$\Delta k_y^{(sup)} = \frac{\pi}{8 w_{max}}$$

dividing the quarter period of the function $\sin(w_{max} \cdot k_y)$ into four parts. Starting with step length $\Delta k^{(a)}$ in the first strip, the step length in each following strip is doubled so long as it does not exceed $\Delta k_y^{(sup)}$. Integration is then performed over strips of constant width $2\Delta k_y^{(sup)}$ until the strip integral becomes sufficiently small i.e.

$$|F_{str}| \leq \varepsilon_2 |F_{temp}|$$

4.3. Computation Time and Efficiency

Computation of the global force from (10) and (11) requires five two-dimensional FFT's (2 FFT's for the eddy current density and 3 FFT's for the excitation field) and one volume integral. On our computer SIEMENS 4004/55 we can execute an in-core FFT of maximum 128·128 complex data. All the 5 FFT's and the volume integral then require 10 minutes computation time. According to (13) the global force is given by a single two-dimensional integral requiring about 40 seconds of computation time only. Compared with (10) and (11), this represents a saving in computer time of a factor of 15.

Therefore our method of computation is highly suitable if only the global force and not the eddy current or force density is required to be analysed. An extensive parameter study of basic systems was done by us on the basis of global force, the results of which are available in a series of papers [2].

5. Results

The results presented below illustrate a variety of subproblems occuring in magnetic levitation. For a complete discussion of the physical aspects of these results we refer to [2, 3] and other references therein. The system data used in the illustrations are as follows.

Figure 5. Normal flux system with rectangular magnet:
$2l = 2$ m, $2b = 0.3$ m, $I = 0.3$ MA, $h_1 = 0.2$ m, $d = 20$ mm,
$\sigma_S = 31$ MA/Vm, $\mu_r = 1$
Null flux system with circular magnet:
$2r = 0.5$ m, $I = 0.6$ MA, $2h_0 = 0.5$ m, $\Delta h = 20$ mm, $d = 5$ mm,
$\sigma_S = 31$ MA/Vm, $\mu_r = 1$

Ferromagnetic system with rectangular magnet:
$2l = 1$ m, $2b = 0.1$ m, $I = 0.3$ m, $h_2 = 0.1$ m, $d = 20$ mm,
$\sigma_S = 10$ MA/Vm, $\mu_r = 1000$

Figure 6. Null flux system with 5 rectangular magnets of alternating polarity:
$2l = 1.15$ m, $2b = 0.3$ m, $q = 0.25$ m, $I = 0.6$ MA,
$2h_0 = 0.5$ m, $\Delta h = 50$ mm, $d = 5$ mm, $\sigma_S = 31$ MA/Vm, $\mu_r = 1$,
$F_{L0} = 125$ kN

Figure 7. Normal and null flux:
$2l = 1.15$ m, $2b = 0.3$ m, $\sigma_S = 31$ MA/Vm, $\mu_r = 1$
Ferromagnetic:
$2l = 1$ m, $2b = 0.1$ m, $\sigma_S = 0.1$ MA/Vm, $\mu_r = 1000$
Normal flux and ferromagnetic:
$I = 0.3$ MA, $d = 20$ mm
Null flux:
$I = 0.6$ MA, $d = 5$ mm, $2h_0 = 0.5$ m

Figure 8. Normal flux (upper row): $h_1 = 0.2$ m, $d = 20$ mm
Null flux (lower row): $2h_0 = 0.4$ m, $\Delta h = 20$ mm, $d = 5$ mm
Normal and null flux: $2l = 1$ m, $2b = 0.3$ m, $\sigma_S = 31$ MA/Vm, $\mu_r = 1$
——$v_x = 30$ m/s, $v_p = 0$; ---$v_x = 30$ m/s, $v_p = 2$ m/s
-o-$v_x = 150$ m/s, $v_p = 0$; -x-$v_x = 150$ m/s, $v_p = 2$ m/s
where p=z and y for left and right column, respectively

Figures 9 and 10. Null flux system with two rectangular magnets of different polarity:
$2l = 1.5$ m, $2b = 0.3$ m, $q = 0.75$ m, $I = 1$ MA, $2h_0 = 0.7$ m,
$\Delta h = 10$ mm, $d = 12$ mm, $\sigma_S = 31$ MA/Vm, $\mu_r = 1$, $v_x = 140$ m/s

5.1. Global Forces

The Figures 5 and 6 show velocity characteristics for lift and drag forces and specific losses in basic levitation systems.

In Figure 5a the situation in a normal flux system with rectangular magnet is illustrated. The effect of magnet form on the forces was also investigated. For example, Figure 5b shows the forces in a null flux system with a pair of circular excitation magnets. Figure 5c represents the forces which act upon a rectangular coil situated below a ferromagnetic track sheet. The lift force decreases because the electrodynamic repulsion between the coil and the track sheet is superimposed on the magnetostatic attraction between them.

Figure 6 shows the transition of a conceptual vehicle with a null flux system from the rolling into the freely floating state. As long as the lift force is smaller than the vehicle weight G, the vehicle rolls on wheels with a fixed sag Δh (deviation from the midplane of the track sheet). When the lift force exceeds the weight, the sag adjusts itself according to the relation

$$F_L(\Delta h) - G = 0 \qquad (18)$$

and the vehicle starts floating. In our computer codes, the relation (18) is solved by Newton's iteration. As a consequence of this method we obtain the derivative of the lift force w.r.t. sag which is physically the mechanical stiffness of the system. With decreasing sag the stiffness increases; with increasing velocity both the quantities approach saturation values.

5.2. System Stiffness

Figure 7 shows suspension stiffness as a function of velocity under constant load conditions for the basic levitation systems. All the 3 diagrams correspond to a constant load of $F_{L0} = 25$ kN. For the normal flux system stiffness remains almost constant with a mean value 0.25 kN/mm corresponding to an eigenfrequency of 1.6 Hz. The system stiffness for the null flux system is much higher (at $v_x = 50$ m/s about 6 times larger) and strongly velocity dependent. The stiffness value at $v_x = 150$ m/s corresponds to an eigenfrequency of 4.4 Hz which is about 3 times higher than that of a normal flux system. The stiffness of a ferromagnetic system is almost velocity independent with a mean value 0.593 kN/mm corresponding to an eigenfrequency of 2.5 Hz.

5.3. Intrinsic Damping

In Figure 8 we illustrate the dependence of normalized side and lift forces on transverse and vertical velocities at constant forward velocity in normal and null flux systems. The perturbing velocities v_y and v_z are assumed to be very small as compared with the forward velocity v_x and taken to be in the range 0-10 m/s. The normalization constant for the forces is $F_0 = \mu_0 I^2/2\pi$. From these curves intrinsic damping of the levitation system may be analysed if the quasi static

forces thus calculated are assumed to remain essentially unchanged in the dynamic situation involving time dependent transverse and/or vertical perturbations (such as side winds etc.). Restricting the perturbation velocity v_p (p=y,z) to a range of about 0-2 m/s where the curves are nearly linear with slope K_p, we can calculate, using Newton's law, the damping time τ_p in seconds for the perturbation velocity v_p as

$$\tau_p = \frac{F_L/F_0}{g \cdot K_p} \qquad (p=y,z) \qquad (19)$$

where g is the gravity acceleration. Since τ_p depends on the normalized lift force, it is independent of the excitation current of the magnets, other parameters remaining constant. An analysis of the physics of intrinsic damping in basic levitation systems is presented in [3].

5.4. Eddy Current and Force Density

Figures 9 and 10 show the eddy current and force density, respectively, in the track for a null flux system with two rectangular magnets of different polarity. Figure 9a is an orthographic projection of the x-component of the eddy current density which shows clearly that the x-component is maximum under the longitudinal conductors of the excitation magnet coils.

The y-component of the eddy current density (Figure 9b) is largest under the transverse conductors of the excitation magnet coils. Since for different polarity of the excitation magnets the currents in the neighbouring pair and in the far pair of transverse conductors each flow in the same direction, both pairs of the inner and external peaks in the y-component each have the same sign. For same polarity the signs, for example of both the right peaks, will be reverse. The eddy current stream lines shown in Figure 9c have a twofold meaning. Firstly they give the direction of the eddy current field; secondly between two neighbouring flow lines the same amount of current always flows i.e. the nearer the lines, the higher is the eddy current density.

The orthographic representation of the lift force distribution (Figure 10a) shows that the major contribution to the lift comes from the longitudinal conductors of the excitation coils while the drag force mainly stems from the transverse conductors. Figure 10b shows lines of constant lift force acting upon a volume element of the track sheet.

6. Track of Finite Width

Recently, we have extended the above semi-analytical method of computation to sheet tracks of finite width. The main difficulty had been as follows: Whereas in the case of infinite sheet track the Fourier components of the exterior and interior magnetic field show a unique one to one correspondence via the boundary conditions, such a correlation does not exist for a track of finite width. It is therefore necessary to reduce the problem to a mathematically well defined interior boundary value problem, the solution of which does not require any knowledge of the exterior field. The results of this calculation will be presented elsewhere.

This work has been supported under the technological program of the Federal Department of Research and Technology of the FRG. The authors alone are responsible for the contents.

References

[1] Reitz, J.R.; Davies, L.C.: J. Appl. Phys. 43 (1972), pp. 1547 - 1553

[2] Urankar, L.: Siemens Forsch.- u. Entw. Ber. 4 (1975), pp. 25 - 32; s. also references herein

[3] Urankar, L.: Siemens Forsch.- u. Entw. Ber. 5 (1975), pp. 110 - 119

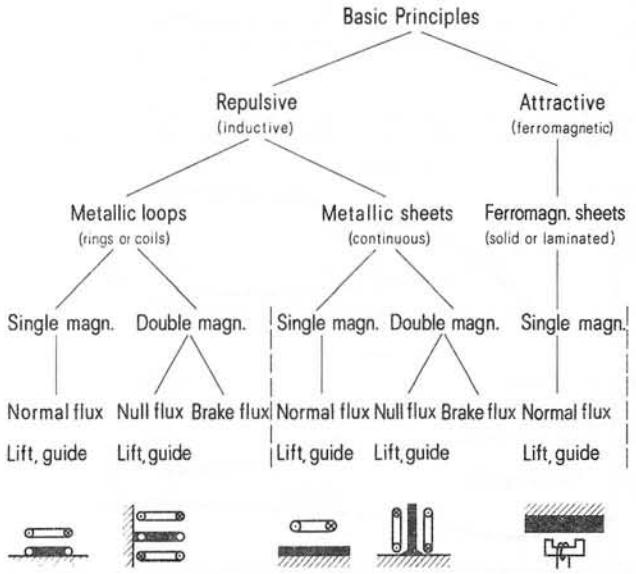

Figure 1: Basic types of magnetic levitation systems

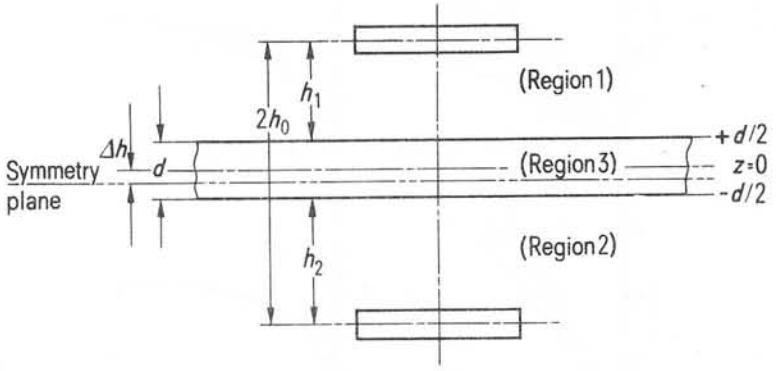

Figure 2: Schematic diagram of arrangement used in this analysis

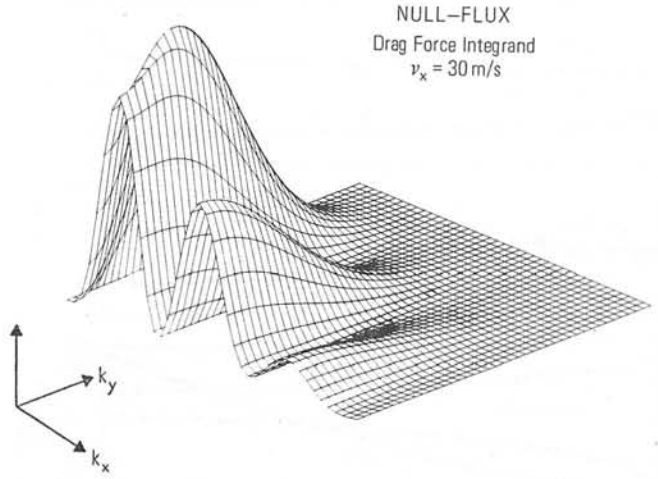

Figure 3: Typical integrand in k-space for global drag force

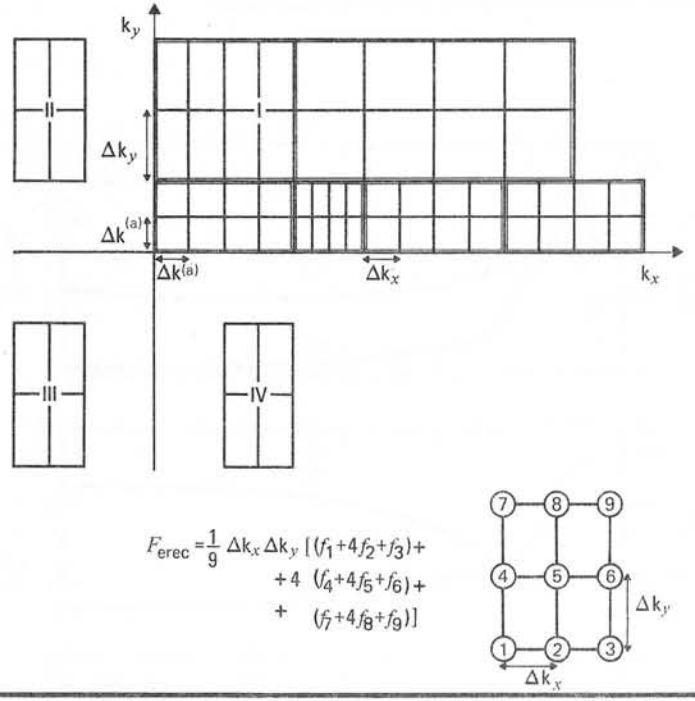

Figure 4: Numerical quadrature in k-space

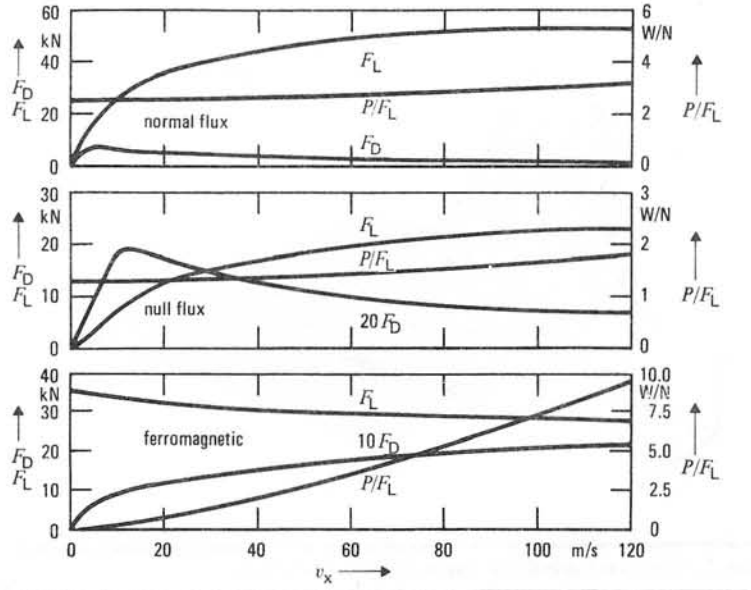

Figure 5: Velocity characteristics for basic levitation systems

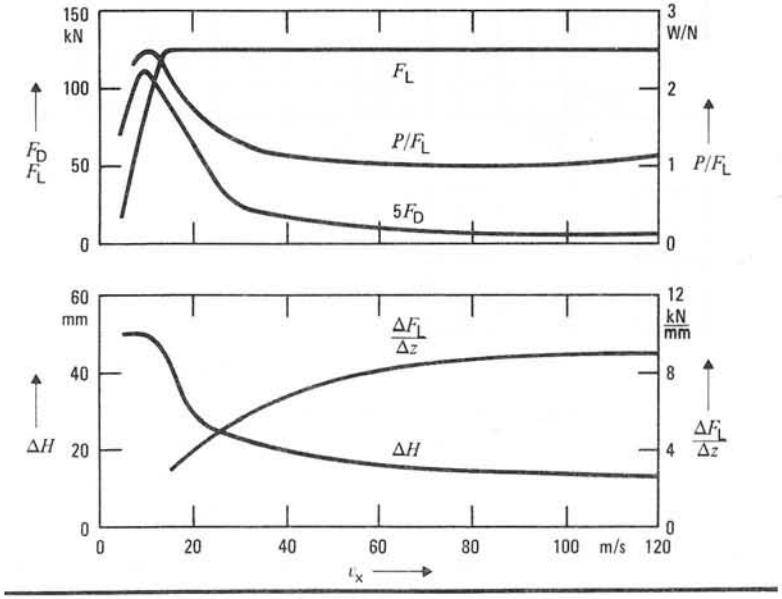

Figure 6: Transition from rolling to freely floating state

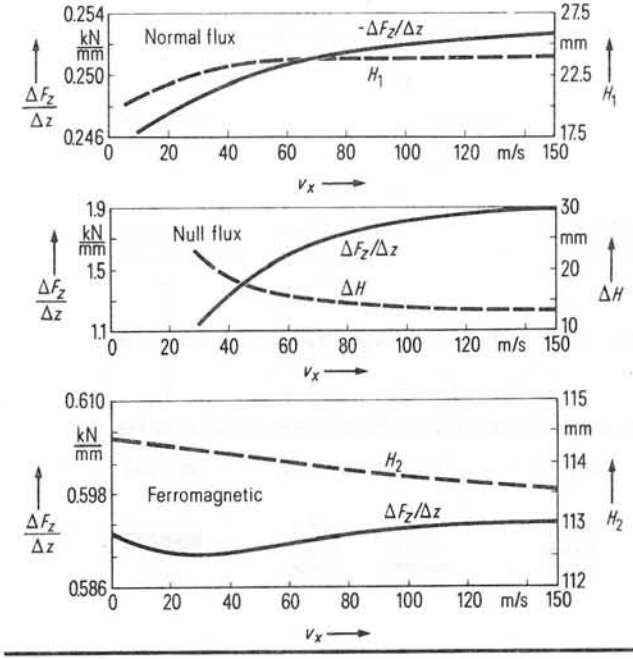

Figure 7: Velocity dependence of system stiffness and levitation height at constand load 25 kN

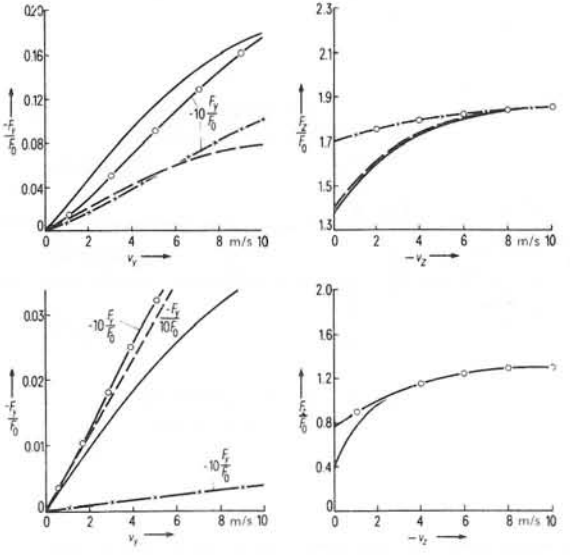

Figure 8: Effect of lateral and vertical velocities on side and lift forces

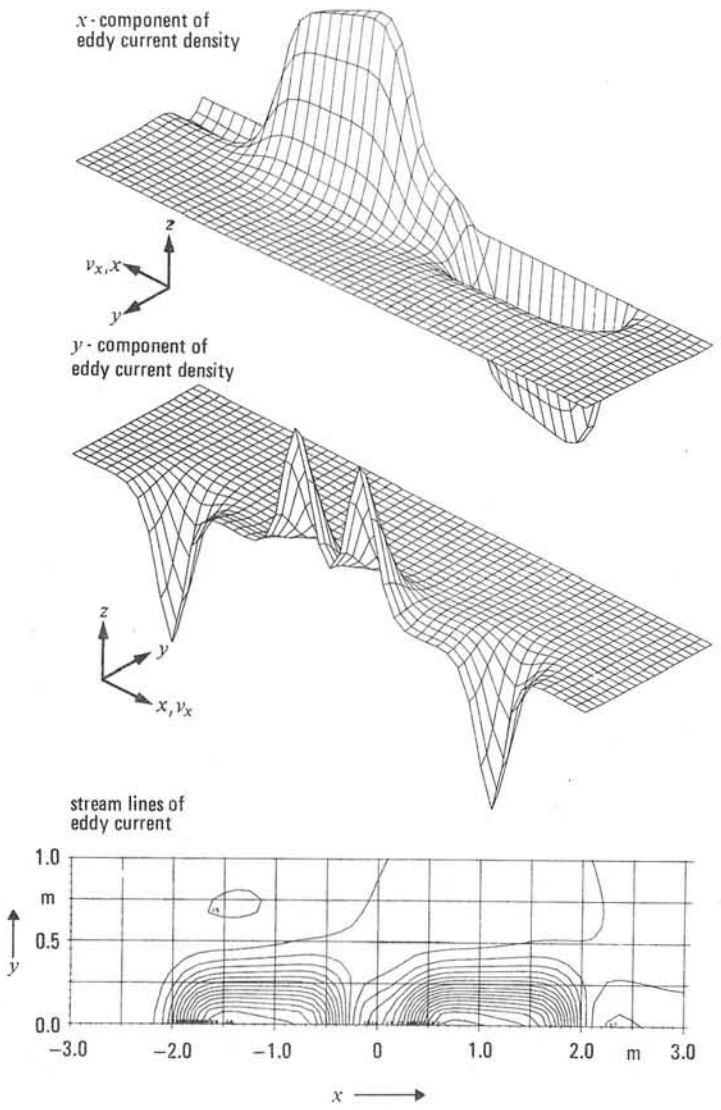

Figure 9: Eddy current density and stream lines in track sheet

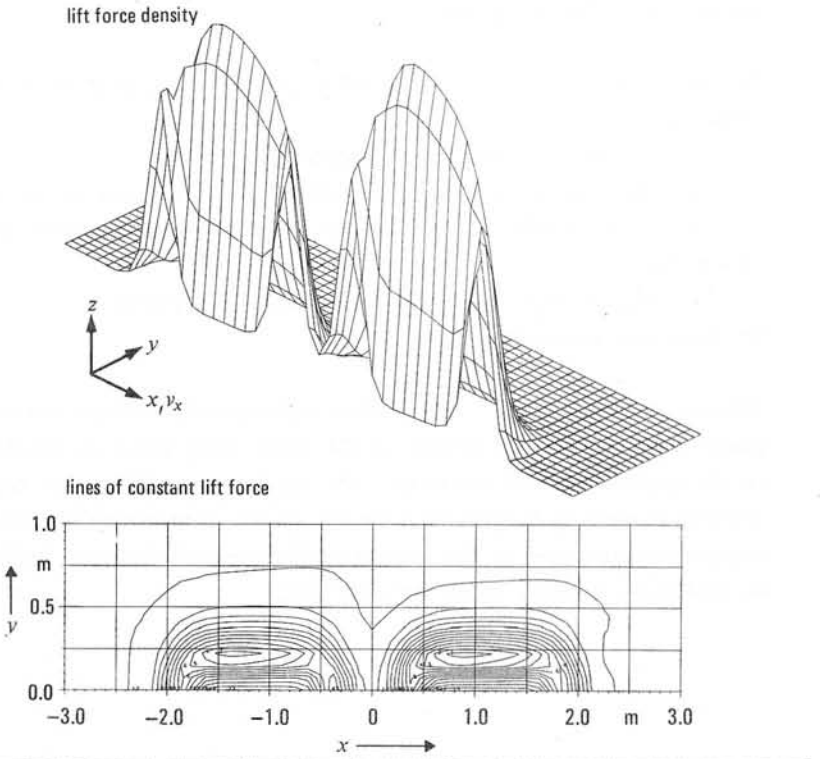

Figure 10: Distribution of lift force acting on track sheet

Discussions following paper:

(Roster, Chain Ltd) Your expression for the force density on the conductor is,

$$\underline{P}\ (x,y,z) = \underline{J}\ (\text{eddy}) \times \underline{B}\ (\text{excitation})$$

This does not appear to account for the self-interaction of the eddy currents. An expression for the force density which includes this effect is,

$$\underline{P}\ (x,y,z) = \underline{J}\ (\text{eddy}) \times \underline{B}\ (\text{excitation}) + \underline{B}\ (\text{eddy})$$

Why have you neglected $\underline{B}$ (eddy)?

(Krause, Siemens) The cross-product between eddy current and its own field leads to internal stress in the sheet track which is uninteresting in the problem at hand and hence left out in eqn. (10). The force density we want to analyse here is due to the interaction between the current distribution in the sheet and the excitation magnet field. An analogous argument holds for eqn. (12).

Three dimensional eddy current calculations

W Wolff, AEG Telefunken, Buchslag, West Germany

I) The solution of the magnetostatic equations

For the solution of the three dimensional magnetostatic equations we used the scalar potential as system quantity.

The basic idea of the applied method is the following.

1)
$$\text{a)} \quad \underline{H} = \underline{H}_i - \operatorname{grad} \phi$$
$$\text{b)} \quad \operatorname{curl} \underline{H} = \operatorname{curl} \underline{H}_i = \underline{i}_{St}$$
$$\text{c)} \quad \operatorname{div} \mu \operatorname{grad} \phi = \operatorname{div} \mu \underline{H}_i$$

The magnetostatic field $\underline{H}$ is split up into two parts. The first one $\underline{H}_i$ only has the same curls as the magnetic field has. Therefore the remaining part is eddy-free and can be expressed by the gradient of a scalar potential ϕ. The scalar potential is defined by an elliptic differential equation (eq. 1c), for which optimized numerical solution methods are well known. Because the curl-field $\underline{H}_i$ can have any sources there is an infinite number of solutions fulfilling eq. 1b). This fact can be used to pick a simple one calculable in a negligible time. Eq. 1b) was solved by discretization, too. Since the solution is not unique, the resulting linear equation system has more unknowns than equations. It is possible to combine the unknowns systematically in such a way that this linear equation system becomes recursive, and so the solution is uncomplicated.

In short, one can say : the magnetostatic problem is solved in a satisfactory way.

II) Extension to the solution of the time dependent Maxwell-equations

a) Basic equations

The question is:
can the described method be extended to the solution of the time dependent Maxwell-equations.

To solve the time dependent Maxwell-equations we

have to distinguish between a given current density $\underline{i}_{St}$ as already introduced in equation 1b) and a current density $\underline{i}_w$, induced by the resulting magnetic field. From here on, the displacement current will be neglected, so the divergence must be zero for both the given and the induced current density and the curl-field $\underline{H}_i$ can also be split up into two parts.

$$\begin{aligned} &\text{a)} \quad \underline{H}_i = \underline{H}_{iSt} + \underline{H}_{iw} \\ &\text{b)} \quad \operatorname{curl} \underline{H}_{iSt} = \underline{i}_{St} \\ &\text{c)} \quad \operatorname{curl} \underline{H}_{iw} = \underline{i}_w \\ &\text{d)} \quad \underline{H} = \underline{H}_{iSt} + \underline{H}_{iw} - \operatorname{grad} \phi \\ &\text{e)} \quad \operatorname{div} \mu \operatorname{grad} \phi = \operatorname{div} \mu (\underline{H}_{iSt} + \underline{H}_{iw}) \end{aligned} \qquad 2)$$

For a known vectorfield $\underline{H}_{iw}$ the equation system does not differ from the magnetostatic one. That means, the solution of the time dependent Maxwell-equations requires the additional calculation of the vectorfield $\underline{H}_{iw}$, only.

According to equation 2c) $\underline{H}_{iw}$ is the vectorpotential of the induced density. To eliminate $\underline{i}_w$, we substitute curl $\underline{H}_{iw}$ in the second Maxwell-equation for $\underline{i}_w$ and obtain eq. 3b).

$$\begin{aligned} &\text{a)} \quad \underline{E} = {}^1\!/\!\delta \; \underline{i}_w = {}^1\!/\!\delta \operatorname{curl} \underline{H}_{iw} \\ &\text{b)} \quad \operatorname{curl} {}^1\!/\!\delta \operatorname{curl} \underline{H}_{iw} = -\frac{d}{dt} \mu (\underline{H}_{iw} + \underline{H}_{iSt} - \operatorname{grad} \phi) \\ &\text{c)} \quad \operatorname{curl} \operatorname{curl} \underline{H}_{iw} = -\delta \frac{d}{dt} \mu (\underline{H}_{iw} + \underline{H}_{iSt} - \operatorname{grad} \phi) \end{aligned} \qquad 3)$$

The total time derivitive is allowed if the velocity is low compared with the velocity of light. If the space, in which the eddy current calculations take place, is surrounded by insulators, boundary conditions at its surface can be formulated. With the further assumption of constant conductivity δ inside this space equation 3b) can be multiplied by δ and we have the more simple equation 3c).

b) Boundary conditions

Outside the eddy current space the eddy current density is zero. So curl $\underline{H}_{iw}$ is zero, too, and $\underline{H}_{iw}$ can be represented by the gradient of a scalar function ϕ_w. Then for the magnetic field we have, according to eq. 2d)

$$\underline{H} = \underline{H}_{St} + \operatorname{grad} \phi_w - \operatorname{grad} \phi$$

Because $\underline{H}$ is defined uniquely by the potential equation 2b), for each ϕ_w the potential ϕ is determined accordingly.

We put ϕ_w = const for the sake of simplicity. That means that outside the eddy current space $\underline{H}_{iw} = 0$ is valid.

Because curl $\underline{H}_{iw}$ is a limited quantity the tangential component H_{iwt} of $\underline{H}_{iw}$ must pass the surface of the eddy current region steadily. So we have the boundary condition, that the tangential component H_{iwt} must be zero at the total surface of the eddy current space.

c) Time dependence

I suppose, for optional time dependence and field dependent permeability the problem is not yet soluble in an acceptable computation time. For the solution of this four dimensional problem additional numerical methods have to be developed especially those, concerning the solution of large linear equation-systems and a suitable discretization of differential equations. Provided all the field quantities have the same time dependence the problem can be reduced to the solution of a three dimensional one. This assumption includes a permeability depending on locus only and is strictly valid for non-ferromagnetica. For ferromagnetica the usual conversion of the permeability curve has to be carried out.

The following considerations provide both a sinusoidal time dependence and time dependent effects caused by moving bodies. In the latter case the restriction has to be made, that the cross section of the moving parts must be constant in the direction of movement.

For all the quantities the time-dependence is expressed by $e^{j\omega t}$ and all the movements are assumed in the X-direction, having the velocity v_x. Eq. 3c) can then be written in the final form eq. 4a)

$$\underline{H}_{iw} = \tilde{\underline{H}}_{iw}\, e^{j\omega t}$$

4)

$$\text{a)}\quad \operatorname{curl}\operatorname{curl}\tilde{\underline{H}}_{iw} + j\omega\mu\tilde{\underline{H}}_{iw} + v_x \frac{\partial}{\partial x}\mu\tilde{\underline{H}}_{iw} = -j\omega\mu\,(\tilde{\underline{H}}_{iSt} - \operatorname{grad}\tilde{\phi}) - v_x \frac{\partial}{\partial x}\mu\,(\tilde{\underline{H}}_{iSt} - \operatorname{grad}\tilde{\phi})$$

$$\text{b)}\quad \operatorname{div}\mu\operatorname{grad}\tilde{\phi} = \operatorname{div}\mu\,(\tilde{\underline{H}}_{iSt} + \tilde{\underline{H}}_{iw})$$

The sign above the quantities signifies that these quantities are the complex amplitude, only.

d) Solution

One is used to the divergence of a vectorpotential being arbitrary. If this holds in our case, too, according to equation 4b), a suitable selection would be $\operatorname{div} \mu \tilde{\underline{H}}_{iw} = 0$, because then the potential $\tilde{\phi}$ does not depend on $\tilde{\underline{H}}_{iw}$, and the calculation of $\tilde{\phi}$ would be definitive. We had the following direct way of calculation : First the computation of $\tilde{\underline{H}}_{iSt}$ needing the given current density, only. Then the computation of $\tilde{\phi}$ for the known $\tilde{\underline{H}}_{iSt}$ and at last the calculation of $\tilde{\underline{H}}_{iw}$.

In reality the solution is more complicated. Because we put $\tilde{\underline{H}}_{iw} = 0$ outside the eddy current space, $\operatorname{div} \mu \tilde{\underline{H}}_{iw}$ cannot be made zero at the surface.

At the surface the normal component of $\tilde{\underline{H}}_{iw}$ jumps according to the jump of the tangential component of the eddy current density, that means, the eddy current causes sources of the magnetic field at the surface, which depend on the resulting field. So we have to solve the two equations 4a) + b) by iteration. We start with an estimated value for $\tilde{\underline{H}}_{iw}$, solve equation 4b) and substitute the result for $\tilde{\phi}$ in equation 4a). The iteration-prescription is:

$$5)\quad \begin{aligned} &a)\quad \operatorname{div} \mu \operatorname{grad} \tilde{\phi}^{(\nu)} = \operatorname{div} \mu \left(\tilde{\underline{H}}_{iSt} + \tilde{\underline{H}}_{iw}^{(\nu-1)}\right) \\ &b)\quad \operatorname{rot} \operatorname{rot} \tilde{\underline{H}}_{iw}^{(\nu)} - \mu v_x \frac{\partial}{\partial x} \tilde{\underline{H}}_{iw}^{(\nu)} = \\ &\qquad \mu v_x \frac{\partial}{\partial x} \left(\tilde{\underline{H}}_{iSt} + \operatorname{grad} \tilde{\phi}^{(\nu)}\right) \end{aligned}$$

With the yielded value for $\tilde{\underline{H}}_{iw}$ we calculate an improved approximation for $\tilde{\phi}$ by means of equation 4b) and start again. The procedure will be stopped if the power balance is fulfilled sufficiently.

e) Discretization

For discretization of equation 5b) the same grid is used as for discretizing the potential equation 5a). In this grid the scalar potential $\tilde{\phi}$ is defined at the nodes, marked as dots in Fig. 5. The components of the magnetic field $\tilde{\underline{H}}$ are calculated by dividing the difference of two neighbouring potentials by their distance. So the component directed from one node to the other one is defined in the

middle of the two nodes. Because of this lay down the according components of $\underline{\tilde{H}}_{iSt}$ and $\underline{\tilde{H}}_{iw}$ are defined at the same positions.

In order to calculate the x-components of $\underline{\tilde{H}}_{iw}$, for example, one has to integrate over all the planes parallel to the grid planes x = constant. At the boundary of each integration plane, $\tilde{H}_{iwx}$ is tangential component with respect to the total eddy current space and therefore zero. So we obtain equation systems containing the unknown components of one plane only.

By introducing a suitable numbering at each integration plane, it is possible to calculate the components of $\underline{\tilde{H}}_{iw}$ directly, for example, by means of Gaussian algorithm.

If no moving bodies are present convergence is uncritical. With a velocity unequal zero, however, the above mentioned iteration procedure diverges if one starts with $\underline{\tilde{H}}_{iw}^{(o)} = 0$. Convergence is obtained, if one starts with $\underline{\tilde{H}}_{iw}^{(o)}$ necessary for total field displacement in the eddy current spaces, the so called ideal diamagnetic case ($\mu = 0$).

III) Some results

a) Electrodynamic levitation systems

For example the forces in electrodynamic levitation systems were calculated. Fig. 1 shows the set-up as used for basic experiments.

In principle, it is a rectongular coil moving with constant velocity above a conducting plate. The plate is infinite in the direction of movement and has constant cross section. It is 10 mm thick and 160 mm wide. The coil has a length of 200 mm, a width of 85 mm and a cross section of 15 x 15 mm^2. The exciting current is 48000 A.

The complete lines of Fig. 2 show the levitation force and the drag force, caused by the eddy current in the plate, versus the velocity of the coil. The parameter is the distance Z_o between the coil and the plate. In the lower curves the distance is 90 mm and in the upper curves 70 mm. The levitation force increases constantly with increasing velocity.

The drag force has a maximum at about 15 m/sec. The broken lines show the respective measured results. The discrepancies are mainly caused by the limitations of the experimental model set-up:

The infinite plate was represented by a round strip mounted on a rotating disc, so that the velocity was not uniform and the distance Z_o was enlarged by the reaction force, during experiment.

Fig. 3 shows the current flow patterns at the upper surface of the plate for 18 km/h, 36 km/h and 540 km/h. In the patterns for 18 km/h two eddies can be seen, caused by the increase and decrease of the magnetic field of the coil. The centre of the eddies moves with increasing velocity opposite the direction of movement, as it can be seen comparing the patterns for 36 km/h with those for 18 km/h. At 540 km/h the rear-eddy has vanished and the front-eddy has shifted its centre to the centre of the coil.

Because of the symmetric set-up with regard to the y-direction, the side forces are zero in the cases dealt with before. For small displacements a linear increasing destabilizing side force occurs. Fig. 4 shows the side force versus the displacement .

b) Eddy current calculations in iron rotors

To demonstrate an application in material with locus dependent permeability the eddy current distribution was calculated in an iron rotor. For sake of simplicity rotor and stator are fixed and the excitation consists of one coil, only.

At first, the magnetic field was calculated for dc-excitation regarding a field dependent permeability. This permeability distribution remained unchanged during the eddy current calculations.

Fig. 6 shows the real component of the magnetic field in the symmetry plane caused by an ac-excitation and the eddy current. In the rotor the magnetic field is mainly displaced.

Fig. 7 shows the imaginary component.

Fig. 8 shows the real component of the eddy current at the surface of the rotor and fig. 9 the imaginary component.

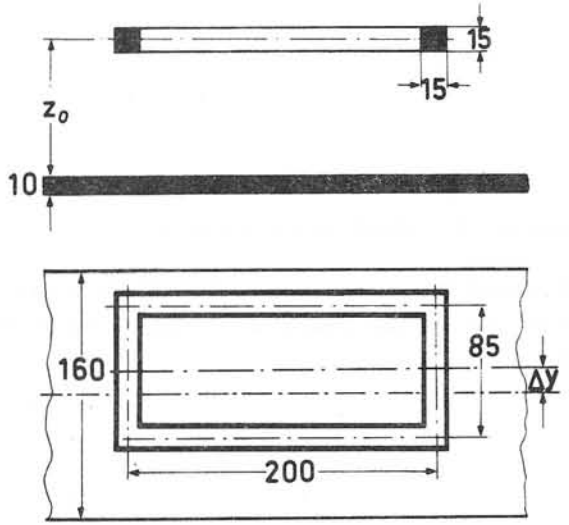

Maße in mm

The model set up

Fig 1

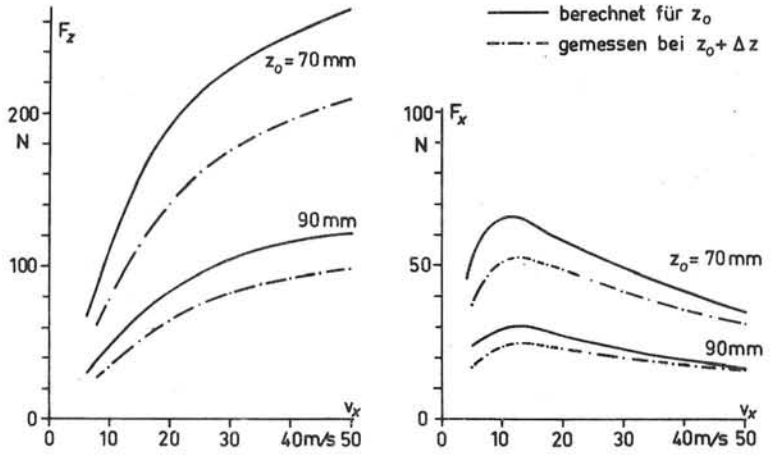

Levitation-and drag-force versus v_x

Fig 2

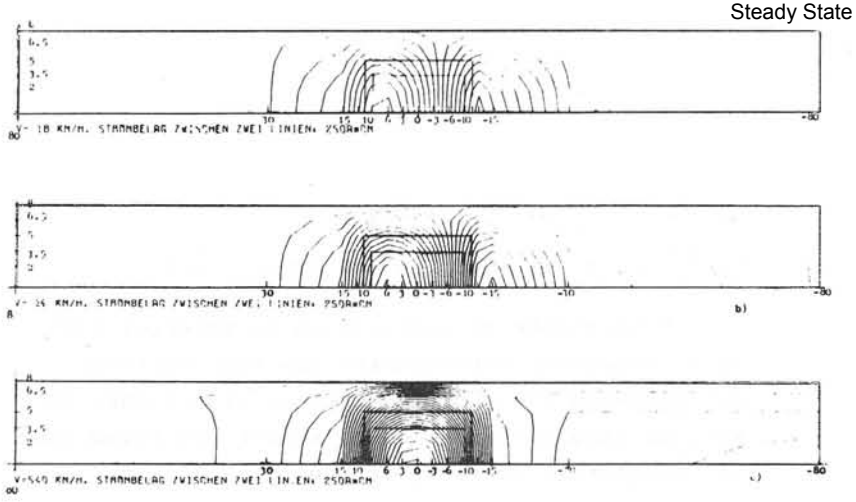

Eddy current patterns

a) v_x = 18 km/h

b) v_x = 36 km/h

c) v_x = 540 km/h

Fig 3

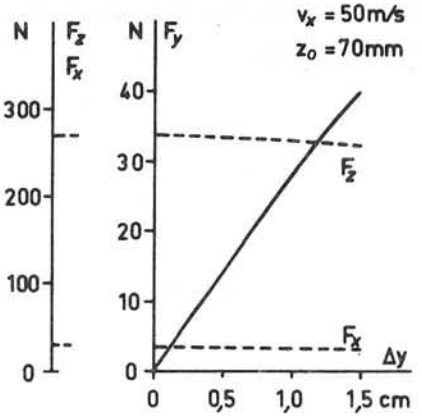

v_x m/s	50	13,9
z_0 mm	70	90
$\left(\frac{\partial F_x}{\partial y}\right)_0$ N/cm	−0,6	−0,7
$\left(\frac{\partial F_y}{\partial y}\right)_0$ N/cm	27,7	7,5
$\left(\frac{\partial F_z}{\partial y}\right)_0$ N/cm	−4,2	−1,7

Side-drag-and levitation-force versus eccentricity Δy

Fig 4

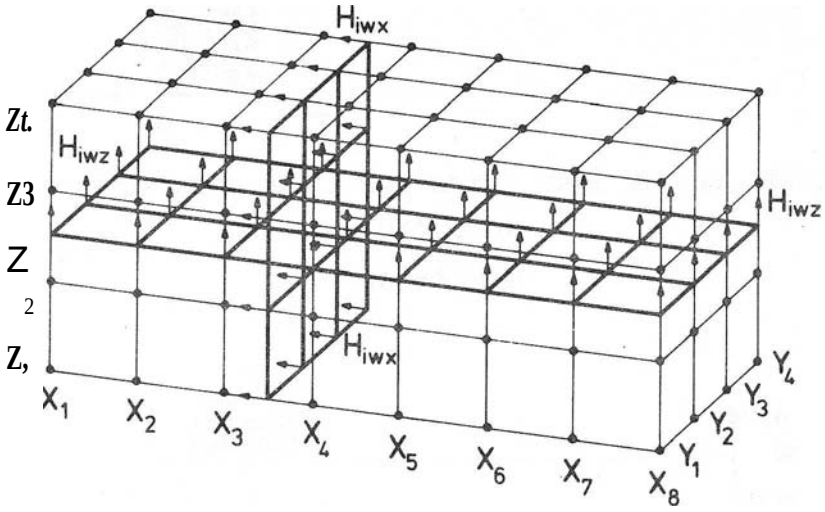

Integration planes for discretization of the vectorpotential equations concerning the components H_{iwx} and H_{iwz}

Fig 5

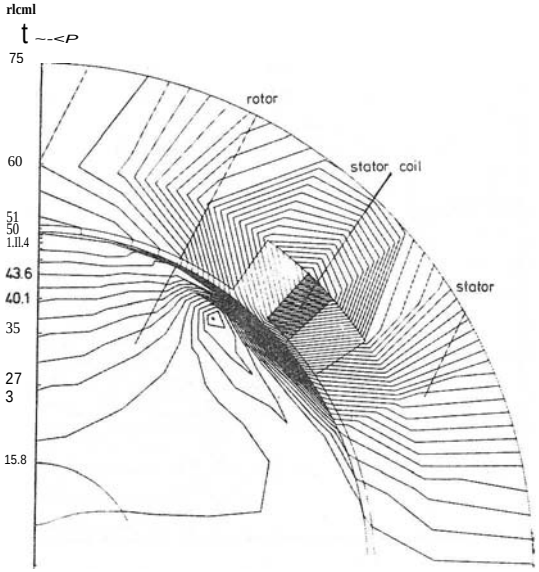

Induction (real component) In symmetry-plane z= 0 cm
O.5T.cm

Fig 6

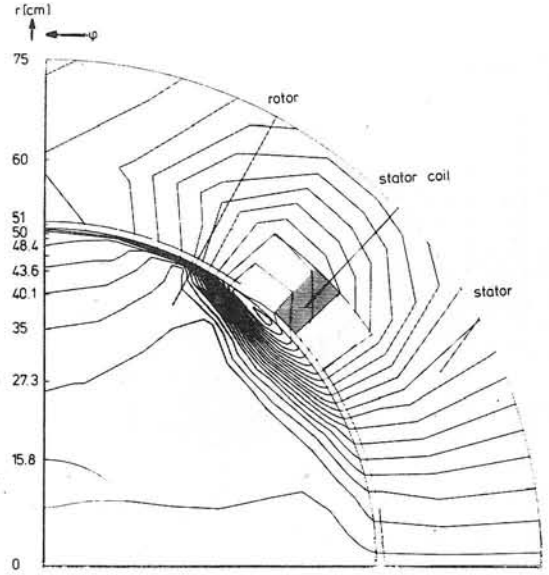

Induction (imaginary component) in
symmetry-plane z = 0 cm
0.6 T*cm

Fig 7

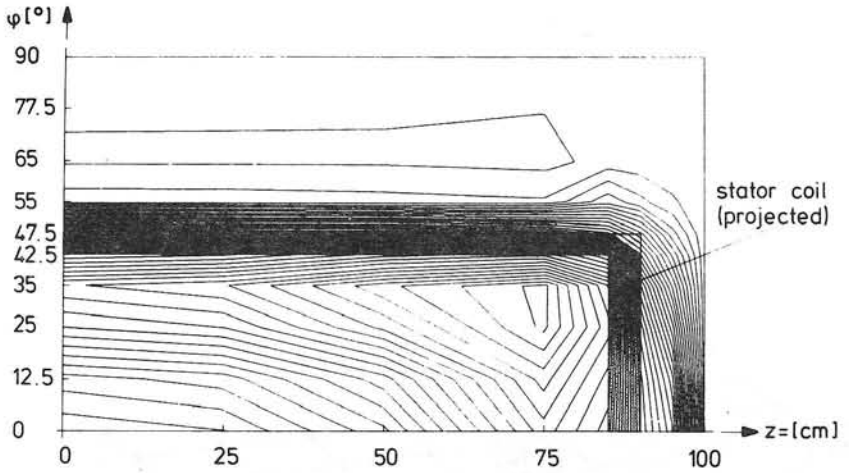

Eddy - current (real component) at the rotor surface
(r = 50 cm)
0.5 kA*cm

Fig 8

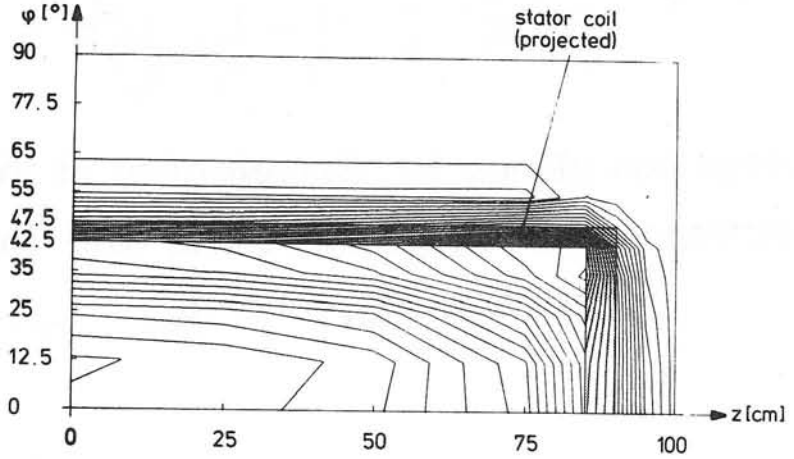

Eddy - current (imaginary component) at the rotor surface
(r = 50 cm)
0.5 kA * cm

Fig 9

Discussions following paper:

(Miller, Leeds) I would like to ask Dr Wolff what boundary condition he uses at the edges of the strip conductor, where the eddy-current is deflected into the transverse direction. When this problem is approached using magnetic vector portential A there appears to be some uncertainty about this boundary condition. In physical terms my question asks whether charge appears on the strip edges.

(Wolff) The above derived boundary conditions for the vector potential are also valid at the edges. Whether charge appears or not cannot be answered by me, because we do not calculate the electrical field especially.

(Carpenter, IC) Dr Wolff's formulation is somewhat similar to that which we shall describe in paper number 38, but with one important difference. The electric vector potential function which Dr Wolff denotes H_{ist} is, as he points out, one of a range of possible functions. We have used the symbol T. in conducting plate problems such as that described by Dr Wolff the component of current normal to the plate surface is usually negligible, and, as we have shown in paper no 7, this makes it possible to restrict T to a single component. The calculation is then reduced to two functions only (T and Ω, in our notation). I would like to ask Dr Wolff if he has considered this possibility. In general (as shown in paper 7) the three components of J can always be described by a T function which is limited to two components, and I wonder if there is any advantage in using three.

It is perhaps worth pointing out that Dr Jacob's equations in terms of a current flow function (paper 38) is essentially the same as Dr Wolff's but with the equivalent of the single-component T function.

(Wolff) Because of the lay boundary condition that the vector-potential is zero outside the eddy current space the three components of the vector-potential are determined uniquely. The advantage of the boundary condition at the surface of the eddy current space are the small equation systems for calculating the components of the vector-potential.

EFFICIENCY OF NUMERICAL TECHNIQUES FOR COMPUTING EDDY CURRENTS IN TWO AND THREE DIMENSIONS

C.J. Carpenter* and E.A. Wyatt*

ABSTRACT

The paper reports recent work on numerical techniques for solving eddy current problems in terms of a scalar, instead of the conventional vector, magnetic potential function. A method described previously for thin plates has been extended to large-section conductors, and gives high convergence rates when solved by iterative methods provided that suitable numerical techniques are used. These techniques are described in the paper. The method is particularly well suited to three-dimensional problems, but it also gives better convergence than the conventional method of calculation in many two-dimensional problems of practical interest, particularly in electrical machines.

PRINCIPLE SYMBOLS:

B	magnetic flux density	T	electric vector potential (equ.6)
d	depth of penetration (equ.10)	$\underline{x}$	solution vector
E	electric field intensity	x,y,z.	coordinates
$\underline{f}$	column vector of constants	α	travelling-wave term (equ.22)
$\underline{H}$	magnetic field intensity	β	constant given by equ.23
h	mesh interval	μ	permeability
J	current density	σ	conductivity
L	coefficient matrix	τ	time
N	mesh element ratio (fig.1)	Ω	magnetic scalar potential
p	pole pitch	ω	angular frequency

* Electrical Engineering Department, Imperial College, London SW7 2AZ.

1) Introduction

Eddy currents induced by leakage fluxes are of increasing importance in large electromagnetic devices such as turbo-generators, transformers, and the like, where increasing sizes and ratings may lead to severe heating problems. Eddy currents are induced in all conducting parts in the vicinity of the windings, particularly in the end-regions; and the end-surfaces of the core commonly need some form of screening. The eddy current and loss densities are difficult to predict because the problem is three-dimensional and the iron parts may be laminated and are liable to severe saturation. The magnetic vector potential, like the field vectors, has three components and, in general, it has to be supplemented by an electrostatic scalar potential, so that field calculations in these terms become formidable.

The obvious advantages of a magnetic scalar-potential formulation in magnetostatic problems, some aspects of which are discussed in a companion paper[1], assume an even greater significance in computing eddy currents. It is necessary to compute only one function outside the conductors, and excellent convergence is normally obtained when the differential equation is solved iteratively. A supplementary current-flow function has to be used inside the conducting regions, and this is, in general, a vector quantity, but it can usually be limited to one component, and it has been found to be well-behaved numerically when applied to problems in which the current flow is confined to thin sheets[2]. This formulation can be applied to conductors of large cross-section either by assuming continuous conducting properties, by replacing them by a stack of thin plates, or using an "onion skin" model consisting of a set of concentric layers. Some of the possibilities have been discussed elsewhere [1,3].

In the type of problem considered here the more important conductors consist of laminated iron cores, or non-magnetic plates whose thickness is limited (although it may often be substantially greater than the depth of penetration at the working frequency). Under these conditions the current density component normal to the major conductor surfaces is negligible (i.e. the z-component in fig.1), and it is

convenient to assume that it is zero in all conductors, whether laminated or not. The effect of removing this restriction will be discussed separately.

One of the devices of interest is a linear induction motor consisting of a conducting plate in an air gap between two iron surfaces, one carrying a winding in slots. This machine has been studied partly because the flux distributions are easily obtained experimentally. The principal parameters are given in figure 1. The winding generates a flux wave travelling in the y direction, and gives three-dimensional flux and current-flow patterns for which a two-dimensional description is adequate. This simplifies experimental work and is directly applicable to many end-field problems.[1] Varying the pole-pitch in the numerical model of the machine changes the field conditions from a rapid variation in the y direction, at one extreme, to a simple two-dimensional result, at the other, when the pole-pitch is infinite. The more general three-dimensional problem has been studied previously[2] using thin plates.

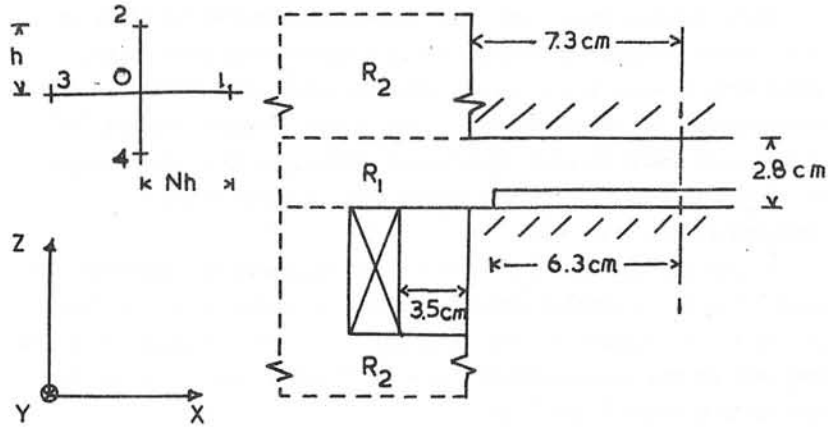

Fig. 1 Induction machine geometry.

Machine 380 mm long, pole pitch 95 mm
"Duralumin" plate, resistivity 3.02×10^{-8} Ωm, thickness 6.35 mm
Mesh Nh = 4.67 mm h = 2 mm in region R_1
h = 4.5 mm in region R_2

Early experience[3] with the scalar-potential method suggested that it had very considerable advantages in eddy-current problems not only in three dimensions, but also in two, because of its numerical behaviour when solved iteratively. This has now been more closely studied and the behaviour of different numerical formulations compared. The object of the paper is to report some of the results of these studies, and the preferred numerical formulation. The method is applicable to both transient and steady-state problems, but for the present purpose all time variations are assumed to be sinusoidal, with angular frequency ω.

2) Formulation

The problem is to solve simultaneously the magnetic field equations

$$\text{curl } H = J \qquad (1$$

$$\text{div } B = 0 \qquad (2$$

together with

$$\text{curl } E = -j\omega B \qquad (3$$

$$\text{div } J = 0 \qquad (4$$

in which all the quantities are vectors with three space components, each of which is complex. The usual two-dimensional method is to satisfy equation 2 implicitly by expressing B as the curl of the magnetic vector potential, A, giving

$$\nabla^2 A = (j/d^2)(A - \text{grad } V) \qquad (5$$

where A is assumed to have zero divergence (Coulomb gauge). The electrostatic potential, V, adds an electric field component which is constant inside each conductor in a two-dimensional problem, but is not in three dimensions, where surface charges appear at all the conductor surfaces as a consequence of equation 4.

One alternative is to use an electric vector potential, T, defined by

$$\text{curl } T = J \qquad (6$$

and to confine T to a simple function by placing some other constraints on it and allowing it to have an arbitrary divergence. As is shown in

reference 1, T can be restricted to one component, T_z, inside the conductor, with zero value outside and a constant value in any conductor hole, provided that J_z is zero. Assuming uniform conductivity, σ, equation 3 becomes

$$\nabla^2_{x,y} T_z = \partial^2 T_z/\partial x^2 + \partial^2 T_z/\partial y^2 = j\,\omega\,\sigma B_z \qquad (7a$$

when expressed in terms of T in Cartesian co-ordinates. Here T_z is operated on only in the x and y directions. From equations 1 and 6

$$H = T - \text{grad}\ \Omega \qquad (8$$

where Ω denotes a magnetic scalar potential function. It follows from equation 2 that, in a non-magnetic conductor,

$$\nabla^2 \Omega = \partial T_z/\partial z \qquad (9$$

where the ∇^2 operator refers to all three directions, in the usual way. Outside the conductors (or in windings in which J, and therefore T, is specified[1]) H can be obtained by computing Ω, whilst in the eddy-current regions both equations 7a and 9 have to be solved. The sources of Ω - i.e. the right hand side of equation 9 - are equivalent to magnetic poles distributed through the volume of the conductor, but concentrated primarily at the upper and lower surfaces where T is discontinuous. Substituting from equation 8 in 7a,

$$\nabla^2_{x,y} T_z = (j/d^2)(T_z - \partial\Omega/\partial z) \qquad (7b$$

where d is the depth of penetration defined by

$$d^2 = 1/\omega\mu_o\sigma \qquad (10$$

The pair of equations, 9 and 7b have to be solved simultaneously for Ω and T_z, respectively. One is Poisson's equation, and the other a form of the Helmholtz equation, but with a two-dimensional operator and an additional source term.

In a travelling-wave type of solution all quantities are assumed to vary sinusoidally with y, and with time τ, so that T_z, for example, takes the form

$$T_z(x,z)\exp j(\omega\tau - \pi y/p + \phi)$$

so that the second derivative terms in y can be written

$$\partial^2 T_z/\partial y^2 = -(\pi/p)^2 T_z \qquad (11$$

and likewise for Ω.

In expressing these equations in discrete form the Ω nd T_z functions inside the conductors are not restricted to a common node array, and the first-order derivatives on the right-hand sides of equations 9 and 10 suggest some advantages in computing them in two staggered arrays. The directional properties of the various terms, together with the discontinuities in both grad Ω and T at the conductor surfaces, introduce a range of possible numerical treatments, and each of the pairs of simultaneous equations obtained can be solved by elimination, line, or point iteration in various combinations.

These possibilities have been somewhat restricted by adopting a first-order (linear) interpolation in a rectangular node array, since this is well suited to the problem under consideration. An investigation of staggered meshes (the"split- branch" formulation[4]) showed that these have no significant advantages in either accuracy or numerical behaviour over a single mesh in which Ω and T_z are computed at the same nodes.

In general the conductor surface may intersect the mesh between nodes, but it is usually convenient to place nodes on it, as shown in fig 1. To compute T_z from equation 7 at a surface node, 0, H_z is required at the discontinuity. From equation 8, the H_z value midway between nodes 0 and 2 is

$$(H_z)_{02} = (\Omega_0 - \Omega_2)/h \qquad (12$$

and between 0 and 4,

$$(H_z)_{40} = (T_0 + T_4)/2 - (\Omega_0 - \Omega_4)/h \qquad (13$$

Here the z suffix has been dropped from T_z as it is superfluous. The two values can be averaged, or alternatively H_z at node 0 can be

derived from the underside values according to

$$(H_z)_o = (H_z)_{40} + (\partial H_z/\partial z)_0 \, h/2 \qquad (14$$

where

$$(\partial H_z/\partial z)_0 = -(\partial H_x/\partial x + \partial H_y/\partial y)_0$$

since div H is zero. Hence

$$(\partial H_z/\partial z)_0 = (\partial^2\Omega/\partial x^2 + \partial^2\Omega/\partial y^2)_o \qquad (15$$

and this can be expressed in terms of the nodal values of Ω in the usual way. The required H_z can likewise be derived entirely in terms of Ω from values on the surface and above by substituting from equations 12 and 15 in

$$(H_z)_0 = (H_z)_{02} - (\partial H_z/\partial z)_0 \, h/2 \qquad (16$$

The results obtained from equations 14 and 16 will be identical when the solution has converged and the continuity condition (equation 2) has been met, and likewise adding 14 and 16 together shows that averaging the H_z values above and below the node also gives the same final result. But at the earlier stages of the calculation the continuity condition is not satisfied, and it has been found that the different formulations give very large differences in numerical behaviour when iterated. In general, the use of asymmetric expressions for H_z has been found to produce poor convergence, and can lead to numerical instability, depending on the sequence and method by which the Ω and T functions are computed. No such difficulty has been encountered when using the symmetrical expressions

$$(H_z)_0 = [(H_z)_{02} + (H_z)_{40}]/2 \qquad (17$$

where the two terms are given by equations 12 and 13, and this form of dependence has therefore been adopted.

At the conductor surface the discontinuity in the right-hand side of equation 9 can be represented by treating it as a sheet source, in which the equivalent pole density is numerically equal to T_z, per unit area. Alternatively, from equation 8,

$$\partial H_z/\partial z = \partial T_z/\partial z - \partial^2\Omega/\partial z^2$$

so that equation 9 can be written

$$\nabla^2_{x,y}\Omega = \partial H_z/\partial z \qquad (18$$

where

$$(\partial H_z/\partial z)_0 = [(H_z)_{02} - (H_z)_{40}]/h \qquad (19$$

Hence the nodal forms of equations 7 and 9 at the conductor surfaces are

$$T_1 + T_3 + jN^2\beta\,[(\Omega_2-\Omega_4)/h - T_4/2] - (2 + jN^2\beta/2 + \alpha)T_o = 0 \qquad (20$$

$$\Omega_1+\Omega_3 + N^2[\Omega_2 + \Omega_4 + (T_o+T_4)h/2] - (2 + 2N^2 + \alpha)\Omega_o = 0 \qquad (21$$

where

$$\alpha = (\pi Nh/p)^2 \qquad (22$$

and

$$\beta = h^2/2d^2 \qquad (23$$

When equation 21 is derived by the equivalent pole-sheet approach the $(T_0+T_4)/2$ term is replaced by T_0, and this provides an alternative approximation of the same accuracy. More general expressions for T_0 and Ω_0 can be derived in the same way for conductor interfaces at which the conductivity takes different values on the two sides, neither zero. At nodes at which the conductivity is uniform, equations 7 and 9 become:

$$T_1+T_3 + jN^2\beta(\Omega_2 - \Omega_4)/h - (2+j2N^2\beta + \alpha)T_o = 0 \qquad (24$$

$$\Omega_1+\Omega_3 + N^2[\Omega_2 + \Omega_4 + (T_4-T_2)h/2] - (2+2N^2+\alpha)\,\Omega_o = 0 \qquad (25$$

3. Methods of solution

The method was compared with the conventional magnetic vector potential (A) formulation in an initial study of the linear motor. To simplify the A calculation the problem was assumed to be two-dimensional. Consequently the pole pitch was made infinite. The scalar potential, when calculated by simple point iteration with unity acceleration factor, required 850 iterations to reduce the maximum error to 2×10^{-5} of the maximum potential in a rectangular mesh of 202 nodes (with machine proportions somewhat different from those shown in fig.1). The dominating effect of the iron surface made the convergence of the A calculation too slow to be practicable without various acceleration techniques (including specifying the flux linkage instead of the excitation current), so that quantitative comparison is difficult and is not necessarily very meaningful because it is problem-dependent. But, in general terms, the well-known advantages of the scalar-potential formulation in regions bounded by iron, because the Neumann condition which is imposed on A is replaced by the Dirichlet condition, are retained in eddy-current calculations. It has been found that the ratio of the convergence rates is reduced as the frequency is raised, but it is greatly in favour of the scalar potential formulation at the working frequency of the machine.

Nevertheless, the preliminary results showed room for further improvement, and experimentation with different methods of computing Ω and T_z showed that not all of them converged well, whilst some diverged. The numerical behaviour was therefore examined more closely. The full set of finite difference equations for all nodal T_z and Ω values takes the form

$$L_1 \underline{x}_1(\Omega, T_z) = \underline{f}_1 \qquad (26$$

where L_1 is a sparce coefficient matrix, $\underline{x}_1$ is the vector of T_z and Ω values, and $\underline{f}_1$ is a constant vector that incorporates the boundary conditions. Although the values of the elements of L_1 depend on the way in which H_z and $\partial H_z/\partial z$ are approximated numerically, L_1 has some properties that are independent of the finite difference approximation used. The finite direction graph technique described by Varga[5] shows that L_1 is not consistantly ordered and does not satisfy Young's "Property A." Furthermore, L_1 cannot be diagonally dominant, though it may approach this condition when the simultaneous equations are suitably manipulated. The manipulation takes the form of elimination of some T_z and Ω terms. The equations are derived from two different coupling conditions, namely the induced current equation 7, and the magnetic continuity equation 9, and numerical experimentation has shown that best convergence rates can be achieved if these are separated. That is, 26 is separated into two simultaneous matrix equations of the form

$$L_2 \underline{x}_2(T_z) = \underline{f}_2 + \underline{g}_2(\Omega) \qquad (27)$$

$$L_3 \underline{x}_3(\Omega) = \underline{f}_3 + \underline{g}_3(T_z) \qquad (28)$$

where $\underline{f}_2$ and $\underline{f}_3$ incorporate the boundary conditions, whilst $\underline{g}_2$ and $\underline{g}_3$ are functions of Ω and T_z respectively. The coefficient matrices L_2 and L_3 depend on the numerical approximation adopted. It is found that L_2 and L_3 are consistently ordered and satisfy Young's "Property A", although neither is diagonally dominant. Furthermore, L_2, but not L_3, can be tri-diagonal. It has been found that the T_z calculation is less well-conditioned than the Ω one (partly because the operator differentiating T_z has one less dimension than that operating on Ω) and improvements depend on an increase in the number of T_z iterations. This causes relatively little increase in the computing time per complete cycle because the T_z calculation is confined to nodes in conductors. There are advantages in solving equation 27 by matrix inversion, particularly when the finite-diference approximation chosen makes L_2 tri-diagonal, and this gives a part line-iteration method.

In a typical calculation, the substitution of equations 27 and 28 for 26 and computing T_z by 10 Gauss-Seidel iterations per step of the main iteration cycle improved convergence by a factor of 5 (to 173 cycles). The computing time was reduced by a factor of 3.5.

One consequence of the consistent ordering of the L_3 matrix is that the Carré- Stoll method[6,7] may be used to calculate the best acceleration factor, and this has been found to work well in practice.

4) Results

The linear motor used for test purposes was excited by a 3-phase winding arranged in 3 slots per pole in the laminated block on the underside of the air gap (fig.1). The computation method was tested for various thicknesses and positions of the conducting plate as well as at different frequencies, but experimental measurements were limited to a plate having the thickness shown in fig. 1 placed on the lower iron surface. This left an air gap above the plate in which the flux density measurements were relatively unaffected by slot harmonics. The plate width was reduced below the normal value to increase leakage effects. For the field calculation a mesh of 661 interior nodes was chosen with approximately square elements in the end-region R_2, and rectangular elements with a length-breadth ratio N of 2.25 in the air-gap region R_1. The scalar potential field sources consisted of current sheets on the surface of the bottom laminated core, together with sheet pole-type sources on the end-winding surfaces (the T' function of ref.1).

A contour plot of the real part of the Ω function is given in fig.2. Here the field in the R_2 regions is compressed by treating all nodes, for plotting purposes, as having the same spacing as in the region R_1. The imaginary part of Ω in the air gap and in the plate is drawn to an enlarged scale in fig. 3. The diagrams show the discontinuity in the normal gradient of Ω at the plate surface which is caused by the discontinuity in T.

As is typical with these proportions, the variation of T with z is comparatively small, although the depth of penetration d is only 20% greater than the plate thickness. The variation of T with x and y over the entire plate is shown in fig.4 for one instant of time (the calculation assumes no end-effects in the y direction). Since T varies sinusoidally with y, as well as in time, the real and imaginary parts are obtained by choosing appropriate sections of the diagram. It is noteworthy that T(x) is approximately sinusoidal.

The solution converged to a potential error of 2×10^{-5} of the maximum potential in 74 iterations, and the convergence rate was found to be virtually independent of frequency over a range of 40 to 1. The acceleration factor, computed by the Carré-Stoll method, settled to a final value of 1.707 + j 0.0047, with a sufficiently high convergence rate to make its initial value (unity) unimportant.

Computed and measured values of the magnitudes of the two large flux-density components are plotted in fig. 5 as a function of x. The measurements shown were made in the mid-plane of the machine, where end-effects were expected to be least. Somewhat higher values were observed in other planes. Under travelling-wave conditions, equation 8 reduces to

$$H_y = - j(\pi / p)\ \Omega$$

so that the y component of B provides a direct measure of Ω. The purpose of the machine is to produce force in the y direction, and this force was measured and compared with the computed value to obtain a convenient criterion of solution accuracy averaged over the plate. The calculated force was 4.4% less than that measured.

The agreement between the calculations and measurements provided adequate confirmation of the former, in view of the approximations made, particularly the neglect of end-effects. Since the programme is a small one it could be readily extended to include these[2], but a more detailed study was not considered worthwhile. The principal objective was to investigate the numerical behaviour of the Ω and T functions for plate thicknesses representative of practical devices, and this behaviour is little affected by the way in which the y variations are modelled.

5) Conclusions

When computing eddy currents numerically the formulation can be expressed in terms of one of a range of possible quantities, all vectors, including the four field vectors (H,B,E,J) and the two vector potentials (A and T). The work described has confirmed the substantial advantages in choosing an electric vector potential, T, as the current describing function, defined so that it is constant or zero outside the conductors.

As in magnetostatic applications, this reduces the field problem in the non-conducting regions to that of computing a function Ω which is both a scalar and which is well-behaved numerically in regions bounded by iron. Inside laminated and plate conductors the associated T function can be limited to one component. Its interaction with Ω can be expressed numerically in a variety of ways, and many, although by no means all, of these possibilities have now been explored. Poor convergence, and even divergence, has been experienced with some, but the preferred methods give excellent convergence in a device which typifies many power-frequency applications.

The method assigns Ω and T values to the same nodes and is suitable for line iteration of the T values. Accelerated point iteration gives convergence which is very much better than that of the magnetic vector potential A function in regions bounded by iron, and the technique is well suited to both two- and three-dimensional calculations. The form of the matrices is such that the Carré-Stoll method for computing acceleration factors automatically is very effective.

6) Acknowledgements

The work has been supported financially by the Science Research Council. The authors are grateful to many colleagues for helpful discussions, particularly Dr. C.W. Norman (Westfield College) and Dr. D. A. Lowther (Imperial College).

7) References

1) Carpenter, C.J. and Locke, D. "Numerical models of 3-dimensional end-winding arrays" Compumag 1976

2) Carpenter, C.J. and Djurović, M "3-dimensional numerical solution of eddy currents in thin plates" Proc.I.E.E. 1975 122 pp 681-688

3) Carpenter, C.J. "Computation of magnetic fields and eddy currents" 5th Int.Conf. on Magnet Technology Rome 1975 pp 147-158

4) Carpenter, C.J. "A network approach to the numerical solution of eddy-current problems" Trans. I.E.E.E.1975 MAG-11 pp 1517-1522

5) Varga, R.S."Matrix Iterative Analysis", Prentice Hall 1962.

6) Carré, B.A. " The determination of the optimum accelerating factor for succesive over-relaxation"Cmput.J. 1961 4 pp 73-8

7) Stoll,R.L. "Solution of linear steady-state eddy-current problems by complex successive overrelaxation" Proc.I.E.E. 1970 117 pp 1317-23

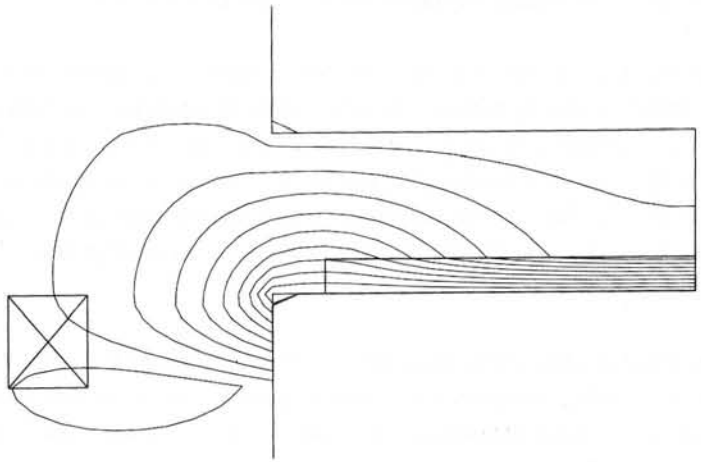

Fig. 2 Real part of Ω
β = 0.0276

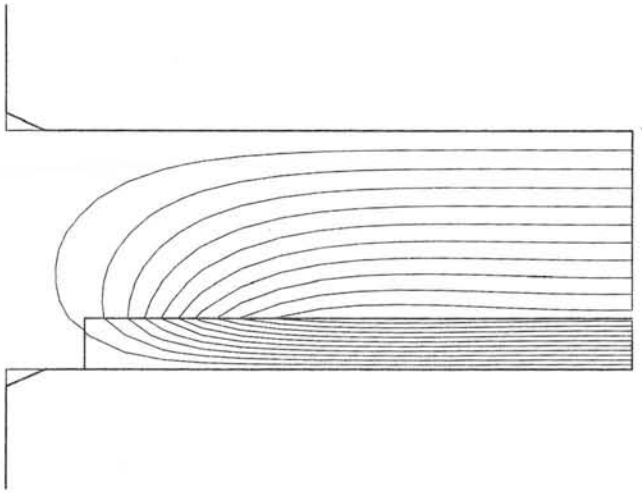

Fig. 3 Imaginary part of Ω

Ω_{max} = -29.2 Ω_{min} = 0

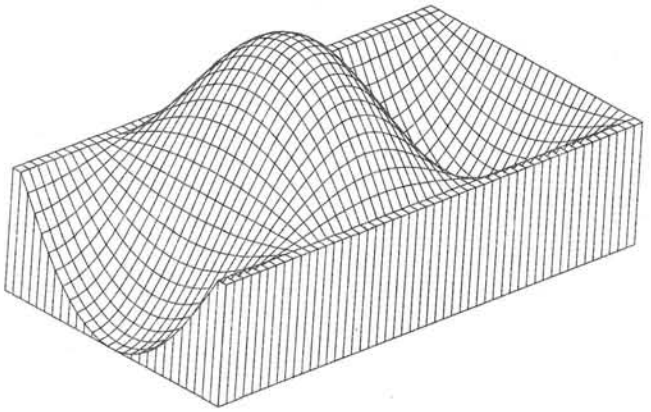

Fig. 4 T variation in typical layer of plate

T_{max} = 6520

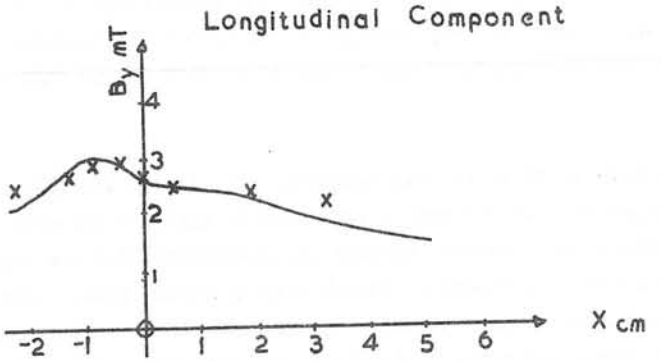

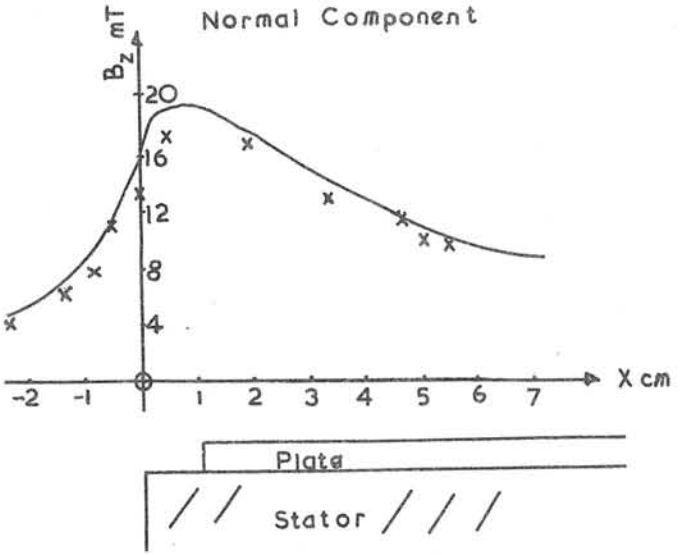

Fig. 5 Magnitude of B in air gap

Measured in machine centre-plane 2mm below top iron surface

Discussions following paper:

(Perin, CERN) I should like to point out that the vector T was used, for the static case, about 20 years ago for the computation of the AGS magnets at BNL. Again a long time ago it was used by R Christian in his magnetostatic program Sybil and by myself at CERN in the MARE program.

(Wyatt) I thank Mr Perin for his comments. It is all too easy to give the impression that the method presented is entirely new when this is not the case. Maxwell himself was responsible for the idea of using a current flow function, though only in scalar form. Our contribution is that we have extended the flow function concept, using the electric vector potential T, in order to solve eddy currents in two and three dimensions.

THE CALCULATION OF MAGNETIC FLUXES AND EDDY CURRENTS IN GENERATOR STATOR CORES

DAVID A.H. JACOBS

Research Department, C.E.G.B., Leatherhead, Great Britain

ABSTRACT

The time dependent electromagnetic fields in stator cores of large generators have been determined by a numerical solution procedure. The outline complex three dimensional geometry is modelled, and the saturable laminated structure of the core is included. The method has been ratified with measurements from large generators, and can be used to investigate the changes in the electromagnetic characteristics of generators occasioned by design modifications, changes in material, or material properties, and other alterations.

NOMENCLATURE

$\underline{A}$	Vector potential
$\underline{B}$	Magnetic flux density vector
$\underline{E}$	Electric field strength vector
$\underline{H}$	Magnetic field strength vector
H_o	Saturation magnetic field in the Fröhlich permeability relation
i	$= \sqrt{-1}$
$\underline{J}$	Current density vector
q	Source term in the stream function equation
r	Radial coordinate
t	Time
$\underline{x} = (r,\theta,z)$	Position vector
z	Axial coordinate
$\underline{\hat{z}}$	Unit axial vector
γ	Stacking factor
$\underline{\underline{\mu}}$	Permeability tensor
$\bar{\mu},\mu_{21},\mu_{22}$	Fourier components of permeability components
μ_o	Permeability of free space
μ_1	Zero field relative permeability of iron
μ_2	Limiting relative permeability of iron
$\xi = \psi_{11} + i\psi_{12}$	
$\underline{\underline{\sigma}}$	Electrical conductivity tensor
ϕ	Magnetic scalar potential
ϕ_{11},ϕ_{12}	Fourier components of ϕ
ψ	Eddy current stream function
ψ_{11},ψ_{12}	Fourier components of ψ
ω	Angular velocity of rotor
Superscript e	Induced eddy current component
Superscript i	Value in iron
Superscript n	Iteration number
Subscripts r,θ,z	Vector components

1. INTRODUCTION

It is highly desirable to put the art of designing large generators onto a firm scientific footing. Moreover during the life of a generator, the type of use and the load conditions it has to meet are likely to vary very considerably, and in order to be able to use the generator most efficiently it is necessary to predict the behaviour and characteristics under these different conditions. In this paper we concentrate on the derivation of the electromagnetic solution in the end region of a generator, including the radial air gap, the stator conductor slots and the stator core. The model developed includes a description of the three dimensional geometry, the radial cooling ducts, Pistoye slots, variations in the laminate constitution of the stator core, and the eddy currents in the laminate.

The aim of this work is to determine the relationships between the electromagnetic state of a generator and the thermal losses, both total and also local distribution, due to the induced eddy currents in the stator core. In principal, since some electromagnetic losses are inevitable, at least in conventional machines, suitable forms of cooling must be used where necessary to dissipate the induced thermal generation, and the channels incoporated in, for example, the stator through which the coolant passes, interact with the electromagnetic characteristics. It is therefore necessary to consider the cooling arrangements, together with the thermal conduction and convection treatment of the stator core and coolant, bound in with the electromagnetics. However in this paper, for simplicity and brevity, we only consider the electromagnetic problems.

2. REDUCTION OF THE BASIC FIELD EQUATIONS

The iron stator of a generator is not only a complicated geometrical shape, being basically cylindrical with axial teeth cut on the inside bore, together with radial and axial cooling ducts, Pistoye slots, etc., but it is also composed of a laminated material designed to confine the induced eddy currents to flow in planes normal to the machine axis. With existing computers it is not possible to represent the individual laminations explicitly, nor is it strictly necessary; instead in our model the laminated structure of the core is replaced by an equivalent homogeneous material with anisotropic non-linear properties. This will be considered more fully in section 7. We use cylindrical polar coordinates (r,θ,z) to describe the geometrical configuration which together with the associated simplifications will be considered in section 3.

The effect of hysteresis is ignored throughout the calculation, although as explained in section 9 the thermal generation caused by hysteresis effects can be estimated from the derived electromagnetic field solution.

We now derive the partial differential equations from the basic field equations. Within the stator core we assume that no eddy currents flow in the axial direction because of its laminated structure, so that the conservation of charge gives

$$\text{div } \underline{J}^e = \frac{1}{r}\frac{\partial}{\partial r}(r J_r^e) + \frac{1}{r}\frac{\partial J_\theta^e}{\partial \theta} = 0 . \qquad \ldots (2.1)$$

This implies that $\underline{J}^e$ can be defined by an eddy current stream function $\psi(r,\theta,z,t)$ with

$$\underline{J}^e = \hat{\underline{z}} \times (\text{grad } \psi) , \qquad \ldots (2.2)$$

where ψ can be defined to be continuous in the axial direction in accordance with the homogeneous laminated representation of the core. Maxwell's third equation gives, ignoring displacement currents, that

$$\text{curl } \underline{H} = \underline{J} . \qquad \ldots (2.3)$$

Away from the regions in which stator currents are present, using equation (2.2) this implies that

$$\hat{\underline{z}}.(\text{curl } \underline{H}) = 0 \qquad \ldots (2.4)$$

so that a magnetic scalar potential ϕ can be defined where

$$H_r = \frac{\partial \phi}{\partial r} \quad \text{and} \quad H_\theta = \frac{1}{r}\frac{\partial \phi}{\partial \theta} . \qquad \ldots (2.5)$$

By using the other two components of equation (2.3) we find that

$$\underline{H} = \text{grad}\phi - \hat{\underline{z}}\psi . \qquad \ldots (2.6)$$

[Currents in the stator bar conductors are incorporated by defining 'cuts' along specific coordinate lines which connect the conductors to the boundary and across which the magnetic potential is made discontinuous, the magnitude of the discontinuity being proportional to the stator current.] The relation (2.6) is a mathematical expression for the fact

that in addition to the magnetic scalar potential contributing to the magnetic field, the eddy currents generated in the lamination by the impinging axial flux act in a manner to reduce the magnitude of this axial flux (Lenz's Law).

The remaining Maxwell equations

$$\text{div } \underline{B} = 0 \quad \text{and} \quad \text{curl } \underline{E} = -\frac{\partial \underline{B}}{\partial t} \qquad \ldots (2.7) \text{ and } (2.8)$$

together with the constitutive relations

$$\underline{J} = \underline{\underline{\sigma}}\,\underline{E} \quad \text{and} \quad \underline{B} = \underline{\underline{\mu}}\,\underline{H} \qquad \ldots (2.9) \text{ and } (2.10)$$

give two partial differential equations for the magnetic scalar potential ϕ and the eddy current stream function ψ, namely

$$\frac{1}{r}\frac{\partial}{\partial r}\left(r\mu_r \frac{\partial \phi}{\partial r}\right) + \frac{1}{r^2}\frac{\partial}{\partial \theta}\left(\mu_\theta \frac{\partial \phi}{\partial \theta}\right) + \frac{\partial}{\partial z}\left(\mu_z \frac{\partial \phi}{\partial z}\right) = \frac{\partial}{\partial z}\left(\mu_z \psi\right) \qquad \ldots (2.11)$$

$$\text{and } \frac{1}{\gamma\sigma_r^i r}\frac{\partial}{\partial r}\left(r\frac{\partial \psi}{\partial r}\right) + \frac{1}{\gamma\sigma_\theta^i r^2}\frac{\partial^2 \psi}{\partial \theta^2} = -\mu_o \frac{\partial}{\partial t}\left(\mu_z\left(\frac{\partial \phi}{\partial z} - \psi\right)\right). \qquad \ldots (2.12)$$

We have assumed that $\underline{\underline{\mu}}$ the permeability tensor for the equivalent homogeneous material is

$$\underline{\underline{\mu}} = \mu_o \begin{bmatrix} \mu_r & 0 & 0 \\ 0 & \mu_\theta & 0 \\ 0 & 0 & \mu_z \end{bmatrix} \qquad \ldots (2.13)$$

and that the conductivity tensor $\gamma\underline{\underline{\sigma}}^i$ for this material is

$$\gamma\underline{\underline{\sigma}}^i = \gamma \begin{bmatrix} \sigma_r^i & 0 & 0 \\ 0 & \sigma_\theta^i & 0 \\ 0 & 0 & 0 \end{bmatrix} \qquad \ldots (2.14)$$

The important characteristics of equations (2.11) and (2.12) are:

(a) The electromagnetic solution in the three dimensional region is given in terms of only two quantities, ϕ and ψ, in place of the three components of the vector potential $\underline{A}$ where $\underline{B} = \nabla \times \underline{A}$, or of the magnetic field $\underline{H}$.

(b) The equation (2.11) is a second order partial differential equation with only spatial derivatives, i.e. there are no time derivatives; considering ϕ as the dependent variable, given ψ, the equation is a non-linear three dimensional Poisson type elliptic equation.

(c) The equation (2.12) is a second order partial differential equation with only two second spatial derivative terms; considering ψ as the dependent variable, given ϕ, the equation is a second order equation in the spatial variables (r,θ) and first order in the time derivative: it is a second order parabolic equation of the heat conduction form. It will be seen later (Section 7) that μ_z is almost constant in an axial plane, and hence the equation is virtually linear.

3. REPRESENTATION OF THE GEOMETRY

To obtain a reasonably tractable problem for the finite difference representation using cylindrical polar coordinates (r,θ,z) all boundaries in the problem are assumed to lie along cylindrical coordinate surfaces, i.e. they are either parts of (a) surfaces of cylinders (r = constant), or (b) planes through the machine axis (θ = constant), or (c) planes perpendicular to the machine axis (z = constant). Thus, in particular, the stator conductor slots are not parallel sided, as in reality, but lie on radial lines from the centre of the generator. A three dimensional perspective view of the region considered is shown in Fig. 1. The stator core can have a stepped end, and radial ducts and steps can be incorporated at axial nodal positions, i.e. the bore can be of variable diameter. The boundary just above the magnetic material of the rotor body can also have a varying diameter. A typical cross section along the axis is illustrated in Fig. 2. An eddy current screen at the end of the stator can be incorporated by using a stepped stator and by specifying different properties at different axial positions in the "stator". In practice the radial cooling ducts have not been modelled explicitly because of the restricted number of axial nodes. A typical cross-section normal to the axis of the machine through the stator core is shown in Fig. 3 where we have assumed that only one tooth pitch of the stator is being considered. The Pistoye slot, if present, is modelled by a line cut in the core material in a plane θ = constant, of specified axial and radial extent across which no eddy currents pass. The radial penetration of the slot can vary with axial distance. The Pistoye slot has no direct effect on the magnetic potential ϕ. The offset of the Pistoye slot from the centre of the core teeth is not explicitly

represented where this offset alternates on adjacent laminations; however the homogeneous laminated material used to represent the core means that a centrally positioned slot models the 'average' position.

Other minor and non-imperative assumptions on the geometrical configuration are described in Section 8.

4. THE TEMPORAL VARIATION-FOURIER SYNTHESIS

The magnetic scalar potential and the eddy current stream function are dependent on the three spatial coordinates (r,θ,z) and, in addition, they vary temporally since the magnetic field generated by the currents in the rotor windings rotate at the machine speed. The rate of rotation is relatively large, and we are predominantly interested in the limiting periodic behaviour of the fields when a periodic input is imposed by the rotor. An expansion in a Fourier time series is therefore used with

$$\left.\begin{matrix}\phi(\underline{x},t)\\ \psi(\underline{x},t)\end{matrix}\right\} = f(\underline{x},t) = \sum_{\substack{n=1\\ n\ \text{odd}}}^{\infty} (f_{n1}(\underline{x})\cos n\omega t + f_{n2}(\underline{x})\sin n\omega t) \ . \qquad \ldots (4.1)$$

The series is truncated after a finite number of terms: typically either only the first, or the first and third harmonics are sought. Substituting the relevant expansions of the form of (4.1) into equations (2.11) and (2.12), and then by multiplying each equation by cosnωt or sinnωt and integrating with respect to time over a period of oscillation, we obtain partial differential equations involving the Fourier components of ϕ and ψ. Considering only the first harmonic variations here, and throughout the remainder of the paper, we obtain the equations

$$\begin{aligned}&\frac{1}{r}\frac{\partial}{\partial r}\left(r(\bar{\mu}_r + \mu_{22r})\frac{\partial\phi_{11}}{\partial r}\right) + \frac{1}{r^2}\frac{\partial}{\partial\theta}\left((\bar{\mu}_\theta + \mu_{22\theta})\frac{\partial\phi_{11}}{\partial\theta}\right)\\ &\quad + \frac{\partial}{\partial z}\left((\bar{\mu}_z + \mu_{22z})\frac{\partial\phi_{11}}{\partial z}\right)\\ &\quad + \frac{1}{r}\frac{\partial}{\partial r}\left(r\mu_{21r}\frac{\partial\phi_{12}}{\partial r}\right) + \frac{1}{r^2}\frac{\partial}{\partial\theta}\left(\mu_{21\theta}\frac{\partial\phi_{12}}{\partial\theta}\right) + \frac{\partial}{\partial z}\left(\mu_{21z}\frac{\partial\phi_{12}}{\partial z}\right)\\ &\quad = \frac{\partial}{\partial z}\left((\bar{\mu}_z + \mu_{22z})\,\psi_{11} + \mu_{21z}\,\psi_{12}\right) \qquad \ldots (4.2a)\end{aligned}$$

and a similar equation (4.2b) with ϕ_{11} and ϕ_{12} interchanged, ψ_{11} and ψ_{12} interchanged and with the sign of the terms involving μ_{22}'s changed. For the stream function components we use the complex variable

$$\xi = \psi_{11} + i\psi_{12} \qquad \ldots (4.3)$$

which enables the two equations for the components to be written in compact form as

$$\frac{1}{\sigma_r}\frac{1}{r}\frac{\partial}{\partial r}\left(r\frac{\partial\xi}{\partial r}\right) + \frac{1}{\sigma_\theta}\frac{1}{r^2}\frac{\partial^2\xi}{\partial\theta^2} + i\mu_o\omega\bar{\mu}_z\gamma\xi = q + i\mu_o\omega\bar{\mu}_z\gamma\frac{\partial}{\partial z}\left(\phi_{11} + i\phi_{12}\right) \qquad \ldots (4.4)$$

$$\text{with} \quad q = \omega\gamma\mu_o\left\{(i\mu_{22z} - \mu_{21z})\left(\frac{\partial\phi_{11}}{\partial z} - \psi_{11}\right) + (i\,\mu_{21z} + \mu_{22z})\left(\frac{\partial\phi_{12}}{\partial z} - \psi_{12}\right)\right\} \qquad \ldots (4.5)$$

$$\text{where} \quad \bar{\mu}_* = \frac{\omega}{\pi}\int_o^{\pi/\omega} \mu_*(\underline{H})\,dt \qquad \ldots (4.6a)$$

$$\text{and} \quad \mu_{22*} = \frac{\omega}{\pi}\int_o^{\pi/\omega} \mu_*(\underline{H})\cos 2\omega t\,dt, \quad \mu_{21*} = \frac{\omega}{\pi}\int_o^{\pi/\omega} \mu_*(\underline{H})\sin n\omega t\,dt, \qquad \ldots (4.6b)$$

(where the * can be r, θ or z).

Note that the expressions (4.6) are the Fourier coefficients of the permeability components, and are functions of the field values $\underline{H}$. Hence the equations (4.2) and the associated equation, are grossly non-linear for typical $\underline{B} \sim \underline{H}$ relationships (see Section 8).

The equations (4.2) and (4.4) have been written in the form in which they are solved: the right hand side is regarded as a source term, and the Fourier components of the permeability are held fixed for each cycle of iterations. This iterative procedure is based on the premise that the equations for the magnetic potential and the eddy current stream function are only relatively weakly linked in most of the region under consideration, and that this linking can be relegated to a 'source' term in each equation only recalculated after each cycle of iterations.

5. BOUNDARY CONDITIONS

The external boundaries of the region considered have been selected to be those at which the values of ϕ and ψ or their gradients

are known to a good degree of accuracy: this implies that the normal or tangential component of the field must be known. However the region must be as small as possible so that the maximum resolution and accuracy can be attained consistent with the numerical solution procedure employed, and the computer available.

With reference to Fig. 4 which illustrates the region considered, the boundary conditions on the magnetic scalar potential ϕ are:

(a) $\frac{\partial\phi}{\partial z} = 0$ on the outer axial casing of the generator, ABCD.

(b) $\frac{\partial\phi}{\partial z} = 0$ at the axial 'centre' of the stator core, LMNP.

(c) $\frac{\partial\phi}{\partial r} = 0$ at the radial extremity of the core, BCNM.

[These three conditions are the mathematical expression for the boundary condition that no magnetic flux leaves these surfaces.]

(d) The potential, or its normal gradient must be specified on the rotor surface AEFLPJKD. This can be derived from models in which the rotor is treated in considerable detail, but the stator is modelled more crudely; or, alternatively, at least to a first approximation, we can assume that all the potential is lost in the radial air gap and hence derive the boundary potential given the magnitude of the radial flux entering the stator tooth.

(e) The magnetic potential on one plane (θ = constant) which bisects a stator tooth is phase displaced from that of the other mid tooth face according to the formula

$$\phi_{BMLFEA}(r,z,t) = \phi_{CNPJKD}(r,z,t - {}^{\theta_1}/\omega)$$

where θ_1 is the angle $A\hat{O}D$. This is a periodic boundary condition. (For open circuit calculations, this boundary condition is accurate when the mid planes of adjacent teeth are considered, and so only one tooth pitch need be examined, whereas on load it is strictly only correct when all the teeth within one phase band are considered.)

The boundary conditions on the eddy current stream function ψ are:

(a) $\psi = 0$ on the surfaces of the stator core parallel to the axis of the machine, namely the surfaces GMNH,UVWQ,XYZT,QQ_1R_1R,TT_1S_1S and on the base and sides of the conductor slot. Across all these surfaces, which include the Pistoye slot, no eddy currents pass.

(b) $\psi_{GMRWVU}(r,z,t) = \psi_{HNSZYX}(r,z,t - {}^{\theta_1}/\omega)$ as for (e) above.

Internal material boundaries must also be treated with care. At the boundaries between materials of different permeabilities, the tangential component of $\underline{H}$ and the normal component of $\underline{B}$ are continuous. When working in terms of the magnetic scalar potential ϕ and seeking solutions satisfying div $\underline{B} = 0$, where $\underline{B} = \underline{\mu}(\text{grad}\ \phi - \hat{z}\psi)$, these internal boundary conditions are automatically satisfied by ensuring that all boundaries are defined by nodal points.

6. THE FINITE DIFFERENCE DISCRETIZATION

In place of deriving an analytic solution to equations (4.2) and (4.4) for the Fourier components of ϕ and ψ, we characterize the variables by a finite set of values, and use finite difference methods to derive the algebraic equations for these nodal values. The nodal points used to describe the region are defined by the intersection of coordinate planes in the cylindrical polar coordinate system. With the region as shown in Fig. 1, about 18 radial nodal lines, 21 circumferential and 14 axial are used. These are spaced non-uniformly so as to obtain the greatest resolution in the regions of most interest. Thus about 5000 nodes are used, of which about one half are within the stator core. [These restrictions on the number of nodal coordinates produce a computer code which occupies less than 250 K bytes of core, which happens to be both convenient and beneficial on our computer, an IBM 370/168.]

The finite difference equations are derived from the analytic equations producing sets of difference equations for the nodal values of the variables ϕ_{11},ϕ_{12},ψ_{11} and ψ_{12}. (Note that the eddy current stream function is only defined in the stator core region.) The coefficients of the difference equations for the potential components depend on the local values of the permeability, and have therefore to be recalculated after each cycle of iterations.

7. THE HOMOGENEOUS LAMINATE REPRESENTATION

The differential equations (4.2) and (4.4) require knowledge of the values of the Fourier components of the vector components of permeability. If we assume that $\mu_r = \mu_\theta$ (see Section 8), then the transverse permeability μ_r and the axial permeability μ_z of the laminated core must be related to the field magnitude in the core material. However the D.C. saturation characteristics of the core plate iron are generally

known, not those of the laminated material. The magnitude of the magnetic field in the iron is related to the vector components by

$$(H^i)^2 = (H_r^i)^2 + (H_\theta^i)^2 + (H_z^i)^2 . \quad \ldots (7.1)$$

The transverse field in the iron is equal to the transverse field in the equivalent homogeneous material ($H_r^i = H_r$, $H_\theta^i = H_\theta$), ... (7.2)
but in the axial direction, across the laminations, the magnetic flux density is continuous so that $\mu^i H_z^i = \mu_z H_z$. ... (7.3)

From the definition of the stacking factor

$$1/\mu_z = 1 - \gamma + \gamma/\mu^i \quad \text{and} \quad \mu_\theta = \mu_r = \gamma\mu^i + (1-\gamma) \quad \ldots (7.4)$$

so that $$H_z^i = \frac{H_z}{\gamma + (1-\gamma)\mu^i} . \quad \ldots (7.5)$$

If a specified saturation relation between μ^i and the magnitude of $\underline{H}^i$ is used (see Section 8), the equations can be formed into an iterative procedure for H^i and μ^i given H_r, H_θ and H_z. The permeability components μ_r, μ_θ, μ_z of the equivalent material are then derived from equations (7.4).

8. FURTHER APPROXIMATIONS

To facilitate the derivation of the difference equations, and their subsequent solution, several further approximations listed below are used. None of these is essential, and given the facilities to run larger computer programs, they could all be relaxed.

(a) $\mu_r = \mu_\theta$ This simplification models a non-grain orientated core plate, and can easily be relaxed at the expense of increased computer run time.

(b) $\mu^i = \mu_1 + \dfrac{\mu_2}{1 + |\underline{H}^i|/H_o}$ Namely the D.C. permeability in the iron comprising the laminated core is related to the instantaneous magnitude of the local magnetic field by a Fröhlich law with the addition of a constant. This algebraic relationship can be fitted to the $\underline{B} \sim \underline{H}$ curves of most core plate iron with a reasonable degree of accuracy. Being algebraic, it is easily evaluated on the computer which has to be done very frequently since the Fourier components of the A.C. permeability are taken as the weighted integrated averages (expressions 4.6) over a cycle. In fact to save computation, the latter integrals can be approximated analytically given the above permeability relationship for the first few iterations.

(c) The separate core plate sections which make up the core are not modelled explicitly, so that the butt joints between them, and the eddy current circuit closures are not modelled.

(d) The radial cooling ducts and any magnetically transparent laminations are not explicitly incorporated because of the restriction on the number of axial coordinate positions. Instead they are implicitly incorporated by suitable adjustments to the axial stacking factor. Their effect is therefore spread over a portion of the core.

(e) The axial cooling ducts are not modelled in the electromagnetic computer codes.

(f) Tooth wedge notches and other small geometrical non-uniformities are not included in the electromagnetic solution.

Both the features (e) and (f) could be included at the expense of program complexity.

(g) At present, the generator is only being considered in open circuit mode. Thus the stator current bars and end connections are not modelled, and, in addition, the periodic boundary conditions on both ϕ and ψ can be accurately applied to adjacent teeth, thus only one tooth pitch is considered. On load conditions can be considered by including the model of the stator conductors and end conditions described in Section 2.

9. THE NUMERICAL SOLUTION PROCEDURE

The finite difference equations are solved in as implicit a form as possible, that is in the equations (4.2) and (4.4) only the terms on the right hand side are calculated with the values of ϕ and ψ from the old iterative solution, except for the Fourier components of the permeability.

To proceed from one solution (ϕ^n, ψ^n) the following steps are followed:

(i) Derive the required Fourier components of the permeability components throughout the iron from the local value of the magnetic field vector and the permeability law.

(ii) Calculate the 'source' terms (the right hand sides) of equations (4.2) and (4.4) at each nodal point.

(iii) Determine a new solution to the magnetic potential, ϕ^{n+1} to a reasonable degree of accuracy.

(iv) Determine a new solution to the eddy current stream function ψ^{n+1} to a reasonable degree of accuracy.

The cycle (i)-(iv) is then repeated until convergence.

The iterative procedure used for steps (iii) and (iv) has been selected to be that most suited to the geometry of the region (which is relatively very thin in the circumferential direction compared to typical radial and axial distances, and this non-uniformity is even further accentuated by the anisotropic permeability), and to the boundary conditions (in particular the periodic boundary conditions which relate the values of the dependent variables at the extremities of circular arcs): namely a line iterative technique, with the implicit lines of nodal points taken as arcs of circles. The subsystems of equations comprising the pairs of algebraic equations for the two Fourier components of each variable ϕ and ψ for the nodes which lie on one such arc are solved simultaneously. This ensures that the periodic boundary conditions are satisfied exactly. An acceleration parameter is used, and new values are used as soon as they are available in all subsequent calculations. Because ϕ_{11} and ϕ_{12} do not have the same differential operator on the left hand side of equations (4.2a) and (4.2b) (the sign of the μ_{22} components are opposite in the two equations), the solution for the components of the potential requires the inversion of a nine diagonal matrix. Whereas for the stream function, we can work with the complex variable ξ and for which the inversion of a tri-diagonal matrix with the additional terms representing the periodic boundary conditions is only required.

It is difficult to optimise the iterative acceleration parameters, especially those for the potential ϕ, because of the non-linear form of the equations. Many accleration devices are also incorporated to enhance the rate of convergence.

Typically one starts with a reasonably good initial approximation, or from the previous solution with different geometry, etc., on backing store in the computer. A subsequent solution can then be obtained in about 3 to 5 minutes on an IBM 370/168 computer. The program derives the values of ϕ and ψ at the nodal points of the grid, and these are then transferred to backing store. A second program processes these results and calculates the vector components of the magnetic field, of the magnetic flux density, of the eddy currents, and from the latter, the rate of thermal generation in the stator core can be determined. The thermal generation caused by hysteresis effects can be calculated from an empirical expression (Steel, 1974) involving the magnitude of the transverse magnetic field. A third program comprises a heat conduction calculation of the core, using the thermal generation rates previously obtained. A finer grid is used for this purpose, and, of course, radial cooling ducts, axial cooling ducts, and tooth wedges, etc., are all modelled. This program gives the temperature at up to 10000 nodal points per packet, a packet comprising those laminations between two radial cooling ducts.

10. VALIDATION OF THE NUMERICAL MODEL

A comprehensive series of investigations has been made with the programs to ensure satisfactory operation. The electromagnetic solution procedure has been used to solve several problems in which a known analytic solution was sought, for example the derivation of two dimensional (r,θ) magnetic fields in a pair of adjacent annuli with known, but different, permeabilities. Subsequently the results have been compared with measured variations on 500 MW generators on open circuit test. The results (which are to be reported elsewhere) indicate acceptably good agreement considering the simple boundary condition imposed on the rotor surface, namely zero axial field and the potential calculated to produce the necessary radial magnetic flux in the centre of the generator and assuming that all the potential is lost in the radial air gap. Typical results will not be discussed here since they also will be described elsewhere; instead some of the salient features already resulting from our investigations are described; other investigations yet to be made will be detailed. They indicate the great generality and versatility of the method, and the increased understanding which the results produce.

11. SOME RESULTS OBTAINED, INVESTIGATIONS TO FOLLOW

One of the purposes of this programme of work has been to increase our understanding of the factors determining the variations in thermal generation in large generators, and several investigations have already been made with regard to the Pistoye slot length, both radial depth and axial extent, and variations in stacking factor. The results to be described were derived for geometry typical of 500 MW generators. Only open circuit conditions have been considered, and the stator end screen has not been modelled.

It is evident, for example, from the results obtained so far that the Pistoye slot is an important feature in predicting the thermal generation rate. These subdivide the laminated area in the stator tooth, typically, into two parts in which the eddy currents can circulate. The

magnitude of these currents are therefore reduced, and the results demonstrate this. However, because the eddy currents are reduced, so the axial flux is allowed to penetrate further. (The Pistoye slots need not necessarily be in the centre of the tooth, nor need they extend radially to the base of the conductor slot, they could extend further, or less far, or they could be of varying length. However, here we only consider the simple case in which they divide the tooth into two equal parts.) At some point axially the Pistoye slots are not cut in the laminations (unless they extend the whole axial length of the machine) and at that point, if any axial flux is still present, there is bound to be an increased thermal generation because of the enlarged eddy current circulations, all other things remaining unchanged. The program can, and has, been used to estimate the magnitude of this increase for various configurations.

Test results have been obtained with different configurations of radial cooling ducts. Their effect on the electromagnetic solution has been through the stacking factor which is decreased to model the ducting arrangement; the presence of the air is thus smeared out over an axial interval. Thus the amount of core plate is reduced, and it is therefore to be expected, and this has been verified, that the thermal generation rates decrease. Temperature calculations show these effects are generally amplified since the cooling efficiency is enhanced. The inclusion of asbestos laminations carrying instrumentation in the core plate has also been demonstrated to have significant effects on the thermal generation.

These examples are just a brief illustration of the type of results which can be derived from our model.

Planned future investigations include on-load calculations, calculations with radial cooling ducts included explicitly, the effect of axial cooling ducts, stepped stator ends, end screen designs, etc. As computers increase in size and more detailed investigations are sought, it is envisaged that the program will be enlarged to incorporate many additional details.

12. ACKNOWLEDGEMENTS

The development of the work described in this paper owes much to the invaluable contributions by Dr C.J. Myerscough, Dr M.L.J. Rollason and Mr J.G. Steel, and the programming has been assisted by Mrs M.E. Down, Mrs J. Linn and Mr P. Rutter.

The work was carried out at the Central Electricity Research Laboratories and the paper is published by permission of the Central Electricity Generating Board.

13. REFERENCE

Steel, J.G., 1974, 'Soft Magnetic Materials in Large Turbo-Alternators', Trans. I.E.E.E. MAG-10 (2) pp. 151-154.

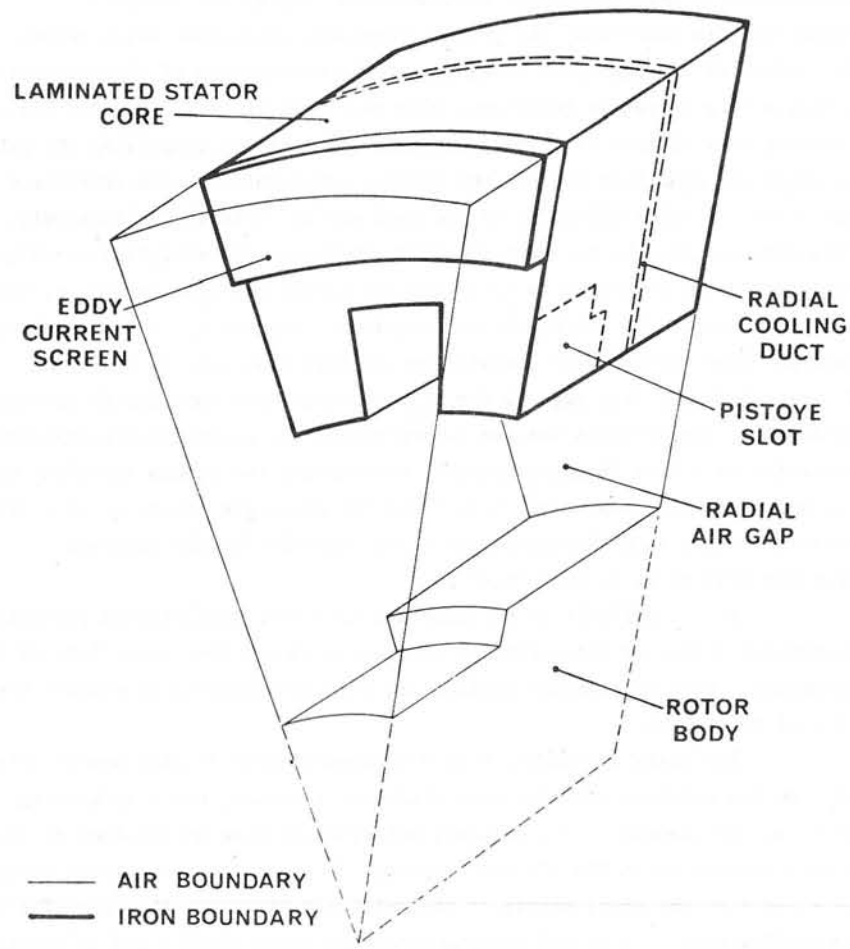

FIG1 A PERSPECTIVE VIEW OF THE REGION IN WHICH THE ELECTROMAGNETIC FIELD SOLUTION IS SOUGHT (THE STATOR AND ROTOR CONDUCTORS ARE NOT SHOWN)

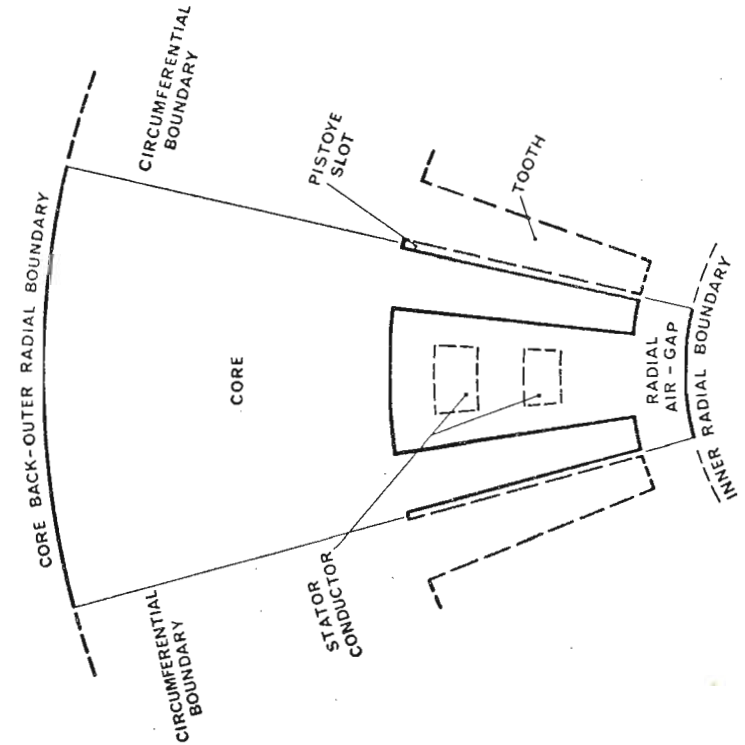

FIG3 CROSS SECTION NORMAL TO THE ROTOR AXIS OF THE REGION CONSIDERED (THROUGH THE STATOR CORE)

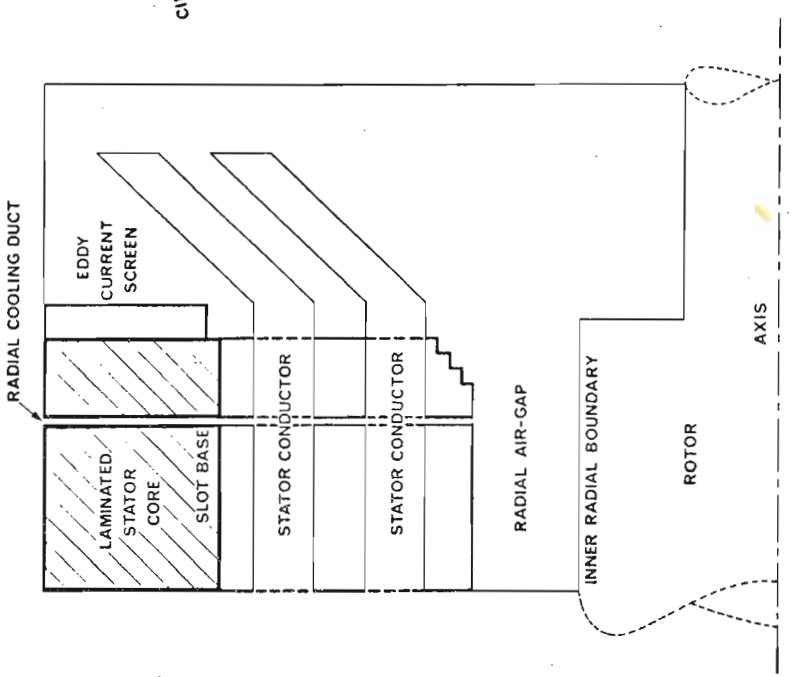

FIG2 CROSS SECTION THROUGH THE ROTOR AXIS AND THE CENTRE OF A STATOR SLOT

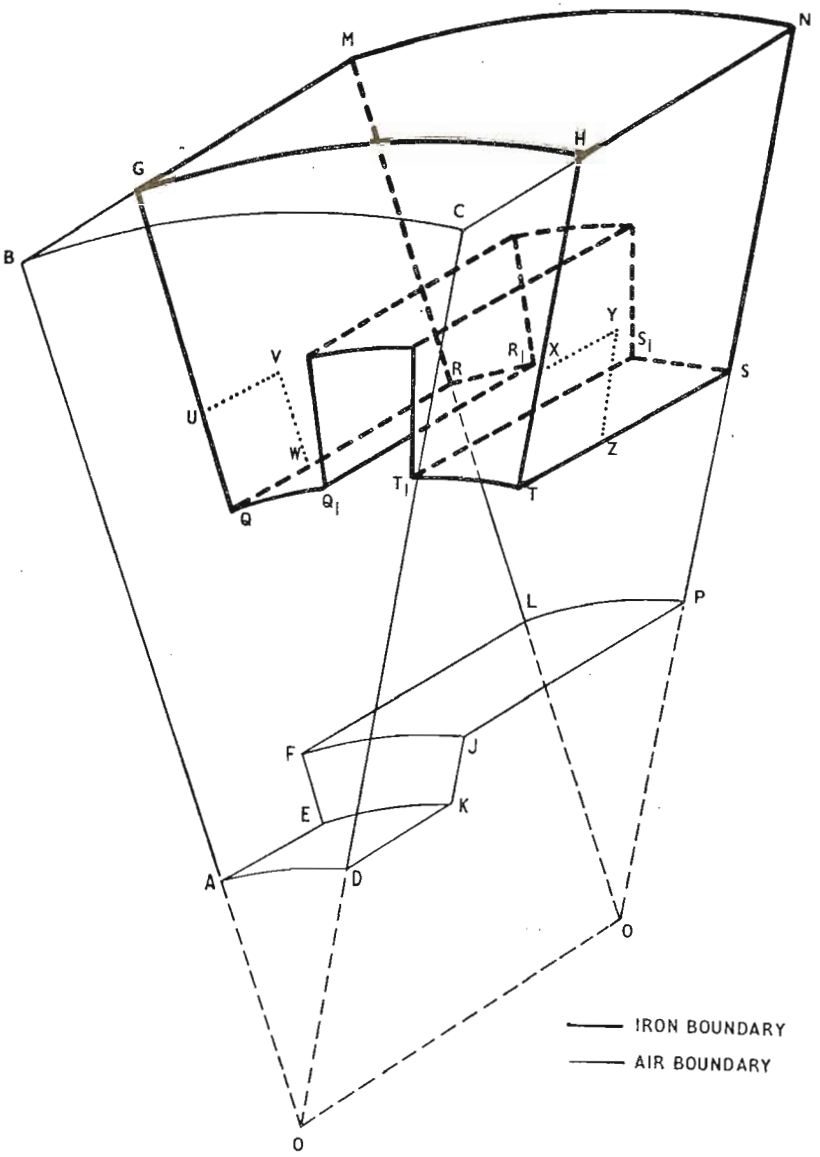

FIG.4 REGION OF THE GENERATOR IN WHICH THE FIELD SOLUTION IS SOUGHT

Discussions following paper:

(Trowbridge) Will you comment on the use of your program for 3D conductor regins ie when there are no constraints on the direction of current flow.

(Jacobs) Such a problem would require additional dependent variables if one is going to consider eddy currents flowing in all three directions and not confined to laminations. Concerning three dimensional conductors these will be included in the next version of the program to be released which is now in an advanced stage of development. There are no inherent difficulties foreseen, and a method similar to that described by Dr Carpenter earlier is being used.

(Ratti, Univ Rome) The author has presented a nice piece of work, for which he must be congratulated.

On these two points we would like to have more detailed information:

(a) The check of convergence is one of the various refinements spoken of by the Author, to reduce the run time: how is this check achieved and what are the benefits obtained?

(b) The program is said to be expensive (something which is rarely recognised by research workers): can the author compare the cost with other methods and/or with the overall cost of the machine under investigation?

(Jacobs) (a) The primary initial check on the rate of convergence is based on the normalized residual and the maximum percentage charge actually applied at any point of the grid. Subsequently we compare the results from such a "well-converged" solution with one for which a further significant set of iterations have been used. As we proceed with the iteration those lines for which convergence is satisfied are not considered again for several further iterations thus saving computation. The fields, fluxes and thermal generation rates often seem to be "better" converged than the potential.

(b) Compared with typical computer programs it seems expensive; but it is not a typical program! A generator costs the order of £10^6 and replacement costs for a 660 Mw machine per day are substantially more than the cost of running our IBM 370/168 computer for a day. They are therefore cheap in that sense.

(Reece, GEC) The work described assumes that the density on the rotor surface is known. When both conductors are studied, with the need to represent both stator and rotor current effects, what is the procedure proposed and what will be the effect on computation time and cost?

(Jacobs) In order to include both rotor and stator conductors, we are developing another program similar to that described by Mr Preston earlier today in which the circumferential variation is treated as a Fourier series and thereby reduce the problem to two space dimensions and time. We will ignore eddy currents in the stator initially at least, and from the imposed stator and rotor conductors and the phase difference between them we will derive the scalar potential on the rotor surface. This will be in the form of circumferential harmonics which will then be used as the boundary condition or the inner radial boundary in the three space dimensional problem.

The determination of magnetic fields in power transformers

by

P.B.Johns,M.Sc.,Ph.D.,C.Eng.,MIEE, A.Wright,Ph.D.,D.Sc.,C.Eng.,FIEE
and J.E.Sitch,B.A.,M.Eng.,Ph.D.
of the University of Nottingham.

1. Introduction

There are many situations where designers must assess the densities of magnetic and/or electric fields. As an example, it is necessary to determine the mechanical forces which may be exerted on the windings of large power transformers. These forces may reach very high levels during system fault conditions and they must be assessed with reasonable accuracy so that the windings may be braced to withstand them. Clearly the forces can be readily determined by calculating the magnetic flux densities at the positions of the individual conductors for various operating conditions.

There are a considerable number of possible numerical methods which may be used for tackling dynamic magnetic problems of this type and in particular there are several well-developed finite-difference routines for solving both transient and steady state eddy-current problems in two dimensions[1]. One of the difficulties encountered, especially with transient analyses, centres around the stability of the method. The fastest finite-difference routines are those which are explicit but they are inherently unstable for large time steps. Implicit finite-difference routines, whilst stable, can require an unacceptable amount of computation.

Recently a method in which the space to be considered is assumed to contain a matrix of transmission lines (TLM method) has been developed for use in communication studies. The method is explicit and also unconditionally stable. The purpose of this paper is to describe the TLM method and show how it may be used to deal with power-frequency problems such as that referred to above.

2. Transmission line modelling of fields

In the TLM method a region to be studied is divided into a mesh of equal-sized volumes, or areas in the case of two-dimensional problems, and a corresponding matrix of loss-free transmission lines, which are appropriately interconnected at their junctions, is assumed to exist.

For a two-dimensional study, four transmission lines are assumed to meet at the mid-points of each of the elements in the mesh as shown in Fig.1. All lines associated with mesh elements in a particular uniform medium have the same propagation velocity and characteristic impedance, proportional to $(\mu\varepsilon)^{-0.5}$ and $(\mu/\varepsilon)^{0.5}$ respectively. For a medium of infinite permeability the propagation velocity would be zero and the characteristic impedance infinite, which implies that currents would not flow into any transmission lines used to represent such a region and open circuits could therefore be placed at its boundaries. This representation is clearly correct because H fields could not be set up in an infinitely permeable material.

The network of lines is excited by launching ideal delta functions (impulses) into it at appropriate points and these travel along the lines until they reach junctions or nodes. Scattering processes then take place and the scattered pulses travel on to neighbouring nodes. A numerical routine must be employed to keep track of the impulses and scattering processes in a somewhat similar manner to that which is used in the Bewley Lattice diagram when actual transmission lines are studied.

If the model was completely loss free, the pulses would not be damped and permanent oscillatory conditions would be set up. Considering the transformer problem as an example it is clear that eddy currents would flow in conducting material in the window due to the changing magnetic field and there would be a resultant power loss. Similarly any conductors forming a winding connected to a load would carry current, leading to the dissipation of power and damping. It could therefore be considered that the window space contains a lossy dielectric. Difficulties would be introduced if allowance was made for this by assuming lines with distributed conductance (G) because of the distortion of the pulses which would result. This may be overcome however if the mesh is fine enough by including lumped conductances at the junctions of the lines as shown in Fig.2. In practice the conductors and dielectric are not uniformly distributed across the window space and allowance may be made for this by including shunt conductances (G) at the appropriate nodes. In many problems the values assigned to these conductances may be made artificially high to increase the damping and accelerate the computations.

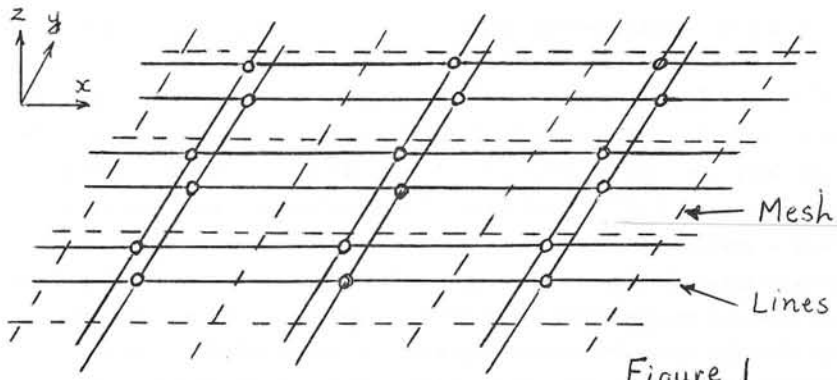

Figure 1

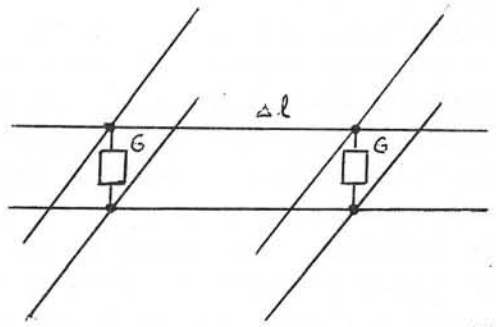

Figure 2

If fields set up by direct currents are to be determined then the input pulses to the model should be maintained constant and the phenomena by which the fields are set up in spaces are being correctly modelled. This process may be done in real time. When fields set up by time varying currents are to be calculated however it may be necessary to introduce time-scaling because the actual time needed to propagate a flux wave across a space will be so short relative to the period of the input signal that an extremely large number of time steps would have to be used to obtain a solution. This topic is dealt with in more detail later.

2.1. Inputs to model

To determine the magnetic fields set up when currents are driven into certain conductors, e.g. into the primary-winding conductors of a transformer, pulses of current are injected into the appropriate elements of the mesh. The magnitude of the pulse injected into any element, at any instant, is made equal to the m.m.f. provided by the conductors in the element at the instant, i.e. the total current flowing into the element. Scattering of the pulses then proceeds as described in the next section.

2.2. Scattering process in a two dimensional space

At a node with no shunt conductance an incoming current wave on one line sees the three other lines in parallel and consequently the reflection coefficient (R) is given by :-

$$R = \frac{3Y_o - Y_o}{3Y_o + Y_o} = 0{\cdot}5$$

where Y_o (= $1/Z_o$) is the characteristic admittance of each line.

The transmission coefficient (T) to each of the three parallel output lines is :-

$$T = \frac{-2 \times 3Y_o}{3(3Y_o + Y_o)} = -0{\cdot}5$$

The above expressions are based on the convention that currents flowing towards a node are regarded as positive.

When a shunt conductance of GY_o is present at a function the reflection and transmission coefficients are then modified to :-

$$R = \frac{Y_o(3 + G) - Y_o}{Y_o(3 + G) + Y_o} = \frac{2 + G}{4 + G}$$

$$\text{and } T = \frac{-2Y_o}{Y_o(3 + G) + Y_o} = \frac{-2}{4 + G}$$

If the conductors in the window are connected to an external source or load the currents flowing in them depend on external factors as well as the material parameters. The type of node used in this case has a current generator connected across the junction as shown in Fig.3. Any shunt conductance is effectively in series with the current source and may therefore be ignored in the scattering equations. The resulting outgoing waves ($b_1 \rightarrow b_4$) are given by expressions of the form

$$b_1 = Ra_1 + Ta_2 + Ta_3 + Ta_4 - \frac{I}{4}$$

$$b_2 = Ta_1 + Ra_2 + Ta_3 + Ta_4 - \frac{I}{4}$$

in which $a_1 \rightarrow a_4$ are the incoming waves to the node.

It is shown in Appendix 1 that the above procedure accurately models Maxwell's equations.

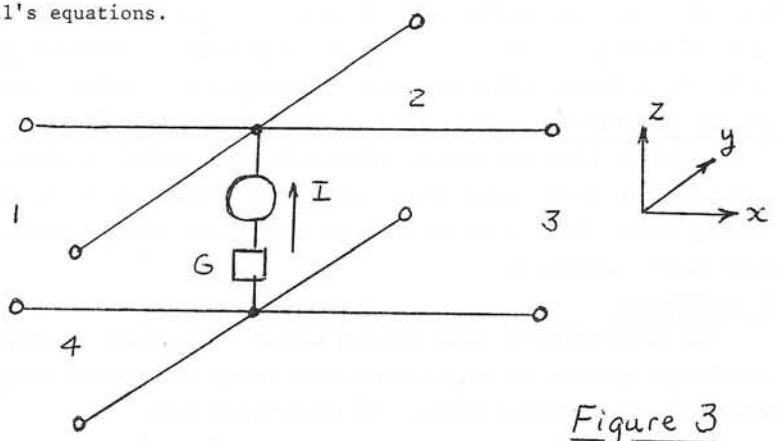

Figure 3

2.3. Time scaling

When dealing with direct current conditions it is possible as in microwave studies to calculate in real time. When solving behaviour obtained with power-frequency inputs however, the number of time steps involved would be excessive. This can readily be seen from the following illustration. For a mesh with 1 cm centres the time steps would have to be $(3 \times 10^{10})^{-1}$s assuming propagation to be at the velocity of light and to calculate 40 ms of real time, i.e. 2 cycles, would require $1{\cdot}2 \times 10^{9}$ steps.

This situation can be avoided by assuming high values of permeability and permittivity for the medium and thus artificially reducing the propagation velocity. To keep the levels of the travelling waves of current and voltage unchanged the characteristic impedance, which is proportional to $(\mu/\varepsilon)^{0{\cdot}5}$, should be maintained constant. It will be seen therefore that if μ and ε are multiplied by the same factor k, time steps may be increased by the same factor.

It must be realised that this change has the effect of increasing the displacement currents in steady state because of the increased shunt capacitances of the transmission lines and as a result they do not bear the correct relationships to the conduction currents. In practice however the displacement currents in power-frequency problems are extremely small relative to the conduction currents and they can be increased by several orders of magnitude without becoming sufficiently large relative to the conduction currents to cause significant errors in computing magnetic field distributions. An indication of these effects is given in the later sections dealing with actual calculated values.

3. Power transformer studies

While the TLM method can be applied to three-dimensional problems initial studies of power transformer magnetic fields have been done on a two-dimensional basis. It was assumed that the transformer had an infinitely permeable core surrounding a rectangular window through which the conductors of the primary and secondary windings passed. It was thus necessary to divide the window area into a mesh of square elements with transmission lines between their centres. At the boundary of the window the lines were terminated in open circuits.

In practice one of the windings may be tapped to allow the transformation ratios to be varied and in these circumstances some of the conductors might not be carrying current at particular times. To allow complete generality the model was therefore arranged with input impulse currents at each of the nodes where primary winding conductors are present. At any instant each of these currents is made equal to the ampere conductors (ampere turns) present in the particular element of the mesh. As stated earlier each of the secondary winding conductors must carry the same current because of the series connection of the turns. This result would not be obtained by connecting equal conductances across each of the nodes at the positions of the secondary winding conductors, because of the different voltages which appear across the nodes. In the model therefore it is necessary to include a path at each of these nodes through which flows a current equal to the product of the sum of the voltages across the nodes and the conductance of the secondary winding and load. In addition, conductances may be included in parallel with these current paths to allow for eddy currents within the conductors.

The computation proceeds by injecting the appropriate current impulses at each particular time step and taking account of the currents present because of the impulses injected at earlier time steps. In this way the complete current pattern is determined for each time step and the program runs until the changes over a time step are below a particular level in the case of d.c. problems or until repetetive behaviour is obtained in a.c. steady-state studies.

3.1. D.C. Magnetic field calculations

In these examples, time only enters into the problem as a means of proceeding to a solution; although the time taken to reach a steady state may be of some interest to designers of pulse-transformers, the time scaling in these examples has been chosen to ensure the fastest possible convergence rather than accurate modelling of transients. All the results shown here are in windows in an infinitely permeable medium. The first example is of a situation where the individual conductors are smaller in cross section than the mesh size, consequently the current in each element is easily defined. Tables 1, 2 and 3 show the current density and H-field profiles for this model. Part of the "primary" is unexcited to simulate the effect of using a tapped winding. We may check the results by integrating H.dℓ along rectangular paths, this indicates errors of less than 0·5%, due to incomplete convergence. In this model mesh size is not fixed by any external consideration, the current density is in units of $A/\Delta\ell^2$ and $H.\Delta\ell$ is printed out for the H-field, this easy spatial scaling only applies to D.C. models. The second example is a window with comparatively large conductors. The primary winding is driven from a voltage source and the secondary drives a resistive load. In the steady D.C. state the current density is constant across the conductor; the results presented below Tables 4, 5 and 6 were obtained after 300 iterations, the solution is within 1% of its steady value after 200 iterations.

3.2. Transient calculations

These are very similar to the D.C. computations with the exception that the time evolution of the solution is now of interest. Tables 7 and 8 show the build-up of H-field in a window filled with short-circuited windings. The units of time are seconds for a mesh size of 0.1 m.

The tables are drawn for different time scalings table 7 has c "slowed down" to 0·0707 m sec^{-1} while in table 8 the modified propagation velocity is 0·707 m sec^{-1}. The agreement between the results shows that if the problem is correctly specified the use of time scaling can result in economical transient models.

3.3. A.C. models

To date A.C. modelling has been restricted to the time domain, although steady-state modelling is also possible. The primary voltage is input as a function of time and the primary and secondary currents, and secondary voltage are found as functions of time. If the time-scaling is done correctly, the displacement current may be kept to a small fraction of the conduction current, and although this means the transmission line matrix is no longer critically damped, convergence to within a few percent is achieved in about 500 time steps for the 9 x 9 element model.

The leakage reactance may be computed from the model, it increases in size relative to the copper resistance as the inverse of the velocity scaling ratio. Thus it is possible to compute the leakage reactance under fault conditions.

4. Conclusions

The feasibility of using the TLM method to calculate the fields in transformer windows has been demonstrated by the preliminary results which have been obtained using a two-dimensional mesh.

The method models the way in which the fields build up and steady-state behaviour is approached through the transient conditions. Although time scaling is necessary in dealing with power-frequency problems it has been shown that this may be done with acceptable accuracy and the method provides an explicit and unconditionally stable routine. This is thought to be unique and of considerable importance.

The method may be extended to deal with non-uniform media and three-dimensional meshes.

5. Acknowledgements

Dr. Johns is spending a year on sabbatical leave at the University of Manitoba. He wishes to thank Dr. A. Wexler for the many interesting discussions on this and like topics, and the Department of Electrical Engineering for their hospitality.

Thanks are also due to Dr. S. Akhtarzad of the University of Nottingham for helpful comments on this paper and to the University of Nottingham for facilities made available during its preparation.

6. References

1. R. L. Stoll, 'The analysis of eddy currents', Clarendon Press, Oxford, 1974.
2. M. Djurovic and C. J. Carpenter, '3-dimensional computation of transformer leakage fields and associated losses', Trans. I.E.E.E., Mag-11, 5, p.1535-1537, September 1975.
3. S. Akhtarzad and P. B. Johns, 'Three-dimensional TLM computer analysis of microstrip resonators', Trans. I.E.E.E., MTT-23, 12, p.990-997, December 1975.

4. C. J. Carpenter and M. Djurovic, 'Three-dimensional numerical solution of eddy currents in thin plates', Proc. IEE, Vol.122, No.6, p.681-688, June 1975.

5. S. Akhtarzad and P. B. Johns, 'Generalised elements for the TLM method of numerical analysis', Proc. IEE, Vol.122, No.12, p.1349-1352, December 1975.

6. P. B. Johns, 'The solution of inhomogeneous waveguide problems using a transmission-line matrix, Trans IEEE, MTT-22, 3, p.209-215, March 1974.

7. S. Akhtarzad and P. B. Johns, 'The solution of Maxwell's equations in three space dimensions and time by the TLM method of numerical analysis', Proc. IEE, Vol.122, No.12, p.1344-1348, December 1975.

8. G. F. Slater, 'The use of finite transmission-line elements in numerical analysis', Ph.D. thesis, Nottingham University, 1973.

7. Appendices

Appendix 1. Modelling Equations

Consider an element, such as the one shown in Fig.A.1.

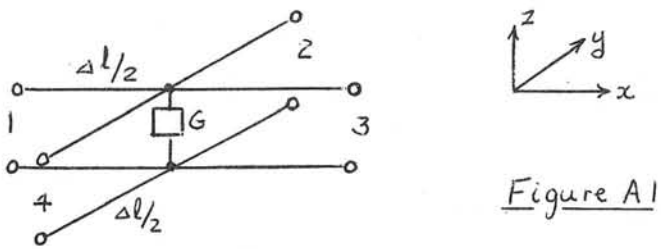

Figure A1

The incident current wave at port 1 is denoted by $a_1(t)$, while the scattered wave is $b_1(t)$. The voltage across the junction may be expressed in terms of the ingoing waves :-

$$V_c(t + \tfrac{\tau}{2}) = -(a_1(t) + a_2(t) + a_3(t) + a_4(t)).T.Z$$

where $\tau = \frac{\Delta\ell}{v}$, the time step.

It may also be expressed as a function of the outgoing waves

$$V_c(t = \tfrac{\tau}{2}) = -(b_1(t) + b_2(t) + b_3(t) + b_4(t)) \frac{T}{R+3T} .Z$$

Now

$$\frac{T}{R+3T} = \frac{2}{4-G}$$

These two equations may be combined to give :-

$$2(V_c(t + \tfrac{\tau}{2}) - V_c(t - \tfrac{\tau}{2})) + \frac{G}{2}(V_c(t + \tfrac{\tau}{2}) + V_c(t - \tfrac{\tau}{2}))$$

$$= (a_1(t) + b_1(t) + a_2(t) + b_2(t) + a_3(t) + b_3(t) + a_4(t) + b_4(t))Z$$

This simplifies to

$$2\tau \frac{\partial V_c(t)}{\partial t} + GV_c(t) = Z\,\Delta\ell\,(-\frac{\partial I_x}{\partial x} - \frac{\partial I_y}{\partial y})$$

$$\frac{2}{vZ}\frac{\partial V_c}{\partial t} + \frac{G}{\Delta\ell Z}V_c = -\frac{\partial I_x}{\partial x} - \frac{\partial I_y}{\partial y}$$

So setting

$$\frac{2}{vZ} \equiv \epsilon,\ \frac{G}{\Delta\ell.Z} \equiv \sigma,\ V_c \equiv E_z/\Delta_z,\ I_y \equiv Hx.\Delta\ell,\ I_x \equiv -H_y.\Delta\ell$$

where $\Delta x = \Delta_y = \Delta\ell$, the space step and $\Delta z = 1m$, we obtain the magnetic circuit law assuming no external electric sources or sinks.

At a point where there is a conductor connected to an external circuit the node has a current generator connected across it, and the following equations apply :-

$$V_c(t + \tfrac{\tau}{2}) = (\tfrac{1}{2}(a_1(t) + a_2(t) + a_3(t) + a_4(t)) + \tfrac{I}{4}(t - \tfrac{\tau}{2}))Z$$

$$V_c(t - \tfrac{\tau}{2}) = -(\tfrac{1}{2}(b_1(t) + b_2(t) + b_3(t) + b_4(t)) + \tfrac{I}{4}(t - \tfrac{\tau}{2}))Z$$

$$\frac{2}{vZ}\frac{\partial V_c}{\partial t} - \frac{I}{\Delta\ell} = -\frac{\partial I_x}{\partial x} - \frac{\partial I_y}{\partial y}$$

So we may set $-\frac{I}{\Delta\ell} \equiv Jz$ to obtain the general magnetic circuit law.

Similarly we may compute the currents at an intersection

$$I_x(t + \tfrac{\tau}{2}) = \tfrac{1}{2}(a_1(t) + b_1(t + \tau) - a_3(t) - b_3(t + \tau))$$

Substituting for the reflected waves (1 + T - R = 2) :-

$$I_x(t = \tfrac{\tau}{2}) = (a_1(t) - a_3(t))$$

Also

$$I_x(t - \tfrac{\tau}{2}) = (-b_1(t) + b_3(t))$$

Using central differences we may combine these two equations to yield :-

$$(I_x(t - \tfrac{\tau}{2}) - I_x(t + \tfrac{\tau}{2})) = (a_3(t) - b_3(t)) - (a_1(t) - b_1(t))$$

$$- \frac{\partial I_x}{\partial t} \cdot \frac{Z}{v} = \frac{\partial V}{\partial x}$$

So with the same equivalents as before and with $\frac{Z}{v} \equiv \mu$, we get the law of electromagnetic induction.

Combining our equations together we may obtain expressions for the characteristic impedance and velocity of propagation of the transmission lines in the matrix in terms of the characteristic impedance of the medium and the velocity of electromagnetic propagation within the medium

$$Z = \sqrt{2}\, Z_o = \sqrt{\frac{2\mu}{\varepsilon}}$$

$$v = \sqrt{2}\, c = \sqrt{\frac{2}{\mu\varepsilon}}$$

Appendix 2. Time scaling

We wish to keep the magnetic relaxation time ($\tau_m = \sigma.\mu$) constant, but vary σ and μ to reduce the propagation velocity. Denoting time-scaled quantities by a prime we may write :-

$$\tau_m = \sigma.\mu = \sigma'.\mu'$$

$$\mu' = \mu \left(\frac{c}{c'}\right)^2 , \quad \sigma' = \sigma \left(\frac{c'}{c}\right)^2$$

$$Z_o' = Z_o \frac{c}{c'}$$

Now we require $\sigma' >> \omega\varepsilon$ which means $c' >> \sqrt{\frac{\omega\varepsilon}{\sigma}} \cdot c$

For copper ($\omega = 2.\pi.50$ radians $sec.^{-1}$ $\varepsilon = \varepsilon_o$, $\sigma = 5.8 \times 10^7$ S m^{-1}, $c = 3 \times 10^8$ m sec^{-1}) we obtain

$$c' >> 2.07 \text{ m sec}^{-1}.$$

Table 1. Jz

1·0	1·0	1·0	1·0	-0·733	-0·733	-0·733	-0·733	-0·733
1·0	1·0	1·0	1·0	-0·733	-0·733	-0·733	-0·733	-0·733
1·0	1·0	1·0	1·0	-0·733	-0·733	-0·733	-0·733	-0·733
1·0	1·0	1·0	1·0	-0·733	-0·733	-0·733	-0·733	-0·733
1·0	1·0	1·0	1·0	-0·733	-0·733	-0·733	-0·733	-0·733
1·0	1·0	1·0	1·0	-0·733	-0·733	-0·733	-0·733	-0·733
1·0	1·0	1·0	0	-0·733	-0·733	-0·733	-0·733	-0·733
1·0	1·0	1·0	0	-0·733	-0·733	-0·733	-0·733	-0·733
1·0	1·0	1·0	0	-0·733	-0·733	-0·733	-0·733	-0·733

Table 2. Hx

-·023	-·023	-·023	-·022	-·020	-·018	-·016	-·014	-·013
-·064	-·065	-·066	-·066	-·061	-·054	-·047	-·042	-·039
-·101	-·105	-·111	-·112	-·103	-·090	-·077	-·067	-·062
-·137	-·147	-·161	-·170	-·151	-·126	-·103	-·087	-·079
-·167	-·185	-·220	-·255	-·207	-·158	-·122	-·100	-·089
-·176	-·206	-·276	-·425	-·263	-·177	-·128	-·100	-·088
-·153	-·183	-·253	-·402	-·242	-·159	-·112	-·086	-·075
-·103	-·120	-·154	-·190	-·146	-·104	-·075	-·058	-·050
-·036	-·042	-·051	-·058	-·048	-·036	-·026	-·020	-·018

Table 3. Hy

-·479	-1·437	-2·394	-3·351	-3·443	-2·671	-1·904	-1·141	-·380
-·479	-1·437	-2·393	-3·348	-3·438	-2·667	-1·900	-1·138	-·379
-·480	-1·440	-2·394	-3·345	-3·431	-2·657	-1·892	-1·133	-·377
-·483	-1·447	-2·400	-3·341	-3·416	-2·640	-1·877	-1·123	-·374
-·490	-1·463	-2·418	-3·335	-3·387	-2·609	-1·853	-1·109	-·369
-·502	-1·500	-2·470	-3·328	-3·319	-2·555	-1·819	-1·090	-·363
-·519	-1·564	-2·636	-3·322	-3·139	-2·474	-1·777	-1·069	-·357
-·531	-1·599	-2·680	-3·317	-3·075	-2·425	-1·747	-1·053	-·352
-·536	-1·614	-2·706	-3·314	-3·053	-2·403	-1·731	-1·044	-·349

Table 4. Jz

0	0	0	0	0	0	0	0	0
0	3·339	3·339	3·339	0	-3·339	-3·339	-3·339	0
0	3·339	3·339	3·339	0	-3·339	-3·339	-3·339	0
0	3·339	3·339	3·339	0	-3·339	-3·339	-3·339	0
0	0	0	0	0	0	0	0	0
0	3·339	3·339	3·339	0	-3·339	-3·339	-3·339	0
0	3·339	3·339	3·339	0	-3·339	-3·339	-3·339	0
0	3·339	3·339	3·339	0	-3·339	-3·339	-3·339	0
0	0	0	0	0	0	0	0	0

Table 5. Hx

·349	·809	·881	·698	0	-·698	-·881	-·809	-·349
·585	1·145	1·226	·941	0	-·941	-1·226	-1·145	-·585
-263	·289	·268	·170	0	-·170	-·268	-·289	-·263
-·0855	-·520	-·612	-·528	0	·528	·612	·520	·0856
0	0	0	0	0	0	0	0	0
·0855	·520	·612	·528	0	-·528	-·612	-·520	-·0856
-·263	-·289	-·268	-·170	0	·170	·268	·289	·263
-·585	-1·145	-1·226	-·941	0	·941	1·226	1·145	·585
-·349	-·809	·881	-·698	0	·698	·881	·809	·349

Table 6. Hy

-·349	-1·506	-3·195	-4·774	-5·472	-4·774	-3·195	-1·506	-·349
·112	-·974	-3·306	-5·655	-6·869	-5·655	-3·306	-·974	4·112
·211	-·865	-3·399	-6·000	-7·354	-6·000	-3·399	-·865	·211
·138	-·968	-3·424	-5·923	-7·210	-5·923	-3·424	-·968	·138
-·223	-1·392	-3·407	-5·388	-6·299	-5·388	-3·407	-1·392	-·223
·138	-·968	-3·424	-5·923	-7·210	-5·923	-3·424	-·968	·138
·211	-·865	-3·399	-6·000	-7·354	-6·000	-3·399	-·865	·211
·112	-·974	-3·306	-5·655	-6·869	-5·655	-3·306	-·973	·112
-·349	-1·506	-3·195	-4·774	-5·472	-4·774	-3·195	-1·506	-·349

Table 7

Time	Node 1	2	3	4	5
5	-9.30	3.78	20.27	9.37	5.38
10	-8.57	8.04	26.63	17.43	15.47
15	-7.97	9.83	29.61	21.68	18.84
20	-7.57	10.41	29.80	22.10	20.12
25	-7.58	10.52	30.0	22.17	20.20

Table 8

Time	Node 1	2	3	4	5
5	-9.18	5.86	22.83	13.20	10.16
10	-8.35	8.24	26.54	17.87	15.34
15	-7.97	9.34	28.26	20.03	17.73
20	-7.79	9.87	29.09	21.07	18.90
25	-7.70	10.14	29.50	21.59	19.46

THE COMPUTATION OF EDDY CURRENT LOSSES IN SOLID IRON UNDER VARIOUS SURFACE CONDITIONS

Dr. D.A. Lowther* and E.A. Wyatt*

Abstract

The paper compares the computation of eddy current losses by different methods. The rectangular B-H curve approximation is used to study the effects of sinusoidal and non-sinusoidal surface electric and magnetic fields.

The non sinusoidal form is convenient both for external field calculations and the analysis of experimental data. The Frohlich curve approach is examined under similar conditions of non-sinusoidal surface H. The extension of both methods to two-dimensions is examined.

1) Introduction

The severe heating problems which can occur in large transformers and turbo-alternators have given rise to the need for an accurate prediction of the power losses. This requires a detailed description of the field distribution both inside, and external to, the core.

The problem may be conveniently divided into two parts in order to simplify the calculations. The first part involves predicting the loss distribution inside a magnetically non-linear core for a given surface field distribution. The second is to find a simple model which allows the calculation of the exterior field, avoiding complex interface conditions.

*Department of Electrical Engineering,
Imperial College of Science and Technology,
London. S.W. 7

At the levels of magnetisation encountered in these applications the hysteresis loss is negligible and the eddy current loss is the major component. The purpose of this paper is to compare different methods of computing the losses in a non-linear medium. The resultant solutions may be expressed in terms of surface impedance. This concept is useful for comparing the various methods and can be used in the computation of the external field.

Two different approaches have been used in the published work. These may be classed according to the way in which the magnetisation characteristic is represented. In the simpler, and historically earlier method described by MacLean, Agarwal et al (references 1-6) a rectangular approximation to the characteristic is used. This leads to an algebraic solution in one-dimension and can give a useful indication of the behaviour of the field inside the material.

The more complex method employs a more realistic representation of the magnetisation characteristic and uses time stepping techniques (references 7-12). This method has become popular as large computers have become available and it gives the field distribution in the material accurately.

Because many electromagnetic devices operate under "current forced" conditions, attention has been restricted to the boundary condition of sinusoidal surface H in most of the published analyses. However, this can be considered as a limiting condition; the other limit being that of sinusoidal surface E (or total flux). Because, in practice, the surface conditions may vary between the two extremes and are, in general, non-sinusoidal, the analysis in this paper deals mainly with the sinusoidal surface E situation. In addition, the analysis is extended to include surface waveforms which are non-sinusoidal in time. This is useful as far as comparisons with experimental results are concerned.

In regions in which the non-linear medium is subject to a high level of incident normal flux, which turns along the surface after entering,

a two-dimensional analysis is required. Such an analysis will be considered briefly.

2) The Finite Difference Model

The finite difference model is taken to include all those models using time-stepping techniques (references 7-12) and in this approach the magnetisation curve may be represented by a single function or, alternatively, the actual curve may be stored at discreet points and curve fitting employed. Many different finite difference schemes have been employed. Examples include the Crank-Nicolson[9] and Dufort-Frankel techniques[7]. In practice both the E and H surface waveforms are non-sinusoidal in time.

2.1) The Sinusoidal Surface E Analysis

When the sinusoidal surface E condition is imposed a difficulty arises which is not present if the sinusoidal surface H solution is sought. The difficulty is that the non-linearity considered is magnetic and thus concerns the relationship between B and H rather than E and J. The method used here is similar to that described by Lim and Hammond[7] who used a Dufort-Frankel time-stepping scheme in conjunction with a Frohlich magnetisation characteristic.

If the material conductivity, σ, is assumed constant and the permeability is a function of B as well as the spatial coordinates, the following governing equation for E may be derived from Maxwell's Equations used in conjuction with the constitutive relations;

$$\nabla^2 \underline{E} = \frac{\partial}{\partial t} \quad (\text{curl } \mu \underline{H}) \qquad (1)$$

which can be further modified to give

$$\nabla^2 \underline{E} = \frac{\partial}{\partial t} \quad (\mu\sigma \underline{E} - \underline{H} \times \text{grad } \mu) \qquad (2)$$

If (2) is applied in conjunction with

$$\text{div} \underline{B} = 0 \qquad (3)$$

all of Maxwell's equations are satisfied.

A convenient experimental model of the one-dimensional diffusion problem is a steel rod of circular cross-section subject to sinusoidal surface conditions. It is thus appropriate to consider the circular cylindrical coordinate form of equation (2) which is:

$$\frac{1}{r} \frac{\partial}{\partial r} \left(r \frac{\partial E}{\partial r} z \right) = \frac{\partial}{\partial t} \left(\mu\sigma E_z + H_\theta \frac{\partial \mu}{\partial r} \right) \qquad (4)$$

The subscripts may be dropped because there is only one component of E and one of H. Equations (2) and (4) , however, require that the time derivative of the permeability be known and this is an inconvenience.

A simpler equation can be obtained from equation (1) by substituting $\underline{B}$ for $\mu\underline{H}$ and noting that

$$\frac{\partial B}{\partial r} = \frac{dB}{dH} \frac{\partial H}{\partial r}$$

The equivalent form of equation (4) is then;

$$\frac{1}{r} \frac{\partial}{\partial r} \left(r \frac{\partial E}{\partial r} \right) = \sigma \frac{dB}{dH} \frac{\partial E}{\partial t} \qquad (5)$$

from which the following finite difference equation may be derived using central differences:

$$E(i,j+1) = Q(E(i,j-1)\ (\beta r\ (\Delta r)^2 - 2r\Delta t) + \Delta t\ E(i+1,j)\ (2r + \Delta r) + E(i-1,j)\ (2r - \Delta r))) \qquad (5a)$$

where

$$\beta = \sigma \frac{dB}{dH} \quad , \quad Q = \frac{1}{r(2\Delta t + \beta(\Delta r)^2)}$$

The relationship between B and H is defined by the Frohlich curve:

$$B = \frac{H}{a + b|H|}$$

in which H and B are in the same direction.

At each step the H distribution must be calculated from that of E so that the magnetisation curve can be used. Because curl $\underline{H} = \underline{J}$

$$E = \frac{1}{r} \frac{\partial (rH)}{\partial r} \qquad (7)$$

and integration with respect to r yields

$$H = \frac{\sigma}{r} \int_{o}^{r} r E \, dr \qquad (8)$$

With this modification the calculation of the field distribution follows the method of Lim and Hammond[7], using the DuFort-Frankel time-stepping scheme.

2.2) Surface Impedance.

From the solution, the fundamental components of the field vectors at the surface can be obtained by harmonic analysis. If either E or H is sinusoidal at the surface, the total power loss in the material may be determined by applying the Poynting Vector to their fundamental components. This loss can be regarded as occurring in the real part of a complex surface impedance. The quadrature component of the impedance may be used to describe the reactive volt-amp absorption. This surface impedance can then be used to terminate the exterior network.

The concept of a surface impedance is useful as a basis for comparison of methods and as a check against experimental results.

3) The Approximate Model

The approximate model in which the magnetisation curve is represented by a rectangular characteristic has been described by several authors (references 1-6). It restricts the flux penetration to a surface layer in which the material is saturated either one way or the other; the switching point between the two magnetisation directions defining a wavefront. An algebraic expression is obtained for the E and H waveforms.

As with the finite difference methods, much of the published literature considers the sinusoidal surface H condition. The following analysis considers the condition of sinusoidal surface E (as in the preceeding section) and, in addition, the analysis is extended to include the non-sinusoidal surface fields.

3.1) Sinusoidal Surface E

Using a modified form of Maxwell's equations and the co-ordinate system of figure 2, the field at a distance x from the surface is given by:

$$\frac{H}{x} = \sigma E \qquad (9)$$

$$\text{and} \quad E = 2B\frac{dx}{dt} = E_o \sin\omega t \qquad (10)$$

After integration these equations give a wavefront depth of

$$x = \frac{E_o}{2\omega B_o} (1 - \cos\omega t) \qquad (11)$$

and the solution for H is

$$H = \frac{\sigma E_o^2}{\omega B_o} \sin\omega t \sin^2 \frac{\omega t}{2} \qquad (12)$$

As in the finite difference method the resultant solutions for the surface values of E and H may be harmonically analysed. If either waveform is purely sinusoidal, the loss may be obtained from the fundamental components by Fourier analysis. The fundamental component of H is:

$$H = H' (-4 \cos\omega t + 3\pi \sin\omega t) \qquad (13)$$

where H' is defined in equation (A.1) of the appendix. If E = E, i.e. is purely real

$$H = H' (3\pi - 4j) \qquad (14)$$

Again a surface impedance may be used to describe the resistive and reactive components of the total volt-amps. If this impedance is considered to consist of series components, their values are given by

equation (A.2). The impedance shows the power factor to be 0.9206 so that the phase angle is 23° . This result may be compared with that for the sinusoidal H condition given by McConnell[4] and Agarwal[5]. In the latter case the impedance is that given in equation (A.3) and the power factor is 0.8944 giving a phase angle of 26.6°.

These two solutions can be compared on a basis of the same peak value of the fundamental component of E and the ratio of the magnitudes of the two impedances is then

$$|Z_{se}| / |Z_{sh}| = 2.04745 \qquad (15)$$

This indicates that the power loss for the condition of sinusoidal surface E is double that for sinusoidal surface H. This point is confirmed by the finite difference solutions.

3.2) Non-sinusoidal Surface Fields

The above approach allows a further generalisation to include non-sinusoidal surface excitations by expressing the surface waveforms in Fourier series form.

The derivation described below is in terms of H although the treatment for E follows a similar procedure.

If the surface H distribution is given by

$$H = H_{1s} \sin \omega t + H_{1c} \cos \omega t + H_{3s} \sin 3\omega t + H_{3c} \cos 3\omega t + \ldots \qquad (16)$$

and equation (10) is modified to become

$$\frac{H}{x} = 2\sigma B_o \frac{dx}{dt} \qquad (17)$$

the resultant equation for the depth of penetration any time, E, is given by

$$x = \sqrt{\frac{2}{\omega\sigma B_o}} H'^{\frac{1}{2}} \qquad (18)$$

where H is defined by equation (A.7) of the appendix. The solution for E is then

$$E = \sqrt{\frac{\omega B_o}{2\sigma}} \frac{H}{H'^{\frac{1}{2}}} \qquad (19)$$

Equation (18) assumes that x = 0, and hence H = 0, at time t = 0 so that the time origin has to be displaced to the point at which H = 0.

As before, a harmonic analysis can be used to yield a surface impedance, although the impedance now has harmonic components so that the surface layer must include a series of harmonic generators.

Agarwal[5] has modified the saturation flux density by a factor of 0.75 so as to predict the loss (but not the VAr's) accurately when the surface H is sinusoidal. This factor has been shown to be dependant on the magnetisation level[13]. In the sinusoidal surface E condition a similar approach can be employed to model the loss accurately.

The advantage of the rectangular magnetisation characteristic lies in the simplicity with which the surface impedance may be derived. The approximation is satisfactory at the large values of surface magnetisation which occur in many problems of interest.

4) Results

The results in figures 3 to 6 show the E and H waveforms predicted for a specific B - H curve for sinusoidal surface E and H. As can be seen, the waveforms are similar in form for both methods and as the magnetisation level is increased the similarity increases. The effect is shown more clearly in the surface impedance results.

The method of section 2 can be adapted so that a finite final slope is included on the B - H curve but the effect is small, as has been noted elsewhere[6]. It would seem that the difference between the approximate and finite difference methods is largely due to the fact that the finite difference solution allows for the initial slope in the B - H characteristic.

The extra loss caused by assuming a step change in flux density requires a reduction in the saturation flux density to obtain accurate predictions.

This result suggests that a modification of the rectangular curve to one having a finite initial slope would improve the agreement between the two methods considerably.

5) Extensions To Two-dimensions

Both methods may be extended to give field solutions in two dimensions, as is necessary when the flux density normal to the surface is large. This condition is commonly met in practice in the end region of a turbo-alternator or around a transformer leg.

The finite difference approach in two-dimensions may be formulated in terms of magnetic vector potential, A , which has only one component. This function was chosen because it is often employed in two-dimensional linear eddy-current problems.

The governing equation for A is

$$\nabla^2 A_z = \mu\sigma \left[\frac{\partial A}{\partial t}_z + \frac{\partial V}{\partial z} \right] - \left[\frac{\partial A}{\partial x}_z \frac{\partial 1/\mu}{\partial x} - \frac{\partial A}{\partial y}_z \frac{\partial 1/\mu}{\partial y} \right] \quad (20)$$

which may be approximated by a nodal (DuFort-Frankel) finite difference method. Care is needed in the treatment of interface conditions which include restrictions both on μ and the normal gradient of A.

The approximate approach may also be adapted to two-dimensions although the wavefront, which is the key to the algebraic treatment of the one-dimensional problem, no longer becomes as clearly defined since the angle through which the magnetisation vector switches is not necessarily 180 degrees. The evaluation of H is complicated by the variation of the current density within the saturated region. The solution is still of the surface layer type and is only applicable to high magnetisation level problems.

Two-dimensional calculations using these two approaches are being made and it is hoped to publish the results at a later date.

6) Conclusions

The foregoing analyses have shown that the most commonly used methods of treating non-linearity can be adapted to allow for any specified surface E or H time variation. A comparison between the results for sinusoidal H and E (the two limits) indicates a region within which the practical condition must occur. The methods have concentrated on the fact that sinusoidal surface E may be regarded as a limiting condition on the waveforms encountered in practice.

The surface layer concept, together with that of a characteristic surface impedance, can simplify external field calculations considerably. In addition, they provide an extremely useful point of reference between different analyses and experimental measurements.

7) References

1. Rosenberg E. "Eddy Currents in Iron Masses", The Elecrician, 1923, pp 188-191
2. Haberland G. and Haberland F. "Alternating fields in Saturated Solid Iron", Archiv fur Elektrotechnic, Berlin, Germany, Vol 30, 1936, pp 126-133.
3. Maclean W."Theory of Strong Electromagnetic Waves in Massive Iron", Journal of Applied Physics, 25 (10) 1954, pp 1267-1270
4. McConnell M.M. "Eddy Current Phenomena in Ferromagnetic Materials", Trans AIEE pt I (Mag) 73, 1954 pp 226-235.
5. Agarwal P."Eddy Current Losses in Solid and Laminated Iron", Trans AIEE, ptI (Mag) 78, 1959, pp 169-181
6. Shevez W.L. "A Modified Limiting Non-Linear Theory of Eddy Current Phenomena in Solid Iron", Trans AIEE pt (Mag) 81, 1962 pp 48-55
7. Lim K.K. and Hammond P. "Numerical Method for determining the Electromagnetic field in saturated Steel Plates." Proc IEE, 119,(11), 1972 pp 1667-1673.
8. Neyfem A.H.and Asfar O.R. "An analytical solution of the Nonlinear

Eddy Current Losses in Ferromagnetic Materials" IEEE Trans Mag - 10, 1974 pp 32- - 331

9. Poritsky H. and Butler J.M. "A-C Flux Penetration into Magnetic Materials with Saturation" Trans AIEE, 1964, COM - 83, pp 99-111.

10. Gillott D.M. and Calvert J.F. "Eddy Current Loss in Saturated Solid Magnetic Plates, Rods, and Conductors". AIEE 1965, MAG - 1, pp 126-137

11. Ahamed S.V. and Erdelyi E.A "Non-Linear Theory of Salient Pole Machines", IEEE Trans PAS - 85, 1966, pp 61-70

12. Bullingham J.M. and Bernal M.J.M. "Investigation of the Effect of Non-Linear B-H Loops on the calculation of Eddy Current Losses", Proc IEE 114 (8) 1967, pp 1174-1176

13. Freeman E.M. "Universal Loss Chart for the calculation of Eddy Current Losses in thick steel plates", Proc IEE, 118 (1), pp278-279

Appendix

The following equations are used in the approximate model of section 3.

$$H' = \frac{\sigma E_o^2}{12\omega B_o \pi} \qquad (A.1)$$

$$Z_{se} = \frac{E}{H} = \frac{12\omega B_o \pi}{\sigma E_o}\left[\frac{3\pi_2+4j}{9\pi^2+16}\right] \qquad (A.2)$$

$$Z_{sh} = \frac{E}{H} = \frac{16}{3\pi}\left[\frac{\omega B_o}{2H_o\sigma}\right]^{\frac{1}{2}}\left[1 + j\tfrac{1}{2}\right] \qquad (A.3)$$

for the same peak fundamental component of E

$$Z_{sh} = \frac{E}{H} = \frac{16B_o\omega\sqrt{80}}{9\pi^2 E_o\sigma}\left[1 + j\tfrac{1}{2}\right] \qquad (A.4)$$

$$\frac{|Z_{se}|}{|Z_{sh}|} = \frac{27\pi 3}{40\ (9\pi^2+16)^{\frac{1}{2}}} = 2.0475 \qquad (A.5)$$

for the same condition, the ratio of penetration depths is

$$\frac{\delta e}{\delta h} = 0.949 \qquad (A.6)$$

$$H' = \sum_{n=1,3,5}^{\infty}\left(H_{ns}\ \sin^2\frac{n\omega t}{2} + Hn_c \sin\frac{n\omega t}{2}\ \cos n\frac{\omega t}{2}\right) \qquad (A.7)$$

Acknowledgements

The authors would like to thank Mr. C.J. Carpenter of Imperial College for helpful discussions, and the Science Research Council for financial support.

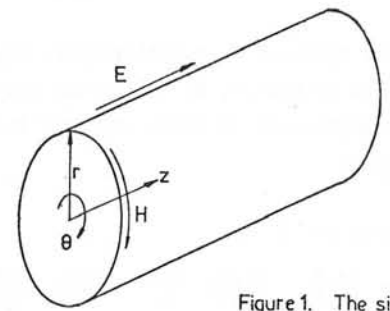

Figure 1. The sinusoidal E model

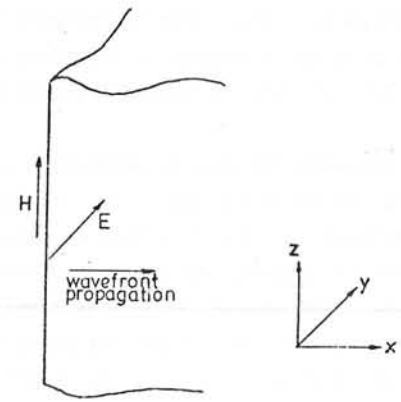

Figure 2. The rectangular B-H curve model

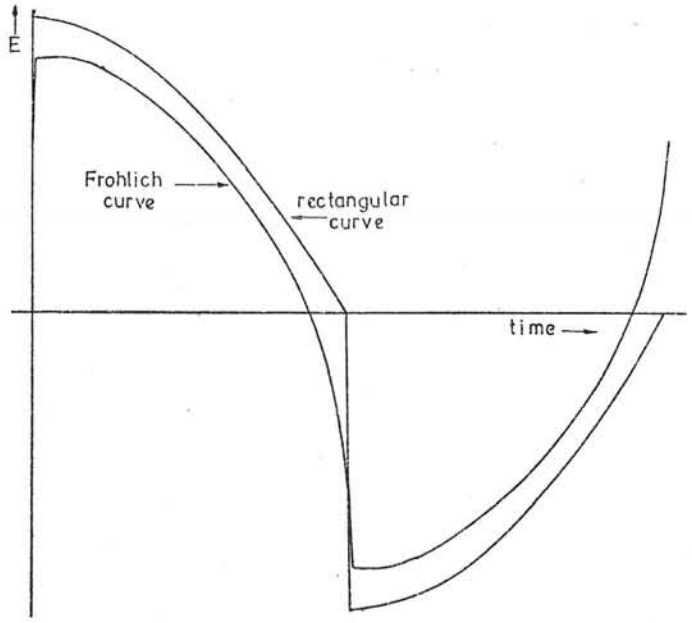

Figure 3. Surface E waveforms for sinusoidal surface H

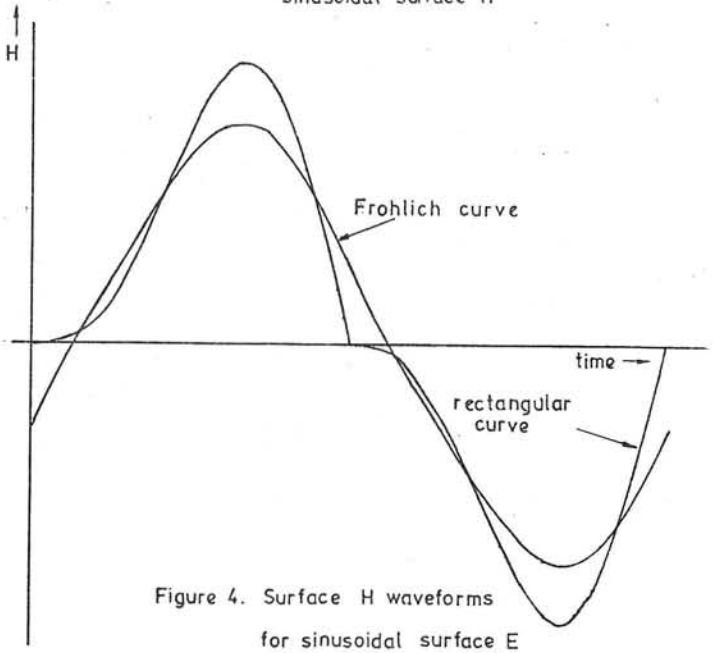

Figure 4. Surface H waveforms for sinusoidal surface E

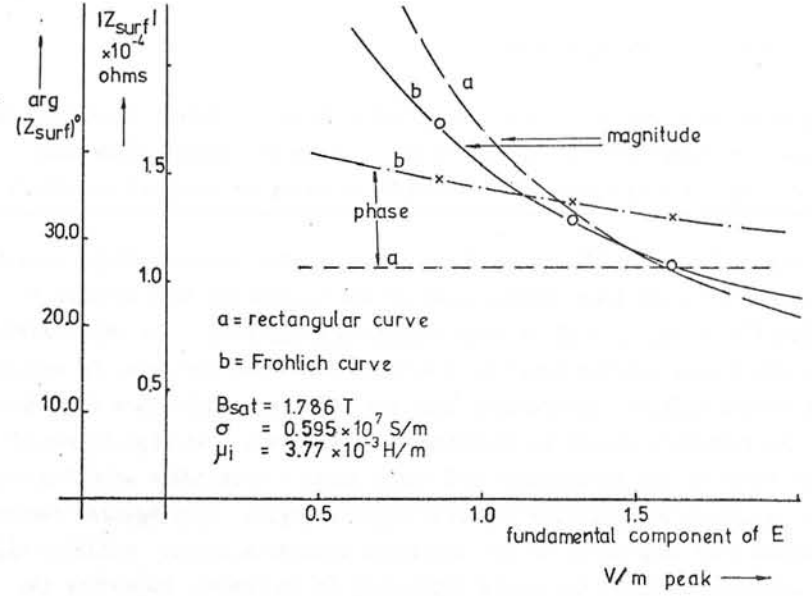

Figure 5. Surface impedance against E for sinusoidal surface H

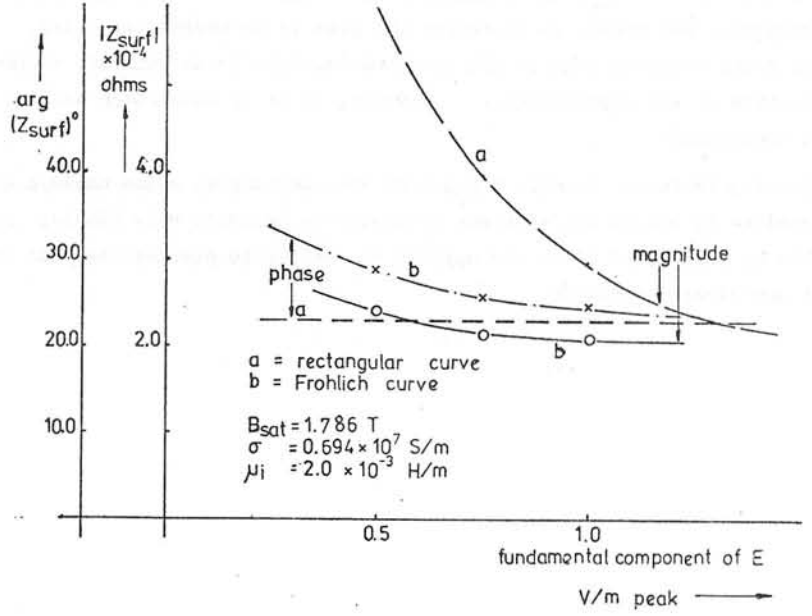

Figure 6. Surface impedance against E for sinusoidal surface E

Discussions following paper:

(Hammond, Southampton) The loss in solid iron is closely predicted by using a rectangular B-H characteristic. Does the author think that this loss could be obtained very simply by using an energy functional?

(Lowther, Imperial College) The rectangular B-H characteristic predicts the loss in solid iron closely only if the saturation flux density is reduced by a factor such as that suggested by Agarwal. In representing the non-linear surface layer by a surface impedance (in order to simplify the exterior field calculation) both the phase and quadrature components of the impedance should be accurately represented. At high levels of magnetisation the rectangular B-H curve gives a reasonable solution for the magnitude but produces an error inphase angle. The Agarwal factor reduces both components of the impedance whereas a better solution might be a method in which the phase angle only is increased, improving the accuracy of both components of the impedance.

With the above proviso the concept of an energy functional, employing a rectangular B-H curve, to represent the loss is an interesting idea. This would overcome some of the problems involved in an accurate representation of the non-linearity. However, it is an idea which we have not considered.

Following Professor Hammond's paper at the conference, which employs this technique to obtain the relevant parameter of interest very simply; we would be interested if he has applied the method to predict the loss in the non-linear situation.

EVALUATION OF THE AIR-GAP FIELD IN SHORT-STATOR LINEAR ASYNCHRONOUS MOTORS

G. Figalli - G. Gentile - E. Pagano - V. Vaccaro

1. Generalities

One of the essential problems to be considered in the study of the performances of short-stator linear asynchronous motors, is the determination of the air-gap magnetic field. In this evaluation, it is necessary to take into account the actual geometry of the stator and therefore the real map of the magnetic field both at the end and at the top and bottom sides. This implies that the air-gap magnetic field can not be identified with an ideal field in which all the lines are parallel and have equal and finite lengths. By introducing suitable simplified hypotheses, different approximate solutions can be obtained if the motor has a periodical configuration. These hypotesis have been validated by the agreement between the theoretical and experimental results obtained up to now.

A mathematical model based on an improved representation of the air - gap fiel map can be useful for application to a wide range of motor configuration. For this purpose the air-gap permeance can be expressed by means of a function of exponential type, which satisfactorily expresses the actual air-gap magnetic field. Allowing for symmetric conditions, the air -gap permeance can be approximated by an even function of x and z (see fig. 1), which vanishes at infinity. This function can be expressed in the form:

$$\lambda(x,z)=\frac{1}{\delta(x,z)}\;\lambda_0\sum_{i}^{n}\exp\left[-\left(\frac{x-x_i}{A_0}\right)^2\right]\sum_{j}^{m}\exp\left[-\left(\frac{z-z_j}{B_0}\right)^2\right] \qquad (1)$$

In this relation for each given pair of values of n and m, the constants A_o, B_o, x_i, z_i, are calculated to obtain the nearest approximation. A constant trend of the air-gap permeance inside the dominion D ($|x|\leqslant l_x/2$, $|z|\leqslant l_z/2$) is imposed together with a more or less quickly decreasing trend at the outside. For this purpose, first of all, a study has been done to determine the optimus value of x_i, A_o, and y_i, B_o, which give the minimum of the functions:

$$\Delta_x(x_i,A_0)=\int_0^{l_{x/2}}\left[\lambda(x,0)-\lambda(0,0)\right]^2 dx+k_x\int_{l_x^{\infty}}^{\infty}\lambda^2(x,0)\,dx\,,$$

$$\Delta_z(z_i,B_0)=\int_0^{l_{z/2}}\left[\lambda(0,z)-\lambda(0,0)\right]^2 dz+k_z\int_{l_z^{\infty}}^{\infty}\lambda^2(0,z)\,dz\,.$$

In these expressions, k_x and k_z are two constants chosen to give the decided weight of the error of the approximation inside the dominions D and D_∞ ($|x|\geqslant l_x^{\infty}$, $|z|\geqslant l_z^{\infty}$). The air-gap field in the dominion D_∞ is supposed to be zero.

2. Mathematical Model

In the study of steady-state operations of short stator linear induction motors, it is useful to make some approximations, i.e. neglect saturation phenomena and displacement currents, assign an infinite permeability to the inductor. If the z-component of the inductor current is only considered, the second Maxwell equation is:

$$\frac{\partial}{\partial x}\left[B(x,z,t)\cdot\delta(x,z)\right]=\mu_0 A_{z1}(x,z,t)+\mu_0 y_1 G_{z2}(x,z,t) \qquad (2)$$

In this equation, it is also assumed that the induction field B has the same direction as the y-axis. This assumption generally made in the technical literature, does not alter the B distribuction on the rotor. Ohm's law combined with the first Maxwell equation gives the following equation:

$$\frac{\partial^2 G_{z2}}{\partial x^2}+\frac{\partial^2 G_{z2}}{\partial x^2}-\chi\frac{\partial}{\partial x}\left(\frac{\partial B}{\partial t}+v\frac{\partial B}{\partial x}\right)=0 \qquad (3)$$

This equation together with equation (2) makes it possible to determine the functoon $B(x,z,t)$ on the rotor whenever the function A_{z1} is assigned. The latter depends on the time variation law of the inductor currents and on the geometric structure of the inductor windings. Referring to a symmetrical system of sinusoidal currents, one can write the linear current density as:

$$A_{z1}(x,z,t)=\sqrt{2}\,I\sum_{1}^{p}e\sum_{1}^{3}i\sum_{1}^{q}r\cdot f_x(x)\cdot f_z(z)\exp\left[j(\omega t-2\pi[i-1]/3)\right]$$

if all the pole windings are series connected and if we set:

$$f_x(x)=\frac{1}{\sqrt{2\pi}\,S_c g'}\left\{\exp\left[-(x-x_{e,i,r})^2/(2S_c^2 g'^2)\right]-\exp\left[-(x-x_{e,i,r})/(2S_c^2 g'^2)\right]\right\}$$

$$f_z(z)=\frac{1}{\sqrt{2\pi}\,af'}\int_{-\infty}^{z}\left\{\exp\left[-(z+a)^2/(2a^2 f'^2)\right]\exp\left[-(z-a)^2/(2a^2 f'^2)\right]\right\}dz$$

This assumption implies that the distribution of the inductor currents is supposed to give rise to a Gaussian distribution of linear current density in the slot opening along the x-axis and to an integrated Gaussian distribution along the z-axis (see fig. 2).

Since at the steady-state the forcing variables are sinusoidal, all other variables will be also, i.e.:

$$B(x,z,t) = \dot{B}(x,z)\exp[j\omega t]$$

$$G_{z2}(x,z,t) = \dot{G}_{z2}(x,z)\exp[j\omega t]$$

$$A_{z1}(x,z,t) = \dot{A}_{z1}(x,z)\exp[j\omega t]$$

Some other properties are now examined. The vector B has zero divergence. Due to the magnetic symmetry with respect to the z axis, this property is summarized in the following equation:

$$\int_{-\infty}^{\infty} \dot{B}(x,z)\,dx = 0 \qquad (4)$$

Performing the Fourier transform along the x-axis, the equation (4) becomes $\tilde{B}(0, z) = 0$. The intrinsic structure of the physical model implies that the B_1 and B_2 components of the resulting air-gap induction field, separately generated by the current distributions on the stator and in the rotor, are zero i.e.:

$$\tilde{B}_1(0,z) = \tilde{B}_2(0,z) = 0 \qquad (5)$$

On the other end the equation (2) can be written in the form:

$$\dot{B}(x,z) = \lambda(x,z)\left\{\mu_0\left[\int_{-\infty}^{x}\dot{A}_{z1}(x,z)dx + y_1\int_{-\infty}^{x}\dot{G}_{z2}(x,z)dx\right] + k_1(z) + k_2(z)\right\} \qquad (2')$$

In this equation we denote with k_1 and k_2 two integration functions. These functions must satisfy the condition (5), namely

$$k_1(z) = -\mu_0 \sum_{1}^{n}{}_{i}\int_{-\infty}^{\infty}\frac{\tilde{A}_{z1}(\xi,z')}{j\xi}\exp\left[-\frac{A_0^2}{4}\xi^2 - j\xi x_i\right]d\xi \qquad (6)$$

$$k_2(z) = -\mu_0 y_1 \sum_{1}^{n}{}_{i}\int_{-\infty}^{\infty}\frac{\tilde{G}_{z2}(\xi,z)}{j\xi}\exp\left[-\frac{A_0^2}{4}\xi^2 - j\xi x_i\right]d\xi \qquad (6)$$

Performing the double Fourier-transform of equations (2) and (3) and taking into account the properties of the integration functions we obtain as a result the integral equation:

$$\tilde{\tilde{B}}(\xi,\eta) = \mu_0\int_{-\infty}^{\infty}\int_{-\infty}^{\infty}\frac{\tilde{\tilde{A}}_z(\gamma,\nu)}{j\gamma}\,\tilde{\tilde{\lambda}}(\xi-\gamma,\eta-\nu)\,d\gamma\,d\nu + \mu_0 y_1\int_{-\infty}^{\infty}\int_{-\infty}^{\infty}\frac{\tilde{\tilde{B}}(\gamma,\nu)(v\gamma+\omega)}{j(\gamma^2+\nu^2)}\cdot$$

$$\cdot\,\tilde{\tilde{\lambda}}(\xi-\gamma,\eta-\nu)\,d\gamma\,d\nu \qquad (7)$$

where the function G_{z2} is eliminated.

To solve the equation (7) it is necessery to assign an adequate form to the function $\lambda(x, z)$, which represents the air-gap permeance. Referring to the relation (1), performing the double Fourier-transform, introducing in the equation (7) and making a normalization of the variable ξ, η over the quantities $A_0^2/4$ and $B_0^2/4$ we obtain the final equation. This equation is an integral equation of the Fredholm type, second kind, of two variables. The inspection of the kernel suggests an expansion of Hermite polynomials as functions of ξ , η . Performing the same expansion of the forcing function $\tilde{\tilde{A}}_{z1}(\xi,\eta)$ we can predict the form of the function $\tilde{\tilde{B}}(\xi,\eta)$:

$$\tilde{\tilde{\lambda}}(\xi,\eta) = \lambda_0 A_0 B_0 \pi \sum_{1}^{n}{}_{i}\sum_{1}^{m}{}_{k}\exp\left[-(A_0^2\xi^2 + B_0^2\eta^2)/4\right]\exp\left[-j(x_i\xi + z_k\eta)\right]$$

$$\tilde{\tilde{B}}(\xi,\eta) = C\exp\left[-(\xi^2+\eta^2)\right]\sum_{1}^{n,m}{}_{i,k}\exp\left[-j(Dx_i\xi + Fz_k\eta)\right]\sum_{0}^{\infty}{}_{h,\ell}\,\bar{H}_h(\xi)\,H_\ell(\eta)\,B_{h,\ell,i,k} \qquad (8)$$

$$\bar{H}_h(\xi) = H_h(\xi) - H_h(0)$$

where the quantities $B_{h,l,i,k}$ are the unknowns to be determined and where $D = 2/A_0$, $F = 2/B_0$, $C = \mu_0\lambda_0 B_0\pi\lambda_0$ is set. Inserting the expression found in equation (2') and performing all the eventual algebra, the procedure leads to a system of infinite equations with infinite unknowns $B_{h,l,i,h}$. Truncation of the system which is equivalent to a degeneration of the kernel and an approximation of the forcing function leads to the matrix equation:

$$B = H + \Lambda k\, B$$

whose solution is: $B = [I-\Lambda k]^{-1} H$

whose [I] is the identity matrix

LIST OF SYMBOLS

a	halfwidth of the rotor.
$A_{z1}(x, z)$	linear current density at the stator air-gap surface.
$B(x, z)$	air-gap induction.
f', g'	numerical coefficients.
$\tilde{f}$, $\tilde{\tilde{f}}$	single and double Fourier-Transform of the function f .
$G_{z2}(x, z)$	current density.
I	effective value of the inductor phase current.
p	number of pole-pairs.
q	number of slots per pole and per phase.
S_c	halfwidth of inductor slots.
$x_{e,r,i}$, $x'_{e,r,i}$	abscissae of the slots for clockwise and counterclockwise currents.
v	mutual velocity between stator and rotor.
$\delta(x, z)$	lenght of the air-gap field-lines.
$\lambda(x, z)$	air-gap permeance.
μ_0	permeability.
χ	electric conductivity.
ω	angular frequency.

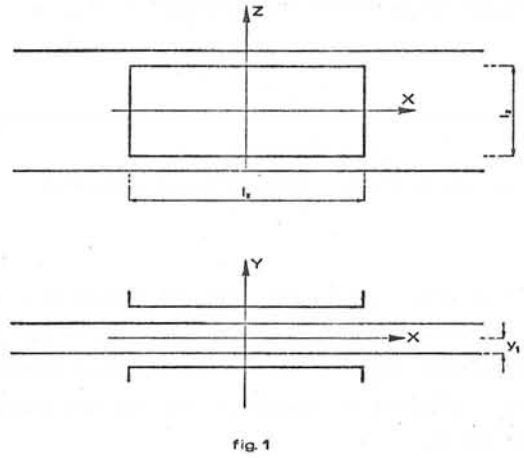

fig. 1

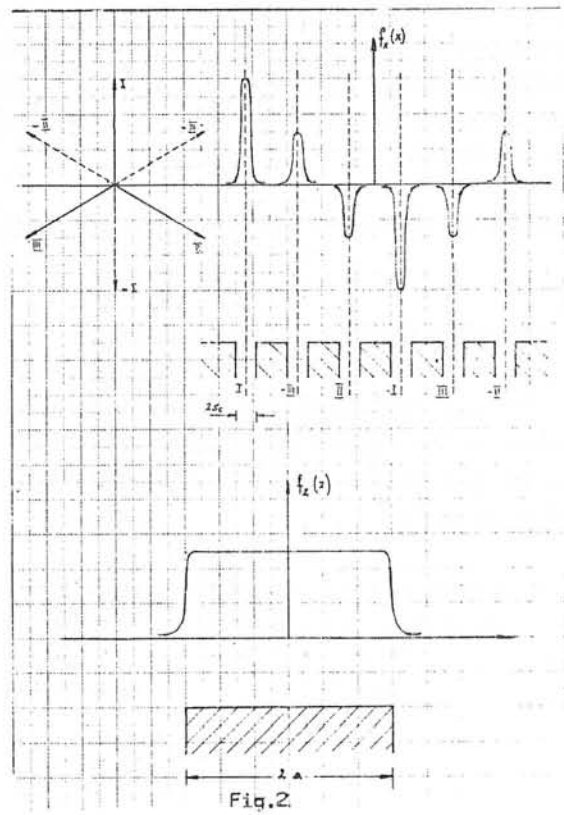

Fig.2

NUMERICAL DETERMINATION OF AN EQUIVALENT COMPLEX PERMEABILITY FOR SATURATED STEEL

Alain BOSSAVIT
Electricité de France (92140 Clamart, France)

This work has been done in relation with the design of a mathematical model of an induction furnace for slabs. The geometry of the furnace is such that a monodimensional study is valid, leading to a coupled system of non-linear partial differential equations, one for the temperature, one for the magnetic field.

A numerical treatment of this system is quite feasible, but time - consuming. The introduction of an *equivalent permeability* (see [1]) for saturated steel is a useful device to reduce the complexity of this system, for it allows one to solve the field equation in closed form, leaving only the heat equation to be solved.

The organization of the paper will be described at the end of the first paragraph.

1. - DEFINITION OF THE EQUIVALENT PERMEABILITY. ITS PURPOSE

We consider an infinite steel block, limited by the y Oz plane, and a current sheet parallel to this plane, at the abscissa $-\ell$, ℓ being the air-gap. Its resistance is r and its inductance s per square-meter and a voltage $v(t) = V \sin \omega t$ is applied.

The steel is characterized by its (constant) resistivity σ and its magnetization curve, linking the induction $b(t,x)$ and the magnetic field $h(t,x)$ by the relation

$$b(t,x) = b(h(t,x)) \tag{1}$$

The evolution of the field is given by the parabolic equation

$$\frac{\partial}{\partial t} b(h(t,x)) - \frac{\partial}{\partial x}\left(\sigma^{-1} \frac{\partial h}{\partial x}\right) = 0, \qquad x \geqslant 0, \tag{2}$$

with the boundary condition

$$(\mu_o \ell + s) \frac{\partial h}{\partial t}(t,0) + r\, h(t,0) - \sigma^{-1} \frac{\partial h}{\partial x}(t,0) = v(t). \tag{3}$$

Having obtained the *periodic solution* of (2) (3), we can compute the *mean power* P and the *quadratic mean intensity* J under the applied voltage V.

Let us now imagine a steel of complex permeability

$$\mu = \mu_o \mu_r \exp(i\theta) \tag{4}$$

heated by the same inductor. In this ideal material, the field would be $\mathcal{R}e\,[\exp(i\omega t)\, H(x)]$ where H is the solution of

$$\begin{cases} i\,\omega\,\sigma\,\mu\, H(x) - \dfrac{\partial^2}{\partial x^2} H(x) = 0, & x \geqslant 0, \\ \left[i\,\omega(\mu_o \ell + s) + r\right] H(0) - \sigma^{-1} \dfrac{\partial H}{\partial x}(0) = V \end{cases} \tag{5}$$

From (5) the mean power P' and the mean quadratic intensity J' are easily found, as functions of μ_r and θ.

We define the equivalent complex permeability as the solution of the system of two equations

$$P = P'(\mu_r, \theta), \quad J = J'(\mu_r, \theta) \tag{6}$$

A priori, μ_r and θ depend on a lot of parameters, and we shall examine this dependence in the next paragraph.

Let us remark that this ideal steel with equivalent permeability behaves like real steel with respect to P and J. These are the major parameters in heating applications, for J determines the power loss in the

coil, so that the heating power can be exactly determined. The comparison between P and J is also important to design the compensating capacitors.

This approach has a flaw : the exact *distribution* of power in the steel is not accurately predicted if one refers to (5) instead of (2) (3), but this is a minor disadvantage, for this power is dissipated in a very narrow skin depth (an the heat diffusion helps to smooth off the differences).

On the other hand, the simplification brought on by (5) in comparison with (2) (3) is obvious, *if the equivalent permeability is known.*

We shall attempt, in the coming paragraphs, to compute this permeability. In § 2, we put the equations in non-dimensional form, and make apparent the occurence of a *small parameter* ε. Setting $\varepsilon = 0$, we obtain a *classical formula* for the equivalent permeability. In § 3, we expose an approximate method, valid for small ε, which results in *corrections* to this formula. Detailed charts and curves for these correcting terms are given in § 4.

2. - EQUATIONS IN NON-DIMENSIONAL FORM. THE SMALL PARAMETER

Let us define new variables by

$$(7)\quad b = b_o \bar{b},\ \bar{t} = \omega t,\ h = H\bar{h},\ v = V\bar{v},\ x = \delta\bar{x}$$

and introduce the classical penetration depth

$$(8)\quad \delta_o = \sqrt{2/\sigma\ \omega\ \mu_o}\ .$$

Three non-dimensional parameters appear :

$$(9)\quad \rho = r\ \sigma\ \delta_o,\quad \lambda = \sigma\ \omega\ \delta_o(\mu_o\ \ell + s),\quad \varepsilon = \delta/\delta_o$$

If we decide that

$$(10)\quad \delta = (H/\sigma\ \omega\ b)^{1/2},\ H = \sigma\ \delta\ V = \sigma\ V^2/\omega b,$$

the equations (2) and (3) become (ignoring the bars)

$$(11)\quad \frac{\partial}{\partial t}\ \beta_\varepsilon\ (h) - \frac{\partial^2 h}{\partial x^2} = 0,\qquad x \geqslant 0,$$

$$(12)\quad \lambda\varepsilon\ \frac{dh}{dt} + \rho\varepsilon\ h - \frac{\partial h}{\partial x} = \sin t,\quad \text{for } x = 0$$

where β is the non dimensional magnetization characteristic. For saturated steel under high applied fields, it is customary to adopt the following representation of the b-h relation (figure 1) :

$$(13)\quad b = b_o\ \mathrm{sgn}(h) + \mu_o\ h$$

If b_o is taken as the new induction unit, (13) takes the non-dimensional form

$$(14)\quad \beta_\varepsilon(h) = \mathrm{sgn}(h) + 2\ \varepsilon^2\ h$$

When $\varepsilon = 0$, (11) (12) reduce to a classical equation (cf. Agarwal, [2]). The instantaneous field is (cf. fig. 2).

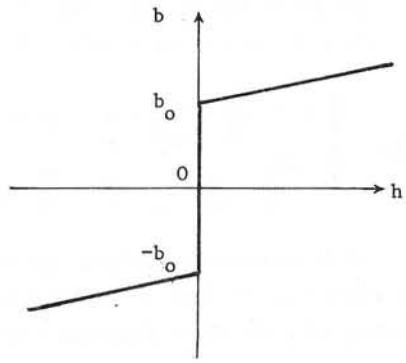

Figure 1

The b-h curve for intense fields

$$(15)\quad h(t,x) = (\sin^2 t/2 - x)\ \sin t \text{ if } x \leqslant \alpha(t) = \sin^2 t/2$$

$$= 0 \qquad \text{if } x \geqslant \alpha(t)$$

This allows to interpret δ and H in (7) : δ is the maximum depth of penetration of the field and $H = (32/5)^{1/2}$ Hm, where Hm = J is the mean quadratic field on the edge of the slab.

The factor ε is thus *a ratio of two penetration depths* (under and above the point of Curie) and it takes small values (0.1 to 0.3) in standard situations.

This fact justifies Agarwal's approximation ($\varepsilon = 0$). A straight - forward computation leads to the following expression for the equivalent

permeability when ε tends to zero :

$$(16) \qquad \boxed{\mu = 1.6 \frac{\mu_o}{\varepsilon^2} \exp\left[i(2 \operatorname{Arctan} 1/2 - \pi/2)\right]}$$

This must be understood as the first term of an asymptotic series in ε and we shall attempt to estimate the next term.

3. - A CORRECTION TO FORMULA (16)

Let us return to (11) (12). If we introduce the zeros $\{\alpha_i(t),\ i = 1,2,\ldots\}$ of h in x, (11) is *equivalent* to

$$(17) \qquad \begin{cases} 2\varepsilon^2 \dfrac{\partial h}{\partial t} - \dfrac{\partial^2 h}{\partial x^2} = 0 & \text{if } x \neq \alpha_i \\ 2 \dfrac{d\alpha_i}{dt} + \dfrac{\partial h}{\partial x}(\alpha_i + 0) - \dfrac{\partial h}{\partial x}(\alpha_i - 0), \quad i = 1,2, \ldots . \end{cases}$$

It is physically obvious (but hard to prove) that h is negligible for all $x > \alpha_1$. So that (11) (12) can be restated in the following form, keeping only the first abscissa α in consideration :

$$(18) \qquad 2\varepsilon^2 \frac{\partial h}{\partial t} - \frac{\partial^2 h}{\partial x^2} = 0\ , \quad x > 0, \quad 0 \leqslant t \leqslant \pi,$$

$$(19) \qquad 2 \frac{d\alpha}{dt} + \frac{\partial h}{\partial x}(\alpha(t)) = 0, \qquad 0 \leqslant t \leqslant \pi,$$

$$(20) \qquad h(\alpha(t)) = 0, \qquad 0 \leqslant t \leqslant \pi,$$

$$(21) \qquad \lambda\varepsilon \frac{dh}{dt}(0,t) + \rho\varepsilon h(0,t) - \frac{\partial h}{\partial x}(0,t) = \sin(t + \gamma(\varepsilon))$$

$$(22) \qquad h(0,0) = h(0,\pi) = 0$$

(A shift $\gamma(\varepsilon)$ in the origin of times has been introduced in (21) to satisfy (22), which ensures the necessary periodicity).

To study (18)... (22) we introduce a new parameter $\zeta = 2\varepsilon^2$ and set

$$(18') \qquad \zeta \frac{\partial h}{\partial t} - \frac{\partial^2 h}{\partial x^2} = 0$$

Developping formally the solution h in terms of ζ and ε, we have

$$(23) \qquad h_{\zeta,\varepsilon} = h_{o,\varepsilon} + \zeta \frac{\partial}{\partial \zeta} h_{o,o} + O(\varepsilon^3)$$

As we wish to obtain $h_{2\varepsilon^2,\varepsilon}$, the following procedure stems from (23) :

- Solve (18') ... (22) with $\zeta = 0$ to get $h_{o,\varepsilon}$
- Differentiate (18') ... (22) with respect to ζ and set ε to zero, to get $\dfrac{\partial h}{\partial \zeta}$,
- combine the results according to (19).

The solution found is accurate to the third order in ε.

The term $h_{o,\varepsilon}$

Let us introduce the new unknown function

$$(24) \qquad u(t) = \int_o^t h(s,0)\, ds$$

The system (18') ... (22) with $\zeta = 0$ becomes

$$(25) \qquad \begin{cases} \lambda\varepsilon \dfrac{du}{dt} + \rho\varepsilon u + 2\sqrt{u} = \displaystyle\int_o^t \sin(s + \gamma(\varepsilon))ds, \quad 0 \leqslant t \leqslant \pi, \\ u(0) = 0 \\ u'(\pi) = 0 \end{cases}$$

a two-point boundary value problem. It has been solved by a shooting method, with a standard iterative procedure on the phase shift γ, and a Runge-Kutta scheme (with precautions near the origin to cope with the stiffness of the differential equation).

The term $\partial h/\partial \zeta$

It can be obtained in closed form easily.

Combination

A computer program has been written for the IBM 370-168 of Electricité de France to carry through these operations, to compare the results with the solution of(5),and to derive the equivalent permeability as a function of the three parameters ε, ρ and λ. About 0.4 second of CPU-time is used for each triplet.It is convenient to express the results in the following form

$$(26) \quad \mu(\varepsilon, \rho, \lambda) = \frac{\nu^2(\varepsilon, \rho, \lambda)}{\varepsilon^2} \exp i \ \theta(\varepsilon, \rho, \lambda)$$

The curves below show how ν et θ vary with ε, ρ and λ.

4. - RESULTS

For a numerical example, let us use the MKSA System.

Reasonable values are :

Frequency : $\omega = 100\ \pi$

Resistance of the sheet : $r = 10^{-6}$ ($\Omega\ m^{-2}$)

Inductance of the sheet : $s = r/\omega$ ($\Omega\ m^{-2}$)

Airgap : $\ell = 0.1$ (m)

Conductivity : $\sigma = 10^{6}$ (Ω^{-1} m)

Applied voltage : V = 10 (V)

Induction at saturation : b = 1.5 (T)

With these values,knowing that $\mu_o = 4\pi\ 10^{-7}$, we obtain

Penetration depth : $\delta = 0.021$ (m)

Mean magnetizing field : Hm = 83000(A/m)

and for the dimensionless parameters

$\varepsilon = 0.298$, $\lambda = 2.88$, $\rho = 0.0712$.

From these figures, and from the examination of our results, we can draw the following conclusion :

Agarwal's formula is valid only for weak magnetizing fields (but strong enough to achieve saturation, of course). For strong fields, as in heating applications, a correction must be provided. This correction depends strongly on the airgap and only to a negligible extent on the impedance of the coil.

REFERENCES

[1] BARRET(P.), Contribution à l'étude du comportement du fer massif en régime alternatif saturé, note HM 010.49, E.D.F., 1972.

[2] AGARWAL (P.D.), Eddy-current losses in solid and laminated iron, *Trans. Amer. Inst. Elect. Engrs.*, 1959, *78*, Pt.II, pp. 169-181.

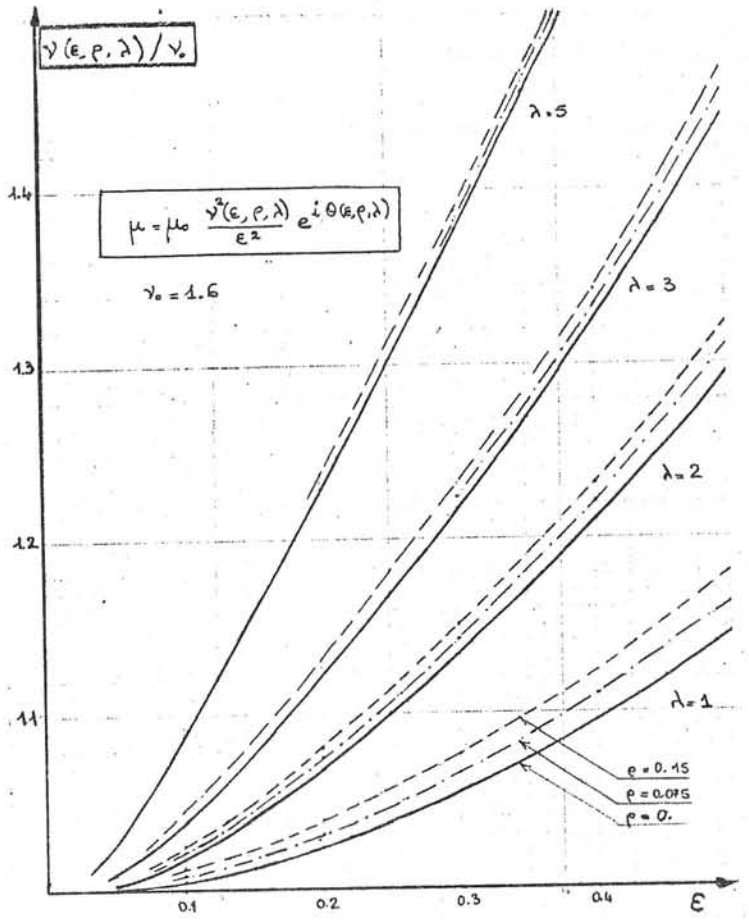

Variation of the modulus of the equivalent permeability

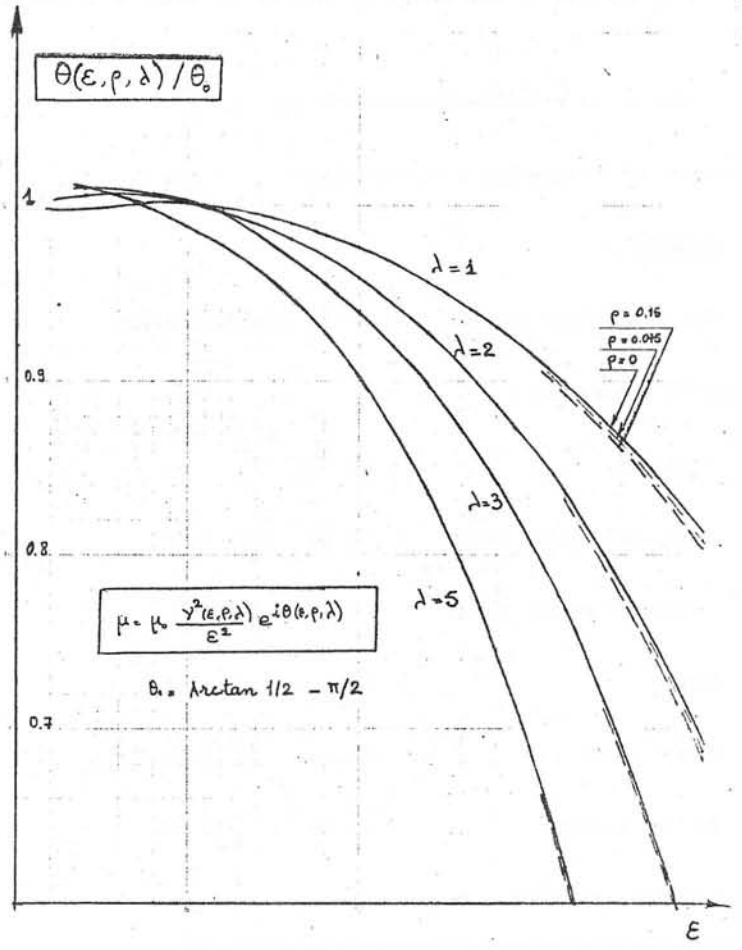

Variation of the argument of the equivalent permeability

A COMPUTERIZED PROGRAM FOR THE NUMERICAL SOLUTION OF HARMONIC FIELDS WITH BOUNDARY CONDITION NON PROPERLY DEFINED

A. Di Napoli, C. Mazzetti, U. Ratti
Electrical Engineering Institute - University of Rome
ROME

Summary

In a previous paper, /1/, an automatic computerized program was defined that, making use of the finite element technique, allows the study of the electromagnetic field relative to large-sized structures involved in high-frequency phenomena.

This program had been used for the determination of the electromagnetic field of a simple resistive divider for high-voltage measurement.

In this paper new devices are introduced that allow to markedly reduce both the storage area involved in the program and the computation time. This proved necessary in so much as the use of the program was so extended as to include the determination of the electromagnetic field of resistive dividers in the presence of electrodes and screens of various shapes and placed in different positions.

Introduction

The present paper represents an intermediate stage for the study of the electromagnetic field relating to large-sized structures involved in high-frequency phenomena. The computation methodology set forth here and applied to the solution of an electromagnetic field of a resistive voltage divider, was extensively illustrated under /1/; Fig. 6 shows the flow-chart, and Appendix 1, the relative equations.

In this paper, a computation subprogram was defined that, through the coefficient matrix inversion, directly solves the system of algebraic equations obtained, by means of the finite element technique, starting from the following differential equations:

$$\nabla^2 V = 0 \quad ; \quad \nabla^2 \dot{H} = \mu\varepsilon \frac{\delta^2 \dot{H}}{\delta t^2} \qquad (1)$$

The program was applied to the study of the electromagnetic field in a system consisting of a resistive voltage divider placed in a test laboratory, in which, unlike the work /1/, there are also present an HV electrode and ring-shaped screens. The system configuration, with the relative boundary conditions, are shown in Fig. 1.

The screens and the electrode are assumed to be made of fiber glass whose surface is metalized by means of a high-conductivity aluminium paint; in this way, they have a mere electrical and non magnetic function /2,3/.

The field distribution analysis was performed concomitantly with the frequency change; it is well known, in fact, that an impulsive wave may be always regarded as a sum of signals having a different frequency, amplitude and phase it ensues that the behaviour of the system under review, vis-à-vis this type of signal, provided that the system may be regarded as linear, is inferred from the results as a function of frequency. The interval considered is that comprised in the range of 0 to 250 kHz: such an interval also involves pulse waves with a rise time in the order of microseconds.

GEOMETRY OF THE SYSTEM AND BOUNDARY CONDITIONS

A system similar to that considered under /1/ was taken into examination, namely, a resistive divider with an anti-inductive winding, placed in a high-voltage laboratory, with both walls and ceiling assumed to be at zero potential.

In respect of the system analyzed under /1/, the resistive column is completed with an electrode placed in correspondence of a high-voltage terminal, as shown under Fig. 1 and 2.

The presence is subsequently considered of an annular screen positioned as in Fig. 1, and the influence is verified that it exerts on the behaviour of the field (Fig.3) and on the potential distribution along the divider (Fig.4), in the assumption of keeping it at the high-voltage terminal potential.

It should be noted that the system thus schematized presents a symmetry axis, and it is therefore possible to study the field behaviour in relation to any planes containing this axis, and to convert the problem under examination from bidimensional to tridimensional. Furthermore, in the plane under review, the system is still symmetrical in respect of the axis of the divider, and it is therefore possible to confine the study to one half plane only. In other words, it is possible to tackle the study of the field in cylindrical coordinates. Moreover, on the basis of the previous assumption of a perfectly anti-inductive winding, it is sufficient to study the phenomenon only in the region external to the divider, as schematically indicated in Fig. 1, where the part of the plane under examination is shown. This region, for the purpose of the application of the finite element technique, was in fact discretized into triangular elements of the first order, as shown in Fig. 2, where it looks thickened in the areas in which a higher electrical gradient was assumed to be present.

The presence of the screens or of the H V electrode has obviously modified in part the boundary conditions and the previously described /1/ field equations, without, however, any changes being made to the functional to be minimized /4,5,6/.

Concerning the boundary conditions relative to the HV electrode and the fixed potential screen, it proved sufficient to impose to the nodes placed on the conducting surfaces a potential equal to that of the high-voltage terminal of the resistive column.

As to segment OO', representing the divisor-air separation surface, it is quite impossible to define "a priori" the value of the displacement currents flowing from such surface, hence the V electric potential and the H_e magnetic field among it. As previously indicated under /1/, it was initially assumed to consider a purely linear potential distribution, and hence, by means of the iterative procedure described in the flow-chart, the actual distribution along the divider was calculated by successive approximations.

The electromagnetic field equations throughout the region under review, are represented by (1) equations, except for the areas placed internally to high-voltage electrode and screens. In this region, owing to the absence of displacement currents, equations (1) are replaced by:

$$\nabla^2 V = 0; \quad \nabla^2 \dot{H} = 0 \qquad (2)$$

Computation Program

The flow chart of the computation program is shown in Fig. 6. In this paragraph two peculiar features of the worked out program are emphasized: the storing of the coefficient matrix of the finite elements and the solution of the two following equation systems obtained by means of the finite element technique (5,6), starting from (1) equations:

$$|N| \cdot |V' + jV''| = 0 \qquad (3)$$

$$\left\{|M| + \omega^2 |T|\right\} \cdot |H'_o \cdot r + jH''_o \cdot r| = 0 \qquad (4)$$

With regard to the first point, it may be observed that we succeeded in considering a hisgh number of nodes, occupying rather reduced storage areas /7/, by storing only the values of the coefficients different from zero that appear in matrices !M! and !N!.

Let us consider, in fact, the node i, j, Fig. 5, being the vertex of six triangles forming the drawn hexagon; it is in fact pointless to assign storage areas to the coefficient tying node i,j to node i+2, j+2 which is certainly equal to zero. In this way, it was possible to store, making use only of triangular elements of the first order, only seven coefficients for each node, thus obtaining a remarkable saving in storage that becomes greater and greater as the number of nodes increases.

The solution of the system of equations (3) and (4) was performed making use of Choleski's decomposition /8/.

It should be reminded that the matrix !N! of (3) is a symmetrical matrix, decomposable in a univocal way into the product of two triangular matrices, of which one is the transposition of the other; equation (3) may be thus written as follows:

$$|N| \cdot |V' + jV''| = |m|^T \cdot |m| \cdot |V' + jV''| = 0 \qquad (5)$$

Premultiplying (5) by the reverse of $!m!^T$, we obtain:

$$|m| \cdot |V' + jV''| = 0 \qquad (6)$$

that, being a triangular matrix, is directly soluble.

In view of the previously mentioned storing of the matrix of only the coefficient different from zero, the one difficulty presented by such a way of working was that of obtaining the algorhythms for the computation of matrix !m! from !N!, writing in !m! only the coefficients different from zero.

Such a way of working involved a storage increase that was, however, offset by a decrease in computation time; this time was reduced to 2/3 of the computation time previously required, by having recourse to the over-relaxation method. It should be also noted that in so doing, the uncertainty is eliminated, that is due to the imperfect knowledge of the overrelaxation coefficient. It should be finally observed that this type of solution is particularly suitable for the problem under examination: in fact, owing to the lack of knowledge of the potential distribution along 00', recourse must be had to successive iterations, during which the matrix to be inverted remains unchanged, and hence, for each iteration, it will suffice to solve the system in respect of the new values of V and of H, calculated along the 00' boundary.

Conclusions and Further Developments

The work carried out highlighted two particular features of the system under review:

- the methodology used for the solution of the system of equations (1);
- the application of the program formulated under /1/, as modified for the study of the divider-screen-electrode-laboratory system.

Concerning the first point, one can be fully satisfied, in view of the saving obtained both in machining time and in the storage area occupied.

As to the second point, although the influence the screen and the electrode exert upon the field behaviour and upon the potential distribution, was duly ascertained, some doubtful points, already present in /1/, still remain in existence. In fact, for frequences below 1kHz, there still exist uncertainties due to the error in the computation of the derivative of !M! (eq. I.6); such uncertainties would be at least reduced by using elements of a higher order than the first one, and we intend to work in the future along these lines.

References

/1/ A. Di Napoli, C. Mazzetti, V. Ratti, "Electromagnetic Field Computation of HV Resistive Divider" - I.C.C.A.D., S. Margherita Ligure, 1976.

/2/ C. Mazzetti, U. Ratti, A. Tomassi, "Dividers for High-Voltage Measurements" - La Goliardica, Roma, 1973.

/3/ B. Heller, A. Veverka, "Les phénomènes de chac dans les machines électriques" - Dunoil, Paris, 1963.

/4/ P. Silvester, M.V.K. CHARI, "Finite Element Solution of Saturable Magnetic Field Problems" - I E E E , Paper 70, TP 130, PWR.

/5/ C.J. Carpenter, "Computer Solution of Field Problems", - Notes of Power System Equipment, London, 1971.

/6/ J.O.C. Zienkiewicz, "The Finite Element Method in Engineering Science" - McGraw-Hill, London, 1971.

/7/ A. Di Napoli, "The Finite Element Method in the Study of Electromagnetic Fields" - La Goliardica, Roma, 1975.

/8/ "Calcul Matricial", Dunod, Paris.

APPENDIX

The flow-chart of the computation program and the algorhythms referred to therein, are reported hereunder (Fig. 6) for a correct understanding of the work.

The equation systems (3), (4), by making use of Choleski's decomposition, may be respectively written as follows:

$$|m| \quad |V' + jV''| = |V'_c + jV''_c| \tag{I.1}$$

$$|n| \; |H'_\vartheta + jH''_\vartheta| = |H'_{\vartheta_c} + jH''_{\vartheta_c}| \tag{I.2}$$

where, as a secondo member, there are placed the voltage and magnetic field vectors fixed at any iteration; !m! and !n! are triangular matrices. From the computation of potential V one goes back to the value of the electric field E_z in the barycenter of the triangles adjacent to the instrument

$$E_r = -\frac{\delta V}{\delta r} \tag{I.3}$$

and, hence, to the displacement currents value:

$$I_s = \frac{dQ}{dt} = \frac{d}{dt}(\varepsilon E_r \cdot 2\pi r l) = j\omega\varepsilon E_r 2\pi r l \tag{I.4}$$

The H values along 00' may be calculated from:

$$H_\vartheta = \frac{I}{2\pi r} \tag{I.5}$$

where I is the current flowing through the divider, less the quantity I_s that flows out of the latter by the capacitive route.

Starting from the value of the magnetic field H_e the electric field E is determined along 00':

$$-\frac{1}{r}\frac{\delta}{\delta r}(H'_\vartheta + jH''_\vartheta) \cdot r = \varepsilon\frac{\delta}{\delta t}(\tilde{E}'_z + j\tilde{E}''_z) \tag{I.6}$$

The knowledge of this component allows to calculate the electromotive force $\Delta V = E_z \cdot \Delta l$ induced by the magnetic field that is added to the resistive dump:

$$V_{new} = V_R + \Delta V \tag{I.7}$$

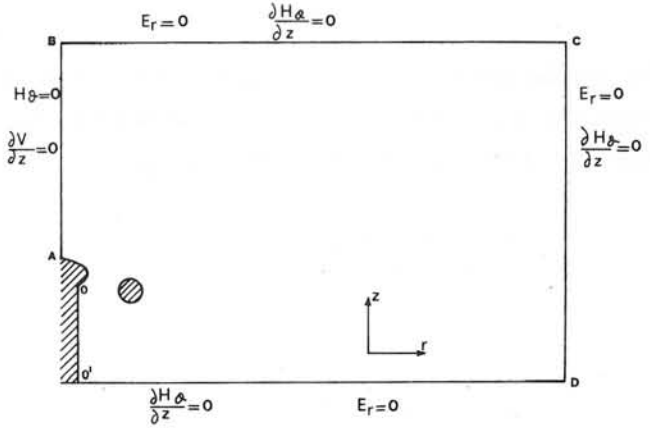

Fig. 1

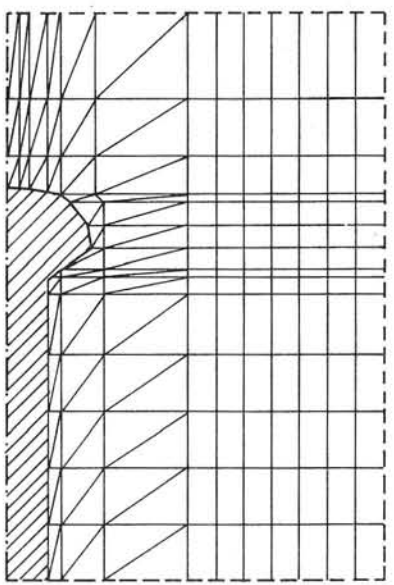

Fig. 2

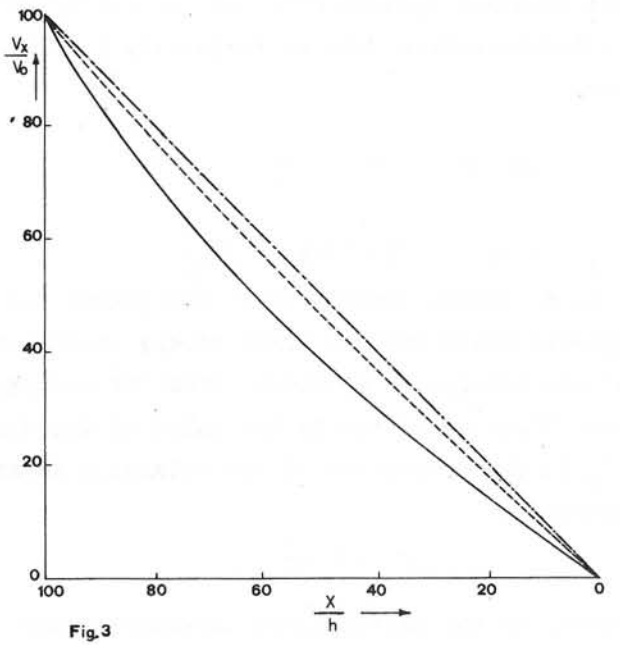

Fig.3

Fig. 3

Potential distribution along the resistive divider at 250 kHz

_____ without screen

---------- with screen

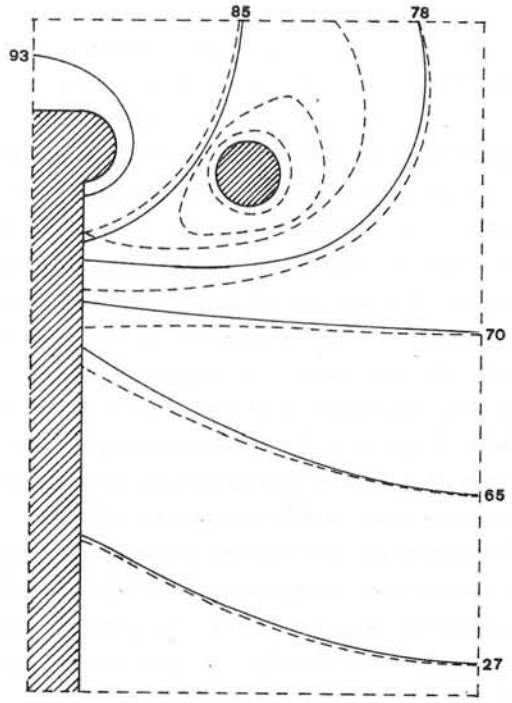

Fig.4
Equipotential lines at 250 kHz
———— without screen
---------- with screen

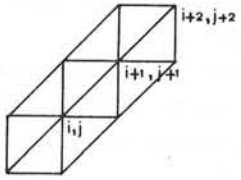

Fig. 5

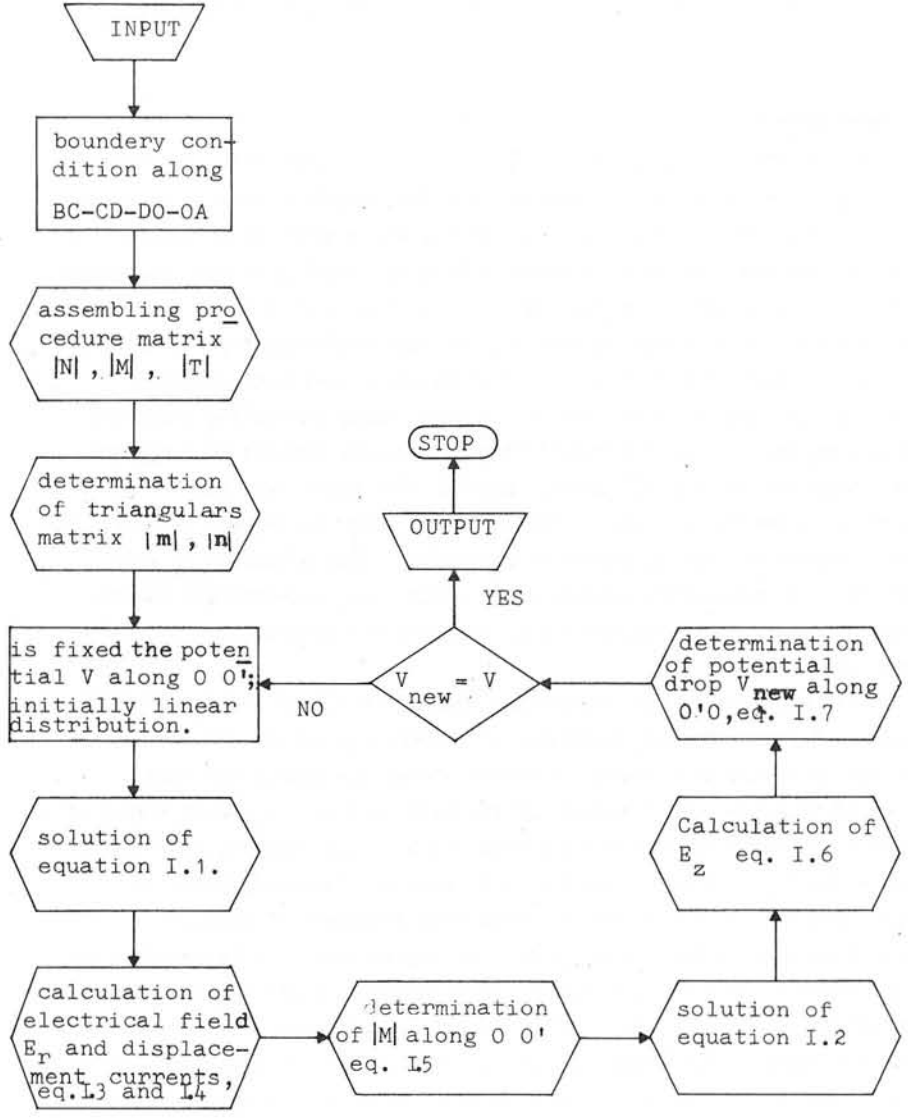

Fig. 6

A COMPUTER METHOD OF CALCULATING THE EDDY CURRENT HEATING OF MAGNETIC MATERIALS, WITH A COMPARISON BETWEEN PREDICTED AND MEASURED RESULTS IN A 2MVA INDUCTION FURNACE

R C GIBSON

1. Introduction

At the Electricity Council Research Centre, Capenhurst, considerable effort is being expended on research into the induction heating of metals. Much of this work is of a practical nature, concerning the development of existing and novel induction heating techniques, leading to the production of full scale industrial prototypes. In parallel with this, a theoretical analysis of induction heating methods has been undertaken by the author.

As a result of this theoretical analysis, a series of computer programs have been written to model various induction heating processes. These programs include the calculation of the eddy current heating, and the subsequent thermal diffusion, together with facilities for controlling the furnace power, frequency and other parameters necessary to model industrial heating processes accurately. Due allowance is made both for the temperature dependence of electrical, magnetic and thermal properties during the heating cycle, and also for saturation of magnetic materials.

This paper describes the methods used to calculate the two-dimensional magnetic field, with eddy currents, in a short cylindrical or flat wide coil of an induction furnace. A finite difference method has been selected as being most suitable for this application. A direct method of solution of the complex coefficient matrix has been adopted, as it has been found to be more efficient of both user and computing time. A detailed analysis is made of the simplified treatment of magnetic saturation used in the method, and it is argued that this is suitable for cases where a low cost calculation giving greater accuracy than orthodox design methods is required. Details are given of tests performed with both non-magnetic and magnetic loads in a 2MVA multilayer billet heater, and the measured results are compared with those calculated using the methods given in this paper.

2. Description of Program and Mathematical Model Used.

The program is essentially in two halves. First the eddy current power distribution is evaluated, and then this is used as source terms in the thermal diffusion equation to calculate the temperature rise in the furnace charge. After a suitable interval, the eddy current heating is recalculated using updated values of physical properties appropriate to the new node temperatures. This cycle of alternate solution of magnetic and thermal fields is continued until the required temperature is obtained. During this heating cycle, such parameters as supply voltage and frequency, furnace power etc. can be altered to model the particular induction heating process being followed. In addition, the program permits furnace power to be controlled in order to provide rapid heating under such thermal constraints as a maximum temperature gradient or a maximum surface temperature. Heat losses from the furnace charge through a thermally insulating refractory are also taken into account.

Figure 1 shows the cross-section of the short circular furnace for which the calculated and measured results are compared in Section 5. A finite difference mesh is fitted to the cross-section as shown, the mesh extending beyond the coil to take adequately into account the stray magnetic field. The electrical and thermal conductivity, heat capacity etc. for each mesh element are interpolated from tabulated values. The derivation of the effective mesh permeability is given in Section 4. The magnetic field equations are written for each node in terms of the vector potential so that in the usual notation

$$\text{curl}\ (1/\mu\ \text{curl}\ A) = -j\,2\pi f \sigma A + J_s \qquad 2.1$$

where μ and σ are assumed constant in time, but can differ for each mesh element. A and J_s are assumed to be sinusoidal functions at frequency F. The method of solution of these equations is given in Section 3.

The thermal diffusion equation can be integrated by a variety of means, in this case a variant of the Runge-Kutta method.

2.1. Calculation of Coil Losses.

The coil losses can be calculated by covering the winding with a finely divided mesh and allowing the program to calculate the eddy current losses in the winding strands in the same way as for the furnace charge. However in a case such as that of Figure 1, where the windings are reasonably well stranded (each strand being not deeper than one penetration depth) a more economic coarse mesh can be used. It is sufficient to assume initially that each strand is perfectly insulating but carrying the requisit source current. Once the magnetic field and the eddy currents in the furnace charge has been evaluated, the ohmic

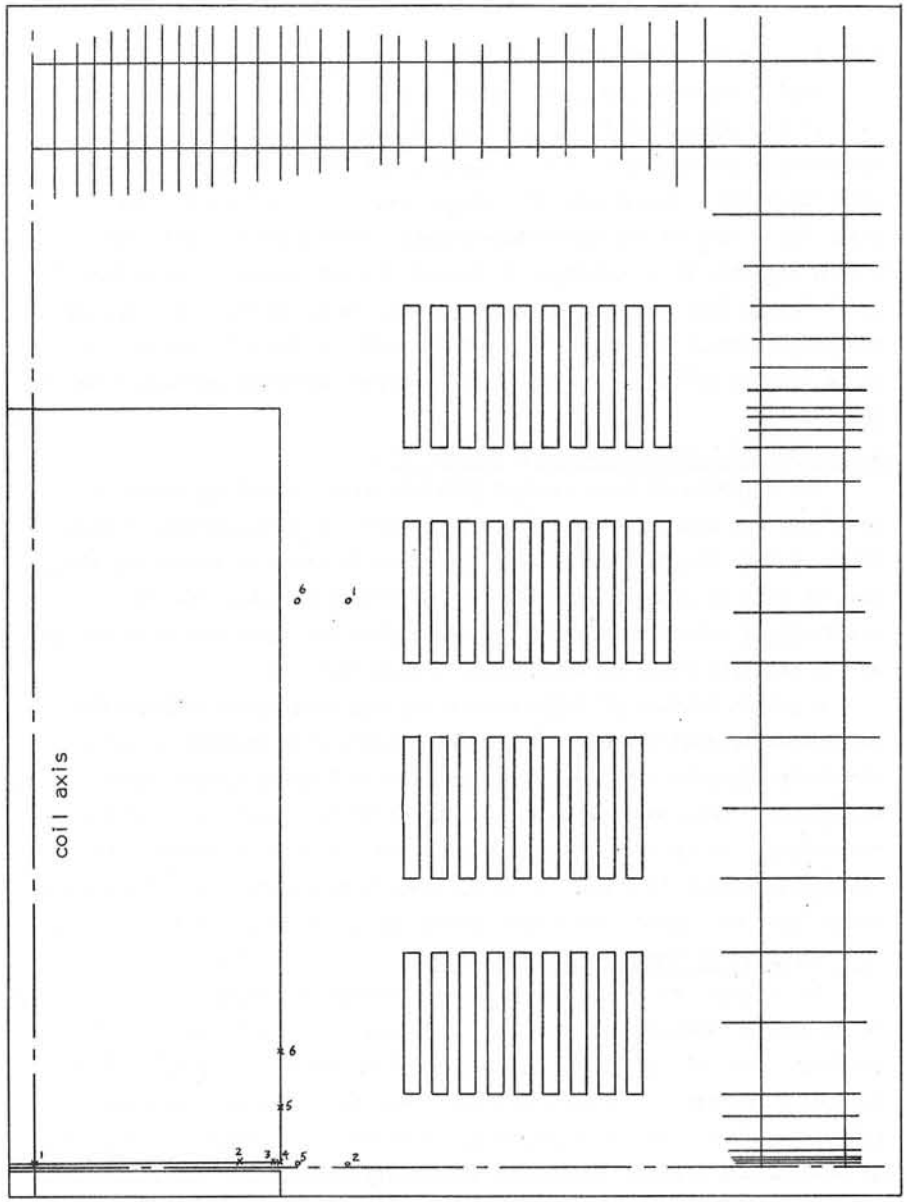

Figure 1 Cross-section of Top Half of 2 MVA Inductor showing Billet, Multi-layer Winding and Finite Difference Mesh

and eddy current winding losses can be simply calculated using the magnetic field passing through each strand. The slight difference between the current distribution initially assumed within each strand, and that which actually occurs as a result of the eddy currents, has negligible effect on the actual magnetic field distribution.

3. Method of Solving Node Equations

A finite difference method was selected, as, although finite element methods are advantageous with irregular geometries, the regular shapes of induction furnaces, with current flows parallel to the surfaces, allow a rectangular mesh to be suitably graded so that the use of excessively fine meshes in unimportant regions can be minimised. The use of a rectangular grid considerably simplifies mesh preparation, an essential feature if the performance of a furnace is to be assessed at short notice. Another important advantage of using a rectangular grid is that more efficient algorithms can be written for the solution of the node field equations; the problems of optimising the band width due to the use of an irregular mesh being avoided.

Iterative methods for solving the matrix of node coefficients have been attempted, but in spite of using line relaxation and other aids, it was found that convergence was relatively slow for complex coefficients with non-uniform meshes and varying physical properties. Problems were also experienced with defining convergence and selecting convergence factors in the complex plane.

A direct method of solution was adopted, and implemented on a UNIVAC 1108 computer as follows. A coefficient matrix for a small problem is shown in Fig. 2. The only core storage required to set up the matrix is for the real arrays f, g, r and the complex array A, A being used both for the source terms J and the solution. A Gaussian elimination method is used, and each line of mx coefficients of the upper triangular matrix is written to the NTRAN backing store while the next line is being formed, using a local complex array of size mx^2. The rapid data transfer to the NTRAN drum occurring simultaneously with the main core calculations and combined with the low core storage requirement allows sets of up to 3000 equations of complex variables to be solved. The time taken on the UNIVAC 1108 is approximately 35 $mx^3 my \mu s$. Fortunately, many induction furnace applications require

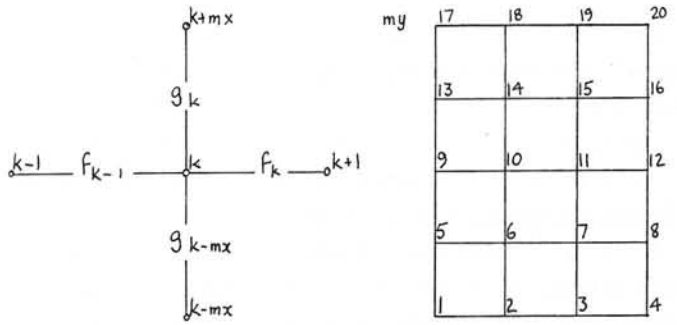

$$e_k = f_k + f_{k-1} + g_k + g_{k-mx} + jr_k$$

$$\begin{bmatrix}
e_1 & -f_1 & & & -g_1 & & & & & & & & & & & & & & & \\
-f_1 & e_2 & -f_2 & & & -g_2 & & & & & & & & & & & & & & \\
 & -f_2 & e_3 & -f_3 & & & -g_3 & & & & & & & & & & & & & \\
 & & -f_3 & e_4 & & & & -g_4 & & & & & & & & & & & & \\
-g_1 & & & & e_5 & -f_5 & & & -g_5 & & & & & & & & & & & \\
 & -g_2 & & & -f_5 & e_6 & -f_6 & & & -g_6 & & & & & & & & & & \\
 & & -g_3 & & & -f_6 & e_7 & -f_7 & & & -g_7 & & & & & & & & & \\
 & & & -g_4 & & & -f_7 & e_8 & & & & -g_8 & & & & & & & & \\
 & & & & -g_5 & & & & e_9 & -f_9 & & & -g_9 & & & & & & & \\
 & & & & & -g_6 & & & -f_9 & e_{10} & -f_{10} & & & -g_{10} & & & & & & \\
 & & & & & & -g_7 & & & -f_{10} & e_{11} & -f_{11} & & & -g_{11} & & & & & \\
 & & & & & & & -g_8 & & & -f_{11} & e_{12} & & & -g_{12} & & & & & \\
 & & & & & & & & -g_9 & & & & e_{13} & -f_{13} & & & -g_{13} & & & \\
 & & & & & & & & & -g_{10} & & & -f_{13} & e_{14} & -f_{14} & & & -g_{14} & & \\
 & & & & & & & & & & -g_{11} & & & -f_{14} & e_{15} & -f_{15} & & & -g_{15} & \\
 & & & & & & & & & & & -g_{12} & & & -f_{15} & e_{16} & & & & -g_{16} \\
 & & & & & & & & & & & & -g_{13} & & & & e_{17} & -f_{17} & & \\
 & & & & & & & & & & & & & -g_{14} & & & -f_{17} & e_{18} & -f_{18} & \\
 & & & & & & & & & & & & & & -g_{15} & & & -f_{18} & e_{19} & -f_{19} \\
 & & & & & & & & & & & & & & & -g_{16} & & & -f_{19} & e_{20}
\end{bmatrix}
\cdot
\begin{bmatrix} A_1 \\ A_2 \\ A_3 \\ A_4 \\ A_5 \\ A_6 \\ A_7 \\ A_8 \\ A_9 \\ A_{10} \\ A_{11} \\ A_{12} \\ A_{13} \\ A_{14} \\ A_{15} \\ A_{16} \\ A_{17} \\ A_{18} \\ A_{19} \\ A_{20} \end{bmatrix}
=
\begin{bmatrix} J_1 \\ J_2 \\ J_3 \\ J_4 \\ J_5 \\ J_6 \\ J_7 \\ J_8 \\ J_9 \\ J_{10} \\ J_{11} \\ J_{12} \\ J_{13} \\ J_{14} \\ J_{15} \\ J_{16} \\ J_{17} \\ J_{18} \\ J_{19} \\ J_{20} \end{bmatrix}$$

To set a boundary node to zero, the coefficient e for that node is multiplied by 10^6 and the source term J is set to zero.

Figure 2. Coefficient Matrix for Small Finite Difference Grid.

long thin grids and so the band width mx is kept relatively small.

When evaluating the matrix coefficients, f, g and r, values of resistivity and permeability are taken appropriate to the local node temperature and magnetic field strength. An extensive error analysis undertaken for a one-dimensional case shows that the second order error for a node at the Curie temperature, where eddy currents pass from a magnetic to a non-magnetic region are not excessive provided a sufficiently fine mesh is taken. It should be noted that in a typical induction furnace the magnetic field strength in the coil airgap can be as high as $10^6 Am^{-1}$, giving a billet surface relative permeability of about 3.

4. Method of Treating Magnetic Saturation.

The solution of eddy current problems with saturating magnetic materials has been attempted by many methods. A disadvantage of most of these is that they are relatively expensive in terms of computing time, and, as will be readily appreciated, not really suitable for the modelling of induction heating processes with the attendant recalculation of the magnetic field as the furnace charge heats up.

A common feature of these more elaborate treatments of magnetic saturation is that the magnetic field strength H is assumed to be a sinusoidal function of time, the flux density B being grossly non-sinusoidal. Less commonly B is considered to be sinusoidal with H non-sinusoidal. It is the author's opinion that in reality, neither of these assumptions is true. It is considered that both H and B are near sinusoidal, or rather that H and $\partial B/\partial t$ are near sinusoidal.

4.1 Analysis of Magnetic Field Waveforms.

It is usual to connect power factor correction capacitors across the mains supply terminals of induction furnaces, and other low power factor devices. For optimum power factor correction the reactive components of current circulate in the series circuit formed by the coil and the capacitors, the value of capacitance being chosen so that the reactance of this series circuit is zero at the supply frequency. The magnitude, however, of this series reactance is much greater at higher frequencies, and so any higher harmonics in the current, and hence airgap and furnace charge surface magnetic field strength waveforms are heavily damped.

Two other features of induction furnace installations merit attention. Firstly, the voltage applied to the coil is known to be

sinusoidal as the load taken by the furnace has little or no effect on the supply system. Secondly it is usual to leave a fairly substantial distance between the furnace charge and the coil to allow for mechanical clearances and thermal insulation.

The significance of these last two points can be demonstrated by considering a very long uniformly wound coil of cross-section area A_c. Inside this coil, parallel to its axis is placed a magnetic core of uniform cross-section area A_m. This magnetic core has a typical B-H characteristic, but has infinite resistivity so that no eddy currents are induced in it. In such a case the magnetic field strength H inside the coil is therefore everywhere parallel to the axis of the coil and of constant magnitude both within the magnetic core, and in the airgap between the coil and the core. The flux density in the magnetic core is μH where μ is a function of H. The instantaneous voltage/turn in the coil is given by

$$v = \frac{\partial}{\partial t}(H(\mu A_m + \mu_o(A_c - A_m))) \qquad 4.1$$

$$= A_m \frac{\partial}{\partial t}(\mu H) + \mu_o(A_c - A_m)\frac{\partial}{\partial t}(H) \qquad 4.2$$

Now if

$$v = V \cos wt \qquad 4.3$$

both sides of equation 4.1 can be integrated with time, and if μ is represented as a function of H by, for instance, the Fröhlich equation

$$\mu = a/(b + |H|) + c \qquad 4.4$$

a table of instantaneous values of H can be calculated corresponding to a number of points on the voltage cosine wave. It is then a simple matter using fast Fourier transforms to obtain a Fourier series expansion for H. From the table of instantaneous values of H it is possible to tabulate the flux density in the magnetic core from the product $\mu.H$. Furthermore, the instantaneous values of flux density can be numerically differentiated to tabulate the expression $\partial(\mu H)/\partial t$. The accuracy of all these numerical calculations can be checked by evaluating v from the computed values of the right hand side of equation 4.2.

This analysis was carried out for a wide range of typical magnetic field strengths, B-H characteristics (including hysteresis), and magnetic core cross-sectional areas. Characteristic waveforms of magnetic field strength, permeability, magnetic core flux density and the time derivative of magnetic core flux density, are shown in Figure 3. Although the wave forms may look distorted, examination of the harmonic content shows in particular that the magnitude of the third harmonic of the H and $\partial(\mu H)/\partial t$ wave forms is less than 30% of the fundamental, no other harmonic being greater than 10%. Also the r.m.s. value of the fundamental is greater than 95% of the r.m.s. value of the total waveform.

4.2 Derivation of Concept of Effective Permeability.

Returning now to the eddy current analysis, equation 2.1 can be rewritten as

$$\text{curl}\,(\rho\,\text{curl}\,H) = -\partial(\mu H)/\partial t \qquad 4.5$$

Now if H is H'sin wt and μ is constant in time, the right hand side of equation 4.5 becomes

$$\mu\partial(H' \sin wt)/\partial t = w\mu H' \cos wt \qquad 4.6$$

or using the notation $H = \mathcal{J}(H'e^{jwt})$ the right hand side of equation 4.5 becomes $-j w\mu H$.

However if μ is a function of H, the above analysis of equation 4.5 is invalid. Looking again at Figure 3, it can be seen that if higher harmonic components are ignored H can still be written as H'sin wt. Also $\partial(\mu H)/\partial t$ can be written as H'' cos wt. If we define

$$H'' = w\mu' H' \qquad 4.7$$

then a new right hand side of equation 4.5 can be written as $-jw\mu' H$.

μ' is defined as the effective permeability. In the analysis of Section 4.1 it was found that for a wide range of cases, μ' corresponded to the permeability calculated for a value of magnetic field strength equal to 0.75 to 0.85 of that of the peak of the fundamental component of the magnetic field strength wave form. It was also found that, for a wide range of typical B-H characteristics, this value of effective permeability is independent of the exact form of the B-H characteristic below the saturation knee.

It is admitted that the extension of the analysis of the magnetic core without eddy currents to cover the case of a magnetic core with eddy currents is not strictly valid. The significant point, however, is that although the relationship between B and H is grossly non-linear, there can exist waveforms of $\partial B/\partial t$ and H which are simultaneously near sinusoidal. As has been noted in Section 4.1 the physical mechanisms occurring in induction furnaces and other similar devices are such as to reduce the magnitude of higher harmonic components of magnetic field

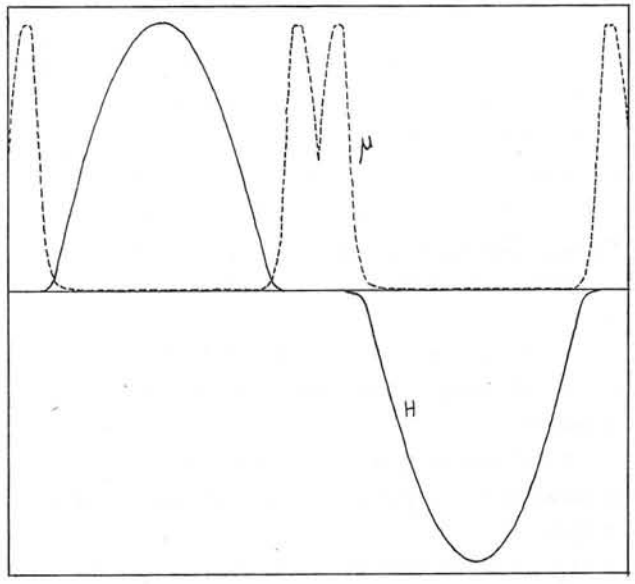

Figure 3(a) Waveform of Magnetic Field Strength H with Corresponding Permeability Waveform μ

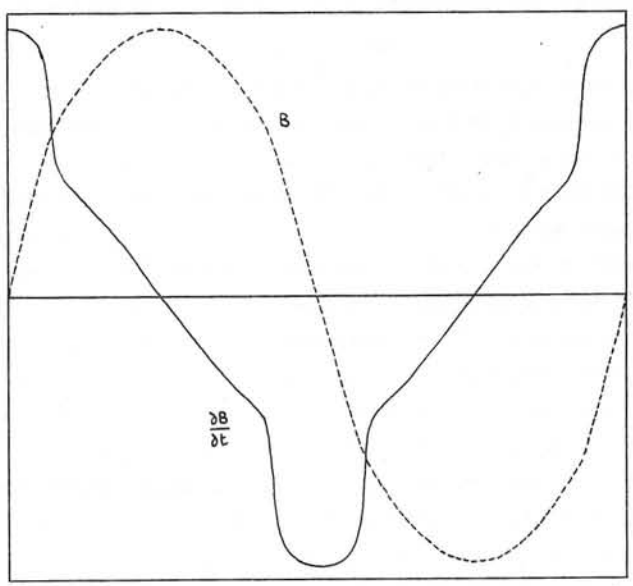

Figure 3(b) Waveforms of Magnetic Flux Density B and $\partial B/\partial t$ Corresponding with Magnetic Field Strength above.

strength and flux density.

It therefore seems reasonable to assume that for problems similar to those encountered in Induction furnace analyses, that is with sinusoidal voltages, and with power factor convection tuned to the supply frequency, it is possible to use the simple concept of a constant effective permeability.

4.3 Simplified Treatment of Magnetic Saturation Used in Program.

The program only considers the fundamental of the magnetic field waveform and uses the concept of effective permeability introduced in Section 4.2. The permeability for each mesh element is calculated using a value 0.8 times the most up to date peak value of the magnetic field strength stored for that mesh element. After solution of the magnetic field, new values of the permeability are calculated and compared with the old values. If agreement is within previously determined limits, (usually 10% is adequate) the program continues to calculate the eddy current power distribution. Should agreement not be achieved, the process is repeated, convergence usually being very rapid with the direct method of solution of the node field equation used.

4.4 Representation of B-H characteristic.

Various methods of expressing permeability as a function of magnetic field strength have been tried, but it has been found adequate to use the simple Frölich expression of equation 4.3 where c tends to μ_o for optimum fit for high values of H (10^4 - 10^6 Am^{-1}). A rapid method of obtaining the coefficients a, b and c is to plot $1/(\mu - c)$ against H for various values of c and to select the value of c that gives the best straight line fit in the region near the maximum value of H that is expected. The slope of this straight line is 1/a and the y-intercept b/a.

5. Comparison of Predicted Performance with Measurements made on a 2 MVA Induction Furnace.

The validity of the mathematical model used in the analysis of induction furnaces, and the accuracy of the method of solution, were tested by comparing predicted performance with measurements taken during heating trials on the prototype 2 MVA 50 Hz cylindrical billet heater with coils using multi-layered windings shown in Figure 1. The winding losses, the terminal voltage, current and power, search coil voltages,

and temperature distribution in the billet, were continuously metered during the course of several heating cycles.

5.1 Tests with Non-magnetic Billets.

The programs were first tested comprehensively with non-magnetic billets, before the complications of magnetic saturation were introduced. The initial tests were made with copper billets, as the physical properties are well documented for the commercially pure metal. Excellent agreement was achieved with electrical measurements such as coil voltage, total power, power factor, coil losses and search coil voltages, and with the rate of temperature rise. A less constructive interpretation could be made of the temperature gradient through the billet however, as the high thermal conductivity of the copper prevented the surface to centre temperature difference from exceeding about 10°C. This was about the same value as the estimated error in the measurements.

In an attempt to increase the surface to centre temperature difference, the tests were repeated using a metal with a much lower thermal conductivity, namely stainless steel. As the physical properties are variable from sample to sample, it was necessary to have the thermal and electrical properties accurately measured as functions of temperature, specimens for this purpose being cut from the billet after the heating tests were completed. To facilitate the measurement of the thermal gradient, the billet was cut into two equal lengths. After thermocouples had been attached to the surfaces thus exposed, the two halves were packed closely together again as shown in Figure 1. A detailed study was also made of temperature corrections for heat lost along the thermocouple wires. The stainless steel billet was heated up to 1200°C and excellent agreement was again obtained, the predicted values of electrical and thermal parameters being within the estimated accuracy of the measured results.

5.2. Tests with Magnetic Billets.

A mild steel billet was prepared in a similar way to the stainless steel billet, and heated from cold, through the Curie temperature, in the 2MVA billet heater. Additional measurements were made by logging the coil voltage and current, together with five search coil voltages on a multi-track tape recorder. This enabled the waveforms to be analysed, and also the inductor power to be determined accurately by taking a true product of the instantaneous current and voltage, and analysing the waveform of this product. Figure 4 shows the terminal voltage and current waveforms, together with the waveform of search coil 5 shown in Figure 1. The values of the third harmonics are 1%, 4% and 15% of the respective fundamentals. It can be seen that the harmonic content is small.

The calculated values of furnace power and voltage, winding losses and search coil voltages taken through the heating cycle were within 15% of the measured values. The coil current was taken as the common parameter for predicting the results. A comparison between calculated and measured values of temperature through the heating cycle can be seen in Figure 5 where the temperatures measured by thermocouples 1, 2 and 3-6, positioned as in Figure 1, are shown. The disparity between predicted and measured values around the 80 second mark largely reflects errors in the measured value taken for the Curie temperature of the billet material. This is a critical comparison as not only does the temperature rise show the instantaneous eddy current power and power distribution, but the graphs also reflect the time integral of power and power distribution.

While agreement is not perfect, the accuracy is quite adequate for predicting furance performance. In particular the thermocouple readings giving the temperature distribution through the billet indicate that the eddy current heating has been calculated with reasonable accuracy.

While calculating the results discussed above, the effect of varying the values of physical properties of the billet material were assessed. The permeability measurements are the most difficult to obtain accurately, but it was found that for the above heating cycle the billet power varied as $\sqrt{\mu}$ for small changes in permeability. This agrees with the analytical results obtained for a cylindrical billet where the penetration depth

$$\delta = (2p/w\mu)^{\frac{1}{2}}$$

is small compared with the billet diameter.

As the sensitivity of the results to changes in the value taken for billet permeability is small, and as noted in Section 4.2 the results are independent of the exact shape of the B-H characteristic below the saturation knee, it is only necessary to measure values of permeability near the peak value of H expected during the course of the heating cycle.

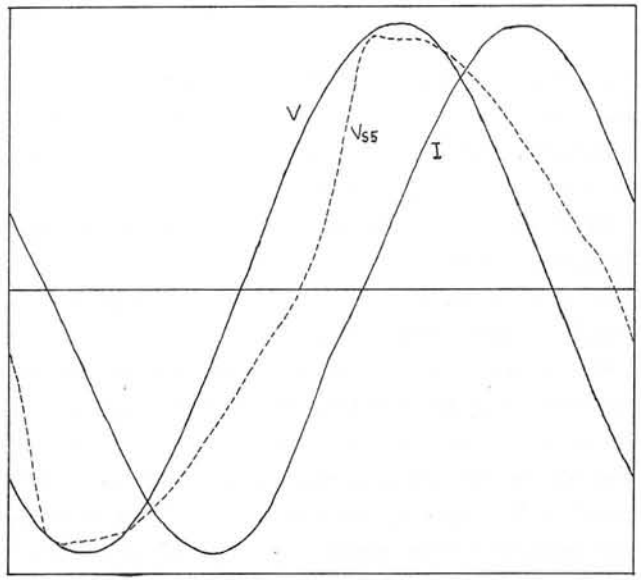

Figure 4. Waveforms of Coil Voltage V, Coil Current I and Search Coil 5 Voltage V_{S5} Taken 4 Seconds from Start of Test with Magnetic Billet.

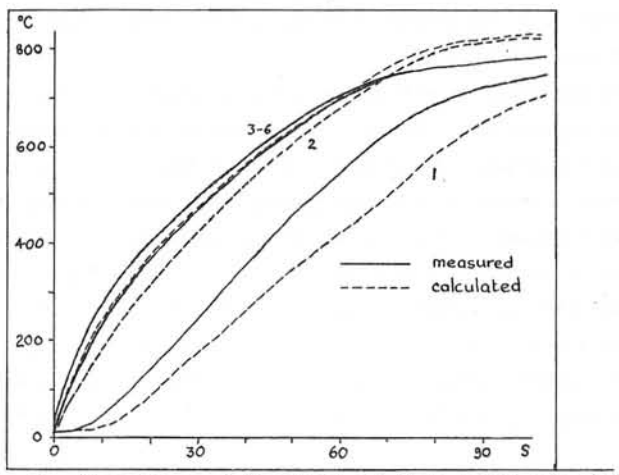

Figure 5. Comparison of Measured and Calculated Temperatures during test with Magnetic Billet.

6. Conclusions

The analytical techniques for modelling induction heating processes, and in particular the treatment of magnetic saturation giving rise to the concept of a linear effective permeability have been tested by comparing predicted and measured results of tests on a 2MVA 50 Hz billet heater.

With non-magnetic billets the agreement between measured and predicted results is very close, being within the accuracies of the techniques used to monitor the heating cycle, and also to measure the physical properties used for the theoretical calculations. Less good agreement is achieved for magnetic billets. The measurements are also more troublesome in this case, and it is difficult to separate out the errors due to the analytical methods used. However, the overall accuracy of the results is within the general tolerances within which the physical properties of industrial steels are known.

The analytical techniques outlined in this paper can therefore be used to compare different furnace designs and the performance of a furnace with different billet materials. While these techniques may not be applicable to all electromagnetic field problems, their use is recommended in many cases where, as in the prediction of induction furnace performance, it is necessary to obtain a theoretical assessment of problems to a greater accuracy and detail than by conventional design methods, and yet remain within a realistic costing for the study of a complete industrial process.

Acknowledgments

The author wishes to thank the Electricity Council for permission to publish this work. The author is also indebted to his colleagues, in particular Mr. I.G. Harvey, for providing the test results.

A METHOD OF CALCULATING EDDY CURRENT LOSSES IN THE ROTOR RETAINING RING OF A TURBOGENERATOR DUE TO THE TOOTH RIPPLE FIELD

BY

D. Howe and T.G. Phemister

C.A. Parsons and Co. Ltd., Newcastle upon Tyne

A method has been developed for calculating the eddy current loss in the rotor retaining ring of a turbogenerator. The airspaces and the conducting ring are considered independently, the two regions being connected by the continuity of the field between the regions.

The airspace has a complicated geometry and a solution of the Laplacian field in this region has been based on the finite element method. The retaining ring has a simple geometry and a solution of the linear diffusion field has been obtained by an analytical method derived from the boundary conditions in that region. Interaction between the regions is calculated by iteration.

The method may have wider application to more general problems.

List of symbols

a	thickness of retaining ring.
$a_i, b_i, c_i, A_m, B_m, C_n, D_n$	coefficients.
$\underline{B}$	magnetic flux density.
b	pole pitch of field component × $1/2\ \pi$
B_x, B_y, B_z	components of flux density
c	length of retaining ring.
$\underline{E}$	electric field strength.
E_m, F_m, G_n, H_n	coefficients.
$\underline{H}$	magnetic field strength.
$\underline{J}$	current density
J	Lagrangian
k	harmonic number, number of stator slots
L	linear operator
p	radius of rotor surface.
P, Q, R, S	coefficients.
r, θ, z	cylindrical polar coordinates.
s	radius of stator bore.
t	time.
V_m	magnetic scalar potential.
V_m'	approximation to V_m
x, y, z	Cartesian coordinates.
Δ	element area.
θ	phase angle.
$\phi_m, \eta_m, \psi_n, \xi_n$	coefficients.
μ_0	permeability of free space.
μ_1	incremental relative permeability along x and z direction.
μ_2	incremental relative permeability along y direction.
ρ	resistivity.
ω	angular frequency.
∇^2	Laplacian operator.

Introduction

The continuing increase in the unit size of turbogenerators is being made possible by the use of improved materials and cooling methods, and by more sophisticated design techniques. With the development of more reliable methods of calculation it is possible to extend the limits of safe design.

The rotor end retaining ring is the most highly stressed component in the generator[1]. The ring is normally shrunk on the end of the rotor body and incorporates some form of bayonet retention against axial forces. It is usual practice to use a non-magnetic steel, although a number of recent designs employ magnetic rings. Serious damage would result should the ring fail. It is important, therefore, to avoid possible areas of locally high temperature. One source of heating is produced by eddy currents induced in the ring by the stator tooth ripple flux.

Tooth ripples are pulsations of the main air-gap flux due to stator slotting. The flux density at points opposite a tooth is greater than at

those opposite adjacent slots, and the resultant ripple travels across the surface of the rotor and induces eddy currents therein. In order to calculate these eddy currents it is necessary to calculate the total field including the reaction field of the unknown eddy currents. The eddy current loss and heating will be strongest in the nose of the retaining ring, which extends into the air-gap, where the tooth ripple field is strongest. Unfortunately, because of differential thermal expansion, a concentration of loss in this area may impair the shrink fit.

The calculation of the eddy current losses is complicated, requiring the solution of Maxwell's equations in three-dimensional cylindrical coordinates. The approach which is described in this paper is based on solving the field in the airspaces and in the conducting ring independently; continuity of the magnetic field between the two regions is established by an iterative process. All fields within the end-region are assumed to vary sinusoidally around the periphery. The electromagnetic equations are formulated in terms of scalar potential, and a finite element numerical method is used for determining the field distribution in the airspaces. The eddy currents induced in the retaining ring are calculated analytically.

2 Method of analysis

Apart from the assumptions which have already been mentioned, two further simplifications have been introduced in order to make the problem mathematically tractable.

Firstly, the analysis is restricted to linear electromagnetic conditions. Except near the polar direct axis a magnetic ring will be heavily saturated by the excitation field. Since the tooth ripple flux is superimposed on this main flux the ring can be considered incrementally linear. The incremental permeability in the peripheral direction is assumed to be dB/dH. In the radial and axial directions the incremental permeability is taken as B/H.

Secondly, the rotor retaining ring of Fig. 1 is represented as a tubular region concentric with the rotor. Such a shape is amenable to analysis, and should not introduce undue error. No attempt has been made, however, to model the singularities at corners in the mathematical analysis.

The fundamental time component of the inducing field at the stator surface will have two harmonics $k \pm 1$, where k is the number of stator slots. Since they are of similar magnitude, they can be treated appoximately as a single time and space harmonic $e^{j(\omega t - \theta)k}$; the relative error is at its greatest on the rotor surface, where it is about $2(s - p)^2/s^2$, p and s being the radii of the rotor surface and stator bore respectively. This fundamental harmonic will have a wavelength equal to the stator slot pitch, and may be calculated, in the air-gap, by the method described by Phemister[2]. Alternatively, this field may be calculated by conformal transformation or, if saturation of the stator teeth is important by a numerical method such as finite elements. The distribution of the tooth ripple flux density around the stator end-surface may similarly be calculated by any appropriate technique. The fundamental component will be obtained from the Fourier expansion of the tooth ripple flux. Since the theory is in terms of sinusoidal functions of arbitrary wavelength and velocity it is possible to combine several such components together to represent any waveform of ripple flux density. In practice, however, only the fundamental is likely to be of importance.

2.1 Equations to be solved

Fig. 2 shows the model of the problem. In the airspace, region 1, cylindrical polar coordinates will be used. The magnetostatic field is described by Laplace's equation,

$$\nabla^2 V_m = 0.$$

When the scalar magnetic potential V_m varies sinusoidally in both space and time

$$V_m = V_m e^{j(\omega t - \theta)k}$$

and Laplace's equation can be reduced to two dimensions

$$\text{i.e. } \frac{\partial^2 V_m}{\partial r^2} + \frac{1}{r}\frac{\partial V_m}{\partial r} + \frac{\partial^2 V_m}{\partial z^2} - \frac{k^2}{r^2} V_m = 0 \qquad \ldots.(1)$$

In the retaining ring, region 2, rectangular Cartesian coordinates are used as shown in Fig. 3. The skin depth at the frequencies considered is low enough to make this a good approximation. The tooth ripple frequency

is low enough for displacement currents to be neglected, and Maxwell's equations take the form

$$Curl\ \underline{H} = \underline{J}, \qquad \ldots.(2)$$

$$Curl\ \underline{E} = -\frac{\partial B}{\partial t} \qquad \ldots.(3)$$

$$\text{and } Div.\ \underline{B} = 0. \qquad \ldots.(4)$$

For the anisotropic permeabilities considered,

$$\left.\begin{aligned} B_x &= \mu_1 H_x, \\ B_y &= \mu_2 H_y \\ \text{and } B_z &= \mu_1 H_z. \end{aligned}\right\} \qquad \ldots.(5)$$

By manipulating equations 2 to 5, it can be shown that

$$\nabla^2 H_x - \frac{\mu_1}{\rho}\frac{\partial H_x}{\partial t} = \frac{\mu_1 - \mu_2}{\mu_1}\frac{\partial^2 H_y}{\partial x \partial y}, \qquad \ldots.(6)$$

$$\frac{\partial^2 H_y}{\partial x^2} + \frac{\partial^2 H_y}{\partial z^2} + \frac{\mu_2}{\mu_1}\frac{\partial^2 H_y}{\partial y^2} - \frac{\mu_2}{\rho}\frac{\partial H_y}{\partial t} = 0, \qquad \ldots.(7)$$

$$\nabla^2 H_z - \frac{\mu_1}{\rho}\frac{\partial H_z}{\partial t} = \frac{\mu_1 - \mu_2}{\mu_1}\frac{\partial^2 H_y}{\partial z \partial y}. \qquad \ldots.(8)$$

Since all the field components are proportional to $e^{j(\omega t - y/b)}$, where $2\pi b$ is the wavelength of the spatial distribution, equations 6 to 8 can be written as

$$\frac{\partial^2 H_x}{\partial x^2} + \frac{\partial^2 H_x}{\partial z^2} - \left(\frac{1}{b^2} + \frac{j\omega\mu_1}{\rho}\right) H_x = -\frac{j}{b}\left(\frac{\mu_1 - \mu_2}{\mu_1}\right)\frac{\partial H_y}{\partial x}, \qquad \ldots.(9)$$

$$\frac{\partial^2 H_y}{\partial x^2} + \frac{\partial^2 H_y}{\partial z^2} - \left(\frac{\mu_2}{\mu_1 b^2} + \frac{j\omega\mu_2}{\rho}\right) H_y = 0, \qquad \ldots.(10)$$

$$\frac{\partial^2 H_z}{\partial x^2} + \frac{\partial^2 H_z}{\partial z^2} - \left(\frac{1}{b^2} + \frac{j\omega\mu_1}{\rho}\right) H_z = -\frac{j}{b}\left(\frac{\mu_1 - \mu_2}{\mu_1}\right)\frac{\partial H_y}{\partial z}, \qquad \ldots.(11)$$

where H_x, H_y, H_z are now functions of r and z only.

Valid solutions of these equations must also satisfy the condition that the normal component of current density is zero on all surfaces, which implies that

$$H_z = jb\frac{\partial H_y}{\partial z} \text{ at } x = 0 \text{ and } x = a \qquad \ldots.(12)$$

$$\text{and } H_x = jb\frac{\partial H_y}{\partial x} \text{ at } z = 0 \text{ and } z = c\ . \qquad \ldots.(13)$$

2.2 Solution for potential field in airspace

The general Lagrangian function for Laplace's equation is

$$J\left[V_m'\right] = 2\ \langle V_m', g\rangle - \langle V_m', LV_m'\rangle.$$

Therefore the variational expression for equation (1) is

$$J\left[V_m'\right] = \iint_R \left[r\left(\frac{\partial V_m'}{\partial r}\right)^2 + r\left(\frac{\partial V_m'}{\partial z}\right)^2 + \frac{k^2}{r}\left(V_m'\right)^2\right] dr dz - \oint_L V_m' r \frac{\partial V_m'}{\partial n}\, dl \qquad \ldots.(14)$$

the line integral is zero for the appropriate boundary conditions. Natural Neumann boundary conditions are given by including the additional term

$$\oint_L V_m' \frac{\partial V_m'}{\partial n}\, dl$$

If 1st order triangular elements are assumed, the trial function V_m' is expressed as a linear function in r and z of the three vertex values.

$$\text{i.e. } V_m'(r,z) = \frac{1}{2\Delta}\sum_{i=1}^{3}\left(a_i + b_i r + c_i z\right)V'_{mi},$$

in which the coefficients depend on the vertex coordinates according to,

$$\left.\begin{aligned} a_1 &= r_3 z_2 - r_2 z_3, \\ b_1 &= z_3 - z_2, \\ c_1 &= r_2 - r_3, \text{ etc.} \end{aligned}\right.$$

By minimizing the Lagrangian equation 14, with respect to the vertex values of V_m' at each node the problem is reduced to the inversion of a matrix of finite order. The coefficients of the resulting matrix can be derived explicitly in terms of the vertex coordinates.

2.3 Boundary conditions on the surface of the retaining ring

It is shown in the appendix that, if a certain condition is satisfied, the following iterative process is exponentially convergent:

(1) An assumed normal flux density on the surface of the retaining ring is used as a boundary condition for the solution of Laplace's equation in the airspace.

(2) H_y on the surface of the retaining ring is calculated from this solution.

(3) Equations 9 to 11 are solved with this H_y as a boundary condition. This gives a new normal flux density to continue the iteration.

Zero normal flux density is a convenient starting point. Convergence can be improved by a suitable weighting of two consecutive solutions.

Over the rotor pole, where the retaining ring is little saturated, the condition for convergence breaks down. An alternative iterative process, with normal flux density used as the boundary condition for the retaining ring, and H_y as boundary condition for the airspace, is then exponentially convergent; this is not discussed in the present paper.

2.4 Solution for the diffusion field in the retaining ring

Completely general solutions of the field equations 9, 10 and 11 for the conducting region of Fig. 3 are presented, and then these solutions are reduced for the particular case of tooth ripple losses.

The method of solution begins by assigning a system of parameters that define H_y at the surface of the ring of Fig. 3:

$$Hy = P \text{ at } x = 0,\ z = 0,$$
$$Q \text{ at } x = 0,\ z = c,$$
$$R \text{ at } x = a,\ z = 0,$$
$$S \text{ at } x = a,\ z = c,$$

$$H_y = P + (Q - P)\frac{z}{c} + \sum_{m=1}^{M} A_m \sin\frac{m\pi z}{c} \text{ at } x = 0,$$

$$= R + (S - R)\frac{z}{c} + \sum_{m=1}^{M} B_m \sin\frac{m\pi z}{c} \text{ at } x = a,$$

$$= P + (R - P)\frac{x}{a} + \sum_{n=1}^{N} C_n \sin\frac{n\pi x}{a} \text{ at } z = 0,$$

$$= Q + (S - Q)\frac{x}{a} + \sum_{n=1}^{N} D_n \sin\frac{n\pi x}{a} \text{ at } z = c.$$

At each iteration these parameters can be obtained by Fourier analysis of the H_y from the solution in the airspace.

It may be verified that, if

$$\phi_m = \sqrt{\frac{m^2\pi^2}{c^2} + \frac{\mu_2}{\mu_1 b^2} + \frac{j\omega\mu_2}{\rho}}, \qquad \ldots(15)$$

$$\psi_n = \sqrt{\frac{n^2\pi^2}{a^2} + \frac{\mu_2}{\mu_1 b^2} + \frac{j\omega\mu_2}{\rho}},$$

$$\text{then } H_y = \left[P + (Q - P)\frac{z}{c}\right]\frac{\sinh\phi_0(a - x)}{\sinh\phi_0 a} + \left[R + (S - R)\frac{z}{c}\right]\frac{\sinh\phi_0 x}{\sinh\phi_0 a}$$

$$+ \sum_{n=1}^{\infty}\frac{2\phi_0^2}{n\pi\psi_n^2}\left[P - (-1)^n R\right]\frac{\sinh\psi_n(c - z)}{\sinh\psi_n c}\sin\frac{n\pi x}{a}$$

$$+ \sum_{n=1}^{\infty}\frac{2\phi_0^2}{n\pi\psi_n^2}\left[Q - (-1)^n S\right]\frac{\sinh\psi_n z}{\sinh\psi_n c}\sin\frac{n\pi x}{a}$$

$$+ \sum_{n=1}^{N}\left[\frac{C_n\sinh\psi_n(c - z) + D_n\sinh\psi_n z}{\sinh\psi_n c}\right]\sin\frac{n\pi x}{a}$$

$$+ \sum_{m=1}^{M}\left[\frac{A_m\sinh\phi_m(a - x) + B_m\sinh\phi_m x}{\sinh\phi_m a}\right]\sin\frac{m\pi z}{c}. \qquad \ldots(16)$$

It follows that, if

$$\eta_m = \sqrt{\frac{m^2\pi^2}{c^2} + \frac{1}{b^2} + \frac{j\omega\mu_1}{\rho}}$$

and $$\xi_n = \sqrt{\frac{n^2\pi^2}{a^2} + \frac{1}{b^2} + \frac{j\omega\mu_1}{\rho}},$$

$$H_x = \frac{j}{b\eta_0^2}\frac{\partial H_y}{\partial x} + \sum_{m=1}^{\infty}\left\{\frac{E_m \cosh \eta_m(a-x) + F_m \cosh \eta_m x}{\sinh \eta_m a}\right\}\sin\frac{m\pi z}{c}$$

$$+ \sum_{n=0}^{\infty}\left\{\frac{G_n \sinh \xi_n(c-z) + H_n \sinh \xi_n z}{\sinh \xi_n c}\right\}\cos\frac{n\pi x}{a} \qquad \ldots(17)$$

and similarly for H_z.

The coefficients of equation (17) can be found from equations (16) and (13). Similarly the coefficients of the expression for H_z can be found from the condition of equation (12). Equation (17) then becomes

$$H_x = \frac{j\sqrt{\frac{\mu_2}{\mu_1}}}{b\,\eta_0\sinh\phi_0 a}\left\{\left(R + (S-R)\frac{z}{c}\right)\cosh\phi_0 x - \left(P + (Q-P)\frac{z}{c}\right)\cosh\phi_0(a-x)\right\}$$

$$- \frac{\omega\mu_1 b}{\rho a\,\eta_0^2\sinh\xi_0 c}\left\{(R-P)\sinh\xi_0(c-z) + (S-Q)\sinh\xi_0 z\right\}$$

$$+ \frac{2j\mu_2}{ab\mu_1}\sum_{n=1}^{\infty}\left\{\left(P-(-1)^n R\right)\sinh\psi_n(c-z) + \left(Q-(-1)^n S\right)\sinh\psi_n z\right\}\frac{\cos\frac{n\pi x}{a}}{\psi_n^2\sinh\psi_n c}$$

$$+ \frac{\pi j}{ab\eta_0^2}\sum_{n=1}^{N} n\left\{\left[\frac{C_n \sinh\left\{\psi_n(c-z)\right\} + D_n \sinh\psi_n z}{\sinh\psi_n c}\right]\right.$$

$$\left. + \frac{j\omega\mu_1 b^2}{\rho}\left[\frac{C_n \sinh\xi_n(c-z) + D_n \sinh\xi_n z}{\sinh\xi_n c}\right]\right\}\cos\frac{n\pi x}{a}$$

$$+ \frac{j}{b\eta_0^2}\sum_{m=1}^{M}\left\{\phi_m\left[\frac{B_m \cosh\phi_m x - A_m \cosh\phi_m(a-x)}{\sinh\phi_m a}\right]\right.$$

$$\left. - \frac{jm^2\pi^2\omega\mu_1 b^2}{\rho c^2\eta_m}\left[\frac{A_m \cosh\eta_m(a-x) - B_m \cosh\eta_m x}{\sinh\eta_m a}\right]\right\}\sin\frac{m\pi z}{c},$$

$\ldots(18)$

and similarly for H_z.

For the particular case of tooth ripple, considerable simplifications can be made since P, Q, A_m and D_n are all zero, and the hyperbolic functions of z and c can be replaced by exponentials, to give:

$$H_x = j\sqrt{\frac{\mu_2}{\mu_1}}\left\{\frac{R + (S-R)\frac{z}{c}}{b\,\eta_0\sinh\phi_0 a}\right\}\cosh\phi_0 x - \frac{\omega\mu_1 b}{\rho a\eta_0^2}\left\{R\,e^{-\xi_0 z} + S\,e^{-\xi_0(c-z)}\right\}$$

$$- \frac{2j\mu_2}{ab\mu_1}\sum_{n=1}^{\infty}\frac{(-1)^n}{\psi_n^2}\left\{R\,e^{-\psi_n z} + S\,e^{-\psi_n(c-z)}\right\}\cos\frac{n\pi x}{a}$$

$$+ \frac{\pi j}{ab\eta_0^2}\sum_{n=1}^{N} n\,C_n\left\{e^{-\psi_n z} + \frac{j\omega\mu_1 b^2}{\rho}e^{-\xi_n z}\right\}\cos\frac{n\pi x}{a}$$

$$+ \frac{j}{b\eta_0^2}\sum_{m=1}^{M} B_m\left\{\phi_m\frac{\cosh\phi_m x}{\sinh\phi_m a} + \frac{jm^2\pi^2\omega\mu_1 b^2}{\rho c^2\eta_m}\frac{\cosh\eta_m x}{\sinh\eta_m a}\right\}\sin\frac{m\pi z}{c}, \qquad \ldots(19)$$

and similarly for H_z.

3 Calculation of eddy current distribution

It now remains to state the relevant boundary conditions for the problem. In region 1, Fig. 2, the field stimulus, which does not include the field of the eddy currents, is the normal component of tooth ripple flux density over the stator surface, *vw*. The boundaries *uv* and *ws* are assumed to be flux lines. On the first iteration, when the retaining ring is represented as an impermeable surface, the part of the boundary *prs* is also a flux line. At the rotor surface, *up*, the scalar magnetic potential is arbitrarily set to zero. The potential function calculated by the finite element method of section 2.2 simultaneously meets these boundary conditions and satisfies the field equation (1).

The tangential field, H_y, at the surface of the retaining ring is calculated from

$$\underline{H} = -\nabla V_m .$$

Thus the constants in the solutions of section 2 can be evaluated.

A correction to the normal component of the field at the surface of the ring is found directly in terms of the parameters derived from the boundary condition, and immediately incorporated into the finite element formulation. In this way interaction between the ring and the airspace can be calculated to any desired accuracy. It will be noted that the 'source' distribution is modified on successive iterations whilst the coefficient matrix for the finite element solution need be assembled only once.

Finally, the eddy current density is obtained from equation (2).

Conclusions

Analytical solutions have been formed in three-dimensional Cartesian coordinates forthe diffusion equation applying to a conducting annulus in a rotating harmonic field. Additionally, a numerical solution is presented for Laplace's equation in three-dimensional cylindrical coordinates. These solutions have been applied to the calculation of eddy currents induced in the rotor retaining ring of a turbogenerator by the tooth ripple field. The conducting and non-conducting regions are connected by the continuity of the field between the regions.

An alternative iterative solution could be developed for regions of high permeability where the present method breaks down.

The solutions may be applied to the study of eddy currents induced by rotating harmonic fields over a wide frequency range. At low frequencies, however, the magnetising force at the inner surface of the ring may no longer be negligible. Therefore in calculating the effect of asynchronous operation, for example, it will be necessary to apply the general solutions and include the area occupied by the rotor end windings as an additional connected region.

Acknowledgements

The authors wish to thank C.A. Parsons and Company Limited for permission to publish this paper.

References

1 VICKERS, V.J. Recent trends in turbogenerators. Proc. IEE, 1974, 121, (11R), p1273-1306.

2 PHEMISTER, T.G. An analytical method of calculating magnetic fields in slotted regions. COMPUMAG, 1976.

APPENDIX

Condition for the convergence of the iterative procedure

It is possible to investigate the convergence of the iterative procedure in a simple model. A two-dimensional field will be considered, with the retaining ring represented by a semi-infinite slab whose boundary with a semi-infinite airspace is at $x = 0$. All fields will be proportional to $e^{j(\omega t - y/b)}$.

If H_o is the value of H_y on the boundary of the slab, then the solutions of equations (9) to (13) are

$$H_y = H_o e^{-\phi_0 x},$$

$$H_x = \frac{-j\mu_2 e^{-\phi_0 x}}{\phi_0 b \mu_1},$$

where ϕ_0 is given by equation (15).

Using

$$H_x = \frac{-j\mu_2 H_o}{\phi_0 b \mu_0}$$

as the boundary condition for the solution in air gives

$$H_x = \frac{-jH_o e^{x/b}}{\phi_0 b} \frac{\mu_2}{\mu_0},$$

$$H_y = \frac{-H_o}{\phi_0 b} \frac{\mu_2 e^{x/b}}{\mu_0}.$$

The iterative procedure will be exponentially convergent if the ratio of the new H_y to the old H_y is less than 1 in absolute value. Thus the iteration will converge if

$$\frac{\mu_0 b |\phi_0|}{\mu_2} > 1.$$

Because the space harmonic number is high and the skin-depth in the retaining ring is small compared with the radius, this criterion for convergence can be applied with little error to the problem of tooth ripple. For the particular generators considered, it guaranteed convergence if $\mu_2 < 10\ \mu_0$ for two-pole or $\mu_2 < 14\ \mu_0$ for four-pole machines. These conditions are certainly satisfied over the heavily saturated parts of the retaining ring since

$$\mu_2 = \frac{\partial B}{\partial H}.$$

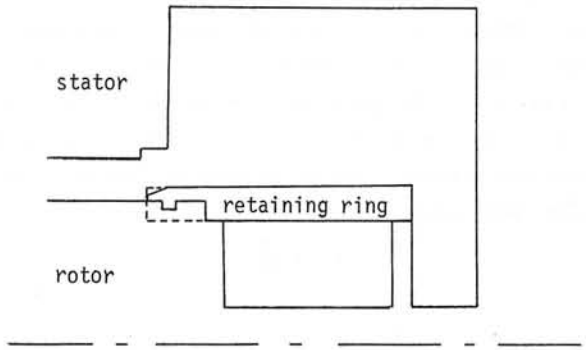

FIG. 1 Representation of rotor retaining ring by tubular region

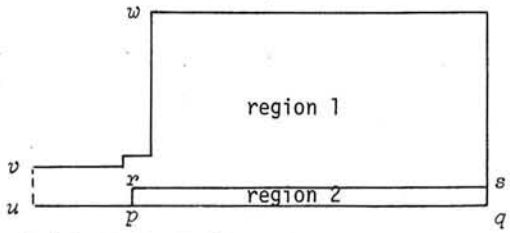

FIG. 2 Model of the field regions

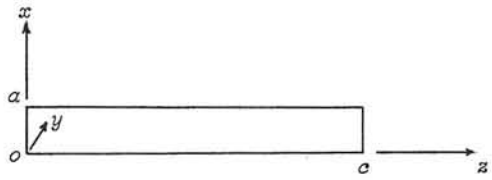

FIG. 3 Model of retaining ring

AN ANALYTICAL APPROACH FOR SOLVING TWO-DIMENSIONAL SATURABLE EDDY-CURRENT PROBLEMS

by J. Muhlhaus, C.E.R.L. Leatherhead

1. INTRODUCTION

The solution of saturable (i.e. non-linear) eddy-current problems is important in many branches of heavy electrical engineering, in particular, with reference to static and rotating electrical machines. The magnetic characteristic of the iron present is usually represented by an algebraic approximation and for one-dimensional problems, numerical solution of the resulting non-linear differential equations is nearly always necessary. For two- and three-dimensional problems, until now, it has always been necessary. Numerical solutions, of course, imply large computing expenditure and anxiety over convergence. A new analytical method for solution of one- and two-dimensional eddy-current problems is presented here and results checked for a one-dimensional case against existing results obtained by a numerical method.

2. THEORY

The eddy-current problem to be solved is that of a semi-infinite ferromagnetic slab excited on its surface by a travelling magnetic field caused, for example, by a sinusoidal current sheet. In other words, both normal and transverse magnetic fields exist at the surface. The origin of coordinates is taken on the surface, the y-axis along the surface and the x-axis into the material. All currents flow in the z-direction, thus giving a two-dimensional problem with x and y variations only (e.g. the screening of a transformer tank from adjacent heavy current bus bars).

There are many algebraic approximations to the B-H curve, but if these B-H relations are substituted into Maxwell's equations, the eventual non-linear differential equations lend themselves only to solution by numerical methods. If power-series solutions are attempted, fields which are infinite at infinite depth (ascending powers of n) or infinite at the surface (ascending powers of $\frac{1}{x}$) are found. Series solutions in ascending powers of exp (-x) were found by the author to be invalid for various representations of the magnetisation curve. Power-series solutions are anyway very unmanageable.

For the present problem, however, four simplifications can be made which will eventually lead to an analytical solution.

(1) All time harmonics can be ignored. Although there will be harmonic loss components, they will in general be much smaller than the loss due to fundamental frequency fields. This means that $\frac{\delta}{\delta t}$ in real time can be replaced by $j\omega$ in the complex domain.

(2) All transverse spatial harmonics can be ignored, that is, the spatial variation in the y-direction parallel to the surface can be considered as $\exp(-jqy)$. Thus if $H_x = h_x(x)\exp(-jqy)$, etc., the equations to be solved are

$$\frac{dh_y}{dx} + jqh_x = J \qquad \ldots (1)$$

$$J = (\omega\sigma/q)b_x \qquad \ldots (2)$$

$$\frac{dJ}{dx} = j\omega\sigma b_y \qquad \ldots (3)$$

$$\frac{db_x}{dx} = jqb_y \qquad \ldots (4)$$

(The capital letter J is used for current density to avoid confusion with $j = \sqrt{(-1)}$).

In the one-dimensional problem of a semi-infinite slab excited on the surface by a sinusoidal tangential magnetic field strength, analytical solutions are possible if the relationship between B and H is assumed to be a step-function, or of the step-function type. In this case a "separating surface" is postulated below the top surface of the slab beyond which no fields exist and at which the magnetic field strength is zero. The magnetic flux density is generally finite or indeterminate at the separating surface, which itself may vary in position with time. The permeability, therefore, will be infinite at the separating surface. An idea of Neiman (1949) was to postulate a separating surface of fixed depth β and to let the permeability variation be

$$\mu = \alpha/(\beta - x)^2, \quad 0 \leq x \leq \beta \qquad \ldots (5)$$

This idea is used in the present two-dimensional problem.

It is a necessary criterion that the pole-pitch should be large. This means that in the slab the flux density is predominately transverse. It is assumed that when the slab is saturated, the transverse magnetic field strength H_y in the slab is much larger than the radial magnetic field strength H_x and that H_x is small; consequently, while the relationship between B_y and H_y is non-linear, that between B_x and H_x is linear.

Combining this statement with the discussion of the previous paragraph, the final two assumptions are therefore

(3) $B_x = \mu_x H_x$ where μ_x is a constant, μ

(4) $B_y = \mu_y H_y$ where $\mu_y = \alpha/(\beta - x)^2$

Appendix 1 gives the analysis of the behaviour of the magnetic field in a slab subject to assumptions (1) to (4) and it is shown that the implied B-H relationship is

$$B = kH^{1-2/n} \qquad \ldots (6)$$

3. COMPARISON OF THE NEW NON-LINEAR THEORY WITH EXISTING ONE-DIMENSIONAL THEORY

It is useful to consider the new non-linear theory under one-dimensional circumstances (i.e. q=0) with existing theories. In effect, the loss is being considered for a semi-infinite slab with tangential sinusoidal magnetic field strength on the surface. Equation (A1.38) is used.

The table shows results for rotor steel of conductivity 5×10^6 mho/m and Ferrosil 253 (a silicon steel) of conductivity 2.5×10^6 mho/m. The best existing non-linear theory is a finite-difference scheme using a Fröhlich approximation to the B-H characteristic, built into a computer program PIFE01 at the C.E.G.B. The values of loss per unit surface area and skin depth at 50 Hz predicted by this program are shown as case nos. 4 and 6 in the table. The other cases are calculations based upon the best-fitted first harmonic curves for rotor steel and Ferrosil 253, the first harmonic curve of the Fröhlich approximation to rotor steel and, for comparison, the actual d.c. curve for rotor steel. The loss per unit area for this last case (case no. 3) gives lower than predicted values at high magnetic field strengths (and thus high saturation) but the other cases agree very well with predictions.

All these results are very encouraging and seem to indicate that the new theory is practical for one-dimensional problems. It is reasonable to expect similarly reliable results for the two-dimensional problem subject to the assumptions of Section 2.

4. CONCLUSION

A new non-linear theory for ferromagnetic material has been developed which agrees closely with existing numerical solutions for one-dimensional eddy-current loss in iron.

5. REFERENCE

Neiman, L.R., 1949, "Surface Effects in Ferromagnetic Bodies". (In Russian), Gosenergoizdat, Moscow-Leningrad.

6. LIST OF SYMBOLS

B	magnetic flux density
H	magnetic field strength
I	current
J	current density
W	total power loss per unit surface area
k,n	constants in the magnetic characteristic $B = kH^{1-2/n}$
m	see equation (A1.10)
q	π/(pole pitch of travelling wave)
α,β	constants in the permeability relation $\mu = \alpha/(\beta-x)^2$
δ	skin depth
μ_x, μ_x	permeability in x and y directions
σ	conductivity
w	angular frequency

APPENDIX I

ANALYSIS OF LOSS IN A NON-LINEAR SLAB

If only fundamental frequency behaviour is required, Maxwell's equations for a non-linear material occupying the half plane $x > 0$ with $\frac{\partial}{\partial z} \equiv 0$ are

$$\frac{\partial H_y}{\partial x} - \frac{\partial H_x}{\partial y} = J_z \qquad \ldots (A1.1)$$

$$\frac{\partial J_z}{\partial x} = j\omega\sigma B_y \qquad \ldots (A1.2)$$

$$\frac{\partial J_z}{\partial y} = -j\omega\sigma B_x \qquad \ldots (A1.3)$$

$$\frac{\partial B_x}{\partial x} + \frac{\partial B_y}{\partial y} = 0 \qquad \ldots (A1.4)$$

where $B_x = \mu_x H_x$ and $B_y = \mu_y H_y$

If only the fundamental component of transverse spatial variation is required, $H_x = h_x(x) \exp(-jqy)$, $H_y = h_y(x) \exp(-jqy)$, etc. The equation relating h_x and h_y then becomes

$$\frac{d^2h_y}{dx^2} = (j\omega\mu_x\sigma + q^2)\ (\mu_y/\mu_x)\ h_y \qquad \ldots (A1.5)$$

If the field distribution is linear in the x-direction, such that $\mu_x = \mu$, but non-linear in the y-direction, such that $\mu_y = \alpha/(\beta-x)^2$, then within the region $0 < x < \beta$,

$$\frac{d^2h_y}{dx^2} = h_y\alpha(j\omega\sigma + q^2/\mu)/(\beta-x)^2 \qquad \ldots (A1.6)$$

Substituting a solution of the form $h_y = A(\beta-x)^{p_1} + B(\beta-x)^{p_2}$ requires that p_1 and p_2 are the roots of the equation

$$p^2 - p - \alpha(j\omega\sigma + q^2/\mu) = 0 \qquad \ldots (A1.7)$$

The required root for the present problem is the one whose real part is positive, so that h_y is zero and not infinite at $x = \beta$, and appropriately, either A or B must be zero. The solution can therefore be written as

$$h_y = H_t(1-x/\beta)^{n+jm} \qquad \ldots (A1.8)$$

where

$$n = \tfrac{1}{2}\{1 + \frac{1}{\sqrt{2}}\left[1 + 4\alpha q^2/\mu + \sqrt{[(1 + 4\alpha q^2/\mu)^2+(4\alpha\omega\sigma)^2]}\right]^{\frac{1}{2}}\} \qquad \ldots (A1.9)$$

and

$$m = \omega\sigma\alpha/(2n-1) = \sqrt{\{n(n-1) - q^2\alpha/\mu\}} \qquad \ldots (A1.10)$$

Therefore

$$h_x = (H_t q/\beta)(m-jn)(1-x/\beta)^{n-1+jm}/(q^2+j\omega\mu\sigma) \qquad \ldots (A1.11)$$

$$b_x = \mu h_x \qquad \ldots (A1.12)$$

$$b_y = (\alpha H_t/\beta^2)(1-x/\beta)^{n-2+jm} \qquad \ldots (A1.13)$$

As $HY = h_y\exp(j\omega t - jqy)$ and $BY = b_y\exp(j\omega t - qy)$, it is seen that the transverse B-H relation in the slab is given by

$$|B| = k|H|^{1-2/n} \qquad \ldots (A1.14)$$

where k is a material constant and the modulus of field strength H, of course, removes its oscillatory variation.

From equation (A1.9), the quantity α can be derived:-

$$\alpha = \{-q^2+\sqrt{[q^4+4n(n-1)\omega^2\sigma^2\mu^2/(2n-1)^2]}\}(2n-1)^2/(2\omega^2\sigma^2\mu) \qquad \ldots (A1.15)$$

and from equation (A1.14), the penetration depth β can be deduced:-

$$\beta = H_t^{1/n}\ \sqrt{(\alpha/k)} \qquad \ldots (A1.16)$$

After further algebraic rearrangement, the field distribution can be written as

$$H_y = H_t(1-x/\beta)^{n+jm}\exp(-jqy) \qquad \ldots (A1.17)$$

$$H_x = -\{(H_t/\beta)(\alpha q/\mu)/[m-j(n-1)]\}(1-x/\beta)^{n-1+jm}\exp(-jqy) \qquad \ldots (A1.18)$$

$$B_y = (\alpha H_t/\beta^2)(1-x/\beta)^{n-2+jm}\exp(-jqy) \qquad \ldots (A1.19)$$

$$B_x = \mu H_x \qquad \ldots (A1.20)$$

As $x^{jm} = \exp\{jm\ \ln(x)\}$ it is seen that the fields decay in an oscillatory fashion as x approaches β. Clearly, given the appropriate values of k and n for the material under consideration, equations (A1.15), (A1.16) and (A1.10) can be used to define the field distribution uniquely in terms of surface tangential magnetic field strength H_t. In particular, the surface normal magnetic flux density is

$$B_n = -(H_t\alpha q/\beta)/[m-j(n-1)] \qquad \ldots (A1.21)$$

The power loss per unit surface area can be deduced either from the Poynting vector or from the integral of $\frac{1}{2\sigma} J_z J_z^*$ over the region $0 < x < \beta$. The result is

$$W = \tfrac{1}{2}(\omega\alpha H_t^2 m/\beta)/[m^2 + (n-1)^2] \qquad \ldots (A1.22)$$

It is useful to examine the skin depth δ. This quantity is different from the depth of penetration β, which marks where the magnetic field strength and current density become zero. It can be calculated only from one-dimensional fields and is defined as that depth within which the actual total current induced would, if uniformly distributed, produce the actual total loss. One-dimensional fields are given when $q = 0$, so the total one-dimensional current is

$$I = \int_0^\beta J_z dx = -\{H_t(2n-1)\sqrt{(n^2-n)}\}/\{[\sqrt{(n^2-n)} - j(n-1)][n + j\ (n^2-n)]\} \qquad \ldots (A1.23)$$

The total loss per unit surface area is $\frac{1}{2}\ II^*/(\sigma\delta)$, and the one-dimensional

loss from equation (A1.22) is $\frac{1}{2} H_t^2 n/(\sigma\beta)$. Equating the two losses gives

$$\delta = \beta/n \qquad \ldots (A1.24)$$

To demonstrate that the field distribution reduces to the well-known distribution for the linear case as $n \to \infty$ and $k = \mu$, it is sufficient to express m and α in terms of n and then proceed to the limit. From equation (A1.16), $\beta \to \sqrt{(\alpha/k)}$ and from equation (A1.15), $\alpha \to \infty$. Thus and $\mu_y \to \alpha/\beta^2 = k = \mu$. By expanding $(n + jm)\ln(1-x/\beta)$ as a series, it is found that

$$\underset{n \to \infty}{\text{Lt}} (n+jm)\ln(1-x/\beta) = -x\sqrt{(q^2 + j\omega\mu\sigma)} \qquad \ldots (A1.25)$$

if the following identity is used:-

$$\sqrt{(q^2+j\omega\mu\sigma)} = \frac{1}{\sqrt{2}} \{q^2+\sqrt{(q^4+\omega^2\mu^2\sigma^2)}\}^{\frac{1}{2}} + j \frac{1}{\sqrt{2}} \{-q^2 + \sqrt{(q^4+\omega^2\mu^2\sigma^2)}\}^{\frac{1}{2}} \qquad \ldots (A1.26)$$

The consequent linear relations are

$$H_y = H_t \exp\{-x\sqrt{(q^2 + j\omega\mu\sigma)}\} \exp(-jqy) \qquad \ldots (A1.27)$$

$$H_x = -jqH_t \exp\{-x\sqrt{(q^2 + j\omega\mu\sigma)}\} \exp(-jqy)/\sqrt{(q^2+\omega\mu\sigma)} \qquad \ldots (A1.28)$$

The power loss reduces to

$$W = \tfrac{1}{2}(\omega\mu H_t^2/\sqrt{2})\left\{\left[-q^2+\sqrt{(q^4+\omega^2\mu^2\sigma^2)}\right]/\left[q^4+\omega^2\mu^2\sigma^2\right]\right\}^{\frac{1}{2}} \qquad \ldots (A1.29)$$

and the skin depth becomes the well-known relation, $\delta = \sqrt{2}/\sqrt{(\omega\mu\sigma)}$. When $n = 2$ and $k = B_s$, the B-H characteristic becomes the non-linear limiting curve, i.e., a step-function curve. (In actual practice, n will be very close to 2). Under such circumstances,

$$\alpha = 9\{-q^2 + \sqrt{(q^4+8\omega^2\sigma^2\mu^2/9)}\}/(2\omega^2\sigma^2\mu) \qquad \ldots (A1.30)$$

$$m = (\omega\sigma\alpha)/3 \qquad \ldots (A1.31)$$

$$\beta = H_t^{\frac{1}{2}} \sqrt{(\alpha/B_s)} \qquad \ldots (A1.32)$$

$$W = \frac{3}{2} \omega^2\sigma(\alpha^3 H_t^3 B_s)^{\frac{1}{2}} / (9+\omega^2\sigma^2\alpha^2) \qquad \ldots (A1.33)$$

and for a one-dimensional field with sinusoidal tangential excitation, $q = 0$ so that

$$W = \sqrt{(\omega B_s/\sigma)}\ H_t^{3/2} /\sqrt{(3\sqrt{2})} \qquad \ldots (A1.34)$$

For small q and general n, the important parameters are:

$$\alpha = (2n-1)\sqrt{(n^2-n)}/(\omega\sigma) \qquad \ldots (A1.35)$$

$$m = \sqrt{(n^2-n)} \qquad \ldots (A1.36)$$

$$\beta = H_t^{1/n}\sqrt{(\alpha/k)} \qquad \ldots (A1.37)$$

$$W = \tfrac{1}{2}H_t^{2-1/n}\ \sqrt{(k\omega/\sigma)}\sqrt{\{n\sqrt{(n^2-n)}/\left[(n-1)(2n-1)\right]\}} \qquad \ldots (A1.38)$$

APPENDIX 2

DERIVATION OF THE BEST-FITTING B-H EQUATION

It is required to derive the best-fitting equation $B = kH^{1-2/n}$, where k and n are constants to be determined, to relate the first harmonic components of magnetic flux density and field strength for a given ferromagnetic material.

For an applied magnetic field strength $H = \hat{H} \cos \omega t$, the d.c. magnetisation curve can be used to obtain the waveform of the flux density B, which can be expanded in harmonics as

$$\Sigma B_r = \Sigma \hat{B}_r \cos r\omega t,$$

that is,

$$B(\omega t) = \hat{B}_1 \cos \omega t + \hat{B}_3 \cos 3\omega t + \hat{B}_5 \cos 5\omega t \ldots \qquad \ldots (A2.1)$$

The amplitude of the first harmonic B_1 in particular is given by,

$$\hat{B}_1 = \frac{1}{\pi} \int_{-\pi}^{\pi} B(\omega t) \cos \omega t\ d(\omega t) \qquad \ldots (A2.2)$$

As $B(\omega t)$ is an odd function of H,

$$\hat{B}_1 = \frac{4}{\pi} \int_{o}^{\pi/2} B(\omega t) \cos\omega t\ d(\omega t) \qquad \ldots (A2.3)$$

When the d.c. magnetisation curve is a step-function, the integral is soluble.

$$\hat{B}_1 = 4B_s/\pi \int_{o}^{\pi/2} \cos\theta d\theta = 4B_s/\pi = 1.273B_s \qquad \ldots (A2.4)$$

Otherwise, the integration must be done numerically, and a first harmonic characteristic can be drawn.

To obtain the best-fitting equation, its form must be redefined as

$$\log B = \log k + (1-2/n)\log H \qquad \ldots (A2.5)$$

where logarithms to the base 10 are convenient to use. Linear regression is used to derive the slope and intercept of this straight line:-

$$(1-2/n) = \{N\Sigma(\log B \log H) - \Sigma\log H\, \Sigma\log B\} / \{N\Sigma(\log H)^2 - (\Sigma\log H)^2\} \qquad \ldots (A2.6)$$

$$\log k = \{\Sigma\log B\Sigma(\log H)^2 - \Sigma\log H\ (\log B \log H)\} / \{N\Sigma(\log H)^2 - (\Sigma\log H)^2\} \qquad \ldots (A2.7)$$

where the summations are over N data points.

ACKNOWLEDGEMENT

The work was carried out at the Central Electricity Research Laboratories and is published by permission of the Central Electricity Generating Board.

Case	Flux Density (T)	Loss per Unit Area (kW/m^2)	Skin Depth (mm)
1	$0.763H^{0.118}$	$0.322 \times 10^{-5} H_t^{1.559}$	$0.0313 H_t^{0.441}$
2	$0.653H^{0.128}$	$0.295 \times 10^{-5} H_t^{1.564}$	$0.0339 H_t^{0.436}$
3	$0.693H^{0.106}$	$0.307 \times 10^{-5} H_t^{1.553}$	$0.0324 H_t^{0.447}$
4	-	$0.18 \times 10^{-5} H_t^{1.622}$	$0.0556 H_t^{0.378}$
5	$1.18 H^{0.0661}$	$0.574 \times 10^{-5} H_t^{1.533}$	$0.0348 H_t^{0.467}$
6	-	$0.498 \times 10^{-5} H_t^{1.555}$	$0.0402 H_t^{0.445}$

N.B. magnetic field strength is in units of A/m

Identity of Cases:

1 first harmonic curve of rotor steel

2 first harmonic curve of Fröhlich approximation to rotor steel

3 d.c. curve of rotor steel

4 existing results using a numerical method for rotor steel

5 first harmonic curve of Ferrosil 253

6 existing results using a numerical methof for Ferrosil 253

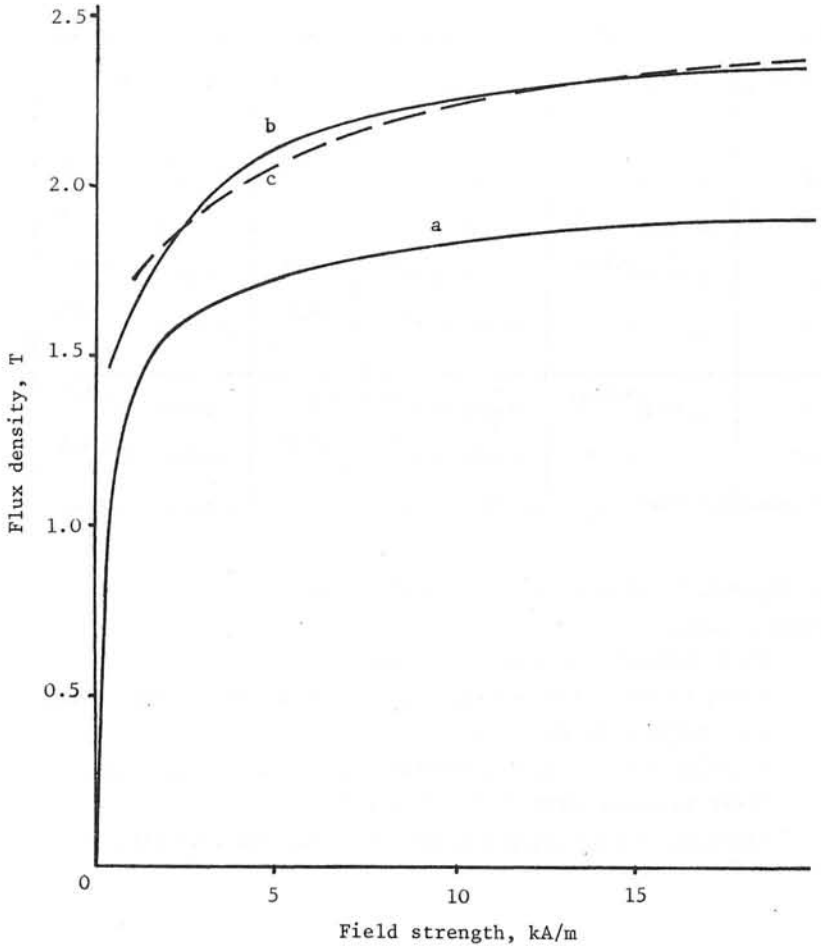

MAGNETIZATION CURVES FOR ROTOR STEEL

a - d.c. curve

b - first harmonic curve

c - best fitted curve of the form $B = kH^{\alpha}$

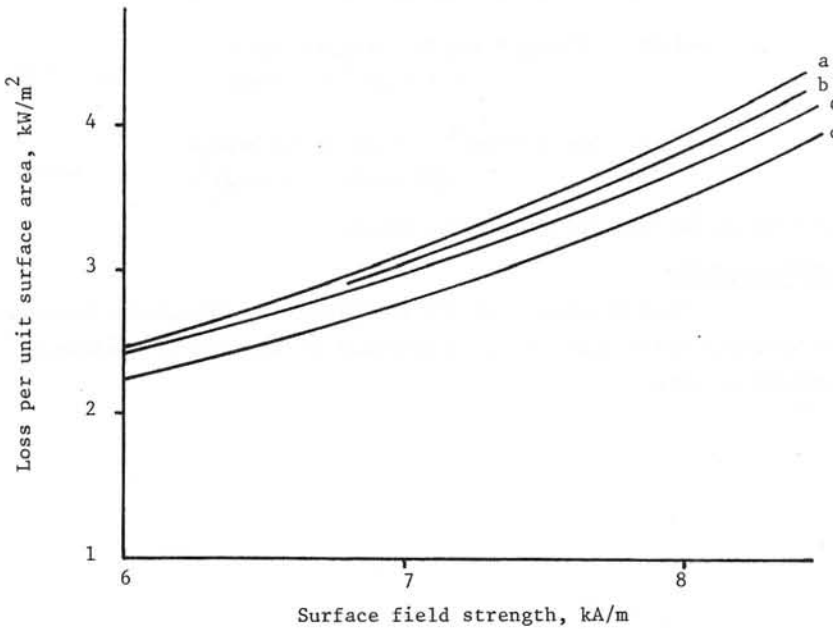

LOSS IN ROTOR STEEL CAUSED BY A TANGENTIAL SINUSOIDAL MAGNETIC FIELD

a - existing results using a numerical method

b - new theory

c - new theory using first harmonic curve of Fröhlich approximation

d - new theory using d.c curve

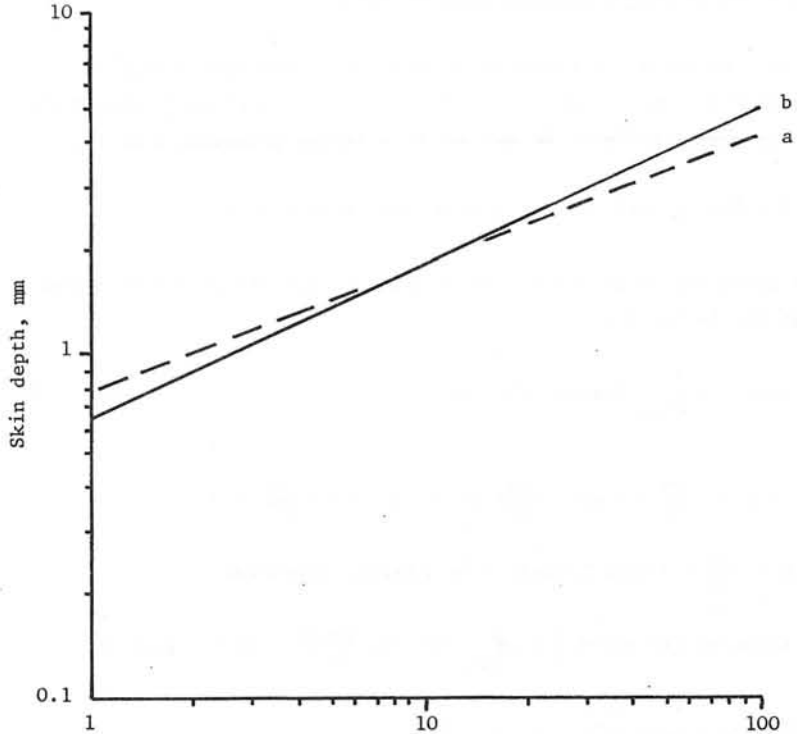

VARIATION OF SKIN DEPTH IN ROTOR STEEL WITH SURFACE MAGNETIC FIELD STRENGTH

a - existing results using a numerical method

b - new theory

CALCULATION OF EDDY CURRENTS IN A CONDUCTOR AND ITS SHEATH BY A FINITE ELEMENT METHOD

by J.C. NEDELEC*, J.L. SABRIE** and J.C. VERITE***

INTRODUCTION AND HYPOTHESIS

The purpose of this work is to determine a map of currents everywhere in the set of conductors and sheaths connecting an alternator to its transformer. All these conductors and sheaths are interacting and eddy currents are developped in their volumes. When these currents are known, it will be easy to determine heatings and stresses appearing.

We suppose in this report there is one conductor C and one sheath G. The generalization to the case of several conductors and sheaths does not bring about new theoretical problems.

We consider the following hypothesis :

- The conductor and its sheath are both concentric cylinders in aluminium. They can be curved.

- We only calculate mean values of the currents according to the thickness which is supposed small. So the thickness will be neglected and current densities will be surfacic ones.

- We know the total applied current.

* École Polytechnique - Centre de Mathématiques Appliquées - Palaiseau France.

** Electricité de France - Etudes et Recherches - Service ERMEL - Clamart - France.

*** Electricité de France - Etudes et Recherches - Service IMA - Clamart - France

EQUATIONS VERIFIED BY THE DENSITY OF CURRENT

Let the Maxwell's equations be curl H = J and curl $E = -\frac{\partial B}{\partial t}$ where J is the current density, E the electric field, B the magnetic induction and H the magnetic field. We may define a vector potential A by :

B = Curl A with div A = 0 so we obtain $\Delta A = -\mu J$

G(x,y) being the Green's function associated with the Dirichlet's problem we obtain for A :

$$A(x) = \mu \int_{G+C} G(x,y).\ J(y).dy \qquad (1)$$

and curl $E = -\frac{\partial B}{\partial t} = -$ curl $(\frac{\partial A}{\partial t})$ gives curl $(E + \frac{\partial A}{\partial t}) = 0$

thus, $E + \frac{\partial A}{\partial t} = -$ grad V, where V is a scalar potential.

Equation (1) gives $\frac{J}{\sigma} + \mu \int_{G+C} G(x,y).\ \frac{\partial J(y)}{\partial t}\ .\ dy = -$ grad V

with $\frac{\partial J(y)}{\partial t} = j\omega J(y)$ when J is harmonic.

Finally, the current density verifies the following equations :

$$\begin{cases} J(x) + j\omega\sigma\mu \int_{G+C} G(x,y).J(y).dy = -\sigma \text{grad } V & (2) \\ J.n = 0 & (3) \\ \text{div } J = 0 & (4) \end{cases}$$

Equation (3) expresses that current lines do not leave G or C, equation (4) expresses continuity of eiectric loads for a stationnary mode.

SIMPLIFIED TWO-DIMENSIONAL PROBLEM

These three equations represent the general case of a three-dimen-

sional problem. A preliminary study has been worked out for a two-dimensional problem corresponding to an imaginary configuration of a rectilinear conductor and a sheath by the side of it and parallel to it (see figure 1). The study may then be realized in a plan perpendicular to their axis x, all the quantities being constant according to x.

For a two-dimensional problem $G(x,y) = \frac{1}{2\Pi} \text{Log}(x-y)$ and equations (3) and (4) are automatically verified.

We have thus to solve the following equation :

$$J(z) + \frac{j\omega\sigma\mu}{2\Pi} \int_{G+C} J(y).\text{Log}|y-z|\,dSy = \sigma(\text{grad } V+\lambda)$$

where λ is a constant vector due to the fact that grad V is not completely defined.

The sheath is then discretized in n sectors according to θ (see below), J being constant in each sector, and the equation becomes :

$$J_K = J_0 - \frac{j\omega\sigma\mu}{2\Pi} \sum_{k'=1}^{n} \int_{S_{K'}} J_{K'}.\text{Log}|M_K M_{K'}|\,dS_{K'} - \frac{j\omega\sigma\mu}{2\Pi} I_A \text{Log}|AM_K|$$

Letter A refers to the conductor, M_K is a point in the Kth sector.

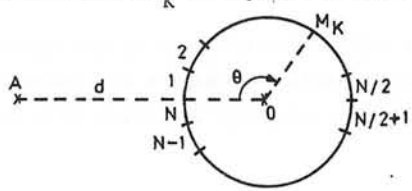

Thus, we obtain a complex linear system the solution of which gives the current anywhere in the sheath. The constant J_0 is calculated by expressing that the currents in the sheath and in the conductor are equal.

Then the magnetic induction has been calculated near G by the following formulas :

$$B_M = \text{curl } A_M = \begin{cases} \frac{1}{\rho} \frac{\partial A_M}{\partial \varphi} \\ \\ -\frac{\partial A_M}{\partial \rho} \end{cases} \qquad \text{with } A_M = \frac{\mu}{2\Pi} \int_{G+C} J(M').\text{Log}|MM'|\,dM'$$

where A_M is the vector potential at point M.

THREE-DIMENSIONAL PROBLEM (see figure 2)

We now have $G(x,y) = \frac{1}{4\Pi|x-y|}$

Let $J' \in L^2(R)$ with div J' = 0 in G and C, and let us rewrite equation (2) in a variationnal form :

$$\int_{G+C} J(x).J'(x).dS_x + \frac{j\omega\sigma\mu}{4\Pi} \int_{G+C} \int_{G+C} \frac{j(y).J'(x).}{|x-y|}\,dSx\,dSy = \tag{2'}$$

$$\sigma V_{Ce} \int_{\Gamma Ce} J'.nCe.d\Gamma_{Ce} + \sigma V_{Ge} \int_{\Gamma Ge} J'.nGe.d\Gamma_{Ge} - \sigma V_{CS} \int_{\Gamma CS} J'.nCS.d\Gamma_{CS} -$$

$$- \sigma V_{GS} \int_{\Gamma GS} J'.nGS.d\Gamma_{GS}$$

Γ_{Ce}, Γ_{CS}, Γ_{Ge}, Γ_{GS} being respectively the extremities of the conductor and of the sheath.

The problem now is to solve the equations (2'), (3) and (4). We use a finite-element method where J(x) is decomposed in a base of known functions wi :

$$J(x) = \sum_{i=1}^{n} \alpha i.wi(x)$$

Then the problem is to determine the n unknowns αi.

DESCRIPTION OF THE FINITE-ELEMENTS AND OF THE BASIC FUNCTIONS

Let Th be a partition of G and C in triangles the vertices of which, Ai, are on G and C. We then define a set of vectorial functions wik :

- To one vertex Ai corresponds one function wi.
- Si, support of wi, is the set of triangles having Ai as vertex.
- wi is constant an each triangle and is in the plane of the triangle.

wi is then defined in the following manner :

Let Γi be the boundary of Si and n the vector perpendicular to Γi in the plane of a triangle Tik of Si. We take wik.n = 0, wik being the restriction of wi on Tik. This condition defines the direction of wik, parallel to the side of Tik belonging to Γi (see below)

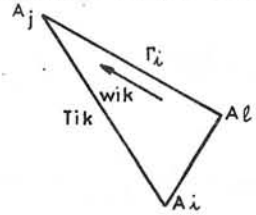

The modulus of wik is defined by the relation :

$$\int_{AiAj} |wik|.n.dS = \pm 1 = -\int_{AiA\ell} |wik|.n.dS \quad \text{i.e. } wik.n.|AiAj| = \pm 1$$

We choose +1 or -1 to have the same direction or rotation for all the wik round the vertices Ai (see below).

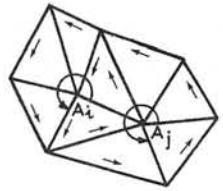

wik are then completely defined.

We have just defined a set of functions but do these functions constitute a base of the functions which are constant on each triangle ?

Let us consider one cylinder C (conductor or sheath). Let N be the number of functions wi on this cylinder.

It is easy to show that these N functions verify the relation :

$$\sum_{i=1}^{N} wi(x) = 0 \quad \forall x \in C$$

Thus these functions don't constitute a base and in particular it can be shown that the circulation of a density of current defined by these functions is zero along any section of the cylinder. If we note that this circulation must be equal to the applied current which is known, the most natural idea is to replace one of the functions wi by a function the support of which is the whole cylinder, which is constant and equal to the density of the applied current when any electric influence is neglected.

Thus the base of functions for a cylinder is constituted by the N-1 former functions wi and the new special one.

Equations (3) and (4) are automatically verified by these functions. Equation (3) is verified because function wik is in the plane of triangle Tik and equation (4) because function wik is constant on Tik, so div wik = 0 on Tik. We now have to solve only equation (2')

LINEAR SYSTEM OBTAINED

Let us always take the case of one conductor and one sheath. There are two special functions, one for the conductor and one for the sheath. Let w_{N-1} and w_N be these two functions if N is the total number of vertices on G+C.

If we replace $J'(x)_N$ in equation (2') successively by the N functions wi(x) and with $J(x) = \sum_{i=1}^{N} \alpha i wi(x)$ we obtain the following system : for k from 1 to N :

$$\int_{G+C} \left(\sum_i \alpha i.wi(x)\right).wk(x).dSx + \frac{j\omega\sigma\mu}{4\Pi} \int_{G+C}\int_{G+C} \frac{\left(\sum_i \alpha i wi(x)\right).wk(y)}{|x-y|}\, dSy.dSx$$

$$= \sigma V_{Ce} \int_{\Gamma_{Ce}} wk(x).nCe.d\Gamma_{Ce} + \sigma V_{Ge} \int_{\Gamma_{Ge}} wk(x).nGe.d\Gamma_{Ge} - \sigma V_{CS} \int_{\Gamma_{CS}} wk(x).nCS.d\Gamma_{Ge}$$

$$- \sigma V_{GS} \int_{\Gamma_{GS}} wk(x).nGS.d\Gamma_{GS}$$

Let us note that by construction, except for the two special functions, the circulation of wi is equal to zero along the extremities of the cylinders. Thus, we obtain, for k from 1 to N :

$$\sum_{i=1}^{N} \alpha i \left[\int_{Si} wi(x).wk(x).dSx + \frac{j\omega\sigma\mu}{4\Pi} \int_{Si}\int_{Sk} \frac{wi(x).wk(y)}{|x-y|}\, dSx.dSy \right]$$

$$= \begin{cases} 0 \text{ for } k < N-1 \\ \sigma V_e \int_{\Gamma_e} wk(x).ne.d\Gamma_e - \sigma V_S \int_{\Gamma_S} wk(x).nS.d\Gamma_S \text{ for } k = N \text{ or } N-1 \end{cases}$$

It is a symmetrical, linear and complex system of N equations with N unknowns αi.

Let us rewrite it in the following partitionned form where A is an (N-2) x (N-2) matrix, u_N and u_{N-1} are vectors :

$$\begin{pmatrix} A & u_{N-1} & u_N \\ u_{N-1}^T & w_{N-1} & v_N \\ u_N^T & v_N & w_N \end{pmatrix} \begin{pmatrix} \alpha \\ \alpha_{N-1} \\ \alpha_N \end{pmatrix} = \begin{pmatrix} 0 \\ \beta_{N-1} \\ \beta_N \end{pmatrix}$$

α_{N-1} and α_N can be determined by expressing that the circulation of the current density at an extremity of each cylinder is equal to the applied current, which is known.

Let I_C and I_G be the applied currents on the conductor and on the sheath and R_C and R_G be the radius.

We have $\int_{\Gamma_{Ge}} J(x).nGe.d\Gamma_{Ge} = I_G = \alpha_{N-1}.w_{N-1}.2\Pi R_G$

and $\int_{\Gamma_{Ce}} J(x).nCe.d\Gamma_{Ce} = I_C = \alpha_N.w_N.2\Pi R_C$

Taking $w_{N-1} = I_G/2\Pi R_G$ and $w_N = I_C/2\Pi R_C$ we have $\alpha_{N-1} = \alpha_N = 1$

We can then rub out the last two equations from the system. β_{N-1} and β_N which are the only terms where appear the applied tensions, are eliminated from the system. So we have only to know the applied currents and the system reduces to :

$$A\alpha + u_{N-1}.\alpha_{N-1} + u_N.\alpha_N = 0 \quad \text{i.e. } A\alpha = -u_{N-1} - u_N$$

It is an (N-2) x (N-2) linear, symmetrical and complex system.

CALCULATION OF THE COEFFICIENTS OF THE SYSTEM

Let aij be a term of the matrix A.

$$aij = \int_{Si} wi(x).wj(x).dSx + \frac{j\omega\sigma\mu}{4\Pi} \int_{Si}\int_{Sj} \frac{wi(x).wj(y)}{|x-y|}\, dSx.dSy$$

Thus, it is necessary, in order to determine the terms of A (or u_{N-1} and u_N), to calculate two types of integrals :

$$Sik = \int_{Si} wi(x).wk(x).dSx \quad \text{and} \quad Dik = \int_{Si}\int_{Sk} \frac{wi(x).wk(y)}{|x-y|}\, dSx.dSy$$

In fact, Si and Sk are sets of triangle. Thus, we have to calculate integrals over triangles :

$$\int_{T_j} wij(x).wk\ell(x).dSk \quad \text{and} \quad \int_{T_j}\int_{T_\ell} \frac{wij(x).xk\ell(y)}{|x-y|}\, dSx.dSy$$

wij(x) and wkℓ(x) are constant or equal to zero on each triangle. So we can put the scalar products wij(x).wkℓ(x) and wij(x).wkℓ(y) out the integrals and we have to calculate :

$$\int_{T_j} dSx \quad \text{and} \quad \int_{T_j} \left[\int_{T_e} \frac{dSy}{|x-y|} \right] dSx$$

The first integral is equal to the surface of T_j.

As for the second integral we have to consider several cases, according as the triangles are far from each other, adjacent or identical.

- If they are far from each other, we calculate the product of the surfaces divided by the distance between the centers of gravity.

- if they are adjacent we use twice a Gauss product formula of degree 5 with 7 points.

- if they are identical the inner integral is analytically calculated and the outer one by a 64 points, 15 th degree triangular Gauss product formula.

RESOLUTION OF THE SYSTEM

The resolution of the system has been performed by a classical direct method which is not necessary to describe here.

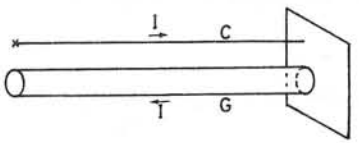

FIGURE 1

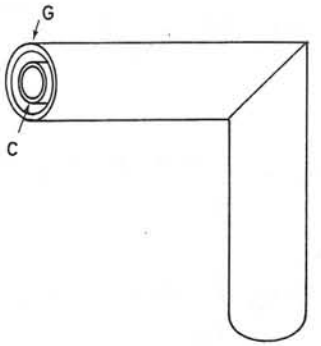

FIGURE 2

BIBLIOGRAPHY

[1] J.L. SABRIE - Liaison alternateur-transformateur ; Examen des méthodes possibles d'étude des efforts et échauffements.
EDF - Rapport interne M16/369 - Novembre 1974

[2] J.C. VERITE - Influences réciproques d'un conducteur filiforme et d'un conducteur cylindrique parcourus par un courant alternatif.
EDF - Rapport interne - HI 1806/02 - Mars 1975

[3] H.A. STROUD - Approximate calculation of multiple integrals.
Prentice-Hall - 1971

[4] J.L. HESS and A.M.O. SMITH - Calculation of potential flow about arbitrary bodies.

[5] O.C. ZIENKIEWICZ and Y.K. CHEUNG - The finite element method in structural and continuous mechanics - Mc Graw-Hill - 1967

[6] R.L. STOLL - The analysis of eddy currents.
Clarendon-Press - Oxford - 1974

[7] J.C. NEDELEC - Curved finite element methods for the solution of singular integral equations on surfaces in R^3.
Rapport - Centre de Mathématiques Appliquées - Ecole Polytechnique - 1976.

[8] M. DJAOUA - Méthode d'éléments finis pour la résolution d'un problème extérieur dans R^3.
Rapport - Centre de Mathématiques Appliquées - Ecole Polytechnique - 1976.

NUMERICAL RESULTS

Two-dimensional problem

The density of current and the induction near the sheath have been calculated.

Curve 1 shows the tangential induction at 1 mm outside G and curve 2 at 1 mm inside G.

Three-dimensional problem

Numerical results have been obtained with the configuration of the figure 2 for two cases :

- Case 1 : The length of the sheath is supposed infinite but there are finite-elements only on a length D. The sheath is isolated from the conductor.

- Case 2 : The sheath is truncated at the distance D from the knee-pipe. The sheath is still isolated from the conductor.

Many tests have been realized with various numbers of vertices and triangles. We give there the results corresponding to the greatest number of elements, with the following values :

Applied current : 375 A	Length D : 2 m
Ray of the sheath : 10 cm	Ray of the conductor : 5 cm
Thickness of the sheath : 0,9 cm	Thickness of the conductor : 0,5 cm
Number of vertices : 496	Number of triangles : 960

Diagram 3 shows the modulus of the density of current obtained in cases 1 and 2 along the generating lines AA' and BB' of the following figure (for the sheath only) :

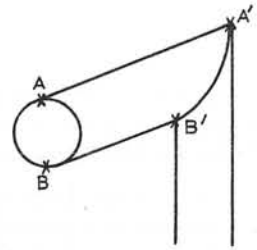

Diagram 4 shows a spreading out in the plane of the diagram of the sheath near the knee-pipe and on both sides of it, in case 1. We can see the finite-elements. Little vectors represent the average density of current on each triangle.

Diagram 5 in the same in case 2.

Conclusion

Obviously, this study has not yet been brought to an end and we have to make several remarks and to underline some difficulties. First of all experimental verifications have to be realized and are worked on at the moment. There are two main difficulties for the numerical results. The first one is that we obtain only average values over triangles and thus it is difficult to well describe the aeras where the density of current rapidly change in direction or modulus because the number of triangles is bounded by the power of the computer, all the more so that we shall have to consider the case of three conductors and three sheaths. The second one is that we don't know very well what hypothesis is to be taken at the extremities of G in order to be in the same conditions as in the experimental device. As for the experimental measurements, it is quite difficult to interpretate them.

Nevertheless, because of the heavy difficulties, especially efforts and heatings, appearing in the new power-stations and our high-power laboratory, we go an actively studying both experimental and numerical aspects of the problem.

DIAGRAM 2

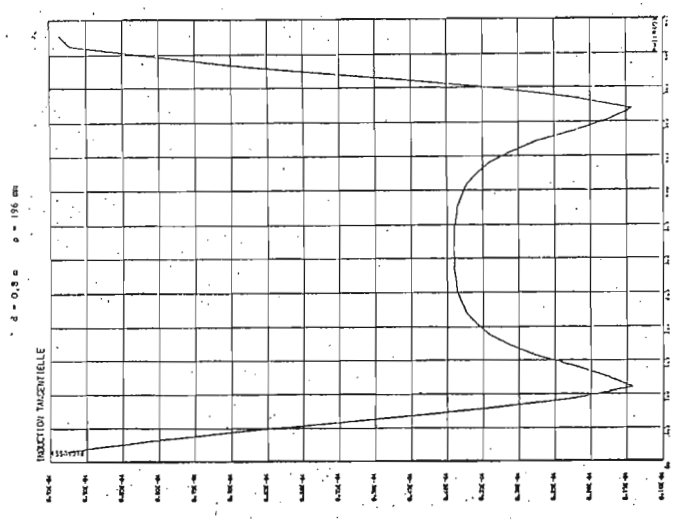

Curve 2 shows tangential induction inside the sheath.

DIAGRAM 1

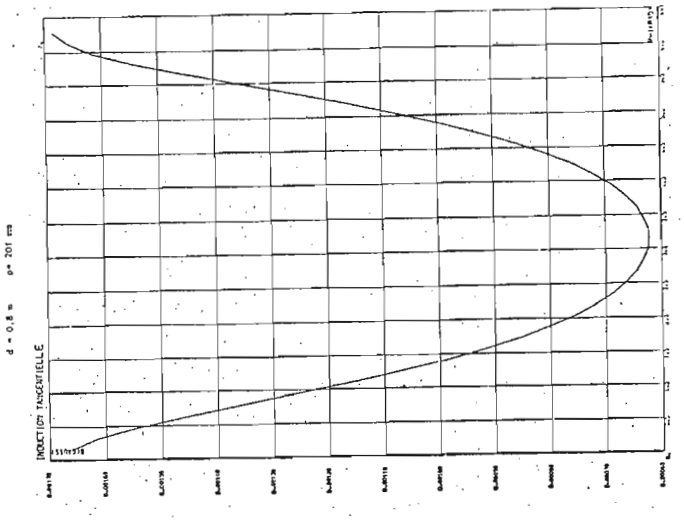

Curve 1 shows tangential induction outside the sheath.

DIAGRAM 3

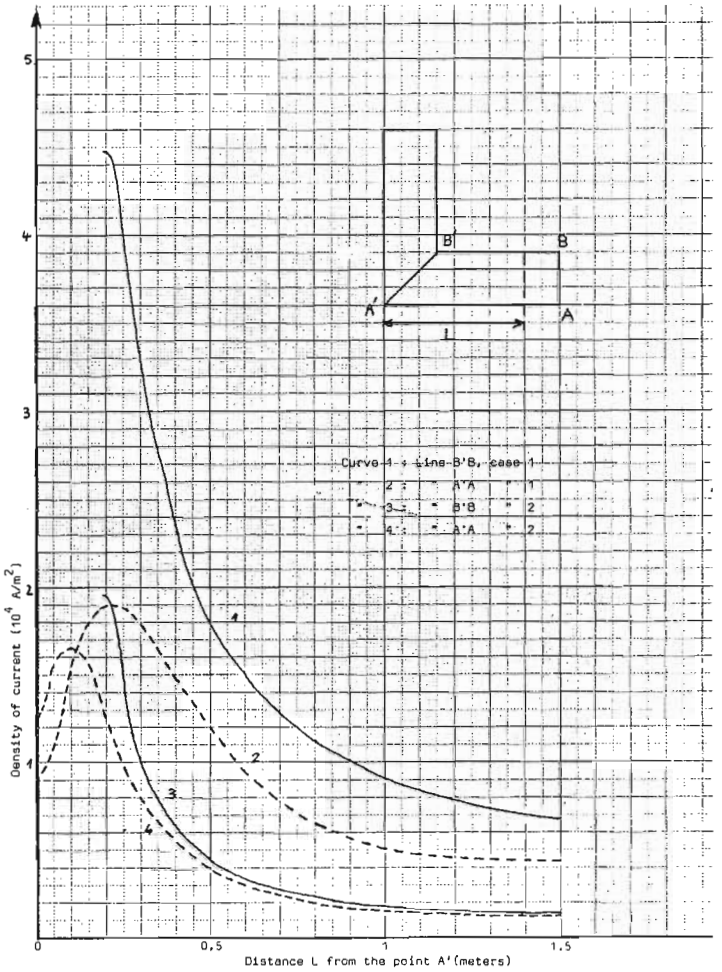

DIAGRAM 5

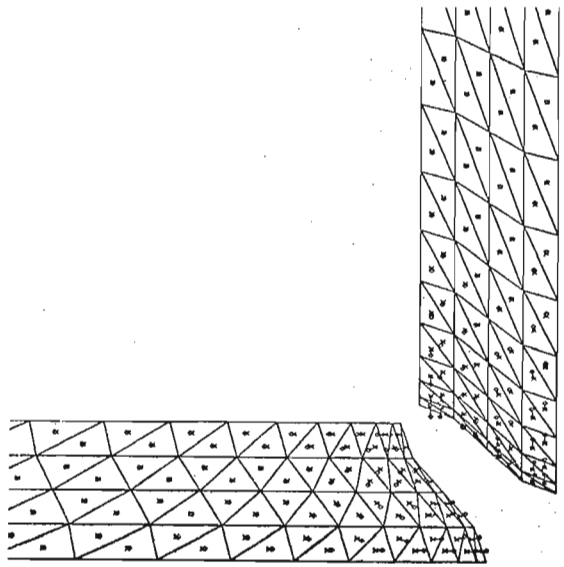

DIAGRAM 4

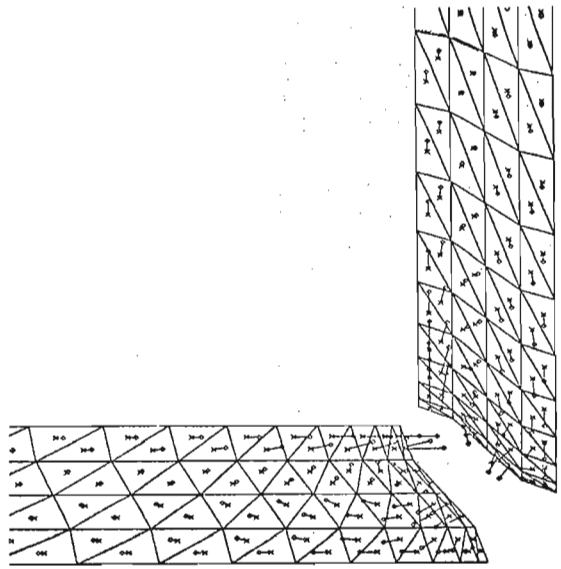

The piece-by-piece solution of eigenvalue problems

by

G. J. Rogers, B.Sc.(Eng.), F.I.M.A.

and

D. S. Benaragama, B.Sc.(Eng.)

Department of Electrical Engineering
The University
Southampton

Summary

A piece-by-piece method is applied to the determination of the eigenvalues and the eigenvectors of the two dimensional scalar Helmholtz Equation. Examples are given for boundary shapes which occur in eddy current problems in electrical machines.

1. Introduction

A piece-by-piece method for the approximate solution of elliptic boundary value problems has been described by Rogers and Cambrell[1]. It has been applied to simple electrical machine problems by Hammond and Rogers[2]. In this paper we extend the technique to the determination of the eigenvalues and the eigenvectors of the scalar Helmholtz equation.

$$\nabla^2 u + \lambda^2 u = 0 \qquad (1)$$

with homogeneous boundary conditions.

In machine problems the effect of eddy currents can be represented by equivalent circuits which can be defined in terms of these eigenvalues and eigenvectors[3]. Here we examine two regions: a basic L-shaped region (Fig. 1) which can represent an induction motor rotor T-bar or the salient pole of a synchronous machine; and the region shown in fig. 2 which represents a cross section through the rotor of a turbo-alternator.

2. The Piece-by-Piece Method

The method is applicable to regions which may be split into sub-regions of such shapes that elementary methods of field solutions may be used in each taken in isolation. At the interface between two sub-regions the field u and its normal derivative $\partial u/\partial n$ must be continuous. We may postulate conceptual sources on the interface to guarantee continuity of one of these quantities. The other continuity constraint then enables integral equations to be formulated for the distribution of the conceptual sources.

Consider the region (R) shown in fig. 3. Let it be divided into two sub-regions R_a and R_b. Within R the field satisfies the scalar Helmholtz equation

$$\nabla^2 u + \lambda^2 u = 0 \qquad (1a)$$

with

$$u = 0 \qquad \text{on } S_1 \qquad (1b)$$

$$\frac{\partial u}{\partial n} = 0 \qquad \text{on } S_2 \qquad (1c)$$

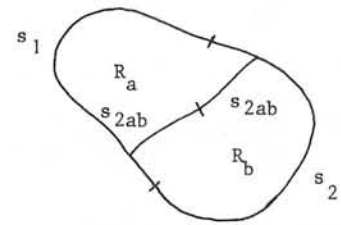

Fig. 3

In each sub-region we may calculate the field u by means of a Green's function, in terms of the field specified on the interface between two regions. On s_{1ab} we assume that u is specified and on s_{2ab} we assume that $\partial u/\partial n$ is specified.

If $G_a(\underline{r}/\underline{r}_o)$ is the Green's function for region R_a, satisfying

$$\nabla^2 G(\underline{r}/\underline{r}_o) + \lambda^2 G(\underline{r}/\underline{r}_o) = -\delta(\underline{r} - \underline{r}_o) \qquad (2)$$

then
$$u(\underline{r}) = \int_{s_{2ab}} G_a(\underline{r}/s)\, \frac{\partial u(s)}{\partial n}\, ds - \int_{s_{1ab}} \frac{\partial G_a(\underline{r}/s)}{\partial n_o}\, u(s)\, ds$$

$$\underline{r} \text{ in } R_a \qquad (3)$$

and similarly

$$u(\underline{r}) = -\int_{s_{2ab}} G_b(\underline{r}/s)\,\frac{\partial u(s)}{\partial n}\,ds - \int_{s_{1ab}} \frac{\partial G_b(\underline{r}/s)}{\partial n_o}\,u(s)\,ds \qquad \underline{r} \text{ in } R_b \qquad (4)$$

For $\underline{r}$ on s_{2ab} u must be continuous and for $\underline{r}$ on s_{1ab} $\partial u/\partial n$ must be continuous in order to satisfy the remaining continuity constraints. Thus

$$\int_{s_{2ab}} \{G_a(s_{2ab}/s) + G_b(s_{2ab}/s)\}\,\frac{\partial u(s)}{\partial n}\,ds + \int_{s_{1ab}} \left\{\frac{\partial G_b(s_{2ab}/s)}{\partial n_o} - \frac{\partial G_a(s_{2ab}/s)}{\partial n_o}\right\} u(s)\,ds = 0 \qquad (5)$$

$$\int_{s_{2ab}} \left\{\frac{\partial G_a(s_{1ab}/s)}{\partial n} - \frac{\partial G_b(s_{1ab}/s)}{\partial n}\right\}\frac{\partial u(s)}{\partial n}\,ds - \int_{s_{1ab}} \left\{\frac{\partial^2 G_a(s_{1ab}/s)}{\partial n \partial n_o} + \frac{\partial^2 G_b(s_{1ab}/s)}{\partial n \partial n_o}\right\} u(s)\,ds = 0 \qquad (6)$$

These coupled integral equations may be solved approximately by Galerkin's method, which leads to a non-linear eigenvalue problem,

$$[A(\lambda)]\,[B] = 0 \qquad (7)$$

where each root of Det $[A(\lambda)] = 0$ is an approximate eigenvalue and the corresponding B is related to the eigenvector .

3. Applications

3.1 The L-shaped Region

With the boundaries specified as shown, figures 1.a and 1.b illustrate the two-axis representation of one half of a salient pole.

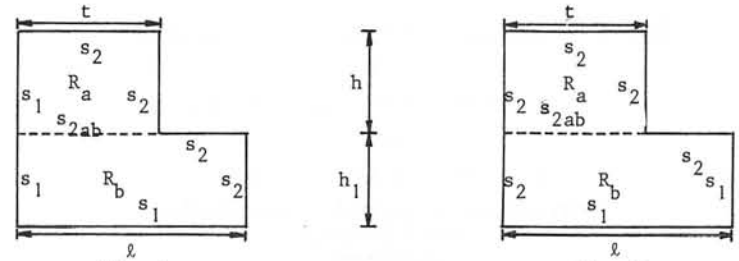

Fig. 1a Fig. 1b

The dominant eigenvalues associated with the direct and quadrature axes for two-pole geometries are given in table 1. Ferriss[4] has calculated the eigenvalues for the L-shaped region (A) and his values are given in parenthesis.

3.2 Cross-section Through the Rotor of a Turbo-alternator

The specification of the boundaries in figures 2.a and 2.b, once again correspond to the two-axis representation of the rotor.

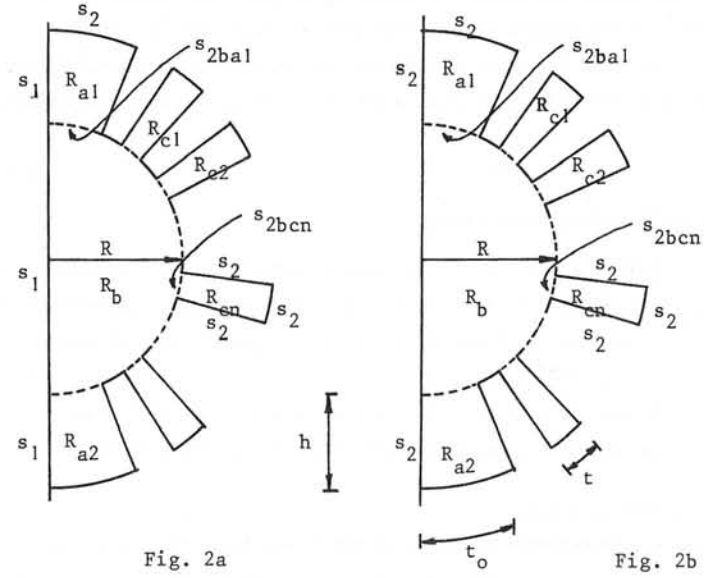

Fig. 2a Fig. 2b

A list of the dominant eigenvalues associated with the two axes for a typical turbo-alternator rotor is given in table 2.

Table 1

(A) $\bar{t}$=0.5 $\bar{h}$=0.5 $\bar{h}_1$=0.5		(B) $\bar{t}$=0.53 $\bar{h}$=0.73 $\bar{h}_1$=0.33	
$\bar{\lambda}^2$ D-Axis	$\bar{\lambda}^2$ Q-Axis	$\bar{\lambda}^2$ D-Axis	$\bar{\lambda}^2$ Q-Axis
11.499 (11.499)	3.221 (3.214)	11.207	2.438
17.255 (17.218)	21.808 (21.792)	25.667	20.573
37.698 (37.697)	34.561 (34.548)	35.321	36.610
70.319 (70.181)	46.810 (46.740)	64.505	45.889
79.749 (79.745)	63.501 (63.404)	79.318	54.515
$\bar{t} = t/\ell$, $\bar{h} = h_1/\ell$,		$\bar{h} = h_1/\ell$, $\bar{\lambda} = \lambda\ell$	

Table 2

t_o=0.58 $\bar{t}$=0.0323 $\bar{h}$=0.414	
$\bar{\lambda}^2$ D-Axis	$\bar{\lambda}^2$ Q-Axis
2.298	1.599
7.821	6.580
10.564	10.065
11.810	11.580
29.397	12.376
$\bar{t}=t/R$, $\bar{t}_o=t_o/R$, $\bar{h}=h/R$, $\bar{\lambda}=\lambda R$	

References

1. Rogers, G.J. and Cambrell, G.K.: 'The piece-by-piece solution of elliptic boundary value problems', Journal Phys. D, Vol. 8, 1975 pp 1615 - 1623
2. Hammond, P. and Rogers, G.J.: 'Use of equivalent fields in electrical-machine studies', Proc. IEE, Vol. 121, 1974, pp 500 - 507
3. Rogers, G.J. and Smith, J.R.: 'Synchronous-machine model including eddy currents', Proc. IEE, Vol. 120, 1973, pp 461 - 468
4. Ferriss, D.H.: 'Solution of mixed boundary value problems in finite domains by Fourier's method', NPL, NAC 16, 1972

SIMPLIFIED INTEGRAL EQUATIONS FOR ALTERNATING-CURRENT DISTRIBUTION IN STRIP-CONDUCTORS AND STRIP-LINE WITH MINIMIZED PROXIMITY EFFECT

Branko D. Popović, D. Sc.
Department of Electrical Engineering
University of Belgrade, Yugoslavia

1 Introduction

In integral equations for alternating-current distribution in parallel cylindrical conductors enter double integrals which are relatively difficult and time-consuming to integrate when solving these equations numerically. This is true even in the case when the conductors are in the form of thin strips. Only when the strips are flat can the integrals be integrated once explicitely.[1]

This paper shows that in the case of thin strip conductors of arbitrary cross-sectional shape the double integrals can be approximated with high accuracy by simple ordinary integrals. Thus the simultaneous integral equations for current distribution in any number of parallel, cylindrical thin strips of arbitrary cross-sectional shape contain only single integrals, and the system can easily be approximately solved using any of the known numerical methods.

If we consider these equations in the case of two identical, symmetrical parallel curved strip conductors, it becomes possible to consider the integral equations not only as equations in current distribution, but also in the shape of the line cross-section. In particular, by shaping the conductors and their distance appropriately, it is possible to have approximately uniform current distribution in the conductors, i.e. to minimize losses. This appears to be the first attempt to reduce skin and proximity effects by an optimization process.

2 Integral equations for current density in parallel conductors

Consider n very long, parallel nonferromagnetic conductors situated in a vacuum, of constant, but otherwise arbitrary cross-sections. Let the z-axis of a coordinate system be parallel to the conductors, and let the conductors strech from z=-b to z=b, with b much larger than the distance between two most distant points of the cross-sections S_j and S_k of any two conductors of the system. Assume that the currents $i_m(t)$, m=1,2,...n, in the conductors are time-harmonic of angular frequency ω, and that, in the complex notation,

$$\sum_{k=1}^{n} \dot{I}_k = 0 \ . \qquad (1)$$

It can be then shown that complex current densities $J_m(x,y)$, m=1,2,...n, in the n conductors satisfy the following set of simultaneous integral equations:

$$J_m(x,y) = \frac{j\omega\mu_0\sigma}{4\pi} \sum_{k=1}^{n} \int_{S_k} J_k(x',y') \times$$

$$\times \ln\{(x-x')^2 + (y-y')^2\}\, dx'dy' + J_{0m} \ ,$$

$$m = 1,2,...n \ . \qquad (2)$$

The J_{0m} are complex constants to be determined, and current density functions are subject to constraints

$$\int_{S_m} J_m(x,y)\, dx\, dy = I_m, \quad m=1,2,...n \ . \qquad (3)$$

Consider now a conductor system consisting of n thin, not necessarily flat strips, of thicknesses d_1, d_2,...d_n (Fig.1). Assume that the strips are such that the middle lines of their cross-sections can be represented by single-valued functions $f_m(x)$, having finite derivatives $f_m'(x)$ at all points of the strips. (By rotating the coordinate system and/or by subdividing the conductors' cross-sections appropriately this condition can be fulfilled in most cases. The other cases, for which $f_m'(x)$ becomes infinite at some points, can be treated by a somewhat more complicated technique, not to be mentioned here.) Let us designate by $g_m(x)$ the functions representing the upper border-lines of the conductors' cross-sections (see Fig.1), i.e.

$$g_m(x) = f_m(x+\Delta x) + \frac{d_m}{2}\sqrt{1 + f_m'(x)^2}\ , \qquad (4)$$

where

$$\Delta x = \frac{d_m}{2}\,\frac{f_m'(x)}{\sqrt{1 + f_m'(x)^2}}\ . \qquad (5)$$

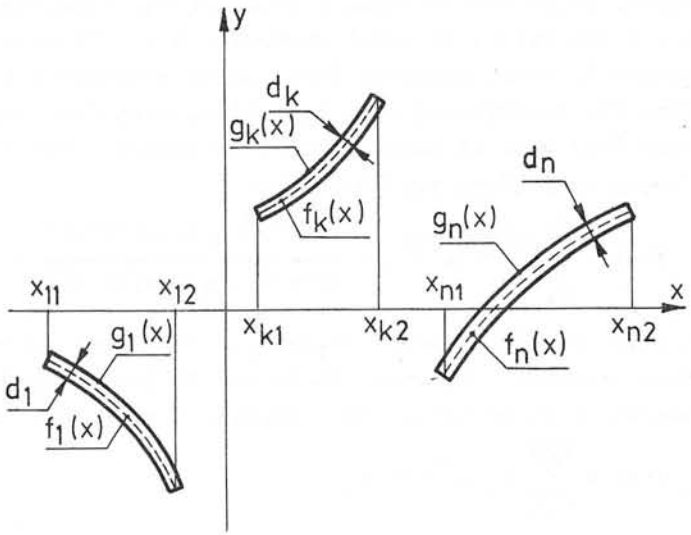

Fig.1. Geometry of cross-section of strip-conductors.

The strips being thin, current density can be assumed constant across the strip thickness, and we can substitute

$$J_k(x',y')\,dx'dy' \text{ by } J_k(x')\,d_k\sqrt{1 + f_k'(x')}\,dx'. \qquad (6)$$

If $k \neq m$ we can set

$$y - y' = f_m(x) - f_k(x')\ , \quad m \neq k\ , \qquad (7)$$

but for $m=k$ this would lead to singular integrals. Therefore we put

$$y - y' = g_m(x) - f_k(x')\ , \quad (m,k=1,2,...n)\ . \qquad (8)$$

Thus from eqn.2 we obtain the following set of approximate integral equations valid for thin strips:

$$J_m(x) = \frac{j\omega\mu_0\sigma}{4\pi}\sum_{k=1}^{n} d_k \int_{x_{k1}}^{x_{k2}} J_k(x')\sqrt{1 + f_k'(x')^2}\ \times$$

$$\times \ln\{(x-x')^2 + [g_m(x)-f_k(x')]^2\}\,dx' + J_{0m}\ ,$$

$$m = 1,2,...n\ . \qquad (9)$$

Similarly, with approximation in eqn.6, eqn.3 becomes

$$d_k \int_{x_{k1}}^{x_{k2}} J_k(x)\sqrt{1 + f_k'(x)}\,dx = I_k\ ,\ k=1,2,...n. \qquad (10)$$

To solve approximately the system of integral equations (9), subject to the n constraints (10), different methods can be used. Perhaps the simplest, and from the computing time probably most convenient, is the so-called point-matching method with polynomial approximation of $J_k(x)$ of the form[1]

$$J_k(x) = \sum_{i=1}^{n_k+1} C_{ki}\,x^{i-1}\ , \quad k=1,2,...n\ . \qquad (11)$$

Here, C_{ki} are complex current-distribution parameters to be determined, and n_k is the order of the polynomial approximation in strip k. With assumed current distribution (11), eqns.9 and 10 become

$$\sum_{i=1}^{n_m+1} C_{mi}\, x^{i-1} = \sum_{k=1}^{n} \sum_{i=1}^{n_k+1} C_{ki}\, G_{ki}(x) + J_{0m} ,$$

$$m = 1,2,\ldots n , \qquad (12)$$

$$\sum_{i=1}^{n_k+1} C_{ki}\, b_{ki} = I_k , \quad k=1,2,\ldots n , \qquad (13)$$

where

$$G_{ki}(x) = \frac{j\omega\mu_0\sigma d_k}{4\pi} \int_{x_{k1}}^{x_{k2}} x'^{(i-1)} \sqrt{1 + f_k'(x')^2} \times$$

$$\times \ln\{(x-x')^2 + [g_m(x)-f_k(x')]^2\}\, dx' ,$$

$$k = 1,2,\ldots n , \qquad (14)$$

and

$$b_{ki} = d_k \int_{x_{k1}}^{x_{k2}} x^{i-1} \sqrt{1 + f_k'(x)^2}\, dx . \qquad (15)$$

Alltogether we have $N = \{\sum_{k=1}^{n} (n_k+1)+n\}$ unknowns (i.e., all the current-distribution parameters C_{ki} and the n constants J_{0m}, m=1,2,...n). In addition to the n equations (13) we therefore need another (N-n) equations, which we obtain by stipulating that eqns.12 hold for (n_k+1) points of the k-th conductor, k=1,2,...n. The simplest choice for these "matching points" is that they be equispaced along the x-axis, i.e.

$$x_{kj} = x_{k1} + (j-1)\, \frac{x_{k2} - x_{k1}}{n_k} , \quad k=1,2,\ldots n ,$$

$$j=1,2,\ldots(n_k+1) . \qquad (16)$$

Eqns.12 thus become

$$\sum_{i=1}^{n_k+1} C_{mi}\, x_{mj}^{i-1} = \sum_{k=1}^{n} \sum_{i=1}^{n_k+1} C_{ki} G_{ki}(x_{mj}) + J_{0m} ,$$

$$m = 1,2,\ldots n, \quad j = 1,2,\ldots(n_m+1) . \qquad (17)$$

These (N-n) equations, together with the n equations (13), have to be solved for the (N-n) current-distribution parameters C_{ki} and the n constants J_{0m}. Both numerical evaluation of the integrals in eqns.14 and 15 and solution of the N complex linear equations (13) and (17) is today a relatively simple matter, and we shall not discuss these topics here.

3 Synthesis of strip-line with minimized proximity effect

In the case of two strip conductors (n=2), symmetrical with respect to the origin and to the x-axis, we have $I_1=-I_2=I$, $J_1(x)=-J_2(x)=J(x)$. The equations (9) become two identical equations, of the form

$$J(x) = \frac{j\omega\mu_0\sigma d}{4\pi} \int_{-x_1}^{x_1} J(x') \sqrt{1 + f'(x')^2} \times$$

$$\times \ln \frac{(x-x')^2 + \{g(x) - f(x')\}^2}{(x-x')^2 + \{g(x) + f(x')\}^2}\, dx' + J_0 . \qquad (18)$$

By physical reasoning it can be concluded that, in principle, there should exist a shape of the conductors for which J(x)=constant, at least approximately. If this is approximately true, equation (18) can be considered as an equation for determining f(x) for which, with J(x)=constant, equation (18) will be approximately satisfied. Obviously, this leads to finding f(x) such that

$$R(x) = \int_{-x_1}^{x_1} \sqrt{1+f'(x')^2}\, \ln \frac{(x-x')^2+\{g(x)-f(x')\}^2}{(x-x')^2+\{g(x)+f(x')\}^2}\, dx' \qquad (19)$$

be constant on the segment $-x_1<x<x_1$. This f(x) cannot be obtained directly. However, it is not difficult to find it approximately by assuming, for example, f(x) in the form

$$f(x) = \sum_{k=1}^{p+1} F_k\, x^{2(k-1)} , \qquad (20)$$

and determining the unknown parameters F_k by an optimization

process so that the expression

$$A = \sum_{i=1}^{q} \left| \frac{R(x_i) - R(0)}{R(0)} \right|^2 , \qquad (21)$$

with x_i representing any set of arbitrary number q of points on the segment $[0,x_1]$, be minimal. This optimization process can also be performed relatively easily by means of an electronic digital computer.

4 Numerical results

Using the theory described in Section 2, numerical results were first obtained for several cases of thin strip conductors for which numerical results already existed. For all the cases of flat thin strips considered in References 1-4, practically the same results were obtained by the present theory. This proved the validity of the present theory which, however, is simpler than any of the available methods for determining current distribution in strip conductors known to the author, particularly if the strips are not flat. As a new example, Fig.2 shows current distribution in three-phase balanced line consisting of three flat strips as shown in the insert of Fig.2. Note considerable asymmetry of current distribution in the strips. Current distributions obtained theoretically in the three strips were practically identical and shifted in phase as expected, although the complete system was solved without postulating the symmetry.

As an example of minimization of skin and proximity effects in a symmetrical two-strip line by shaping the conductors, consider a strip-line having minimal distance of 10 cm, maximal width of 20 cm, made of copper strips (σ=5.7 × × 10^7 S/m) of thickness d=2 mm. By the optimization process using the trial function of the conductor's shape of the form

$$f(x) = 0.05 + F_3 x^4 \quad (x \text{ in metres}) , \qquad (22)$$

it was found that $F_3 \approx 836\ m^{-4}$, i.e.

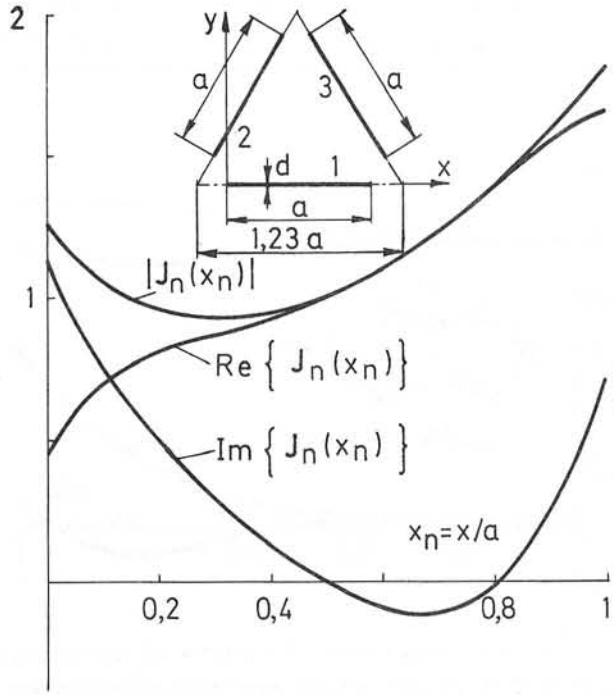

Fig.2. Real part, imaginary part and magnitude of normalized current density $J_n(x_n)=J(x_n)/J(0.5)$ in strip 1 of the symmetrical three-phase strip line shown in the insert. The conductors carry balanced sinusoidal currents, with clockwise phase sequence. a=20 cm, d=0.2 cm, $\sigma=5.7\times10^7$ S/m, f=50Hz, n=4.

$$[f(x)]_{optimal} \approx 0,05 + 836\ x^4 \quad (x \text{ in metres}) . \qquad (23)$$

For that shape of the conductors current distribution was computed using the present method. The results for real and imaginary parts of current density are shown in Fig.3. For comparison, the results for parallel flat strips of the same width (measured along the x-axis) and the distance equal to

the minimal distance between the curved strips are shown in dashed lines. In spite of relatively crude modelling of the strips (using only one optimization parameter, as in eqn.22), the combined skin and proximity effects are seen to be reduced appreciably.

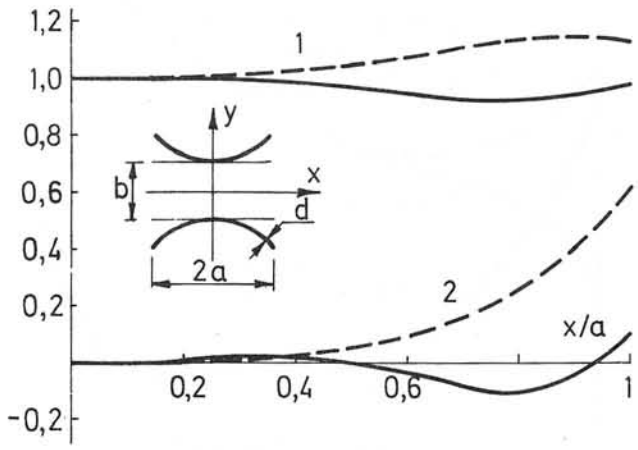

Fig.3. Real (1) and imaginary (2) parts of normalized current density J(x/a)/J(0) in optimized two-strip-conductor line (solid lines) and two parallel flat strips (dashed lines). Cross-sections of the two systems are shown in the insert. a=10 cm, b=10 cm, d=0.2 cm, $\sigma=5.7\times10^{7}$ S/m, f=50 Hz, n=6.

5 Conclusion

A simple method is presented for determining alternating-current distribution in parallel thin strip-conductors of any cross-sectional shape. It is assumed that the strips are thin enough that current density is practically constant across their thickness.

It is shown in addition that a symmetrical two-strip line can be synthesized with approximately constant current density at all points of a strip, i.e. with minimized skin and proximity effects. This appears to be the first attempt to minimize the proximity effect by shaping the conductors.

Numerical results obtained by the present method are in excellent agreement with available experimental and theoretical results. However, the present method appears to be the simplest of all the existing methods, particularly if the strips are of a curved cross-section. Numerical results obtained for an optimized two-strip line show pronounced uniformity of current distribution across the optimal line when compared with similar line consisting of two flat strips.

6 Acknowledgement

The author is grateful to Mr. Antonije Djordjević for preparing the computer programs and for obtaining the numerical results presented in the paper.

7 References

1 POPOVIĆ, B. D., and FILIPOVIĆ, D. N.: "Theory of power-frequency proximity effect for strip conductors", Proc. IEE, 122, (8), pp.839-842

2 HAEFNER, S. J.: "Alternating-current resistance of rectangular conductors", Proc.Inst.Rad.Eng.,1937,25,pp.434-447

3 SILVESTER, P.: "Skin effect in multiple and polyphase conductors", IEEE Trans., PAS-88, (3), pp.231-238

4 POPOVIĆ, B. D., and POPOVIĆ, Z. D.: "Method of determining power frequency current distribution in cylindrical conductors", Proc.IEE, 119, (5), pp.569-574